



University
of Glasgow

Karstensen, Annette Degn (1996) Constraint estimation schemes in fracture mechanics. PhD thesis

<http://theses.gla.ac.uk/7228/>

Copyright and moral rights for this thesis are retained by the author

A copy can be downloaded for personal non-commercial research or study, without prior permission or charge

This thesis cannot be reproduced or quoted extensively from without first obtaining permission in writing from the Author

The content must not be changed in any way or sold commercially in any format or medium without the formal permission of the Author

When referring to this work, full bibliographic details including the author, title, awarding institution and date of the thesis must be given

Constraint Estimation Schemes in Fracture Mechanics

by

Annette Degn Karstensen, M.Sc.

Thesis submitted to the Faculty of Engineering of
University of Glasgow for
the degree of Doctor of Philosophy

April 1996

© Copyright 1996 by Annette Degn Karstensen

Blank Page

Abstract

Elastic-plastic crack tip constraint has been estimated for the common planar crack geometries. These include single edge cracked bars in tension and bending, centre cracked panels, and double edge cracked bars. The description of the stress field has been modified from a one parameter characterisation, based on K or J , to include a second term. The second parameter is a non-singular term, described either in terms of an elastic T -stress or a Q field.

The limits of one and two parameter characterisation are discussed for single edge bars in tension and bending and for centre cracked panels. For the single edge geometries the two parameter characterisation was found to extend the characterisation well beyond the one parameter approach. For the centre cracked panels the two parameter characterisation in terms of a J - Q approach was found to be more accurate than a J - T approach at high levels of deformation.

For the single edge cracked bending and tension geometries the second parameter Q is divided into two components named Q_T and Q_P . Q_T is an elastic term which depends of the elastic T stress and is independent of the distance from the crack tip. The second component, Q_P , arises from global bending on the uncracked ligament. This is a distance dependent term which depends on the level of deformation and can either be expressed as a function of the load normalised by the limit load or as a function of the plastic component of the J -integral.

For single edge bend bars the constraint estimation provides basis for a method of predicting fracture toughness using local failure approach, where the failure criterion is expressed in terms of the stress level ahead of the crack tip. Finally the constraint of mixed mode problem has been analysed and compared with that of pure Mode I problems.

Blank Page

Acknowledgements

My biggest thanks go to Professor John Hancock. He was the best supervisor I could have wished for. I would like to thank him for having such a good time working on my Ph.D. I was also glad that he gave me the opportunity to work with Dr. Covadonga Betegón from University of Oviedo. Although I was in Spain for a short time I learned a lot, and besides Covadonga is good company. I thank my colleague Damane Nekkai for not only being helpful with my work, but also being a good friend. John also equipped me with LaCoste, the best *Sun* SPARC Workstation I could ever have hoped for, I really tied a special knot with that silly computer.

I would like to thank Jem for the part he played through a long period of this project: for helping me changing my "Ænglisk" into English; for looking after LaCoste, and for helping to optimise my computer programs. I appreciated "all of it" - to various degrees.

To Karen and Hilde thanks for feeding me with endless bowls of "Hilde's Pasta Dish" night after night in their cosy flat. Thanks to the Kiwi Jacqui, the first friend I ever made in Glasgow. I am particularly happy for the inspiration for my double backhand, and I am really glad she returned when I needed her most. Yasmine, thanks for being a friend and putting up with me throughout the time I shared your office. I would also like to thank John and Moira for their support. Thanks are due to my sister Vibsen, for supply of my favourite Danish cartoons and strong liquorice.

Finally I would like to thank Professor John Sumpter of DRA, for support in terms of a grant from DRA and thanks to *Civilingeniør Myhrwold Grant*, *Otto Mønsted's Grant* and *the Danish Engineering Association* for their financial support to pay my Ph.D. fees.

Contents

Abstract	iii
Acknowledgements	v
List of Figures	5
List of Tables	15
1 Introduction to Constraint Based Fracture Mechanics	17
2 Single Parameter Fracture Mechanics	19
2.1 Linear Elastic Fracture Mechanics	19
2.1.1 The Stress Intensity Factor	22
2.1.2 The Griffith Criterion	23
2.1.3 Crack Tip Plasticity	25
2.1.4 Validity of Linear-Elastic Fracture Mechanics	27
2.2 Single Parameter Elastic-Plastic Fracture Mechanics	28
2.2.1 Crack Tip Opening Displacement	28
2.2.2 J Characterised Crack Tip Fields	30
2.2.3 Slip Line Fields	32
2.2.4 Slip Line Fields around a Crack Tip	35
2.2.5 Crack Tip Constraint in Large Scale Yielding	36
3 Two Parameter Fracture Mechanics	39
3.1 J Dominated Crack Tip Fields	39
3.2 Elastic Two Parameter Fracture Mechanics	40
3.2.1 T -stress	40
3.2.2 The Effect of T on the Plastic Zone	42
3.2.3 Determination of the T stress	42
3.3 Two Parameter Elastic-Plastic Crack Tip Fields	46
3.3.1 Modified Boundary Layer Formulations	46
3.4 Higher-Order Asymptotic for Non-Linear Crack Tip Fields	48
3.4.1 The Q Approach	48
3.5 The Effect of Constraint on Experimental Toughness Data	50
3.5.1 Constraint Effect on Cleavage Failure	50
3.5.2 Ductile Fracture	54
3.6 Engineering Application	56
3.6.1 Failure Assessment	56
3.6.2 Constraint Based Failure Assessment Diagrams	58

4	Numerical Methods	61
4.1	Numerical Analysis	61
4.1.1	Modified Boundary Layer Formulations	61
4.1.2	Full Field Solutions	62
4.1.3	Material Response	63
4.1.4	Determination of J	64
4.2	Software for Constraint Analysis	66
4.2.1	Program: "ABAQUS to Matlab"	66
4.2.2	Program: Constraint	68
5	Limits to the Characterisation of Crack Tip Fields by One and Two Parameters	75
5.1	Modified Boundary Layer Formulation Results	75
5.2	T-stress in Full Field Solutions	83
5.3	Limits for One Parameter Characterisation	89
5.4	Limits for Two Parameter Characterisation	96
5.4.1	Limits for J - T Characterisation	96
5.4.2	Limits for J - Q Characterisation	98
5.5	Conclusion	100
6	Constraint Estimation Schemes for Edge Cracked Bars in Bending and Tension	107
6.1	J - Q Crack Tip Fields	107
6.2	Constraint Estimation for Single Edge Crack Bars in Bending	109
6.3	Constraint Estimation for Single Edge Cracked Bars in Tension	122
6.4	Discussion	130
6.5	Conclusions	133
7	Constraint Estimation Schemes for Centre Cracked Panels and Double Edge Cracked Bars	139
7.1	Numerical Analysis	139
7.2	Stress Fields of Centre Cracked Panels	139
7.3	Numerical Results for Centre Cracked Panels	140
7.3.1	Numerical Results for Centre Cracked Panels	140
7.3.2	Force to Moment Ratios on the Ligaments of Centre Cracked Panels	145
7.4	Constraint Estimation for Centre Cracked Panels	148
7.4.1	Crack Tip Constraint Estimated by T	148
7.4.2	Crack Tip Constraint Estimated by Q	149
7.4.3	Discussion of Constraint Estimation for Centre Cracked Panels	150
7.5	Stress Field of Double Edge Cracked Bars	152
7.6	Numerical Results for Double Edge Cracked Bars	153
7.7	Constraint Estimation for Double Edge Cracked Bars	154
7.8	Conclusion	155

8	Constraint Effects Modelled by Local Failure Criteria	159
8.1	Approach to a Local Failure Criteria in Cleavage	159
8.1.1	The Scaling Approach	160
8.1.2	The Local Approach	161
8.1.3	Statistical Approach to Local Cleavage Failure	163
8.1.4	Thickness effect	166
8.2	Local Fracture Criteria for Cleavage	168
8.3	Discussion	170
8.4	Conclusion	172
9	Mixed Mode and Mode I Crack Tip Fields Unified by Constraint	175
9.1	Non-hardening Mode I Fields	175
9.2	Non-hardening Mixed Mode Fields	178
9.3	Numerical Model	179
9.4	Results	181
9.4.1	Slip line Fields	181
9.4.2	Strain Hardening	185
9.5	Fracture Criteria	186
9.6	Conclusions	187
10	Conclusion	193
11	References	195

Blank Page

List of Figures

2.1	A crack of length $2a$ subject to a remote stress σ_{app} .	19
2.2	The three modes of loading.	22
2.3	Effect of specimen thickness on Mode I fracture toughness.	23
2.4	Cracked plate at a fixed displacement and fixed load.	24
2.5	Plastic zone shapes for Mises and Tresca yield criteria.	27
2.6	Validation of LEFM and EPFM.	29
2.7	Estimation of (CTOD) from 90° intercept construction.	29
2.8	Arbitrary contour around a crack tip.	30
2.9	Various zones surrounding a crack tip.	32
2.10	The stress state in a slip line field region.	33
2.11	Mohr's circle.	33
2.12	Prandtl slip line field in a region around a crack tip.	35
2.13	Slip line fields for deep and shallow cracked bars in bending after Ewing(1968) and Green(1953).	37
2.14	Slip line fields for a centre cracked panel.	37
2.15	Slip line fields for double edge cracked bars.	38
3.1	The Effect of the T stress on the plastic zone shape in small scale yielding.	42
3.2	The Effect of the T stress on the plastic zone shape in small scale yielding, after Du and Hancock (1991).	43
3.3	Model used to determine T from Eshelby's method, after Kfourri (1986).	44
3.4	Values of the non-dimensional bi-axiality parameter β for SEN and DEN specimens as function of a/W , data after Kfourri (1986).	45
3.5	Illustration of the components of the line spring model.	46
3.6	Model for boundary layer formulation.	47
3.7	Toughness of edge cracked bend bars after Betegón (1990), and Betegón and Hancock (1990) as a function of $\frac{T}{\sigma_0}$.	50
3.8	Critical value of J as a function of $\frac{T}{\sigma_0}$ for 3PB and CCT specimens, low-grade mild steel at -50°C , Sumpter (1993).	51

3.9	Critical value of J as a function of Q for 3PB and CCT specimens, low-grade mild steel at -50°C , after Sumpter and Hancock (1994).	51
3.10	Critical value of J as a function of $\frac{T}{\sigma_0}$ for 3PB and CCT specimens, high strength weld steel at -30°C , Sumpter (1993).	52
3.11	Critical value of J as a function of Q for 3PB and CCT specimens, high strength weld steel at -30°C , after Sumpter and Hancock (1994).	52
3.12	Fracture toughness versus $\frac{T}{\sigma_0}$ for ASTM A515 Grade 70 steels at 20°C from edge cracked bend bars for three thicknesses, after Kirk et al. (1993).	53
3.13	Fracture toughness versus Q for ASTM A515 Grade 70 steels at 20°C from edge cracked bend bars for three thicknesses, after Kirk et al. (1993)	53
3.14	The toughness of a range of through and part through crack geometries parameterised by T , after Hancock, Reuter and Parks (1993).	54
3.15	The CTOD as a function of T at crack extensions of 0, 200 and 400 μm , after Hancock, Reuter and Parks (1993).	54
3.16	The initial slope of CTOD- Δa resistance curve as a function of $\frac{T}{\sigma_0}$, after Hancock, Reuter and Parks (1993).	55
3.17	The initial slope of J - Δa resistance curve as a function of $\frac{T}{\sigma_0}$, after Hancock, Reuter and Parks (1993).	56
3.18	Failure assessment lines as given by R6 Rev 3 and the original form.	57
3.19	Geometry specific failure assessment diagram, single edge bend bars, $n=13$.	58
3.20	Failure assessment diagram expressed as conventional and modified FAD on the same axis, Sumpter Weld Data, single edge cracked bend bars, $n=10$.	59
4.1	The mesh for boundary layer formulation analysis.	62
4.2	The four geometries analysed.	63
4.3	Mesh of a full field solution, with $a/W=0.5$.	64
4.4	The stress-strain relationship based on Ramberg-Osgood power law, for various hardening rates.	65
4.5	Examples of a record in a FIL file.	68
4.6	Form functions for single edge bend, single edge tension, centre crack panels and double edge cracked bars.	71
4.7	Bi-axiality ratio for single edge bend, single edge tension, centre cracked tension and double edge cracked bars geometries.	72
4.8	Numerical results for the non-dimensionalised limit load of SECB bars compared with Miller's (1987) formula.	73
4.9	Numerical results for the non-dimensionalised limit load of SECT bars compared with a curve fit formula.	73

-
- 5.1 The tangential stress directly ahead of the crack in a boundary layer formulation, $\frac{T}{\sigma_0} = -0.7$, ($n=6$). 76
- 5.2 The tangential stress normalised by the yield stress directly ahead of the crack in a modified boundary layer formulation for different values of $\frac{T}{\sigma_0}$, $n=3$. 77
- 5.3 The tangential stress normalised by the yield stress directly ahead of the crack in a modified boundary layer formulation for different values of $\frac{T}{\sigma_0}$, $n=6$. 77
- 5.4 The tangential stress normalised by the yield stress directly ahead of the crack in a modified boundary layer formulation for different values of $\frac{T}{\sigma_0}$, $n=13$. 78
- 5.5 The tangential stress normalised by the yield stress directly ahead of the crack in a modified boundary layer formulation for different values of $\frac{T}{\sigma_0}$, non-hardening. 78
- 5.6 The tangential stress normalised by the yield stress at different distances ahead of the crack tip ($R=\frac{r\sigma_0}{J}$) in a modified boundary layer formulation with different values of $\frac{T}{\sigma_0}$, $n=3$. 79
- 5.7 The tangential stress normalised by the yield stress at different distances ahead of the crack tip ($R=\frac{r\sigma_0}{J}$) in a modified boundary layer formulation with different values of $\frac{T}{\sigma_0}$, $n=6$. 79
- 5.8 The tangential stress normalised by the yield stress at different distances ahead of the crack tip ($R=\frac{r\sigma_0}{J}$) in a modified boundary layer formulation with different values of $\frac{T}{\sigma_0}$, $n=13$. 80
- 5.9 The tangential stress normalised by the yield stress at different distances ahead of the crack tip ($R=\frac{r\sigma_0}{J}$) in a modified boundary layer formulation with different values of $\frac{T}{\sigma_0}$, non-hardening. 80
- 5.10 The modified boundary layer formulation compared for different strain hardening rates, as the tangential stress normalised by the yield stress directly ahead of the crack tip at a distance $r = \frac{2J}{\sigma_0}$ as a function of $\frac{T}{\sigma_0}$. 81
- 5.11 The tangential stress normalised by the yield stress as a function of $\frac{T}{\sigma_0}$ directly ahead of the crack tip at a distance $\frac{r\sigma_0}{J} = 2$. Single edge cracked bend bars, $n=3$. 84
- 5.12 The tangential stress normalised by the yield stress as a function of $\frac{T}{\sigma_0}$ directly ahead of the crack tip at a distance $\frac{r\sigma_0}{J} = 2$. Single edge cracked bend bars, $n=6$. 85
- 5.13 The tangential stress normalised by the yield stress as a function of $\frac{T}{\sigma_0}$ directly ahead of the crack tip at a distance $\frac{r\sigma_0}{J} = 2$. Single edge cracked bend bars, $n=13$. 85
- 5.14 The tangential stress normalised by the yield stress as a function of $\frac{T}{\sigma_0}$ directly ahead of the crack tip at a distance $\frac{r\sigma_0}{J} = 2$. Single edge cracked bend bars, non-hardening. 85

- 5.15 The tangential stress normalised by the yield stress as a function of $\frac{T}{\sigma_0}$ directly ahead of the crack tip at a distance $\frac{r_{cp}}{y} = 2$. Single edge cracked bars in tension, $n=3$. 86
- 5.16 The tangential stress normalised by the yield stress as a function of $\frac{T}{\sigma_0}$ directly ahead of the crack tip at a distance $\frac{r_{cp}}{y} = 2$. Single edge cracked bars in tension, $n=6$. 86
- 5.17 The tangential stress normalised by the yield stress as a function of $\frac{T}{\sigma_0}$ directly ahead of the crack tip at a distance $\frac{r_{cp}}{y} = 2$. Single edge cracked bars in tension, $n=13$. 86
- 5.18 The tangential stress normalised by the yield stress as a function of $\frac{T}{\sigma_0}$ directly ahead of the crack tip at a distance $\frac{r_{cp}}{y} = 2$. Single edge cracked bars in tension, non-hardening. 87
- 5.19 The tangential stress normalised by the yield stress as a function of $\frac{T}{\sigma_0}$ directly ahead of the crack tip at a distance $\frac{r_{cp}}{y} = 2$. Centre cracked panels, $n=3$. 87
- 5.20 The tangential stress normalised by the yield stress as a function of $\frac{T}{\sigma_0}$ directly ahead of the crack tip at a distance $\frac{r_{cp}}{y} = 2$. Centre cracked panels, $n=6$. 87
- 5.21 The tangential stress normalised by the yield stress as a function of $\frac{T}{\sigma_0}$ directly ahead of the crack tip at a distance $\frac{r_{cp}}{y} = 2$. Centre cracked panels, $n=13$. 88
- 5.22 The tangential stress normalised by the yield stress as a function of $\frac{T}{\sigma_0}$ directly ahead of the crack tip at a distance $\frac{r_{cp}}{y} = 2$. Centre cracked panels, non-hardening. 88
- 5.23 The stresses directly ahead of a crack in edge cracked bend bars normalised by the small scale yielding field at a distance $\frac{r_{cp}}{y} = 2$ as a function of $\frac{\sigma_p}{\sigma_0}$. 92
- 5.24 The stresses directly ahead of a crack in edge cracked bars in tension normalised by the small scale yielding field at a distance $\frac{r_{cp}}{y} = 2$ as a function of $\frac{\sigma_p}{\sigma_0}$. 93
- 5.25 The stresses directly ahead of a crack in centre cracked panels normalised by the small scale yielding field at a distance $\frac{r_{cp}}{y} = 2$ as a function of $\frac{\sigma_p}{\sigma_0}$. 94
- 5.26 $\frac{\sigma_p}{\sigma_0}$ at the break down of single parameter characterisation for SECB, SECT and CCP, for hardening rates $n=3, 6, 13$ and non-hardening. 95
- 5.27 The stresses directly ahead of crack in an edge cracked bend bars normalised by the MBLF stress field at a distance $\frac{r_{cp}}{y} = 2$ as a function of $\frac{\sigma_p}{\sigma_0}$. 101
- 5.28 The stresses directly ahead of a crack in edge cracked bars in tension normalised by the MBLF stress field at a distance $\frac{r_{cp}}{y} = 2$ as a function of $\frac{\sigma_p}{\sigma_0}$. 102
- 5.29 The stresses directly ahead of crack in a centre cracked panels normalised by the MBLF stress field at a distance $\frac{r_{cp}}{y} = 2$ as a function of $\frac{\sigma_p}{\sigma_0}$. 103

5.30	$\frac{\sigma_0}{J}$ at the break down of J - T characterisation for SECB, SECT and CCP, for hardening rates $n=3, 6, 13$ and non-hardening.	104
5.31	Q' as a function of $\frac{\sigma_0}{J}$ for single edge bend bar, $n=13$	105
5.32	Q' as a function of $\frac{\sigma_0}{J}$ for CCPs and SECB, $n=13$	105
6.1	The hoop stress directly ahead of a crack SECB, $a/W=0.2, n=13$ at several levels of deformation.	108
6.2	The hoop stress in SECB, normalised by the stress from a modified boundary layer formulation at the same value of T , as a function of load normalised by the limit load, $n=3$.	110
6.3	The hoop stress in SECB, normalised by the stress from a modified boundary layer formulation at the same value of T , as a function of load normalised by the limit load, $n=6$.	110
6.4	The hoop stress in SECB, normalised by the stress from a modified boundary layer formulation at the same value of T , as a function of load normalised by the limit load, $n=13$.	111
6.5	The hoop stress in SECB, normalised by the stress from a modified boundary layer formulation at the same value of T , as a function of load normalised by the limit load, non hardening.	111
6.6	Q_P as a function of $\frac{P}{P_{Limit}}$ for Single edge bend bars at distances $\frac{r_{\sigma_0}}{J}=1, 2$ and 5 from the crack tip.	112
6.7	Q_P as a function of $\frac{P}{P_{Limit}}$ for single edge bend bars at a distance $\frac{r_{\sigma_0}}{J} = 2$ from the crack tip, for all a/W ratios and $n=3$.	112
6.8	Q_P as a function of $\frac{P}{P_{Limit}}$ for single edge bend bars at a distance $\frac{r_{\sigma_0}}{J} = 2$ from the crack tip, for all a/W ratios and $n=6$.	113
6.9	Q_P as a function of $\frac{P}{P_{Limit}}$ for single edge bend bars at a distance $\frac{r_{\sigma_0}}{J} = 2$ from the crack tip, for all a/W ratios and $n=13$.	113
6.10	Q_P as a function of $\frac{P}{P_{Limit}}$ for single edge cracked bend bars at a distance $\frac{r_{\sigma_0}}{J} = 2$ from the crack tip, for all a/W ratios, $n=\infty$.	114
6.11	Q_P as a function of $\frac{J_P}{\sigma_0}$ for single edge cracked bars in bending for all a/W at distances $\frac{r_{\sigma_0}}{J}=1,2,5$ from the crack tip.	117
6.12	Q_P as a function of $\frac{J_P}{\sigma_0}$ for single edge cracked bars in bending for all a/W at a distance $\frac{r_{\sigma_0}}{J}=2$ from the crack tip, $n=3$.	117
6.13	Q_P as a function of $\frac{J_P}{\sigma_0}$ for single edge cracked bars in bending for all a/W at a distance $\frac{r_{\sigma_0}}{J}=2$ from the crack tip, $n=6$.	118
6.14	Q_P as a function of $\frac{J_P}{\sigma_0}$ for single edge cracked bars in bending for all a/W at a distance $\frac{r_{\sigma_0}}{J}=2$ from the crack tip, $n=13$.	118
6.15	Q_P as a function of $\frac{J_P}{\sigma_0}$ for single edge cracked bars in bending for all a/W at a distance $\frac{r_{\sigma_0}}{J}=2$ from the crack tip, non-hardening material.	119
6.16	The hoop stress normalised by the stress from a modified boundary layer formulation for a distance $\frac{r_{\sigma_0}}{J}=2$ at the same value of T , as a function of load normalised by the limit load, $n=3$.	122

- 6.17 The hoop stress normalised by the stress from a modified boundary layer formulation for a distance $\frac{r_{\sigma_0}}{f} = 2$ at the same value of T , as a function of load normalised by the limit load, $n=6$. 123
- 6.18 The hoop stress normalised by the stress from a modified boundary layer formulation for a distance $\frac{r_{\sigma_0}}{f} = 2$ at the same value of T , as a function of load normalised by the limit load, $n=13$. 123
- 6.19 The hoop stress normalised by the stress from a modified boundary layer formulation for a distance $\frac{r_{\sigma_0}}{f} = 2$ at the same value of T , as a function of load normalised by the limit load, non-hardening. 124
- 6.20 Q_P as a function of $\frac{P}{P_{L_{lim}}}$ for single edge cracked bars in tension for all a/W at a distance $\frac{r_{\sigma_0}}{f} = 2$ from the crack tip, $n=3$. Curve fitting value for $k_2(n) = -0.0087$ 124
- 6.21 Q_P as a function of $\frac{P}{P_{L_{lim}}}$ for single edge cracked bars in tension for all a/W at a distance $\frac{r_{\sigma_0}}{f} = 2$ from the crack tip, $n=6$. Curve fitting value for $k_2(n) = -0.0072$ 125
- 6.22 Q_P as a function of $\frac{P}{P_{L_{lim}}}$ for single edge cracked bars in tension for all a/W at a distance $\frac{r_{\sigma_0}}{f} = 2$ from the crack tip, $n=13$. Curve fitting value for $k_2(n) = -0.0041$ 125
- 6.23 Q_P as a function of $\frac{P}{P_{L_{lim}}}$ for single edge cracked bars in tension for all a/W at a distance $\frac{r_{\sigma_0}}{f} = 2$ from the crack tip, non-hardening. 126
- 6.24 Q_P as a function of $\frac{J_P}{c\sigma_0}$ for single edge cracked bars for all a/W at a distance $\frac{r_{\sigma_0}}{f} = 2$ from the crack tip, $n=3$. 126
- 6.25 Q_P as a function of $\frac{J_P}{c\sigma_0}$ for single edge cracked bars for all a/W at a distance $\frac{r_{\sigma_0}}{f} = 2$ from the crack tip, $n=6$. 127
- 6.26 Q_P as a function of $\frac{J_P}{c\sigma_0}$ for single edge cracked bars for all a/W at a distance $\frac{r_{\sigma_0}}{f} = 2$ from the crack tip, $n=13$. 127
- 6.27 Q_P as a function of $\frac{J_P}{c\sigma_0}$ for single edge cracked bars for all a/W at a distance $\frac{r_{\sigma_0}}{f} = 2$ from the crack tip, non-hardening. 128
- 6.28 The hoop stress at a distance $\frac{r_{\sigma_0}}{f} = 2$ directly ahead of a SECB, $a/W=0.2$, $n=13$ at several levels of deformation. 134
- 6.29 The hoop stress at a distance $\frac{r_{\sigma_0}}{f} = 2$ directly ahead of a SECB, $a/W=0.7$, $n=13$ at several levels of deformation. 135
- 6.30 The hoop stress at a distance $\frac{r_{\sigma_0}}{f} = 2$ directly ahead of a SECT, $a/W=0.2$, $n=13$ at several levels of deformation. 136
- 6.31 The hoop stress at a distance $\frac{r_{\sigma_0}}{f} = 2$ directly ahead of a SECT, $a/W=0.7$, $n=13$ at several levels of deformation. 137
- 7.1 Development of plastic flow fields in centre cracked panels. 140
- 7.2 The hoop stress directly ahead of a crack in a centre crack panel, $a/W=0.3$, $n=13$ at several levels of deformations. 140

7.3	The stress directly ahead of a crack in a CCP, normalised by the MBLF stress field at a distance $\frac{r_{c0}}{j}=2$, as function of the load normalised by the limit load, $n=3$.	141
7.4	The stress directly ahead of a crack in a CCP, normalised by the MBLF stress field at a distance $\frac{r_{c0}}{j}=2$, as function of the load normalised by the limit load, $n=6$.	141
7.5	The stress directly ahead of a crack in a CCP, normalised by the MBLF stress field at a distance $\frac{r_{c0}}{j}=2$, as function of the load normalised by the limit load, $n=13$.	142
7.6	The stress directly ahead of a crack in a CCP, normalised by the MBLF stress field at a distance $\frac{r_{c0}}{j}=2$, as function of the load normalised by the limit load, non-hardening.	142
7.7	Q as a function of $\frac{P}{P_{Limit}}$ for CCP for distances $\frac{r_{c0}}{j}=1,2$ and 5 , $n=13$.	143
7.8	Q as a function of $\frac{P}{P_{Limit}}$ for CCP, $n=3$.	143
7.9	Q as a function of $\frac{P}{P_{Limit}}$ for CCP, $n=6$.	144
7.10	Q as a function of $\frac{P}{P_{Limit}}$ for CCP, $n=13$.	144
7.11	Q as a function of $\frac{P}{P_{Limit}}$ for CCP, non hardening material.	144
7.12	Boundary condition and reaction force and moment on the ligament for centre crack panels.	145
7.13	Force eccentricity.	146
7.14	Line of action of the reaction force non dimensionalised by the size of the ligament showed as a function of $\frac{P}{P_{Limit}}$, $n=13$.	147
7.15	Line of action of the reaction force non dimensionalised by the size of the ligament showed as a function of $\frac{P}{P_{Limit}}$, no strain hardening.	147
7.16	Comparison of hoop stress and MBLF solutions at $\frac{r_{c0}}{j}=2$. MBLF solutions were obtained using the elastic T -stress and the plastic corrected T -stress. Data for $a/W=0.1$ after Wang and Park (1994).	149
7.17	Q as a function of $\frac{P}{P_{Limit}}$ for centre cracked panel, $n=6$.	150
7.18	Q as a function of load normalised by limit load for $n=13$, with Q_T for $a/W=0.1$ and $a/W=0.9$.	152
7.19	Slip line fields for double edge cracked bars.	153
7.20	Hoop stress normalised by yield stress directly ahead of a crack in a double edge cracked bar at several levels of deformation, $a/W=0.3$ and $n=13$.	154
7.21	Hoop stress normalised by yield stress directly ahead of a crack in a double edge cracked bar at several levels of deformation, $a/W=0.9$ and $n=13$.	155
7.22	The hoop stress directly ahead of the crack at a distance $\frac{r_{c0}}{j} = 2$ normalised by the modified boundary layer formulation as a function of the load normalised by limit load, strain hardening rates $n=3,6,13$ and non-hardening.	156

- 7.23 Q at a distance $\frac{r_0}{c} = 2$ as a function of the load normalised by limit load, strain hardening rates $n=3,6,13$ and non-hardening. 157
- 7.24 Q as a function of $\frac{P}{P_{Limit}}$ for double edge cracked bar with a second order curve fit, $n=6$. 158
- 7.25 Line of action for reaction force non dimensionalised by the size of the ligament as a function of $\frac{P}{P_{Limit}}$, $n=13$. 158
- 8.1 Schematic J -temperature curve for ductile-brittle transition. 159
- 8.2 Fracture toughness for specimens with various levels of crack tip constraint. 160
- 8.3 Relationship between the normalised J-integral values in SEB specimens with those of SSY conditions which generate equivalent opening mode stresses at $r=4\delta$ (COD) ahead of the crack tip for hardening exponent $n=10$. Dodds, Anderson and Kirk (1991). 161
- 8.4 Schematic illustration of the Ritchie, Knott and Rice model for stress-controlled cleavage fracture directly ahead of a sharp crack. 162
- 8.5 Comparison of the variation of fracture toughness with temperature between experimental values (K_Q and K_{Ic}) for characteristic distance of one and two grain diameters. *H.S.W analysis : Heald, Spink and Worthington (1972)*., diagram from Ritchie, Knott and Rice (1973). 163
- 8.6 Plot of the experimental results as a function of the Weibull stress σ_w . Each vertical segment corresponds to one experiment. Comparison is made with the theoretical prediction of the cumulative probability of failure. Ferritic grain, test temperature 77K, after Beremin (1983). 164
- 8.7 Variation of cleavage fracture toughness vs. τ at various values of σ_u . σ_u is the fracture stress and $\tau = \frac{T}{\sigma_0}$. The lower graph shows the analysis compared with the experimental data of Betegón (1990), after Wang and Parks (1992). 165
- 8.8 Comparison of shapes for contours of principal stresses, for increasing levels of applied loading for hardening exponent, $n=13$ and $a/W=0.5$. The levels of deformation is given in terms of $\frac{c\sigma_0}{E}$. 167
- 8.9 Effective thicknesses for a single edge bend bar $a/W=0.5$, $\frac{a_1}{\sigma_0}=3$. Data after Nevalainen and Dodds (1995), $n=10$ and $E/\sigma_0=500$. 168
- 8.10 The local failure criteria applied on a stress field described by a two parameter characterisation. 169
- 8.11 Local cleavage criteria for deeply crack bend bars; $Q_T = 0$, $n=13$. 170
- 8.12 $\frac{J_c}{J_{c,ssy}}$ as a function of $\frac{r_0}{c}$ with increments of 0.01 for different values of Q_T . $n=13$ and $\sigma_f = 3\sigma_0$. 171
- 8.13 $\frac{J_c}{J_{c,ssy}}$ as a function of Q_T for different values of $\frac{r_0}{c}$. $n=13$ and $\sigma_f = 3\sigma_0$. 172
- 8.14 $\frac{J_c}{J_{c,ssy}}$ as a function of $\frac{r_0}{c}$, $Q_T = 0$ and $n=13$. 173
- 9.1 Prandtl slip stress field in a region around a crack tip. 176

9.2	The Effect of the T stress on the plastic zone shape in small scale yielding, after Du and Hancock (1991).	177
9.3	A mixed mode field with a stress discontinuity (Shih 1974).	178
9.4	The Mode II field after Shih (1974).	179
9.5	The mesh for the mixed mode problems.	180
9.6	Mean stress non-dimensionalised by yield stress as a function of angle for a range of mixities, non-hardening material.	181
9.7	Equivalent stress non-dimensionalised by the yield stress as a function of angle for range of mixities, non-hardening material.	182
9.8	Slip Line field for the family of mixed mode problems.	183
9.9	The displaced model of a mixed mode problem for $K_I = K_{II}$.	184
9.10	The maximum hoop stress as a function of the non-dimensionalised distance from the crack tip, $n=13$.	185
9.11	The maximum hoop stress as a function of the non-dimensionalised distance from the crack tip, $n=6$.	186
9.12	The hoop stress directly ahead of a crack in Mode I as a function of the non-dimensionalised distance from the crack tip for a range of $\frac{T}{\sigma_0}$ values, $n=13$.	187
9.13	$\frac{T}{\sigma_0}$ as a function of mixity for a range of hardening rates.	188
9.14	Q as a function of mixity for a range of hardening rates.	188
9.15	The stress deviation non-dimensionalised by the yield stress directly ahead of Mode I crack for a range of $\frac{T}{\sigma_0}$ values, $n=13$ and $n=6$.	189
9.16	The stress deviation non-dimensionalised by the yield stress at the maximum stress angle for a range of mixities, $n=13$ and $n=6$.	190
9.17	Experimental data in a $J-Q$ locus for 3PB test from Betegón (1991), $n=14$.	191
9.18	Experimental data obtained in 3PB tests and mapped into mixed mode data for $n=13$ in a $J-M^e$ locus, 3PB tests after Betegón (1991).	191

Blank Page

List of Tables

3.1	Values of K_I and β for single edge notched bars in tension.	41
3.2	Values of K_I and β for single edge notched bars in pure bending and three-point bending.	41
3.3	Values of K_I and β for centre cracked panels and double edge cracked bars.	41
3.4	Relations between strain hardening exponent, n , and the second order exponent t , after Sharma and Aravas (1991).	49
3.5	Stress exponents of higher order terms, Mode I, plane strain, from Chao and Ji (1994).	49
3.6	Chemical composition Wt% of 43A.	59
4.1	Record format in FIL file.	67
4.2	Variables to be read into Matlab.	67
4.3	Variables from ABAQUS into Matlab.	69
4.4	Numerical values of $f(\frac{a}{W})$ for centre crack panels.	70
5.1	Curve fitting constants for the small scale yielding field.	82
5.2	Curve fitting constants for the modified boundary layer formulation.	83
5.3	Limits for one parameter characterisation of single edge cracked bend bars.	91
5.4	Limits for one parameter characterisation for single edge cracked tension bars.	91
5.5	Limits for one parameter characterisation for centre cracked panels.	91
5.6	Limits of $J-T$ characterisation single edge cracked bend bars.	97
5.7	Limits of $J-T$ characterisation for single edge cracked tension bars.	97
5.8	Limits of $J-T$ characterisation for centre cracked panels.	98
5.9	Limits for $J-Q$ characterisation for single edge cracked bars in tension and bending	99
6.1	Curve fittings results for the proportionality constant $k_2(n)$ which relates Q_P and $\frac{P}{P_{Limit}}$ for Single Edge Cracked Bend bars, $n=3$.	114

6.2	Curve fittings results for the proportionality constant $k_2(n)$ which relates Q_P and $\frac{P}{P_{L_{limit}}}$ for Single Edge Cracked Bend bars, $n=6$.	115
6.3	Curve fittings results for the proportionality constant $k_2(n)$ which relates Q_P and $\frac{P}{P_{L_{limit}}}$ for Single Edge Cracked Bend bars, $n=13$.	115
6.4	Curve fittings results for the proportionality constant $k_2(n)$ which relates Q_P and $\frac{P}{P_{L_{limit}}}$ for Single Edge Cracked Bend bars, non-hardening, $n=100$ is used for the fit.	116
6.5	L_r^{max} for different values of strain hardening exponent.	116
6.6	Curve fittings results for the proportionality constant $k_1(n)$ which relates Q_P and $\frac{J_P}{c\sigma_0}$ for Single Edge Bend bars, $n=3$.	119
6.7	Curve fittings results for the proportionality constant $k_1(n)$ which relates Q_P and $\frac{J_P}{c\sigma_0}$ for Single Edge Bend bars, $n=6$.	120
6.8	Curve fittings results for the proportionality constant $k_1(n)$ which relates Q_P and $\frac{J_P}{c\sigma_0}$ for Single Edge Bend bars, $n=13$.	120
6.9	Curve fittings results for the proportionality constant $k_1(n)$ which relates Q_P and $\frac{J_P}{c\sigma_0}$ for Single Edge Bend bars, non-hardening.	121
6.10	k_1 and k_2 constants for Single Edge Cracked Bend Bars.	121
6.11	Curve fittings results for proportionality constants $k_2(n)$ which relates Q_P and $\frac{P}{P_{L_{limit}}}$ for Single Edge Cracked Tension bars, $n=6$.	128
6.12	Curve fittings results for proportionality constant $k_2(n)$ which relates Q_P and $\frac{P}{P_{L_{limit}}}$ for Single Edge Tension bars, $n=13$.	129
6.13	Curve fittings results for proportionality constant $k_1(n)$ which relates Q_P and $\frac{J_P}{c\sigma_0}$ for Single Edge Cracked Tension bars, $n=6$.	129
6.14	Curve fittings results for proportionately constant $k_1(n)$ which relates Q_P and $\frac{J_P}{c\sigma_0}$ for Single Edge Cracked Tension bars, $n=13$.	129
6.15	k_1 and k_2 constants for Single Edge Cracked Bars.	131
7.1	Values of the Q estimation schemes for centre cracked panels for hardening rates $n=3, 6, 13$ and non-hardening.	150
7.2	Values of Q calculated using two different approaches.	151
8.1	Data of the fracture toughness for maintaining J-dominance for $T \geq -0.2\sigma_0$ $n=13$, $Q_P=0$.	171
9.1	Elastic mixity for range of plane strain mixed mode fields.	180

Introduction to Constraint Based Fracture Mechanics

The behaviour of real structures does not always correspond to predictions based on the behaviour of perfect materials because of the presence of defects and flaws. Structures respond to extreme loading by either large deformation or fracture. Fracture which originates from defects and flaws is particularly important as it may occur at very low stress levels. The Liberty Ships built during World War II are the best known examples of such catastrophic low stress failures. That experience launched research into fracture mechanics. The main events in the history of fracture mechanics have been chronicled by Sumpter (1993b).

Three important variables are involved in the application of fracture mechanics to a cracked structure: the flaw size, the fracture toughness, and the applied stress. Fracture mechanics quantifies the critical combinations of these three variables.

However the earliest work was not sophisticated, and in the beginning of the twentieth century Charpy (1912) developed a pendulum test that measured the energy of separation in notched metallic specimens. Such tests are now known as impact tests. Impact tests were used to investigate the Liberty ship failures. It was concluded that fracture was much more likely to occur in structures with a low Charpy energy.

In the 1920s Griffith (1921) developed the first quantitative energy-based fracture theory. However it was not until the introduction of the stress intensity factor K by Irwin (1960), as a key parameter for characterising the stress field around a crack tip, that fracture mechanics became a practical engineering tool. The essential aim is to correlate crack extension in two different cracked bodies; for example, a laboratory specimen and an engineering structure. The transferability of fracture toughness is based on the similarity of the near crack tip stress and deformation fields. The similarity is most commonly described using one parameter which describes the strength of a singular crack tip field. In the middle sixties the use of the stress intensity factor was extended by applying the critical value K_{Ic} as a measure of plane strain fracture toughness. The use of tough materials however meant that valid measurements of the elastic stress intensity factor could not be made on realistically sized specimens. The problems were resolved by the development of non-linear fracture mechanics based on the J-integral proposed by Rice (1968b).

A typical fracture toughness is obtained from a deeply cracked bend bar which in fully plasticity develops a high level of constraint. The state of constraint controls the triaxiality at the crack tip, and a high level of constraint implies a highly triaxial stress field. The triaxiality controls the fracture process, and for specimens with a high triaxiality the fracture toughness is known to be low. The standard fracture

toughness test therefore provides a lower bound estimation which ensure a safe but often conservative value of the fracture toughness.

Elastic-plastic crack tip fields do not uniquely exhibit high levels of constraint, and there has been increasing interest in analysing structures and testing specimens with low crack tip constraint. Low values of constraint are associated with enhanced toughness. A primary goal has been to develop a two-parameter description of crack tip fields in order to use constraint enhanced toughness.

This thesis reviews the fundamentals of two parameter fracture mechanics. The first parameter scales the asymptotic singularity at the crack tip measured by K or J , while the second parameter indicates the level of stress triaxiality at the crack tip field. The limits of one and two-parameter characterisation of crack tip fields are then discussed and a theoretical framework for characterising crack tip constraint in terms of the higher order terms in a series expansions of the crack tip stress field is developed. The development of crack tip constraint is systematically examined for a wide range of plane strain geometries and strain hardening rates. Finally mixed mode fields are shown to belong to a similar family as the Mode I fields and the loss of constraint in mixed mode loading can be compared with that of Mode I. It is finally shown that it is possible to map the constraint based Mode I failure loci into mixed mode data.

Single Parameter Fracture Mechanics

This Chapter introduces single parameter fracture mechanics. It is divided into two major sections. The first section is an overview of linear elastic fracture mechanics (LEFM), based on a description of the elastic stress and displacement fields of a sharp crack. The concept of a stress intensity factor and the Griffiths failure criterion are introduced. In the second section the fundamental parameters of elastic-plastic fracture mechanics (EPFM) are described, including the introduction of the J integral and slip line fields.

2.1 Linear Elastic Fracture Mechanics

Inglis (1913) was the first to develop a mathematical solution to quantify the stress field in a centre cracked plate subjected to uniaxial tension. He analysed a linear elastic infinite plate with a central crack subjected to uniform tension as shown in Figure 2.1. Later Westergaard (1939) developed stress function methods for two-dimensional crack problems.

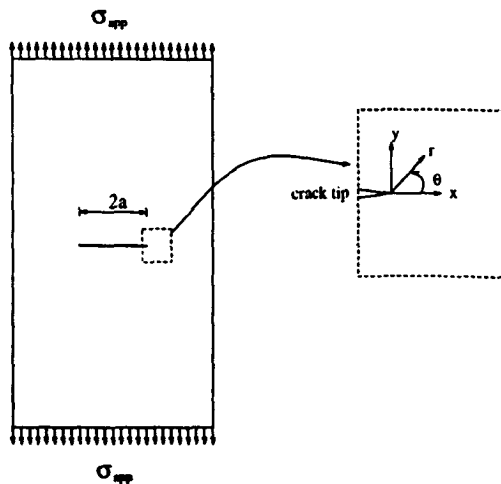


Figure 2.1: A crack of length $2a$ subject to a remote stress σ_{app} .

Several authors (e.g. Broek (1991) and Hellan (1985)) have reviewed the analysis of crack tip stress fields by appropriate Airy stress functions. Solutions are found by satisfying a biharmonic equation and the appropriate boundary conditions.

The Westergaard stress field is given in cylindrical coordinates (r, θ) centred at the crack tip, the co-ordinate system is defined in Figure 2.1.

$$\begin{aligned}\sigma_x &= \frac{\sigma\sqrt{\pi a}}{\sqrt{2\pi r}} \cos \frac{\theta}{2} (1 - \sin \frac{\theta}{2} \sin \frac{3\theta}{2}) \\ \sigma_y &= \frac{\sigma\sqrt{\pi a}}{\sqrt{2\pi r}} \cos \frac{\theta}{2} (1 + \sin \frac{\theta}{2} \sin \frac{3\theta}{2}) \quad (r \ll a) \\ \tau_{xy} &= \frac{\sigma\sqrt{\pi a}}{\sqrt{2\pi r}} \sin \frac{\theta}{2} \cos \frac{\theta}{2} \cos \frac{3\theta}{2}\end{aligned}\quad (2.1)$$

These equations describe the stress field in a region close to the crack tip where the radial distance r is very much less than the crack length a .

The corresponding Cartesian displacements (u, v) can be derived from the stress field through the stress-strain relationship. The stress-strain relationship depends on whether plane strain or plane stress conditions apply. The isotropic stress-strain relationship in its general form is :

$$\begin{aligned}\epsilon_x &= \frac{1}{E} [\sigma_x - \nu(\sigma_y + \sigma_z)] \\ \epsilon_y &= \frac{1}{E} [\sigma_y - \nu(\sigma_x + \sigma_z)] \\ \epsilon_z &= \frac{1}{E} [\sigma_z - \nu(\sigma_x + \sigma_y)] \\ \gamma_{xy} &= \frac{\tau_{xy}}{G} \quad \gamma_{yz} = \frac{\tau_{yz}}{G} \quad \gamma_{zx} = \frac{\tau_{zx}}{G}\end{aligned}\quad (2.2)$$

where ν is Poisson's ratio, E is Young's modulus and G is the shear modulus. For two dimensional problems the strain-displacement equations for the three in-plane strain components are

$$\begin{aligned}\epsilon_x &= \frac{\partial u}{\partial x} \\ \epsilon_y &= \frac{\partial v}{\partial y} \\ \gamma_{xy} &= \frac{\partial u}{\partial y} + \frac{\partial v}{\partial x}\end{aligned}\quad (2.3)$$

Compatibility is ensured by differential equations of the form

$$\frac{\partial^2 \epsilon_x}{\partial y^2} + \frac{\partial^2 \epsilon_y}{\partial x^2} = \frac{\partial^2 \gamma_{xy}}{\partial x \partial y}\quad (2.4)$$

A complete statement of the compatibility equations is given by McClintock and Argon (1966).

In plane stress the in-plane load is assumed to be distributed uniformly over the thickness of a thin plate or membrane and the stress σ_z , τ_{xz} and τ_{zy} and their gradients in the z direction are zero.

$$\begin{aligned}\sigma_z &= \tau_{xy} = \tau_{xz} = 0 \\ \frac{\partial \sigma_z}{\partial z} &= \frac{\partial \tau_{xy}}{\partial z} = \frac{\partial \tau_{xz}}{\partial z} = 0\end{aligned}\quad (2.5)$$

The state of stress is specified by σ_x , σ_y and τ_{xy} . The corresponding strains are determined by reduced stress-strain relations.

$$\begin{aligned}\varepsilon_x &= \frac{1}{E}(\sigma_x - \nu\sigma_y) \\ \varepsilon_y &= \frac{1}{E}(\sigma_y - \nu\sigma_x)\end{aligned}\quad (2.6)$$

The relation between the shear strain and shear stress is defined as

$$\gamma_{xy} = \frac{2(1+\nu)}{E}\tau_{xy}\quad (2.7)$$

Near the centre of thicker plates where plane strain conditions are satisfied, it is assumed that

$$\begin{aligned}\varepsilon_z = \gamma_{xz} = \gamma_{yz} &= 0 \\ \frac{\partial \varepsilon_x}{\partial z} = \frac{\partial \gamma_{yz}}{\partial z} = \frac{\partial \gamma_{xz}}{\partial z} &= 0\end{aligned}\quad (2.8)$$

When those conditions are substituted into the general stress-strain relationship (2.2), the out of plane normal stress σ_z can be found in terms of σ_x and σ_y as:

$$\sigma_z = \nu(\sigma_x + \sigma_y)\quad (2.9)$$

The displacement fields for plane strain and plane stress conditions in a Mode I are found to be of the form:

$$\begin{aligned}u &= 2(1+\nu)\frac{\sigma\sqrt{\pi a}}{E}\sqrt{\frac{r}{2\pi}}\cos\frac{\theta}{2}\left(\kappa - 1 + 2\sin^2\frac{\theta}{2}\right) \\ v &= 2(1+\nu)\frac{\sigma\sqrt{\pi a}}{E}\sqrt{\frac{r}{2\pi}}\sin\frac{\theta}{2}\left(\kappa + 1 - 2\cos^2\frac{\theta}{2}\right)\end{aligned}\quad (2.10)$$

where κ is defined as:

$$\begin{aligned}\kappa &= 3 - 4\nu && \text{plane strain} \\ \kappa &= \frac{3-\nu}{1+\nu} && \text{plane stress}\end{aligned}\quad (2.11)$$

Williams (1957) expressed the elastic stress and displacement field near a crack as a series expansion. The stress field can be expressed by an asymptotic expansion of the form:

$$\sigma_{ij}(r, \theta) = A_{ij}(\theta)r^{-\frac{1}{2}} + B_{ij}(\theta)r^0 + C_{ij}(\theta)r^{\frac{1}{2}} + \dots\quad (2.12)$$

where (r, θ) are polar co-ordinates centred at the crack tip, and σ_{ij} are the Cartesian components of the stress tensor.

In classic linear elastic fracture mechanics the stress field is described by the first term in the expansion, which corresponds to Westergaard's stress field given in Equation (2.1).

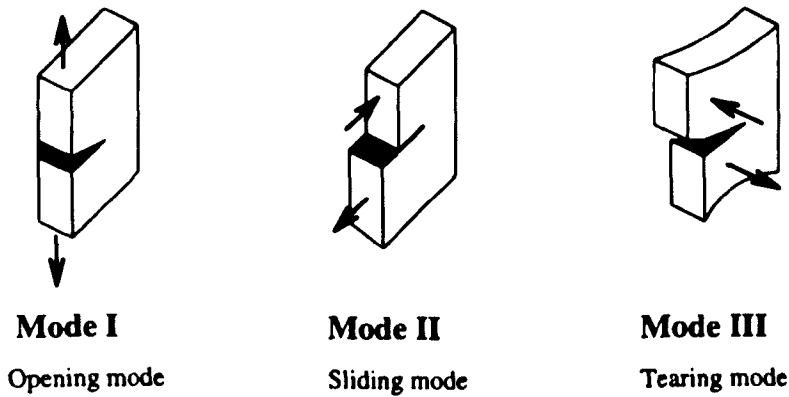


Figure 2.2: *The three modes of loading.*

2.1.1 The Stress Intensity Factor

When a load is applied to a cracked body, the crack surfaces move relative to each other. The response may be divided into three modes, which are illustrated in Figure 2.2. Discussion will largely be centred on Mode I.

It is now convenient to introduce the stress intensity factor K , in Equation (2.1) to describe the magnitude of the elastic crack tip stress field. The stress intensity factor was first described by Irwin (1957) and for a Mode I type crack K is denoted K_I and defined

$$K_I = \lim_{r \rightarrow 0} \sigma_{ij} \sqrt{2\pi r} \quad (\theta = 0) \quad (2.13)$$

For a Griffith crack $K_I = \sigma \sqrt{\pi a}$. The stress intensity factor characterises the crack tip field when the body is largely elastic. K is a function of the remote stress, and the crack length and characterises the strength of the crack tip singularity. Equation (2.13) allows the stress field in Equation (2.1) to be written using the stress intensity factor K_I and universal functions of angle $f_{ij}(\theta)$:

$$\sigma_{ij}(r, \theta) = \frac{K_I}{\sqrt{2\pi r}} f_{ij}(\theta) \quad (2.14)$$

A dimensional argument shows that K_I is proportional to the applied load and the square root of a characteristic dimension such as the crack length, and is a function of the geometry of the cracked structure. Various methods can be used to determine K , and these are reviewed in literature of fracture mechanics; Broek (1991) and Andersen (1995), while K for many common crack problems are given by Rooke and Cartwright (1976) and Murakami (1987).

The critical value of the stress intensity factor K is used as a measure of fracture toughness in small scale yielding (SSY), where the toughness in plane strain differs from the toughness in plane stress. When the thickness is small compared to the size of the plastic zone, the state of stress is normally plane stress, as explained by Andersen (1995). The fracture toughness decreases with thickness until a plateau is reached, where a further decrease in thickness has little or no effect on toughness, as shown in Figure 2.3. The fracture toughness is the critical value of K at which the crack extends and for a Mode I plane strain crack is denoted by K_{Ic} .

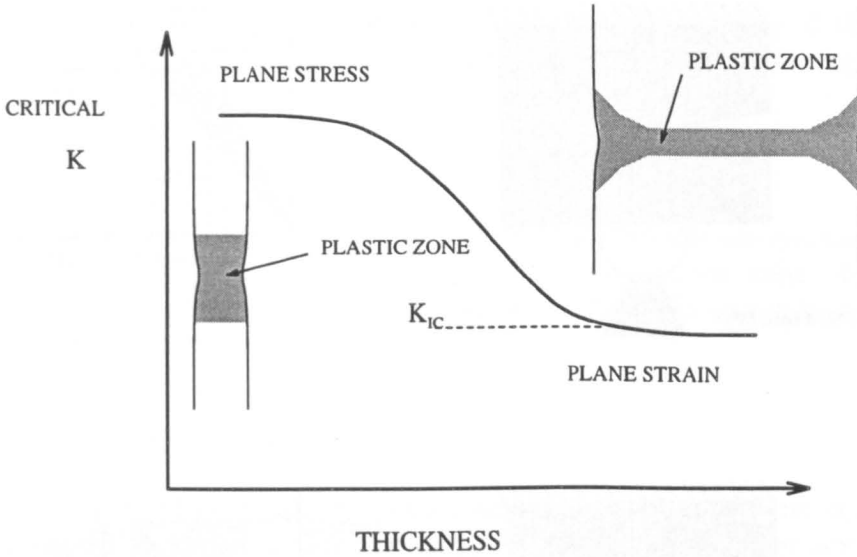


Figure 2.3: Effect of specimen thickness on Mode I fracture toughness.

2.1.2 The Griffith Criterion

Griffith (1921) considered the energetic of crack advance in brittle materials. Glass for example is brittle and fails in a largely linear elastic manner with low energy absorption. Griffith (1921) introduced the concept that the work required to extend a crack is a balance between the released strain energy and the surface energy developed during crack growth. In a centre cracked panel, such as that shown in Figure 2.1 the surface energy is given by:

$$U_{surface} = 2 \cdot 2at\gamma_s \quad (2.15)$$

where γ_s is the surface energy per unit area and t is the thickness of the plate. The total surface energy will increase as the crack grows because the surfaces of solids exhibit a surface tension in a similar manner to liquids.

The potential energy of an elastic body, Π is defined as

$$\Pi = U_{strain} - \mathcal{F} \quad (2.16)$$

where U_{strain} is the strain energy and \mathcal{F} is the work done by external forces. For a cracked plate with a fixed displacement, the work done by external forces is zero and $\Pi = U_{strain}$, as illustrated in Figure 2.4.

For a cracked plate with fixed load, the work from the external forces can be calculated as:

$$\mathcal{F} = P\Delta \quad (2.17)$$

where P is the external force and U_{strain} is determined from

$$U_{strain} = \int_0^\Delta Pd\Delta = \frac{1}{2}P\Delta \quad (2.18)$$

and therefore the potential energy is $\Pi = -U_{strain}$ for a fixed load.

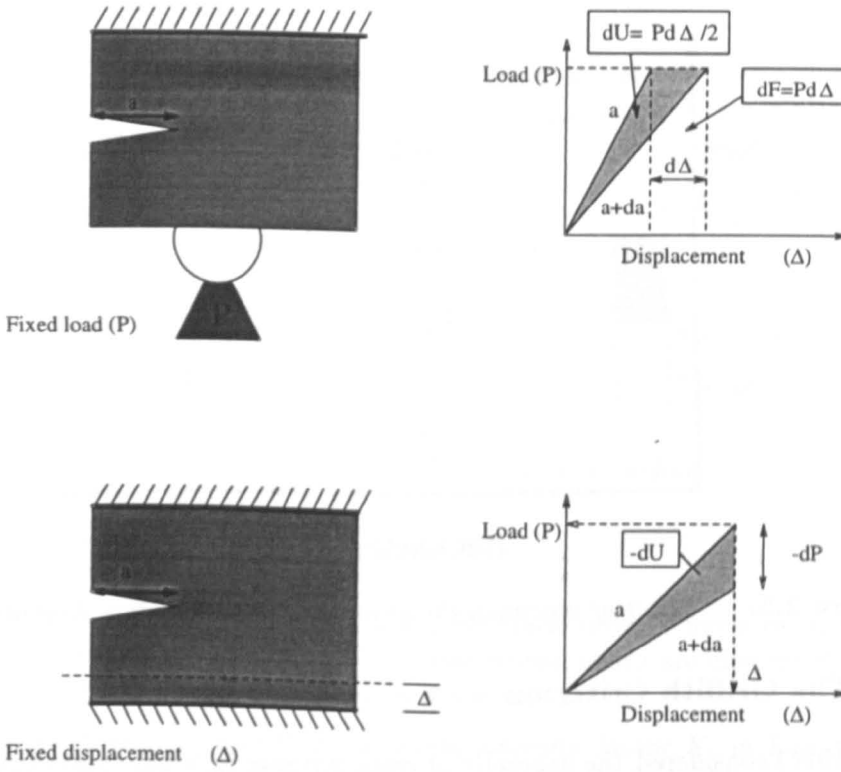


Figure 2.4: Cracked plate at a fixed displacement and fixed load.

Griffith expressed U_{strain} in terms of the stress, using expressions developed by Inglis (1913) for a plate with a crack of length a , with U_{strain} defined as:

$$U_{strain} = \frac{\pi \sigma^2 a^2 t}{E'} \tag{2.19}$$

where E' is Young's modulus for plane stress and $\frac{E}{1-\nu^2}$ for plane strain. Crack growth requires an increase of surface energy balanced by reduction in strain energy:

$$\begin{aligned} \frac{dU_{surface}}{da} &= \frac{dU_{strain}}{da} \\ \frac{2\pi\sigma^2 at}{E'} &= 4t\gamma_s \end{aligned} \tag{2.20}$$

The critical stress σ_{cr} , at a crack extension can now be estimated as:

$$\sigma_{cr} = \sqrt{\frac{2\gamma_s E'}{\pi a}} \tag{2.21}$$

If U_{strain} is the strain energy in a plate of unit thickness, the amount of strain energy released to propagate a crack a distance da is

$$G = \left(\frac{dU_{strain}}{da} \right) = \frac{2\pi\sigma^2 a}{E'} \tag{2.22}$$

Through Equation (2.22) it is possible to relate the critical value of the stress intensity factor (the fracture toughness) to a critical value of the strain energy release rate \mathcal{G}_c :

$$\mathcal{G}_c = \frac{K_I^2}{E'} \quad (2.23)$$

In this case \mathcal{G} has been defined when the applied displacements are constant under fixed grips conditions so that the external load cannot provide work. It can be shown (e.g. Broek (1991)) that \mathcal{G} is always the derivative of the elastic strain energy independent of whether the load is constant or not.

2.1.3 Crack Tip Plasticity

When metals are loaded beyond their elastic limit they yield and deform in a plastic manner. The yield criterion defines the limit of elastic behaviour under any possible combination of stresses. The yield criteria used in engineering is attributable to Tresca (1864) and von Mises (1913). The Tresca criterion predicts yield if the maximum shear τ_{max} exceeds the yield stress in shear k :

$$\sigma_1 - \sigma_3 = 2k \quad (\sigma_1 \geq \sigma_2 \geq \sigma_3) \quad (2.24)$$

von Mises suggested that yield occurred when

$$(\sigma_1 - \sigma_2)^2 + (\sigma_1 - \sigma_3)^2 + (\sigma_2 - \sigma_3)^2 = 2\mathcal{Y}^2 \quad (2.25)$$

where σ_1, σ_2 and σ_3 are principal stresses. Yield occurs when the equivalent stress reaches the uniaxial yield stress σ_0 :

$$\mathcal{Y} \geq \sigma_0 \quad (2.26)$$

The stress field singularity predicted theoretically in LEFM cannot exist in real materials, as the material must start to deform plastically. In order to estimate the extent of crack tip plasticity it is convenient to express the stresses in terms of the principal stresses used in Equations (2.24) and (2.25).

The principal stresses in the plane (σ_1 and σ_2) at any point can be found from the Mohr's circle construction:

$$\sigma_{1,2} = \frac{(\sigma_x + \sigma_y)}{2} \pm \sqrt{\left(\frac{\sigma_x - \sigma_y}{2}\right)^2 + \tau_{xy}^2} \quad (2.27)$$

Substitution of Equation (2.14) and (2.1) into (2.27) gives the principal stresses close to the crack tip:

$$\begin{aligned} \sigma_1 &= \frac{K_I}{\sqrt{2\pi r}} \cos \frac{\theta}{2} \left(1 + \sin \frac{\theta}{2}\right) \\ \sigma_2 &= \frac{K_I}{\sqrt{2\pi r}} \cos \frac{\theta}{2} \left(1 - \sin \frac{\theta}{2}\right) \\ \sigma_3 &= 0 \quad \text{plane stress} \\ \sigma_3 &= \frac{2\nu K_I}{\sqrt{2\pi r}} \cos \frac{\theta}{2} \quad \text{plane strain} \end{aligned} \quad (2.28)$$

A first simple approximation of the size of the plastic zone can be obtained from (2.14) by applying the Tresca yield criterion to the elastic stress field. This provides an estimate of the radius r_y over which the material is yielding ahead of the crack:

$$r_y = \frac{1}{2\pi} \left(\frac{K_I}{\sigma_0} \right)^2 f(\theta) \quad (2.29)$$

The development of the plastic zone depends on whether the crack tip is under plane strain or plane stress. The radius of the plastic zone can be estimated on the basis of von Mises yielding criteria by applying the principal stress field as given in Equation (2.28) into (2.25). The extent of the plastic zone as a function of θ for plane strain is given by:

$$r_p(\theta) = \frac{K}{4\pi\sigma_0} \left(\frac{3}{2} \sin^2 \theta + (1 - 2\nu)^2 (1 + \cos \theta) \right) \quad (2.30)$$

and the plastic zone for plane stress is

$$r_p(\theta) = \frac{K}{4\pi\sigma_0} \left(1 + \frac{3}{2} \sin^2 \theta + \cos \theta \right) \quad (2.31)$$

The Tresca criterion changes the shape of the plastic zone in comparison to the von Mises yield criterion. The zones for Tresca are slightly larger and of a slightly different shape to the von Mises zones. The Tresca yield zone is found in a similar way, the maximum shear stress in plane strain is the larger of $\frac{1}{2}(\sigma_1 - \sigma_2)$ and $\frac{1}{2}(\sigma_1 - \sigma_3)$, and for plane stress $\tau_{max} = \frac{1}{2}\sigma_1$. By applying the principal stresses from Equation (2.28) the Tresca yield zone for plane stress is given as:

$$r_p(\theta) = \frac{K^2}{2\pi\sigma_0^2} \left(\cos \frac{\theta}{2} \left(1 + \sin \frac{\theta}{2} \right) \right)^2 \quad (2.32)$$

In plane strain, it is the larger of :

$$r_p(\theta) = \frac{K^2}{2\pi\sigma_0^2} \cos^2 \frac{\theta}{2} \left((1 - 2\nu + \sin \frac{\theta}{2}) \right)^2 \quad (2.33)$$

$$r_p(\theta) = \frac{K^2}{2\pi\sigma_0^2} \cos^2 \frac{\theta}{2}$$

In Figure 2.5 the boundary of the plastic zone estimated by both the Tresca and Mises criteria are shown.

The effect of crack tip plasticity was initially discussed by Irwin (1948) and Dugdale (1960). Irwin suggested that the crack length is enhanced by plasticity. The effective crack length can be regarded as the length of the crack plus a correction due to the plastic zone size.

Dugdale (1960) considered an effective crack length in plane stress by considering a strip of uniform closing stress equal to the yield stress. By requiring equilibrium between the strip of yield and the applied load, the correction can be calculated.

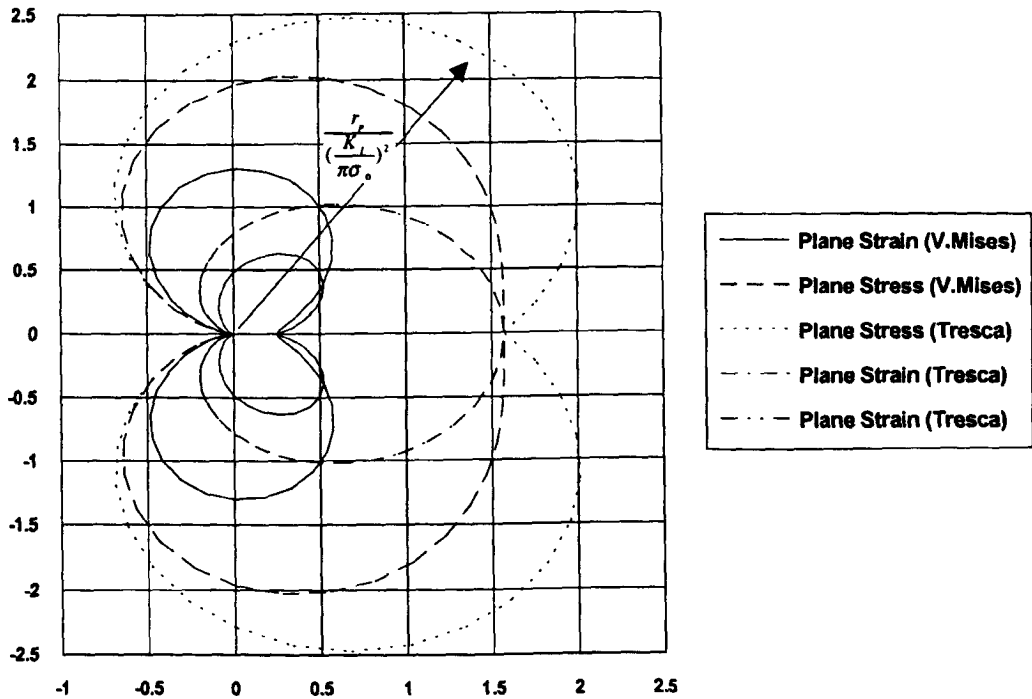


Figure 2.5: Plastic zone shapes for Mises and Tresca yield criteria.

2.1.4 Validity of Linear-Elastic Fracture Mechanics

Linear elastic fracture mechanics can be applied when crack tip plasticity is regarded as a minor perturbation of the elastic field and the material can largely be regarded as linear elastic. When the material fails in a macroscopically elastic manner the critical value of the stress intensity factor is a measure of fracture toughness. Standard test methods for K_{Ic} are given in ASTM (E 339-83 1983) and British Standard (BS-7448 1991b)

Valid LEFM is ensured if the specimen dimensions are large compared to the size of the plastic zone. Bend specimens for K_{Ic} tests normally have a width, W , equal to twice the thickness, B , and are fatigue pre-cracked so the crack length/width ratio (a/W) is between 0.45 and 0.55. The specimens are designed such that all the critical dimensions, a , B and $W-a$, are approximately equal, and when tested each dimension must be large compared to the size of the plastic zone in order to obtain a valid result for K_{Ic} . The size of the plastic zone may be compared with either the crack length a , the ligament ($W - a$) or the thickness B .

When the specimen is fatigue pre-cracked ASTM E339 requires that the peak value of the stress intensity in a single cycle, K_{max} should be no larger than $0.8K_{Ic}$. When the crack approaches the final length, K_{max} should be no larger than $0.6 K_{Ic}$. The requirement is more strict in the final stages of pre-cracking to prevent damage to the material at the crack tip. When the pre-cracked test specimen is loaded to failure the load-displacement response is monitored. The critical value of stress intensity factor is calculated from the critical applied load, P_Q . The standards give the requirements for the determination of P_Q , while the corresponding provisional

stress intensity factor K_Q can be calculated from an expression of the form:

$$K_Q = \frac{P_Q}{B\sqrt{W}} f(a/W) \quad (2.34)$$

where $f(a/W)$ is a dimensionless function of a/W . The provisional stress intensity factor K_Q value computed from (2.34) and is a valid K_{Ic} results if the requirements for validity are met.

The requirements given in ASTM (E 339-83 1983) are:

$$\begin{aligned} a &\geq 2.5 \left(\frac{K_{Ic}}{\sigma_0} \right)^2 \\ B &\geq 2.5 \left(\frac{K_{Ic}}{\sigma_0} \right)^2 \\ W &\geq 5.0 \left(\frac{K_{Ic}}{\sigma_0} \right)^2 \end{aligned} \quad (2.35)$$

If these requirements are satisfied then $K_Q = K_{Ic}$ which is a valid plane strain toughness.

2.2 Single Parameter Elastic-Plastic Fracture Mechanics

When the plastic zone around the crack tip field becomes comparable in size with the dimension of the structural component, or if the criteria given in Equation (2.35) are exceeded, the LEFM approach is no longer valid and elastic-plastic fracture mechanics (EPFM) is required. This is illustrated schematically in Figure 2.6, where FPFM means fully plastic fracture mechanics.

Elastic plastic fracture mechanics is applied to materials that exhibit non-linear behaviour (i.e. plastic deformation). The two different fracture parameters commonly used to characterise crack tip conditions in an elastic plastic material are the crack tip opening displacement (CTOD) introduced by Wells (1961) and the J -integral introduced independently by Cherepanov (1967), Eshelby (1968) and Rice (1968b).

2.2.1 Crack Tip Opening Displacement

The critical value of the crack tip opening displacement (CTOD) was introduced by Wells (1961) as a measure of fracture toughness for steel specimens which were too tough to be characterised by LEFM. An initially sharp crack blunts with plastic deformation, resulting in a finite displacement (δ) at the crack tip. This is denoted the crack tip opening displacement or CTOD. Experimentally, the CTOD or CMOD (crack mouth opening displacement) is determined from measurements of the surface displacement across the crack from which crack extension has occurred, as shown in Figure 2.7. Shih (1981) has suggested that the CTOD should be defined by a 90° line intercept construction at the crack tip, as illustrated in figure 2.7.

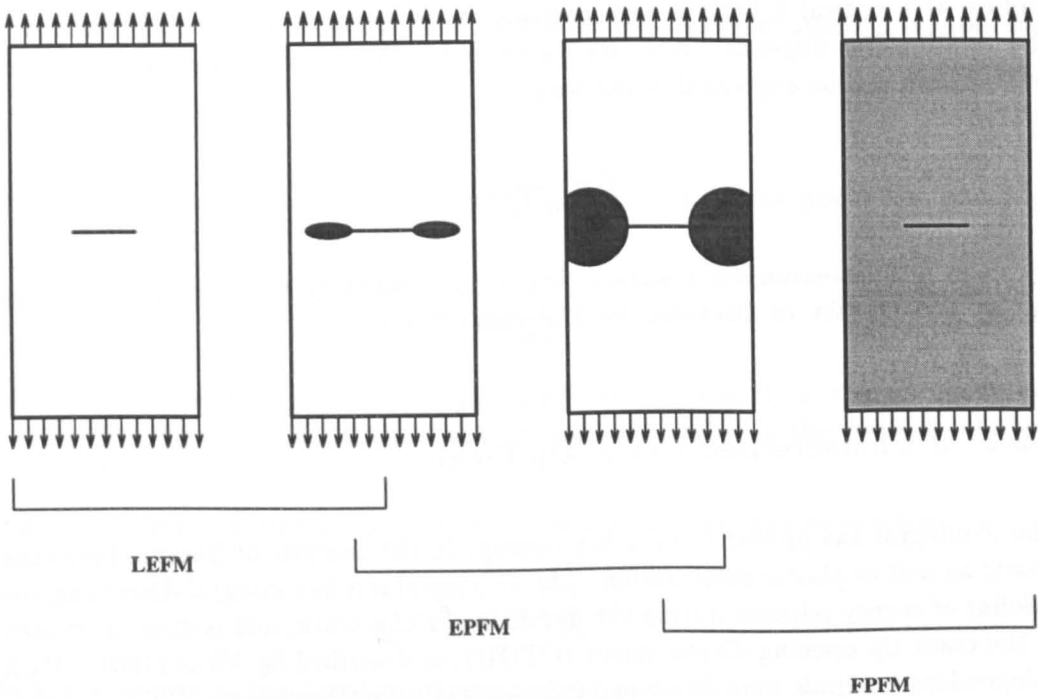


Figure 2.6: Validation of LEFM and EPFM.

Fracture is considered to occur at a critical value of CTOD, δ_c . A relationship between CTOD and the applied stress has been developed through the Bilby, Cottrell and Swindon (1963) non hardening strip yield analysis

$$\delta = \frac{8\sigma_0 a}{\pi E} \ln \sec \left(\frac{\pi \sigma}{2 \sigma_0} \right) \tag{2.36}$$

From a series expansion of the $\ln \sec$ term at low values of $\frac{\sigma}{\sigma_0}$, Equation (2.36) can be reduced to:

$$\delta = \frac{\sigma_0 \pi a}{E \sigma_0} = \frac{K_I^2}{E} = \frac{G}{\sigma_0} \quad (\sigma \ll \sigma_0) \tag{2.37}$$

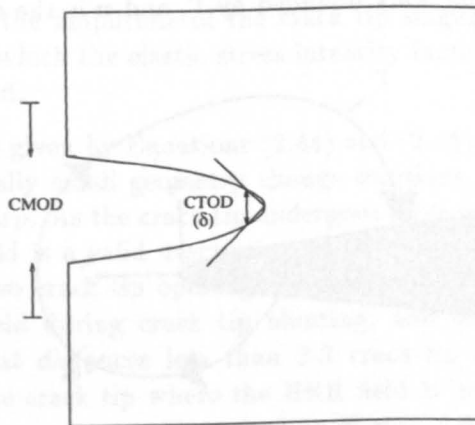


Figure 2.7: Estimation of (CTOD) from 90° intercept construction.

Failure at a critical CTOD is thus identical with failure at K_{IC} or $(\frac{G}{\sigma_0})$, although the relationship depends on strain hardening. Within contained yielding this relationship can be expressed of the form

$$\delta = \frac{K_I}{m\sigma_0 E} \quad (2.38)$$

where m is a dimensionless constant that is approximately 1.0 for plane stress and 2.0 for plane strain, as discussed by Andersen (1995).

2.2.2 J Characterised Crack Tip Fields

The J -integral has proved to be a key concept in the analysis of fracture involving elastic as well as plastic deformation. The J -integral is a line integral describing the amount of energy released during the development of a crack, and is directly related to the crack tip opening displacement (CTOD), as described by Wells (1961). Path independent integrals were developed independently by Cherepanov (1967), Eshelby (1968) and Rice (1968*b*) although their application to fracture mechanics is largely due to Rice. Rice (1968*b*) developed the J -integral for crack problems and expressed the concept in the form

$$J = \int_{\Gamma} W dx_2 - \mathbf{P} \frac{\partial \mathbf{u}}{\partial x_1} ds \quad (2.39)$$

where Γ is the length of the path, as shown in Figure 2.8. The first term in the J -integral is the strain energy density or work of deformation per unit volume, where W is defined as the strain energy density

$$W = \int_0^{\epsilon} \sigma_{ij} d\epsilon_{ij}, \quad i, j = 1, 2, 3 \quad (2.40)$$

The second term in (2.39) is the work done by the external forces, in which \mathbf{P} is the force vector applied to the body bounded by Γ , and \mathbf{u} is the displacement vector.

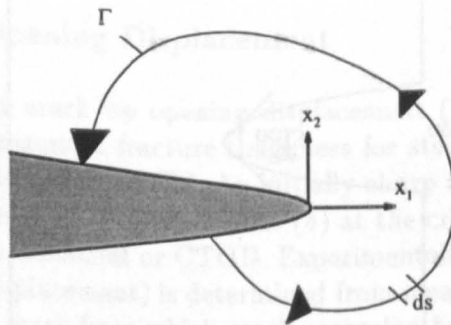


Figure 2.8: Arbitrary contour around a crack tip.

The constitutive law for linear elastic material behaviour in uniaxial tension was given by Hooke (1678)

$$\sigma = \varepsilon E \quad (2.41)$$

In the non-linear regime the stress-strain relationship is the power law given in uniaxial tension by

$$\frac{\varepsilon_p}{\varepsilon_0} = \alpha \left(\frac{\sigma}{\sigma_0} \right)^n \quad (2.42)$$

where σ_0 is a reference stress and ε_0 is a reference strain. E is Young's modulus. ε_p is plastic strain, α is a proportionality constant and n is the strain hardening exponent.

The total strain for elastic-plastic material behaviour can then be written

$$\frac{\varepsilon}{\varepsilon_0} = \frac{\sigma}{\sigma_0} + \alpha \left(\frac{\sigma}{\sigma_0} \right)^n \quad (2.43)$$

Which is known as the Ramberg-Osgood relation.

Hutchinson (1968b), and Rice and Rosengren (1968) independently argued that the crack tip field in a material exhibiting power law behaviour under Mode I loading can be expressed as an asymptotic series. The leading terms of the stress and strain fields have the form:

$$\sigma_{ij} = \sigma_0 \left[\frac{J}{\varepsilon_0 \sigma_0 \alpha I_n r} \right]^{\frac{1}{1+n}} \tilde{\sigma}_{ij}(\theta, n) \quad (2.44)$$

and

$$\varepsilon_{ij} = \frac{\sigma_0 \alpha}{E} \left[\frac{J}{\varepsilon_0 \sigma_0 \alpha I_n r} \right]^{\frac{n}{1+n}} \tilde{\varepsilon}_{ij}(\theta, n) \quad (2.45)$$

Here $\tilde{\sigma}_{ij}(\theta, n)$ and $\tilde{\varepsilon}_{ij}(\theta, n)$ are tabulated functions of their arguments as in Shih (1983), and I_n is an integration constant which is a function of the strain hardening exponent n .

J can be regarded as the amplitude of the crack tip singularity field, in a similar manner to the way in which the elastic stress intensity factor K is the amplitude of the elastic singular field.

The deformation fields given by Equations (2.44) and (2.45) are known as the HRR fields, and are essentially small geometry change solutions, where the crack tip is assumed to remain sharp. As the crack tip undergoes large geometry changes during blunting, the HRR field is a valid description of the deformation field at distances greater than one or two crack tip openings (typically $r \geq \frac{2J}{\sigma_0}$). McMeeking (1977) analysed the stress field during crack tip blunting, and suggested that the HRR field does not apply at distances less than 2-3 crack-tip opening displacements. This region around the crack tip where the HRR field is invalid is called the large deformation or blunting zone, as illustrated in Figure 2.9. In this region the J integral is no longer path-independent, as shown by McMeeking (1977).

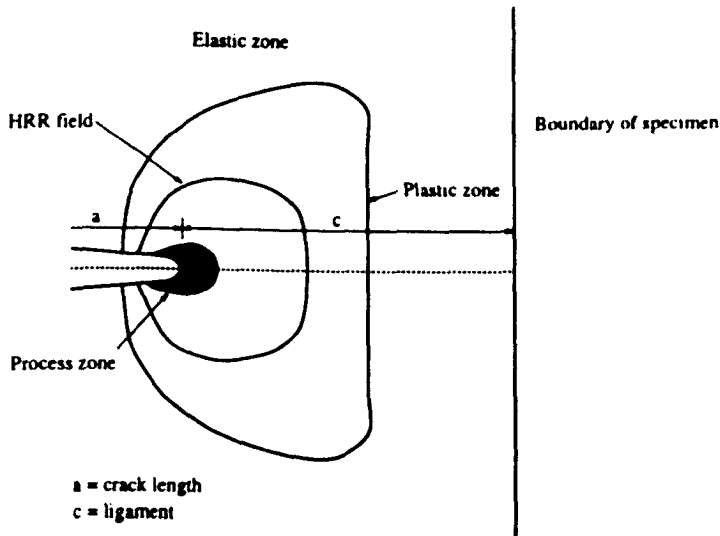


Figure 2.9: Various zones surrounding a crack tip.

For linear elastic materials, n and α are equal to 1 in the Ramberg-Osgood Equation (2.43), and the HRR field is equivalent to the Westergaard field described in Equation (2.1).

Griffiths' analysis of the energetic aspects of fracture mechanics was based on experiments in glass where fracture occurs in a largely elastic manner. Irwin (1948) and Orowan (1955) pointed out that for a crack to propagate, the energy to create this new surface is much larger in ductile materials than in brittle materials. Plastic deformation occurs at the crack tip, and plastic energy is the major term in the energy balance. When crack growth and fracture is associated with plastic deformation, J should be applied rather than \mathcal{G} for describing the fracture toughness.

In the linear elastic case J is identical to \mathcal{G} :

$$J = \mathcal{G} = \frac{K_I^2}{E'} \quad (2.46)$$

Here E' is identified as $E' = E$ for plane stress and $E' = \frac{E}{1-\nu^2}$ for plane strain conditions. Although the identity $J = \mathcal{G}$ applies only to LEFM, J retains its energetic meaning for a non-linear elastic material. Controversy has arisen about its energetic significance for incremental plasticity, as opposed to deformation plasticity, (Turner (1973)). However this problem can be avoided by regarding J as a characterising parameter through its role in the HRR field.

2.2.3 Slip Line Fields

In regions in which the yield criterion is satisfied for a non hardening material under plane strain conditions, there are two orthogonal sets of curvilinear curves on which the maximum shear stress k occurs. These sets of curves are called *slip lines* or *shear lines*. The yield stress in shear, k , is equal to $\mathcal{Y}/2$ for the Tresca criterion and $\mathcal{Y}/\sqrt{3}$ for the von Mises criterion. Since the material is non-hardening, k is constant throughout the plastic region. Under plane strain conditions the stress system is

dictated by the maximum shear stress and a hydrostatic stress whose value is equal to the out of plane stress, σ_z . The orthogonal slip lines or shear lines are denoted α and β lines and is defined in Figure 2.10.

σ_z is given by

$$\sigma_z = \frac{1}{2}(\sigma_1 + \sigma_2) = \frac{1}{2}(\sigma_x + \sigma_y) \tag{2.47}$$

where σ_1 and σ_2 are the in plane principal stresses. Equation (2.47) can be compared with the incompressible elastic plane strain condition given in Equation (2.9) for the case $\nu = 0.5$. The hydrostatic stress is defined as:

$$\sigma_m = \frac{1}{3}(\sigma_1 + \sigma_2 + \sigma_3) = \sigma_z = \sigma_3 \tag{2.48}$$

A non-dimensional stress parameter combining the hydrostatic stress and the von Mises stress is called the triaxiality and is defined as $\frac{\sigma_m}{\bar{\sigma}}$. Triaxiality is used as a measure of constraint, and can be calculated from slip line field theory.

Mohr's circle can be used to describe the stress state, as illustrated in Figure 2.11.

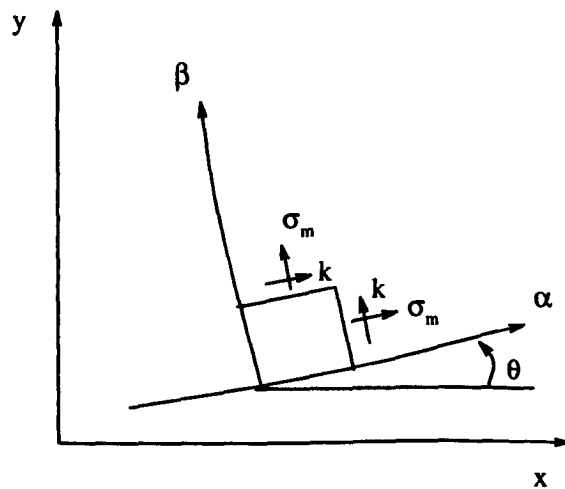


Figure 2.10: The stress state in a slip line field region.

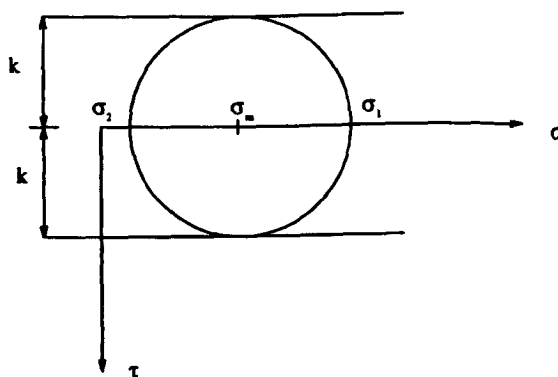


Figure 2.11: Mohr's circle.

The stress field is of the form:

$$\begin{aligned}\sigma_x &= \sigma_m - k \sin 2\vartheta \\ \sigma_y &= \sigma_m + k \sin 2\vartheta \\ \tau_{xy} &= k \cos 2\vartheta\end{aligned}\quad (2.49)$$

The principal stresses σ_1 and σ_2 in the plane can be found by applying Equation (2.49) into Equation (2.27), or simply by reading off the principal stresses on the Mohr's circle in Figure 2.11.

$$\left. \begin{array}{l} \sigma_1 \\ \sigma_2 \end{array} \right\} = \sigma_m \pm k \quad (2.50)$$

$$\sigma_3 = \sigma_m \quad (2.51)$$

Valid slip line fields must satisfy equilibrium conditions. It is convenient to use polar co-ordinates in which the equilibrium equations are of the form

$$\begin{aligned}\frac{\partial \sigma_r}{\partial r} + \frac{1}{r} \frac{\partial \tau_{r\theta}}{\partial \theta} + \frac{\sigma_r - \sigma_\theta}{r} &= 0 \\ \frac{1}{r} \frac{\partial \sigma_\theta}{\partial \theta} + \frac{\partial \tau_{r\theta}}{\partial r} + 2 \frac{\tau_{r\theta}}{r} &= 0\end{aligned}\quad (2.52)$$

Within a centred fan the stress in cylindrical coordinates take a particularly simple form:

$$\begin{aligned}\sigma_r = \sigma_\theta &= \sigma_m \\ \tau_{r\theta} &= \pm k\end{aligned}\quad (2.53)$$

Now from equations (2.53) and (2.52)

$$\begin{aligned}\frac{\partial \sigma_m}{\partial r} &= 0 \\ \frac{1}{r} \frac{\partial \sigma_m}{\partial \theta} \pm 2 \frac{k}{r} &= 0\end{aligned}\quad (2.54)$$

and from the last Equation in (2.54)

$$\sigma_m = 2k\theta + f(r) \quad (2.55)$$

As $\frac{\partial \sigma_m}{\partial r} = 0$ has to be satisfied, $f(r)$ has to be a constant C and this leads to the Hencky equations, which are a statement of the equilibrium conditions in curvilinear co-ordinates:

$$\begin{aligned}\sigma_m &= 2k\theta + C \quad \text{along a } \alpha \text{ line} \\ \sigma_m &= 2k\theta - C \quad \text{along a } \beta \text{ line}\end{aligned}\quad (2.56)$$

2.2.4 Slip Line Fields around a Crack Tip

McClintock (1971) used a slip line field analysis to discuss the stress fields of sharp and blunting cracks in Mode I loading. By analysing different geometries and different modes of loading McClintock demonstrated that no unique slip line field exists in full plasticity. However if plasticity surrounds the tip the full Prandtl (1920) field shown in Figure 2.12 is developed. This is a unique field in which the degree of triaxiality is independent of the type of loading.

The Prandtl field consists of two diamond-shaped regions connected by centred fans. The stress fields in the diamond-shaped regions are constant, but in the centre fan regions the stress fields changes as a function of the angle θ .

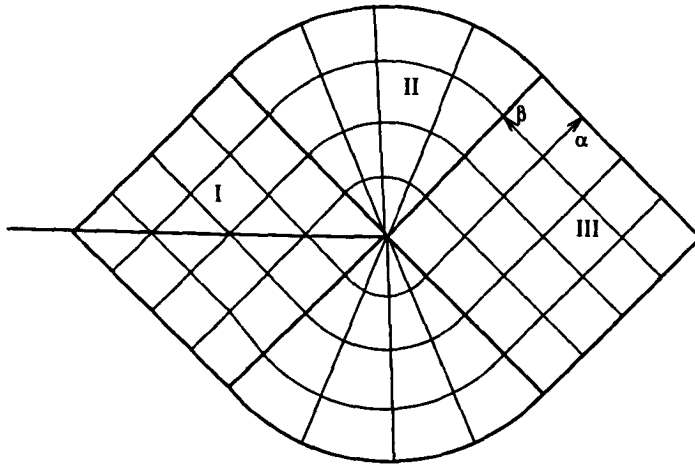


Figure 2.12: *Prandtl slip line field in a region around a crack tip.*

Equation (2.61) reveals that the slip line field is consistent with the HRR field for non-hardening material ($n=\infty$), as described by Hutchinson (1968b). The stresses can be solved starting from the free crack surface, denoted I in Figure 2.12. At the free surface the stresses are

$$\begin{aligned}\sigma_1 &= 2k \\ \sigma_2 &= 0 \\ \sigma_3 &= \sigma_m = k\end{aligned}\tag{2.57}$$

It is convenient to work in cylindrical coordinates (r, θ) centred at the crack tip. When the boundary conditions are applied in Equation (2.57) the stress field in region I can be written as :

$$\begin{aligned}\sigma_r &= k(1 + \cos 2\theta) \\ \sigma_\theta &= k(1 - \cos 2\theta) \\ \tau_{r\theta} &= k \sin(2\theta) \\ \sigma_m &= k\end{aligned}\tag{2.58}$$

The stress field in the centre fan, region II can be calculated from the Hencky Equations Hill (1950). This gives the stress state as:

$$\begin{aligned}\sigma_{\theta} = \sigma_r = \sigma_z = \sigma_m &= k(1 + 3\pi/2 - 2\theta) \\ \sigma_{r\theta} &= k\end{aligned}\tag{2.59}$$

Finally in the diamond ahead of the crack, denoted III, the stresses are:

$$\begin{aligned}\sigma_{\theta} &= k(\pi + 1 + \cos 2\theta) \\ \sigma_r &= k(\pi + 1 - \cos 2\theta) \\ \sigma_z &= \sigma_m = k(1 + \pi) \\ \tau_{r\theta} &= k \sin 2\theta\end{aligned}\tag{2.60}$$

The stress σ_y ahead of the crack tip reaches a value of:

$$\sigma_{y_{max}} = \frac{2 + \pi}{\sqrt{3}} = 2.97\sigma_0\tag{2.61}$$

Slip line models show that triaxial stresses build up along curves from a free boundary, when the slip lines are straight the triaxiality is constant. This can be seen from the Hencky Equations (2.56), as the hydrostatic stress is linearly dependent on the rotation of the slip lines. The level of triaxiality in the full Prandtl field is due to the rotation of the slip lines from the crack flanks.

2.2.5 Crack Tip Constraint in Large Scale Yielding

In small scale yielding the crack tip field can be characterised with a single parameter (K , J or $CTOD$) which can be used as a geometry independent fracture criterion. For small scale yielding the maximum stress is approximately $3\sigma_0$ in a non hardening material.

Green (1953) analysed deeply cracked bend bars and demonstrated that if the crack is sufficiently deep the slip line fields depend only on local notch shape near its root, and loading conditions.

Ewing (1968) used Green's solution and estimated the minimum width for which the deep-notch solution applies. The slip line fields for deep and shallow cracked bend bars are shown in Figure 2.13. Ewing analysed v notches of different angles in pure bending rather than cracked geometries and found that the deeply cracked solution can only be applied when $a/W \geq 0.3$ for an notch angle 3.21° . He also suggested that for shallow cracks the plasticity initiates at the cracked face as well as at the crack tip, and the slip line field develops differently from the deeply cracked geometries.

McClintock (1971) showed with slip line analysis that centre cracked panels are incapable of maintaining significant triaxiality under fully plastic conditions. The slip line field for center cracked panels is shown in Figure 2.14. For the centre cracked

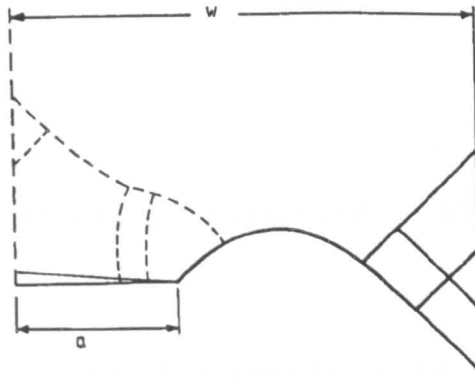


Figure 2.13: Slip line fields for deep and shallow cracked bars in bending after Ewing(1968) and Green(1953).

panels the maximum stress is approximately $\frac{2}{\sqrt{3}}\sigma_0$. A deeply edge cracked plate in bending exhibits maximum principal stresses at the crack tip of approximately $2.5\sigma_0$.

Figure 2.15 shows the slip line field for double edge cracked specimens. Shallow double edge cracked bars exhibit unconstrained flow fields, while for the deeply cracked bars the fully constrained Prandtl field is developed.

McClintock (1971) demonstrated that in large scale yielding the flow field is geometry dependent, and the plane strain crack tip stress fields depends on crack geometry and type of loading. The dependency of geometry and loading mode indicates there is no single parameter which uniquely characterises the crack tip fields beyond small scale yielding.

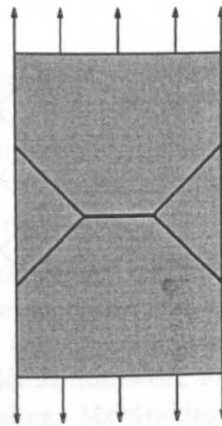


Figure 2.14: Slip line fields for a centre cracked panel.

$$\sigma = \frac{2}{\sqrt{3}}\sigma_0 \psi$$

$$(2.1)$$

where ψ is a dimensionless factor depending on geometry and loading. Falk (1985) analysed single edge cracked bars in tension and bending, and suggested $\psi = 25$ for bending and $\psi = 200$ for tension in agreement with the conclusions of McClintock and Parks.

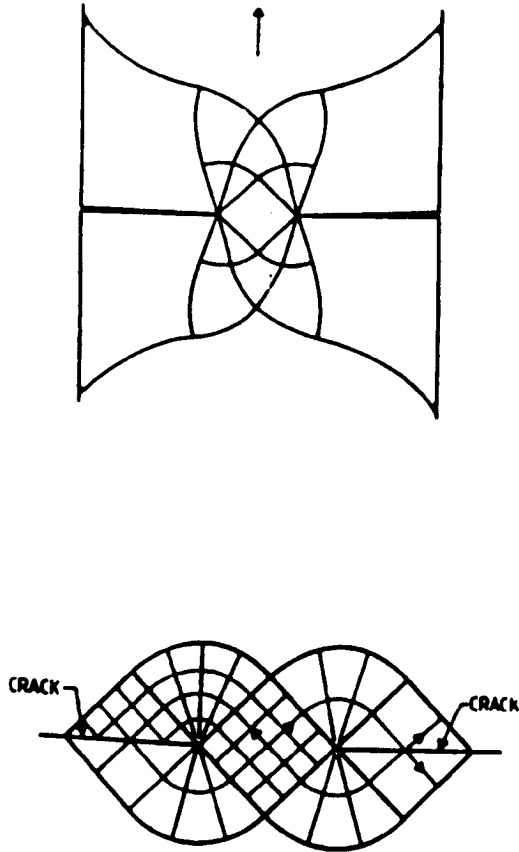


Figure 2.15: *Slip line fields for double edge cracked bars.*

Two Parameter Fracture Mechanics

In this Chapter the fundamentals of two parameter fracture mechanics are reviewed. Firstly the limits of J dominated crack tip fields are discussed, then the significance of the elastic second parameter in the Williams expansion, the T -stress, is described. Under elastic-plastic conditions the level of constraint is quantified by Q .

3.1 J Dominated Crack Tip Fields

The introduction of the J -integral (Rice (1968*b*)) and the ability to characterise crack tip stress fields through the HRR field provides the foundation for single parameter fracture mechanics. Fracture criteria based on J assume that the crack tip stresses can be described by the HRR fields as characterised by the J -integral. J -characterisation is valid as long as the region over which the HRR singularity dominates, completely encompasses the zone of large strains. The region of large strains immediately ahead of the crack tip is defined as the process zone in Figure 2.9. At level of large scale yielding, J no longer uniquely characterises the fields. The conditions under which fields are characterised by J are referred to as conditions for J dominance.

McMeeking and Parks (1979) suggested that fields characterised by J are identical to those observed in small scale yielding when single parameter characterisation is valid. The HRR fields are uniquely characterised by J , but McClintock (1971) demonstrated that fully plastic flow fields in non-hardening materials depend on geometry and the mode of loading.

To investigate this problem, McMeeking and Parks (1979) and Shih and German (1981) examined the levels of stresses ahead of a crack tip, using finite element analysis of deeply cracked bend bars and centre cracked panels. They aimed to develop size requirements for specimens to obtain the level of crack tip triaxiality stress corresponding to small scale yielding. McMeeking and Parks (1979) suggested that for deeply cracked geometries single parameter characterisation can be maintained under condition which depend on the size of the ligament c as long as the plasticity is restricted to the ligament, which is the case for deeply edge cracked bars:

$$J \leq \frac{c\sigma_0}{\mu} \quad (3.1)$$

where μ is a dimensionless factor depending on geometry and loading. Shih (1985) analysed single edge cracked bars in tension and bending, and suggested $\mu \approx 25$ for bending and $\mu \approx 200$ for tension in agreement with the calculations of McMeeking and Parks.

Al-Ani and Hancock (1991) analysed short cracks in tension and bending, where a short crack in tension is $a/W \leq 0.5$ and in bending $a/W \leq 0.3$. They showed that J -dominance is lost at much higher values of μ than given by Shih (1985) leading to extreme size requirements. They also suggested that for short cracks the J dominance is controlled by the crack length rather than the ligament.

3.2 Elastic Two Parameter Fracture Mechanics

The validity for single parameter fracture mechanics characterised by J through the HRR field or the small scale yielding field has been discussed in Chapter 2. J provides a single parameter characterisation of the crack tip stress field for a very limited range of highly constrained loading configurations and deformation levels. Several suggestions to extend the characterisation of the stress field beyond single parameter characterisation have been discussed and the approaches are all classified as two parameter fracture mechanics. Two parameter characterisation of crack tip fields begins with the elastic T -stress which arises from the second term in the Williams expansion.

3.2.1 T -stress

A two parameter approach developed by Bilby *et al.* (1986) and more recently by Betegón and Hancock (1991), Al-Ani and Hancock (1991), and Du and Hancock (1991) is based on the elastic T -stress. T is the second term in the Williams expansion described by Rice (1974a). Neglecting higher order terms, the elastic stress field can thus be expressed in the form:

$$\sigma_{ij}(r, \theta) = \frac{K_I}{\sqrt{2\pi r}} f_{ij}(\theta) + T\delta_{1j}\delta_{i1} \quad (3.2)$$

Here (x, y) are Cartesian co-ordinates, where x coincides with the crack. The T -term in (3.2) is a uniform stress $\sigma_{11}=T$, acting parallel to the crack flanks. T is independent of the distance, r , and becomes significant compared to K at finite distances from the tip. The T -stress has now been tabulated for a wide range of geometries, in which the results are either expressed in terms of a stress concentration factor $\frac{T}{\sigma}$ or as a bi-axiality parameter β following LeEVERS and Radon (1983):

$$\beta = \frac{T\sqrt{\pi a}}{K} \quad (3.3)$$

Results for some important through crack geometries have been given by Sham (1991), LeEVERS and Radon (1983), and KfourI (1986), while Wang and Park (1992) have given results for surface cracked panels. Sham (1991)'s results for a range of a/W ratios of single edge cracked bars under tension and bending are summarised in Tables 3.1) - (3.2. Values of β for centre cracked panels (Nekkal (1991)) and double edge cracked panels (LeEVERS and Radon (1983)) are given in Table 3.3.

a/W	$\frac{K}{\sigma\sqrt{\pi a}}$	$\beta = \frac{T\sqrt{\pi a}}{K}$
0.1	0.11877E1	-0.46436E0
0.2	0.13650E1	-0.43362E0
0.3	0.16570E1	-0.37070E0
0.4	0.21083E1	-0.27762E0
0.5	0.28210E1	-0.15293E0
0.6	0.40254E1	0.69027E-2
0.7	0.63457E1	0.21010E0
0.8	0.11926E2	0.50105E0
0.9	0.34485E2	0.10306E1

Table 3.1: Values of K_I and β for single edge notched bars in tension.

a/W	Pure Bending		Three Point Bending	
	$\frac{K}{\sigma\sqrt{\pi a}}$	$\beta = \frac{T\sqrt{\pi a}}{K}$	$\frac{K}{\sigma\sqrt{\pi a}}$	$\beta = \frac{T\sqrt{\pi a}}{K}$
0.1	0.10458E1	-0.36263E0	0.10234E1	-0.36062E0
0.2	0.10534E1	-0.22852E0	0.10272E1	-0.23295E0
0.3	0.11220E1	-0.73444E-1	0.10937E1	-0.90071E-1
0.4	0.12586E1	0.92115E-1	0.12290E1	0.60928E0
0.5	0.14951E1	0.26160E0	0.14647E1	0.21685E0
0.6	0.19100E1	0.43325E0	0.18787E1	0.37921E0
0.7	0.27210E1	0.61041E0	0.26880E1	0.55311E0
0.8	0.46642E1	0.83862E0	0.46270E1	0.78585E0
0.9	0.12406E2	0.12675E1	0.12358E2	0.12273E1

Table 3.2: Values of K_I and β for single edge notched bars in pure bending and three-point bending.

a/W	Centre Cracked Panels		Double Edge Cracked Bars	
	$\frac{K}{\sigma\sqrt{\pi a}}$	$\beta = \frac{T\sqrt{\pi a}}{K}$	$\frac{K}{\sigma\sqrt{\pi a}}$	$\beta = \frac{T\sqrt{\pi a}}{K}$
0.1	0.1006E1	-0.1017E1	0.12130E1	-0.436E0
0.2	0.1025E1	-0.1034E1	0.12123E1	-0.445E0
0.3	0.1058E1	-0.1051E1	0.12175E1	-0.458E0
0.4	0.1109E1	-0.1068E01	0.12322E1	-0.463E0
0.5	0.1187E1	-0.1085E1	0.12659E1	-0.471E0
0.6	0.1303E1	-0.1102E1	0.13342E1	-0.441E0
0.7	0.1488E1	-0.1261E1	0.14588E1	-0.411E0
0.8	0.1816E1	-0.1460E1	0.16671E1	-0.330E0
0.9	0.2312E1	-0.1930E1	0.19927E1	-0.196E0

Table 3.3: Values of K_I and β for centre cracked panels and double edge cracked bars.

3.2.2 The Effect of T on the Plastic Zone

The introduction of two parameter fracture mechanics originates from the work of Larsson and Carlsson (1973), who demonstrated that the second term in the Williams expansion (2.12) has a significant effect on the shape and size of the plastic zone which develops at the crack tip. The change of shape is illustrated in Figure 3.1. Compressive T stresses both enlarge the maximum radius of the plastic zone and cause the plastic lobes to swing forward. In contrast, tensile (i.e. positive T) stresses cause the plastic zone to decrease in size and to rotate backwards. With the benefit of hindsight it now seems clear that if non-singular stresses affect the size and shape of the plastic zone then they are likely to affect the local stresses within the plastic zone.

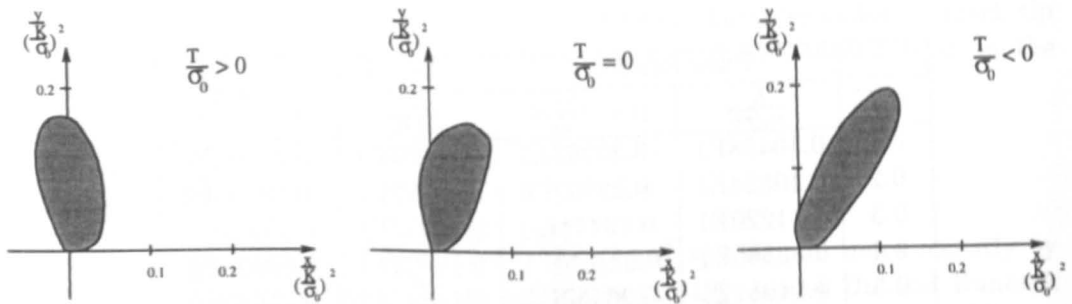


Figure 3.1: The Effect of the T stress on the plastic zone shape in small scale yielding.

Du and Hancock (1991) also described the variation in the size and shape of the plastic zone as a function of the T -stress and explained how the slip line field in non-hardening materials changes with changing T -stress. They showed that the full Prandtl field is obtained only in very constrained geometries when T is positive. In small scale yielding when T is zero an elastic wedge exists on the cracked flank the slip line field is reduced to a diamond ahead of the crack and a centred fan with an angular span of 130° . As T becomes more compressive, the elastic wedge extends and the angular span of the centred fan is reduced. For $\frac{T}{\sigma_0} = -0.7$ the centre fan stops at 78° . The effect of T on the slip line field is shown in Figure 3.2 for different values of T .

3.2.3 Determination of the T stress

The T -stress depends on the geometry and the applied load. Although a range of analytical and numerical techniques have been used to calculate T , increased computing power has enabled finite element analysis to become popular numerical tools to address this class of problem.

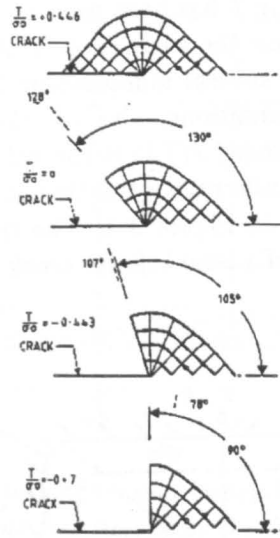


Figure 3.2: *The Effect of the T stress on the plastic zone shape in small scale yielding, after Du and Hancock (1991).*

Direct Methods

In the direct method the T -stress is determined directly from the stress or the displacement fields in a plane strain finite element analysis. In the Williams expansion (2.12), as r tends to zero, third and higher order terms approach zero while the first term is singular and the second term is finite. T can then be calculated from:

$$T = \lim_{r \rightarrow 0} \left(\sigma_{ij} - \frac{K}{\sqrt{2\pi r}} f_{ij}(\theta) \right) \delta_{1j} \delta_{i1} \quad (3.4)$$

The simplest way to calculate T using the direct method is to examine the stress field in the crack flanks. The K term is zero for $\theta = \pi$ because $f_{ij}(\pi) = 0$, and the T -stress is consequently identical to σ_x . However, the use of numerical methods in conjunction with a singular stress field requires that the mesh be highly refined if accurate results are to be obtained.

Weight Function Methods

The weight function method has recently been applied by Sham (1991). The fundamental concept was introduced by Bueckner (1973) and Rice (1972), to evaluate stress intensity factors, and will not be described here in detail. For some simple crack geometries the method is extremely accurate, as it is largely analytic, but for more complex geometries numerical procedures have to be used to determine the weight function; however, accurate results are still obtainable.

Eshelby's Method

Eshelby's method of determining T has been used by several authors, notably Kfourri (1986). The method is based on the evaluation of J contour integrals along paths remote from the crack tip for several independent load cases using finite element analysis under linear elastic conditions. $J(F)$ is the value of J when an external force F is applied on the specimen; $J(f,t)$ is the value of J when a point force f is applied at the crack tip and equilibrating the tractions t act on the outer boundary of the specimen, as illustrated in Figure 3.3. The tractions which correspond to a point force f acting at the tip of a semi-infinite crack in an infinite body are denoted t_0 .

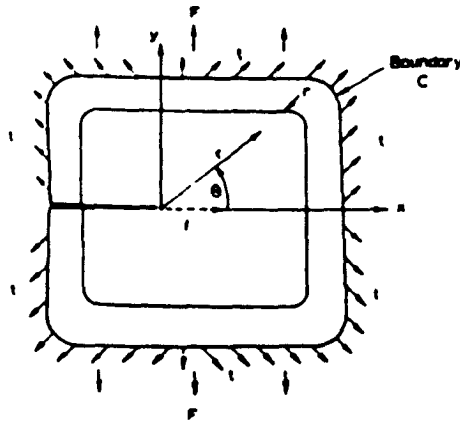


Figure 3.3: Model used to determine T from Eshelby's method, after Kfourri (1986).

The first form of Eshelby's theorem states that:

$$J(F, f, t_0) = J(F) + \frac{Tf}{E'} \quad (3.5)$$

$J(F, f, t_0)$ denotes the superposition of $J(F)$ and $J(f, t_0)$. If the point force is resisted by other tractions, t , which equilibrate f , the second form of Eshelby's theorem gives:

$$J(F, f, t) = J(F) + J(f, t) + \frac{Tf}{E'} + \frac{2K_f K_t}{E'} \quad (3.6)$$

where K_t is the stress intensity factor when the load F is acting on the specimen, and K_f is the stress intensity factor corresponding to the traction ($t-t_0$). Determination of $J(F)$ and $J(F, f, t_0)$ allows T to be determined from Equation (3.5). Alternatively a knowledge of $J(F, f, t)$, $J(f)$ and $J(f, t)$ allows T to be determined from (3.6). Figure 3.4 shows some values of the bi-axiality parameter β obtained from Eshelby's method by Kfourri (1986). The relation between T and β is given by Equation (3.3).

High accuracy can be obtained applying Eshelby's method, but the method needs solutions for two load cases which increase the necessary modelling and analysis. Furthermore, this method is only applicable for two dimensional plane strain problems, while some finite element programs do not allow a point load in the crack tip to be used in conjunction with J determination by virtual crack extension.

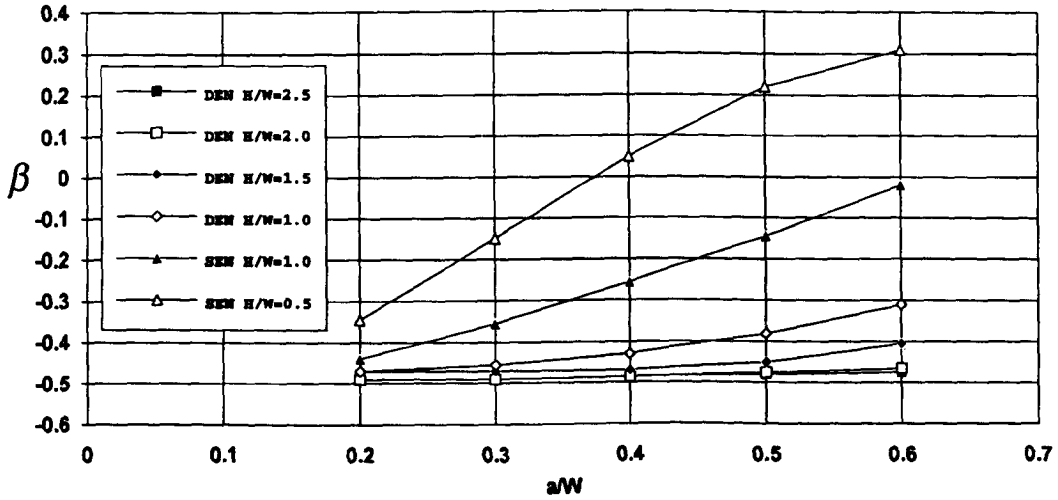


Figure 3.4: Values of the non-dimensional bi-axiality parameter β for SEN and DEN specimens as function of a/W , data after Kfourri (1986).

Line Spring Method

T can be determined for part-through cracks using the line spring method introduced by Rice and Levy (1972). This method was primarily intended to determine the stress intensity factor for plates and shells containing part-through surfaces cracks loaded in tension and bending. Figure 3.5 (a) shows the cross section of a plate with a part-through crack of length $2c$, and of varying depth $a(x)$. The plate is subject to a membrane force N^∞ and a bending moment M^∞ , illustrated in Figure 3.5 (b).

The idea is to divide the plate up into sections on which a local moment and membrane force act. Each section is regarded as an edge cracked bar subjected to both tension and bending, as shown in Figure 3.5 (c). In the linear elastic case the displacement (δ) and rotation (θ) of the cracked specimen corresponding to the local loads $N(x)$ and moments $M(x)$ can be expressed in the form of a generalised elastic spring:

$$\begin{bmatrix} \delta(x) \\ \theta(x) \end{bmatrix} = \begin{bmatrix} C_{11}(x) & C_{12}(x) \\ C_{21}(x) & C_{22}(x) \end{bmatrix} \begin{bmatrix} N(x) \\ M(x) \end{bmatrix} \quad (3.7)$$

Equilibrium and compatibility consistent with defined boundary conditions can then be satisfied by finite element procedures. By superimposing a tension component and a moment T is defined as:

$$T = \beta_T \lambda_T \left(\frac{S_{11}}{t} \right) + \beta_B \lambda_B \left(\frac{6}{t^2} \right) S_{22} \quad (3.8)$$

where the suffices T and B denote tension and bending respectively. β is the bi-axiality parameter and λ is the calibration constant for the stress intensity factor K . K depends on the method of loading and geometry. S_{11} is the tensile force gradient acting on each section and S_{22} is the moment gradient, while t is the plate thickness. Solutions for semi-elliptical surface cracks in plates have been given by Wang and Park (1992) and Al-Ani (1988). More recently MacLennan, Al-Ani and Hancock (1992) and Nekkal and Hancock (1995) have given solutions for semi-elliptical cracks in the chord-brace intersection of a tubular joint.

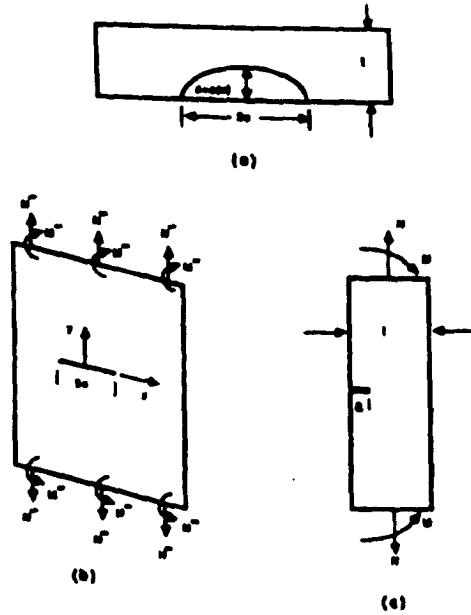


Figure 3.5: Illustration of the components of the line spring model.

3.3 Two Parameter Elastic-Plastic Crack Tip Fields

3.3.1 Modified Boundary Layer Formulations

The boundary layer formulation was introduced by Rice and Tracey (1974) to analyse crack tip plasticity in small scale yielding. Displacements or tractions corresponding to the K -field are applied on the outer boundary of a semi-circular mesh with a semi infinite crack. Small scale yielding condition is satisfied by insuring an elastic surrounding of the plastic zone. By modifying the boundary constraints on the outer boundary by the addition of the non-singular T -stress to the K -field the *modified boundary layer formulations* (MBLF) are developed; the principle is shown schematically in Figure 3.6.

By varying the T -stress in the modified boundary layer formulation, Betegón and Hancock (1991) established the relation between the T -stress and the stress field ahead of the crack for hardening rates $n=13$ and $n=\infty$. Betegón and Hancock (1991) also showed that for geometries with negative T -stresses the stress field decreases, and causes the stresses to fall below the HRR field and lose single parameter characterisation. This corresponds to the introduction of a second order term which Betegón and Hancock (1991) gave as a function of T . Their calculations were based on a non-linear stress-strain response represented by a Ramberg-Osgood power law, with $\epsilon_0 = 0.002$, $\alpha = 3/7$ and $\nu = 0.3$

The small scale yielding field ($T=0$) was used as a reference field for the modified boundary layer formulation, and is here denoted σ_{ssy} . The stress field ahead of the

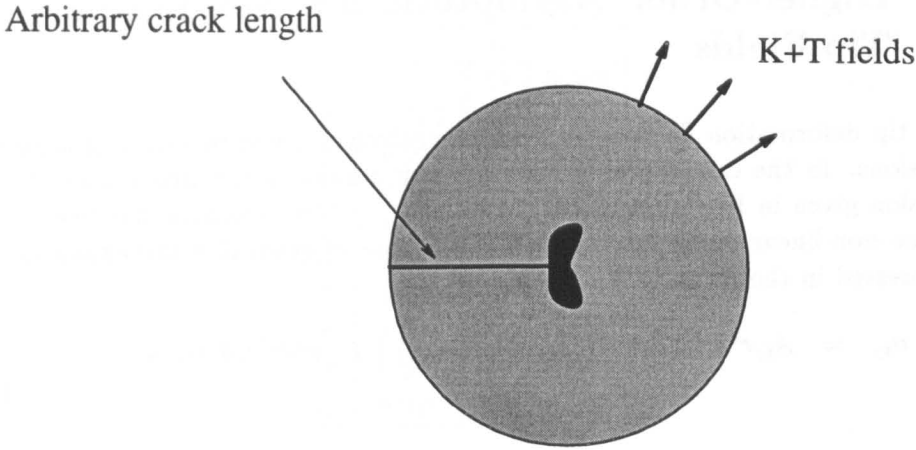


Figure 3.6: Model for boundary layer formulation.

crack tip for $\theta = 0$ was fitted to a second order polynomial:

$$\frac{\sigma_{\text{MBLF}}}{\sigma_0} = \frac{\sigma_{\text{SSY}}}{\sigma_0} + a_1\left(\frac{T}{\sigma_0}\right) + a_2\left(\frac{T}{\sigma_0}\right)^2 \quad (3.9)$$

Betegón and Hancock (1991) suggested the curve fit to (3.9) of the form

$$\begin{aligned} \frac{\sigma_{\text{MBLF}}}{\sigma_0}(r, T) &= \left(\frac{\sigma_{\text{SSY}}}{\sigma_0}\right)_{(r, T=0)} + 0.64\left(\frac{T}{\sigma_0}\right) - 0.4\left(\frac{T}{\sigma_0}\right)^2 \\ n &= 13, \frac{T}{\sigma_0} \leq 0 \end{aligned} \quad (3.10)$$

$$\begin{aligned} \frac{\sigma_{\text{MBLF}}}{\sigma_0}(r, T) &= \left(\frac{\sigma_{\text{SSY}}}{\sigma_0}\right)_{(r, T=0)} + 0.6\left(\frac{T}{\sigma_0}\right) - 0.75\left(\frac{T}{\sigma_0}\right)^2 \\ n &= \infty, \frac{T}{\sigma_0} \leq 0 \end{aligned} \quad (3.11)$$

Wang (1993) used a similar approach when he investigated the near-crack-tip stress field in a modified boundary layer formulation. However, Wang did not use a Ramberg-Osgood stress-strain relationship, he instead applied a power law of the tensile stress/strain relation

$$\varepsilon \begin{cases} \frac{\sigma}{E} & \text{for } \sigma < \sigma_0 \\ \varepsilon_0\left(\frac{\sigma}{\sigma_0}\right)^n & \text{for } \sigma > \sigma_0, \quad 1 < n < \infty \end{cases} \quad (3.12)$$

where $\varepsilon_0 = \frac{\sigma_0}{E}$, and the following material constants were used $\varepsilon_0 = 0.0025$, $n=10$ and $\nu = 0.3$. Wang suggested a three-term polynomial fit in the range $1 < \frac{r\sigma_0}{J} < 6$:

$$\frac{\sigma_{\text{MBLF}}}{\sigma_0} = \frac{\sigma_{\text{SSY}}}{\sigma_0} + a_1\left(\frac{T}{\sigma_0}\right) + a_2\left(\frac{T}{\sigma_0}\right)^2 + a_3\left(\frac{T}{\sigma_0}\right)^3 \quad (3.13)$$

The fitting parameters for $r = \frac{2J}{\sigma_0}$ were $a_1=0.6168$, $a_2=-0.5646$ and $a_3=0.1231$.

3.4 Higher-Order Asymptotic for Non-Linear Crack Tip Fields

Crack tip deformation fields have been extensively studied in terms of asymptotic expansions. In the case of linear elasticity this results in the well known Williams expansion given in Equation (2.12). More recently this technique has been used to examine non-linear crack tip fields. Without loss of generality the expansions can be expressed in the form:

$$\sigma_{ij} = A_{ij}r^s\bar{\sigma}^{(1)}(\theta, n) + B_{ij}r^t\bar{\sigma}^{(2)}(\theta, n) + C_{ij}r^u\bar{\sigma}^{(3)}(\theta, n) + \dots \quad (3.14)$$

$$s < t < u$$

The strength of the singularity is determined by the exponents of the radial distance, r . The dimensionless amplitudes of each term are denoted by A_{ij} , B_{ij} while $\bar{\sigma}^{(l)}(\theta, n)$ ($l=1,2,\dots$) are angular functions which depend upon the strain hardening exponent, n in a Ramberg-Osgood stress-strain relation. In the case of linear elasticity $s=-1/2$, $t=0$, $u=1/2$, while the universal angular functions are tabulated in standard literatures such as Broek (1991).

In non-linear deformation the leading term in the series is identified with the HRR field so that higher order solutions are sought in the form:

$$\sigma_{ij} = \sigma_0 \left(\frac{J}{\alpha \epsilon_0 \sigma_0 L n r} \right)^{\frac{1}{1+n}} \bar{\sigma}^{(1)}(\theta, n) + B_{ij}^{(2)} r^t \bar{\sigma}_{ij}^{(2)}(\theta, n) + C_{ij} r^u \bar{\sigma}^{(3)}(\theta, n) + \dots \quad (3.15)$$

$$s = \frac{1}{n+1} \quad s < t < u$$

Li and Wang (1986), and Sharma and Aravas (1991) have examined two term expansions of this form. The amplitude B_{ij} of the second term is formally arbitrary, and can be considered as a second independent parameter describing the crack tip stress field. B_{ij} is thus dependent on loading, material response and deformation level. In contrast the exponent t is simply a function of the strain hardening exponent, n given in Table 3.4 after Sharma and Aravas (1991).

In contrast Yang, Chao and Sutton (1993a,b) and Xia *et al.* (1993) have sought three and four term expansions. Sutton and co-workers express their results in the form:

$$\frac{\sigma_{\theta\theta}}{\sigma_0} = \left(\frac{J}{\alpha \epsilon_0 \sigma_0 L n L} \right)^{\frac{1}{1+n}} \left[\left(\frac{r}{L} \right)^{s_1} \bar{\sigma}_{\theta\theta}^{(1)}(\theta) + A_2 \left(\frac{r}{L} \right)^{s_2} \bar{\sigma}_{\theta\theta}^{(2)}(\theta) + (A_2)^2 \left(\frac{r}{L} \right)^{s_3} \bar{\sigma}_{\theta\theta}^{(3)}(\theta) \right] \quad (3.16)$$

The exponents of the second and third order terms are again functions of n given in Table 3.5.

3.4.1 The Q Approach

As a simplification of the general expansion in Equation (3.15) O'Dowd and Shih (1991a,b) have introduced a widely accepted notation in which the amplitude of the

n	t	n	t
		11	0.068
2	-0.102	12	0.066
3	-0.013	13	0.065
4	0.033	14	0.063
5	0.55	15	0.061
6	0.065	16	0.059
7	0.069	17	0.057
8	0.071	18	0.056
9	0.071	19	0.054
10	0.070	20	0.053

Table 3.4: Relations between strain hardening exponent, n , and the second order exponent t , after Sharma and Aravas (1991).

n	$s_1 = -1/(n+1)$ (HRR values)	s_2	s_3
3	-0.25	-0.01284	0.2243
4	-0.2	0.03282	0.2656
5	-0.1666	0.05456	0.2758
10	-0.0909	0.06977	0.2304
13	-0.07143	0.06468	0.2008

Table 3.5: Stress exponents of higher order terms, Mode I, plane strain, from Chao and Ji (1994).

second term in the expansion is denoted Q .

$$\frac{\sigma_{ij}}{\sigma_0} = \left(\frac{J}{\alpha \varepsilon_0 \sigma_0 J_n r} \right)^{\frac{1}{n+1}} \hat{\sigma}(\theta, n) + Q \left(\frac{r}{J/\sigma_0} \right)^t \hat{\sigma}(\theta, n) + \dots \quad (3.17)$$

On this basis Q may formally be defined as:

$$Q = \lim_{r \rightarrow 0} \frac{\sigma_{ij} - \sigma_{HRR}}{\left(\frac{r}{J/\sigma_0} \right)^t \hat{\sigma}(\theta, n)} \quad (3.18)$$

However in practise Q is determined in a simpler way. It is argued that the exponent t can be approximated to zero, leading to a distance independent second order term. This simplification allows the crack tip fields to be written in the form:

$$\sigma_{ij} = \sigma_{ij}(Q = 0) + Q \sigma_0 \delta_{ij} \quad (3.19)$$

This approach does however require that the strength of the second order term should be very much less than the leading HRR term. For weakly hardening materials the second order term is non-singular, and the calculations of Sharma and Aravas (1991) and Sutton and co-workers support this idea.

3.5 The Effect of Constraint on Experimental Toughness Data

3.5.1 Constraint Effect on Cleavage Failure

The relationship between the constraint parameter T and cleavage fracture toughness has been discussed by Betegón and Hancock (1990), and Sumpter and Forbes (1992). Both examined the critical value of J for geometries with different levels of constraint. Specimens with the most negative T values were found to be tougher than deeply cracked geometries with positive T values. The experimental results were expressed as a J - T fracture locus as illustrated in Figure 3.7. Figure 3.7 shows Betegón's experimental data plotted as J versus $\frac{T}{\sigma_0}$.

Bend geometries with $a/W < 0.3$ give negative T values, corresponding to the shallowest cracks. For the deeply cracked geometries ($a/W > 0.3$), which is known to have positive T -stress, the toughness was found experimentally to be independent of geometry. The J value at fracture was found to be nearly constant, in accordance with predictions based on modified boundary layer formulation.

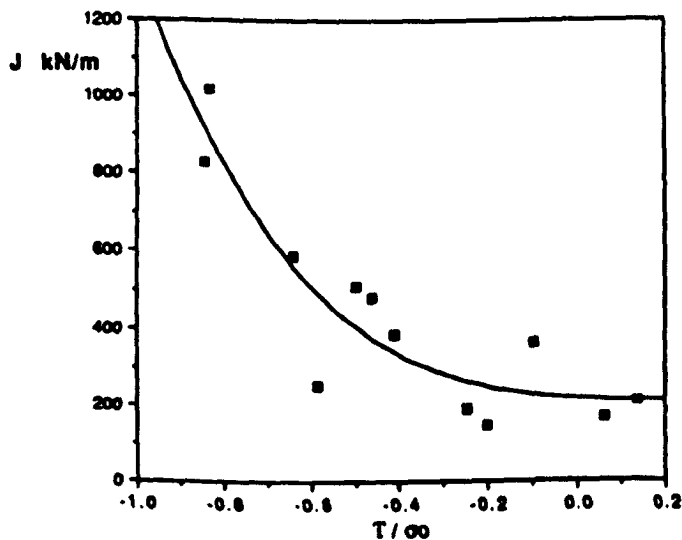


Figure 3.7: Toughness of edge cracked bend bars after Betegón (1990), and Betegón and Hancock (1990) as a function of $\frac{T}{\sigma_0}$.

Toughness tests on a low-grade mild steel at -50°C have recently been reported by Sumpter and Forbes (1992), Sumpter (1993b) and Sumpter and Hancock (1994).

Three point bend specimens (3PB) with a/W ratios between 0.15 and 0.7 were tested along with centre cracked panels (CCP) with a/W ratios between 0.65 and 0.8. Figure 3.8 shows the critical value of J versus $\frac{T}{\sigma_0}$ at cleavage. A comparison between the two types of specimen shows that the highly unconstrained CCT specimens gave slightly higher values of J_c than 3PB specimen, at the same value of $\frac{T}{\sigma_0}$.

Figure 3.9 shows the same data re-analysed in terms of Q . Q is defined in Equation (3.18) and indicates that a rather better correlation of CCT and 3PB specimens can be achieved, although the effect is masked by scatter. The best two parameter characterisation is obtained by applying the elastic-plastic term Q to describe the level of constraint in a $J_c - Q$ locus, though the elastic T stress remains the simplest engineering parameter to index constraint.

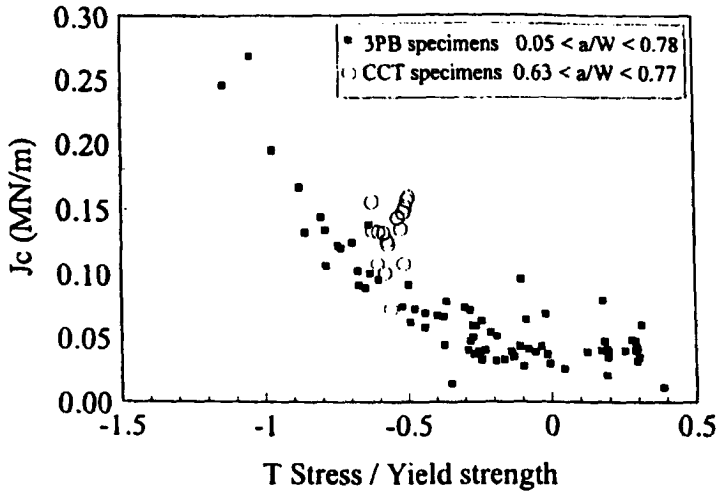


Figure 3.8: Critical value of J as a function of $\frac{T}{\sigma_0}$ for 3PB and CCT specimens, low-grade mild steel at -50°C , Sumpter (1993).

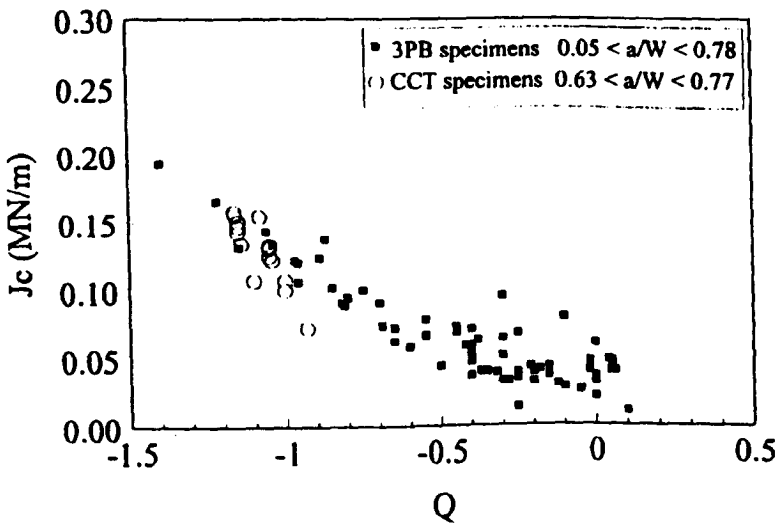


Figure 3.9: Critical value of J as a function of Q for 3PB and CCT specimens, low-grade mild steel at -50°C , after Sumpter and Hancock (1994).

Sumpter and Hancock (1994) also showed data from test specimens in a high strength weld metal with a yield stress about 700 MPa, at a test temperature of -30°C . Figure 3.10 shows the critical value of J as a function of $\frac{T}{\sigma_0}$, while Figure 3.11 shows the same data as a J_c - Q locus. Constraint enhanced toughness was found to be even more significant for this material than for the mild steel, however both J/Q and J/T analyses describe the data well.

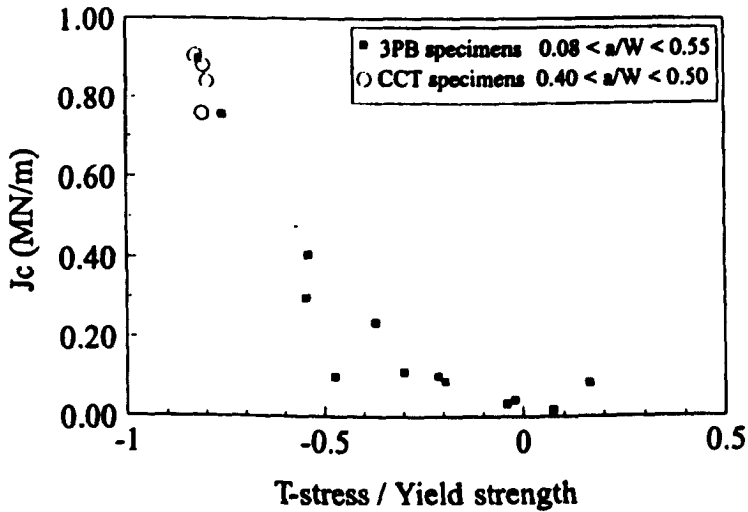


Figure 3.10: Critical value of J as a function of $\frac{T}{\sigma_0}$ for 3PB and CCT specimens, high strength weld steel at -30°C , Sumpter (1999).

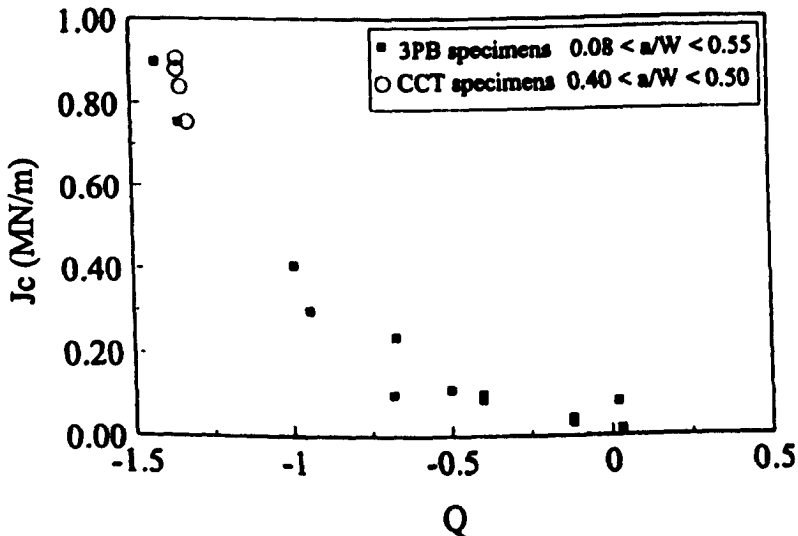


Figure 3.11: Critical value of J as a function of Q for 3PB and CCT specimens, high strength weld steel at -30°C , after Sumpter and Hancock (1994).

Kirk *et al.* (1993), have presented cleavage toughness data for an A515 steel at room temperature, using edge cracked bend bars with different a/W ratios and various thickness. The results show J at fracture as a function of $\frac{T}{\sigma_0}$ in Figure 3.12, and versus Q in Figure 3.13. Comparing Figure 3.12 with Figure 3.13 the data shows geometries with positive values of T presented in terms of Q give negative values of Q ; however, the loss of constraint shown by Kirk is due to global bending in the ligament where T - Q fields are not applicable.

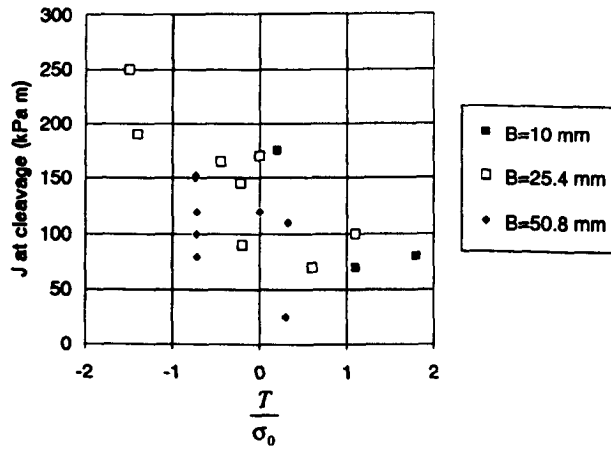


Figure 3.12: Fracture toughness versus $\frac{T}{\sigma_0}$ for ASTM A515 Grade 70 steels at 20°C from edge cracked bend bars for three thicknesses, after Kirk *et al.* (1993).

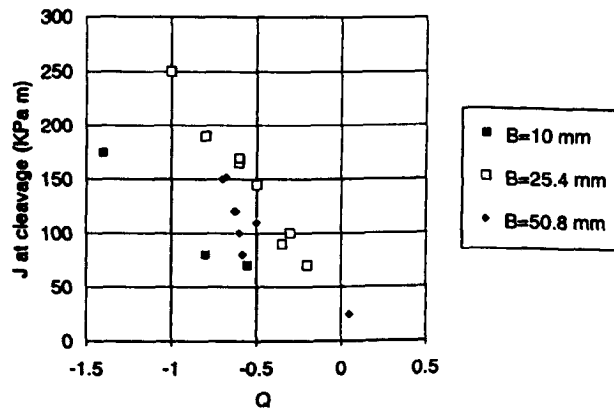


Figure 3.13: Fracture toughness versus Q for ASTM A515 Grade 70 steels at 20°C from edge cracked bend bars for three thicknesses, after Kirk *et al.* (1993)

3.5.2 Ductile Fracture

Hancock, Reuter and Parks (1993) tested samples of an American pressure vessel steel denoted A710 using both cracked geometries and surface cracked plates. Crack extension occurred by stable ductile tearing enabling both J and CTOD to be measured as a function of crack extension Δa . ASTM (1983) suggest J_c at an extension of $200 \mu\text{m}$ to define initiation toughness, and Figure 3.14 shows J for crack extensions $\Delta a=0$, $\Delta a=200 \mu\text{m}$ and $\Delta a=400 \mu\text{m}$. Figure 3.15 shows the corresponding crack tip opening displacement δ as a function of Δa .

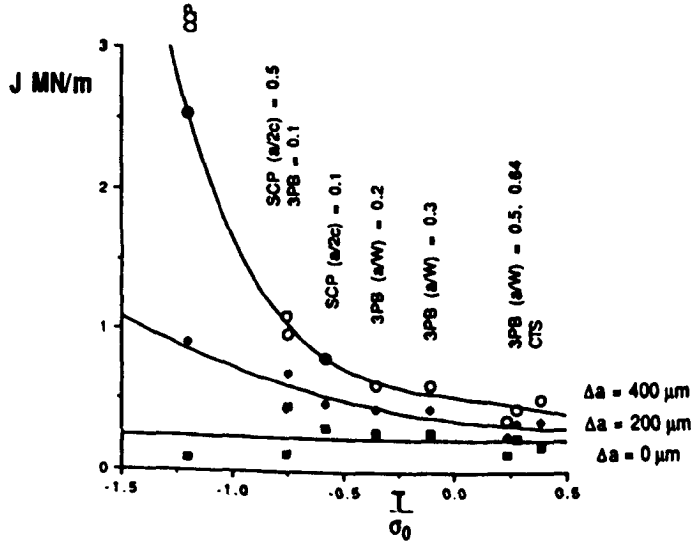


Figure 3.14: The toughness of a range of through and part through crack geometries parameterised by T , after Hancock, Reuter and Parks (1993).

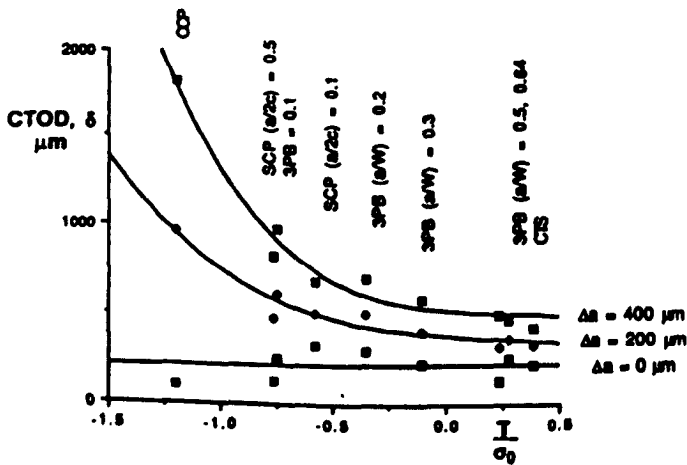


Figure 3.15: The CTOD as a function of T at crack extensions of 0, 200 and $400 \mu\text{m}$, after Hancock, Reuter and Parks (1993).

The results show a marked effect of constraint on toughness after small amounts of crack growth. J_c values for centre cracked panels were approximately 4 times greater than that of highly constrained deeply cracked bend bars and CTS specimens at a crack extension of 200 μm . For higher crack extensions (Δa) the constraint effect is even more pronounced as J_c for the CCP specimen is more than 5 times the values for the deeply cracked bend bars.

Geometries with positive T stresses (deeply crack bend bars and CTS specimen) showed no or only little geometry dependent toughness. For these geometries the near crack tip field is dominated by J , and single parameter characterisation can be applied up to the usual limit of J -dominance. Geometries which are known to have negative values of T showed geometry dependent toughness, which supports the theory that crack tip constraint and the associated toughness are well characterised by T .

The authors noted that the main effect of constraint sensitivity of toughness arises from the effect of constraint on the slope of the resistance curves, as illustrated in Figure 3.16 and 3.17. This data may be compared with the numerical solutions of Varias and Shih (1993) on stable crack growth.

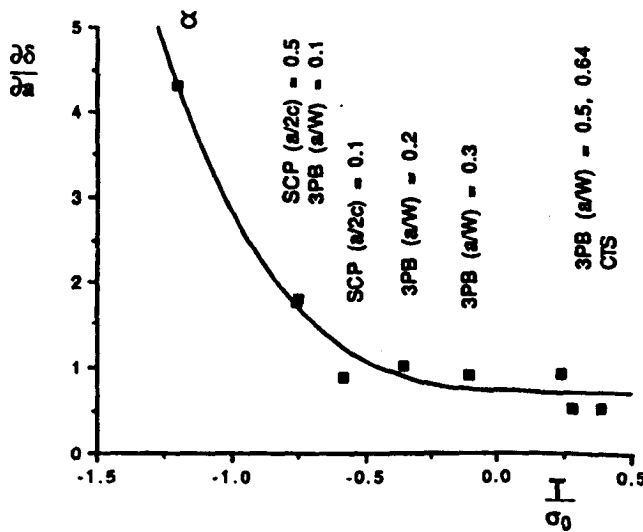


Figure 3.16: *The initial slope of CTOD- Δa resistance curve as a function of $\frac{T}{\sigma_0}$, after Hancock, Reuter and Parks (1993).*

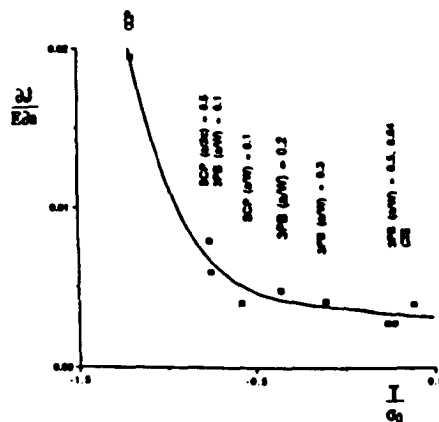


Figure 3.17: The initial slope of J - Δ resistance curve as a function of $\frac{I}{G_0}$, after Hancock, Reuter and Parks (1993).

3.6 Engineering Application

The conventional accepted approach to ensure structural integrity is based on a single parameter, such as the critical value of J or K . Experimental data are obtained from highly constrained deeply cracked bend specimens. This approach is safe because it provides a lower bound toughness, but is also conservative and may lead to unnecessary repairs to and outage of engineering structures.

3.6.1 Failure Assessment

A common engineering approach to failure assessment in the United Kingdom is codified in R6 (1986) and PD6493 (1991). Proximity to failure is judged in relation to plastic collapse or LEM failure. In practise the proximity to collapse is measured by $\frac{P}{P_{Limit}}$ which is the abscissa of the Failure Assessment Diagram (FAD). Proximity to LEM failure is judged by $\frac{K_I}{K_{IC}}$ which is the ordinate. The proximity to fracture under LEM is described by the ratio of the stress intensity factor K_I to an experimentally measured material toughness, K_{mat} .

$$K_r = \frac{K_I}{K_{mat}} \quad (3.20)$$

K_{mat} corresponds to K_{IC} as defined in British Standard (BS-7448 1991b) and ASTM (E 339-83 1983), or alternatively to a small amount of crack growth (0.2 mm). In plane stress the critical plane stress toughness is used rather than K_{IC} .

The first proposed form of a failure assessment diagram was a simple square box. This was proposed by Dowling and Townley (1975). The abscissa is the load non dimensionalised by the limit load, denoted L_r , and the ordinate is the stress intensity factor normalised by the critical value of the stress intensity factor, denoted K_r , Figure 3.18.

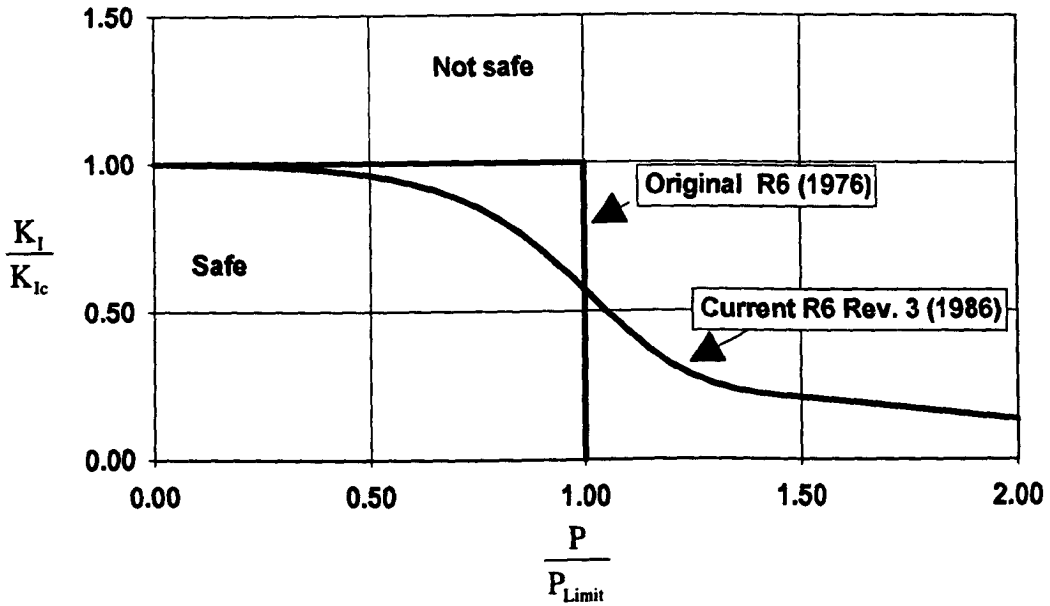


Figure 3.18: Failure assessment lines as given by R6 Rev 3 and the original form.

Failure Assessment Diagrams are truncated at an abscissa value of L_r^{max} defined as

$$L_r^{max} = \frac{\sigma_0 + \sigma_{UTS}}{2\sigma_0} \quad (3.21)$$

R6 gives three options for failure assessment: a general curve, which can be used for materials which do not exhibit a yield discontinuity. A material specific curve, which is suitable for all metals regardless of the stress-stain behaviour, and a Failure Assessment line based on J -integral Analysis, which can be used for all purposes.

The failure locus for the general curve is described by the relationship

$$K_r = (1 - 0.14L_r^2)(0.3 + 0.7 \exp(-0.65L_r^6)) \quad \text{for } L_r \leq L_r^{max} \quad (3.22)$$

The material specific curve is described by the equation:

$$K_r = \sqrt{\frac{E\varepsilon_{true}}{L_r\sigma_0} + \frac{L_r^3\sigma_0}{2E\varepsilon_{true}}} \quad (3.23)$$

The third option is J -Integral analysis, for a specified material and geometry. This method is based on a elastic value of J (J_E) and the total value of J . The abscissa of the failure assessment diagram is given by L_r while the ordinate is defined:

$$K_r = \frac{K_I}{K_{IC}} = \sqrt{\frac{J_E}{J_{IC}}} \quad (3.24)$$

This curve is based on calculations of Kumar, German and Shih (1981). J is divided into an elastic component J (J_E) and plastic component J (J_P), J_E is proportional to $(\frac{P}{P_{Limit}})^2$, and J_P is proportional to $(\frac{P}{P_{Limit}})^{n+1}$. Failure at a critical value of J can then be expressed as a single failure assessment line as a function of $\frac{P}{P_{Limit}}$.

3.6.2 Constraint Based Failure Assessment Diagrams

Conventional failure assessment is based on a single parameter approach defined by the critical value of J or K . MacLennan and Hancock (1995) and Ainsworth and O'Dowd (1995) have introduced the effect of constraint into failure assessment. MacLennan and Hancock (1995) analysed a range of single edge bend bars and centre cracked panels. The centre cracked panels are known to lose constraint for all geometries, while the shallow single edge bend bars lose constraint.

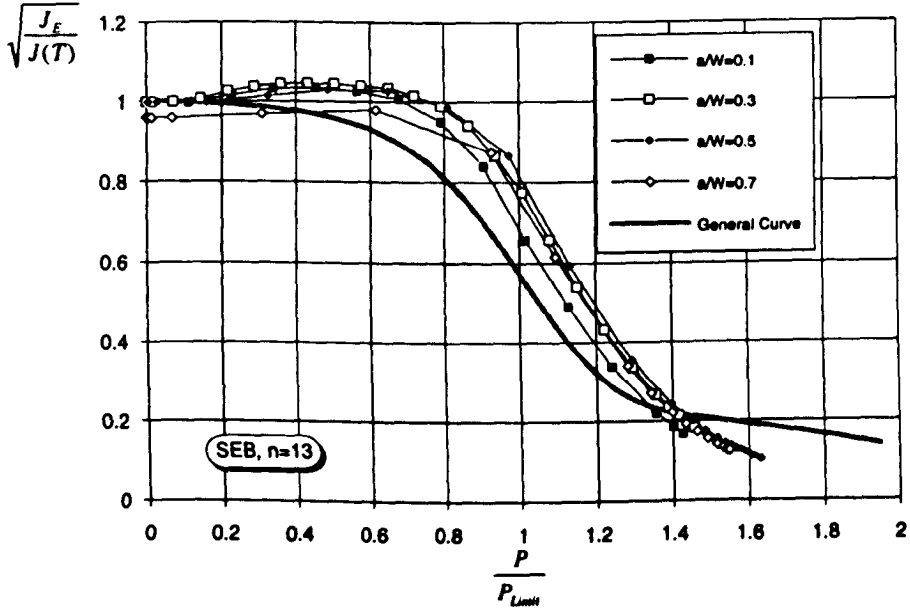


Figure 3.19: Geometry specific failure assessment diagram, single edge bend bars, $n=13$.

The effect of constraint quantified on the fracture toughness $J_C(T)$ was described by MacLennan and Hancock (1995) in terms of T :

$$\frac{J_C(T)}{J_C(T=0)} = \left(\frac{1}{\exp\left(\frac{T}{\sigma_0}\right)} \right)^m \quad \frac{T}{\sigma_0} < 0 \quad (3.25)$$

$$\frac{J_C(T)}{J_C(T=0)} = 1 \quad \frac{T}{\sigma_0} \geq 0$$

The exponent m in Equation (3.25) defines the constraint sensitivity of fracture. m is zero for materials which are constraint insensitive, and non zero values of m correspond to increasing levels of constraint sensitivity. MacLennan and Hancock modified the FAD, so that the elastic component of the J integral is normalised by the constraint matched fracture toughness (T or $Q \neq 0$). The abscissa in the FAD is still the normalised load, but the abscissa is a modified value of K_r denoted K_r^{Mod} and defined as:

$$K_r^{Mod} = \sqrt{\frac{J_E}{J(T)}} \quad (3.26)$$

MacLennan and Hancock (1995) analysed a range of a/W ratios in bending and drew failure assessment lines (FAL).

This method of failure assessment can now be applied to experimental data, and the experimental data of Sumpter (1993b) and Sumpter and Forbes (1992) are shown.

The material was a grade 43A normalised plain carbon steel tested at a temperature of -30° under cleavage failure. The yield stress at this temperature was 700 MPa and the material hardening characteristics were described by $n = 10$ and $\alpha = 0.95$. The chemical composition is given in Table 3.6.

C	Si	Mn	P	S	Cr
0.19	0.04	0.59	0.01	0.032	0.09

Table 3.6: Chemical composition Wt% of 43A.

The modified FAD proposed by MacLennan and Hancock measures the toughness of shallow and deeply cracked bend bars as a function of T or Q , and the failure assessment diagram is then constructed using the constraint matched toughness given in (3.26). By applying this method the advantage of enhanced toughness for specimens with low levels of constraint can be taken into account for defect assessment.

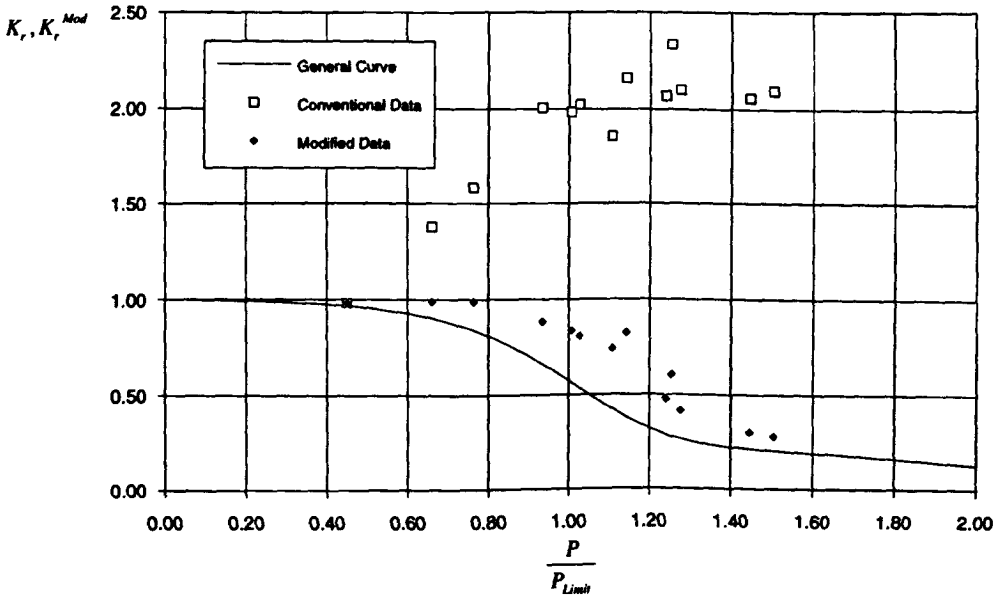


Figure 3.20: Failure assessment diagram expressed as conventional and modified FAD on the same axis, Sumpter Weld Data, single edge cracked bend bars, $n=10$.

Blank Page

Numerical Methods

Two parameter fracture mechanics has been reviewed in Chapter 3. The review has identified that a major problem with constraint based fracture mechanics arises from an inability to determine Q from far field parameters. One of the objective of this Thesis is to find a systematic way to describe levels of crack tip constraint for fundamental geometries. The method for determining stress and deformation field in this thesis has been finite element analysis. The numerical details of the models are described in this chapter. The chapter also describes the material response in a elastic-plastic regime in terms of a Ramberg-Osgood stress-strain relationship. A computer software package has been developed for the purpose of analysing finite element results and calculating various fracture parameters. The structure of this program is discussed.

4.1 Numerical Analysis

Finite element analysis was used to determine crack tip stress and deformation fields. The finite element package used throughout the present work was ABAQUS v.5.3 (1992) on a UNIX *Sun Sparc* station 10 running the Solaris 2.4 operating system.

The meshes were created using PATRAN v.2.4.5 (1988) mounted on a IBM RS/6000 with AIX. The elements were 8 nodes biquadratic isoparametric plane strain elements, using reduced integration and linear pressure interpolation (ABAQUS element type CPE8RH). Analysis was based on small-strain theory using incremental plasticity. Two different type of analysis have been performed. Firstly modified boundary layer formulations have been used to obtain reference fields at different levels of known constraint. Secondly full field solutions of real cracked geometries subject to specific loading have been analysed.

4.1.1 Modified Boundary Layer Formulations

The boundary layer formulation comprises of a semi circular model containing a radial crack where the crack tip is located at the centre and the crack mouth is at the boundary of the model as illustrated in Figure 4.1.

A plane strain displacement field calculated through the singular K -field and the non-singular T -field was applied on the outer boundary of the model.

$$\begin{aligned}
 u &= \frac{K_I}{2G} \sqrt{\frac{r}{2\pi}} \cos\left(\frac{\theta}{2}\right) \left[\kappa - 1 + 2 \sin^2\left(\frac{\theta}{2}\right) \right] + \frac{rT(1-\nu^2) \cos \theta}{E} \\
 v &= \frac{K_I}{2G} \sqrt{\frac{r}{2\pi}} \sin\left(\frac{\theta}{2}\right) \left[\kappa + 1 - 2 \cos^2\left(\frac{\theta}{2}\right) \right] - \frac{rT(1-\nu^2) \sin \theta}{E}
 \end{aligned}
 \tag{4.1}$$

This configuration is referred to as a modified boundary layer formulation (MBLF) and can be regarded as simulating near tip conditions in an arbitrary geometry under contained yielding. The boundary layer formulation may be thought of as being equivalent to cutting out a region around the crack tip and constructing a separate body. The MBLF analysis has to be understood as way of obtaining reference fields for various levels of constraint.

The mesh used for the MBLF had 360 elements and was heavily focused so that the size of the first element was approximately one millionth of the outer radius as shown in Figure 4.1. The crack tip was modelled by a focused mesh of collapsed elements which allowed the 25 crack tip nodes to be coincident but independent.

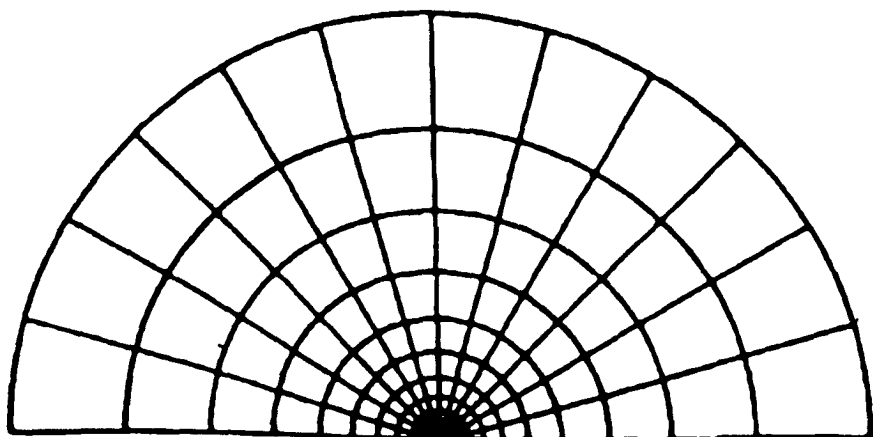


Figure 4.1: *The mesh for boundary layer formulation analysis.*

Boundary conditions were applied in two steps. Initially the displacements corresponding to the T stress were applied, and then in the second step displacements corresponding to an increasing stress intensity factor were applied at a constant value of T . The two step method ensured that T stress was constant during deformation. The small scale yielding field corresponds to ($T=0$) in Equation 4.1.

4.1.2 Full Field Solutions

Numerical solutions were obtained for a range of plane strain cracked geometries as illustrated schematically in Figure 4.2. The geometries included single edge cracked bars in bending (SECB) and tension (SECT), centre cracked panels (CCP) and double edge cracked bars (DEC). For the single edge cracked bars, symmetry allowed half the bar to be modelled, while for centre crack panels and the double edge cracked bars only a quarter was modelled. The single edge bars were loaded by applying force loading at the remote boundary corresponding to either pure tension or pure bending. The centre cracked panels and the double edge cracked bars were displacement loaded in tension. For CCPs the total crack length is denoted $2a$, as shown in Figure 4.2, while for the DEC the crack on each side of the specimen has the same length a .

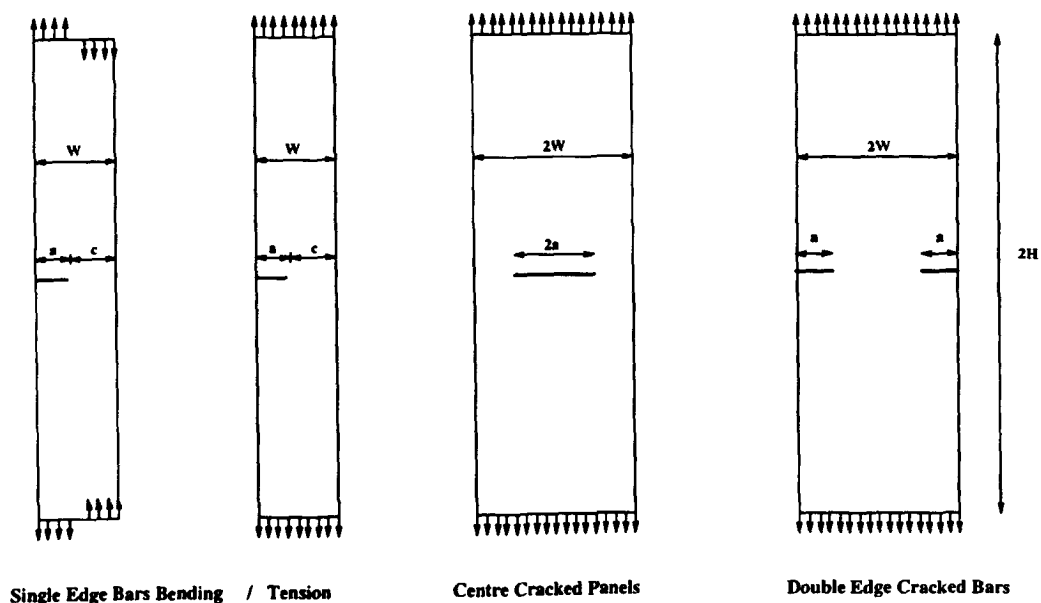


Figure 4.2: The four geometries analysed.

Figure 4.3 shows a typical mesh of a full field solution. The mesh shown corresponds to an (a/W) ratio of 0.5 and has 624 elements. For the single edge geometries the width to height was $1/3$ and for the CCPs and DECs the width to height was $2/3$. The same mesh can be used for all the 4 different type of full field geometries (SECT, SECB, CCP and DEC). For the single edge geometries the load on the model was either tension or bending. For the CCP and DEC symmetry boundary conditions were applied along one of the vertical boundaries as well as on the ligaments. Similarly, one mesh can be used for two different crack lengths. Consider for example a SECT ($a/W=0.4$). By changing the boundary condition on the ligament and the crack flanks the same mesh can be analysed as ($a/W=0.6$). The crack tip was modelled using the same principles as in the MBLF, using a focused mesh of collapsed elements which allowed the 33 crack tip nodes to be coincident but independent.

4.1.3 Material Response

In uniaxial tension the material response can be described by Hooke's law at stresses less than the yield stress σ_0

$$\sigma = E\varepsilon \quad (\sigma \leq \sigma_0) \quad (4.2)$$

where E is Young's modulus. Poisson's ratio, ν , was 0.3. Yield and associated plastic flow was modelled by incremental plasticity under the Prandtl-Reuss flow rules. The plastic response was approximated to a Ramberg-Osgood stress-strain relation which in uniaxial tension can be described by

$$\frac{\varepsilon}{\varepsilon_0} = \frac{\sigma}{\sigma_0} + \alpha \left(\frac{\sigma}{\sigma_0} \right)^n \quad (4.3)$$

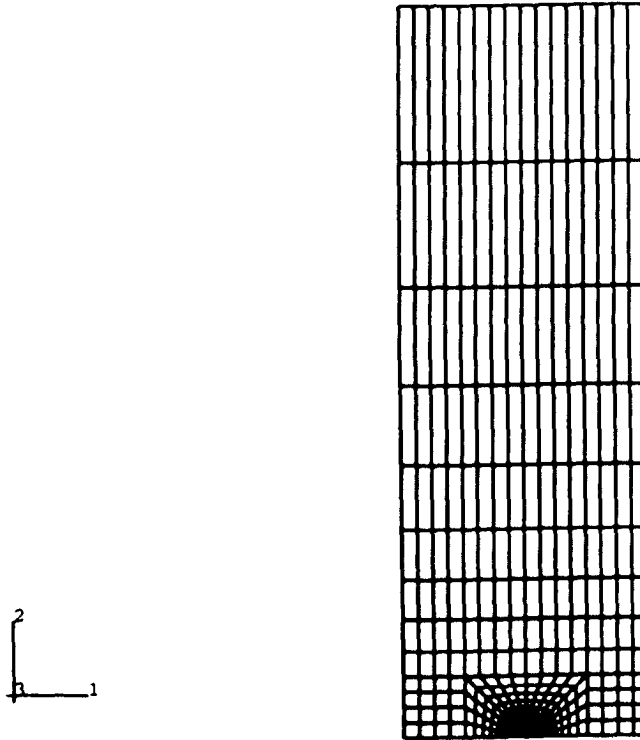


Figure 4.3: Mesh of a full field solution, with $a/W=0.5$.

Numerical calculations were performed with strain hardening exponents of 3, 6, 13 and non-hardening material response, which can be regarded as corresponding to a hardening exponent of infinity. Unless otherwise stated ϵ_0 was 0.001 and $\alpha = \frac{3}{7}$. These stress-strain relationships are shown graphically in Figure 4.4.

4.1.4 Determination of J

J was determined by the virtual crack extension method of Parks (1977), as modified by Li, Shih and Needleman (1985), and implemented in ABAQUS. The J -integral is given by the decrease in total potential energy of the loaded structure caused by an increase in the crack opening area. In terms of a discretised finite element solution the potential energy of a body is given by:

$$\Pi = \frac{1}{2}[\mathbf{u}]^T[\mathbf{K}][\mathbf{u}] - [\mathbf{u}]^T[\mathbf{F}] \quad (4.4)$$

$[\mathbf{u}]$ is a vector with the nodal displacement, $[\mathbf{K}]$ is the stiffness matrix and $[\mathbf{F}]$ is a vector with the applied nodal force. The energy release rate, or change in potential energy under fixed load is:

$$\begin{aligned} \mathcal{G} &= -\left(\frac{\partial \Pi}{\partial a}\right)_{load} \\ &= -\frac{\partial [\mathbf{u}]^T}{\partial a}([\mathbf{K}][\mathbf{u}] - [\mathbf{F}]) - \frac{1}{2}[\mathbf{u}]^T \frac{\partial [\mathbf{K}]}{\partial a}[\mathbf{u}] + [\mathbf{u}]^T \frac{\partial [\mathbf{F}]}{\partial a} \end{aligned} \quad (4.5)$$

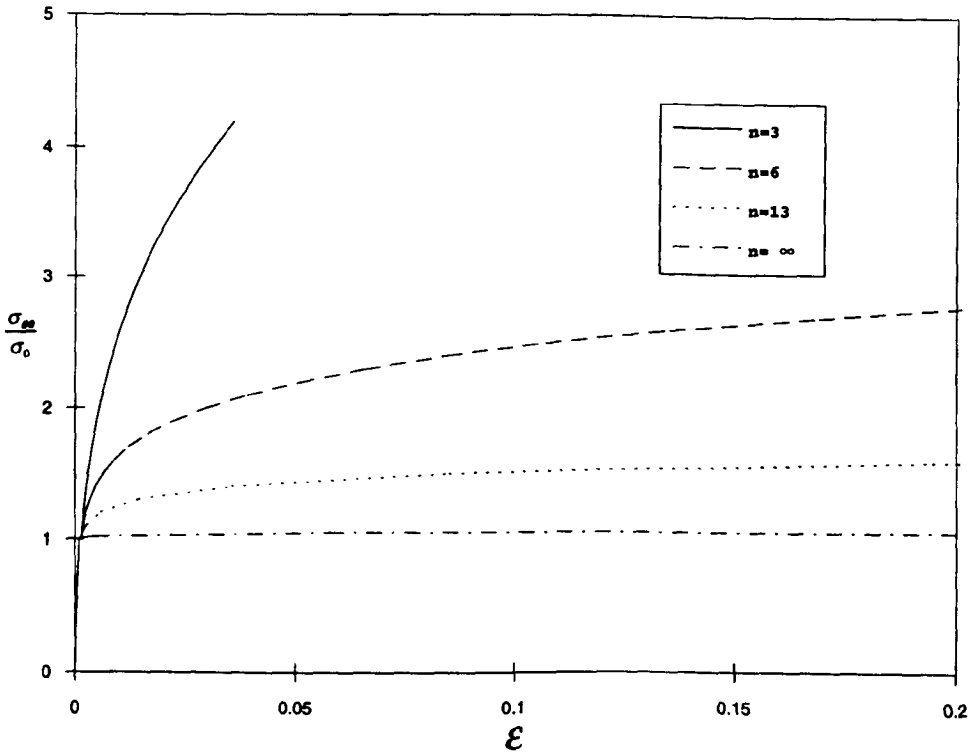


Figure 4.4: *The stress-strain relationship based on Ramberg-Osgood power law, for various hardening rates.*

The basic equation in linear finite element analysis is the relation between force and displacement, which can be written in matrix notation as:

$$[\mathbf{F}] = [\mathbf{K}][\mathbf{u}] \quad (4.6)$$

The consequence of (4.6) in (4.5) is that the first term must be zero and since there is no load on the free crack face the third term must also vanish allowing the energy release rate to be reduced to:

$$\mathcal{G} = \frac{K_I^2}{E}(1 - \nu^2) = -\frac{1}{2}[\mathbf{u}]^T \frac{\partial[\mathbf{K}]}{\partial a} [\mathbf{u}] \quad (4.7)$$

The energy release rate is proportional to the derivative of the stiffness matrix with respect to crack length.

The principle of the calculation of the J integral for a crack extension from a to $a + \delta a$ is to consider only the change in energy of the elements surrounding the crack tip. Each element around the crack tip is distorted so that its stiffness changes. The energy release rate is related to this change in element stiffness:

$$\mathcal{G} = -\frac{1}{2}[\mathbf{u}]^T \left(\sum_{i=1}^N \frac{\partial[k_i]}{\partial a} \right) [\mathbf{u}] \quad (4.8)$$

$[k_i]$ are the elemental stiffness matrices and N is the number of elements surrounding the crack tip. Parks (1974) showed that Equation (4.8) is equivalent to the J integral.

4.2 Software for Constraint Analysis

The results of finite element analyses were written to a *.FIL file in compressed ASCII format. The advantage of ASCII format is the ease with which data can be transferred between computer systems without having to translate the data.

A range of computer programs were written to convert numerical results from the FIL file into a file which could be read by Matlab V.4. (1991). Matlab is a tool for numerical computation and visualisation. Using programs written within Matlab the results obtained from the finite element analysis could be processed into relevant fracture parameters which could not be obtained directly from ABAQUS. Another advantage of using Matlab is that the results could easily be displayed graphically. Post processing of the finite element analysis results have been divided into 3 steps. The programs have been included on a DOS format 3¹/₂" floppy disc at the back of this thesis. The Matlab programs were written and run on Matlab version 4.2a for UNIX workstations.

Step 1: The program "abamat" is written using UNIX shell commands. It is a package using Make with a Makefile, and a lex program. The lex program removes the line breaks from the FIL file to create a continuous data stream readable by Matlab. The Makefile applies the lex program and makes the old FIL file into a new FIL file with a continuous data stream.

Step 2: is the main program written and executed in a language implemented in Matlab. This main program is called "ABAQUS to Matlab". In this step the FEA results are read into Matlab and saved in a Matlab format.

Step 3: is another Matlab program written and executed within Matlab. The programs use the result from the FEA now in a Matlab format, to calculate the relevant fracture mechanics parameters. This program is called "constraint".

4.2.1 Program: "ABAQUS to Matlab"

The main feature when transferring FEA data from ABAQUS to Matlab is the way the FIL file is built up. The FIL file is built on the principle that all words are of the same length, whether they contain integers, floating point numbers, or character strings. The results are written as a sequence of records. Table 4.1 shows how each record is built up. At the beginning of each record is the number of items in the record. With a knowledge of the number of items in a record, the program can identify the end of a record and then stop reading this particular record. The second item in a record is a label, and the rest of the record is data - either node/element numbers or results (e.g. stress or strain).

The record label identifies the type of data, for example when the program reads the label 1901, ABAQUS to Matlab recognises the label as a record containing nodal definition, as shown in Figure 4.5. When the label is recognised by the program the data are read into the Matlab file and can be used for calculations. The program recognises 18 different labels as given in Table 4.2. If the label is not recognised the program skips to the end of the record and reads the next record.

The beginning of each record is indicated by a *, followed by the character D, A or I indicating the type of data. Each floating point number in a result file record begins

Location	Length	Description
1	1	Record length (items)
2	1	Record type key (label)
3,4 ..	(items-2)	Attributes (stresses, strain etc.)

Table 4.1: *Record format in FIL file.*

Label	Variable
2000	Increment start
2001	Increment end
1921	Date, Version etc.
1901	Coordinates in the full model
1931	Nodes numbers in node sets
1932	Continuation of 1931
1933	Element numbers in element sets
1934	Continuation of 1933
1991	<i>J</i> -integral
1999	Total energy
1	Element header (element or node numbers)
11	Stresses
12	Stress invariant
21	Strains
22	Plastic strains
101	Nodal displacements
104	Reaction forces
107	Coordinates for specified node set

Table 4.2: *Variables to be read into Matlab.*

with the character D, followed by the number in double precision. Each character string begins with the character A, followed by eight characters. Each integer begins with the character I, followed by a two digit integer giving the number of decimal digits in the integer, followed by the integer itself, an example of a record is given in Figure 4.5. The program "ABAQUStoMatlab" is built up of a series of subroutines.

- file_reader
 - From the file name, the type of geometry (SECT, SECB, CCP or DEC) is known as well as the strain hardening rate, and the crack length. For example a single edge cracked bar in tension, $n=13$ and $a/W=0.4$ would be called *SEC0413*. If the analysis is a modified boundary layer formulation the file is named MBLF.
- read_header
 - Reads the number of items and the label. The label is a number which identifies the type of record (stress, strain etc.)
- read_integer
 - Reads an integer from the input stream.
- read_text
 - Reads a text string from the input.
- read_float
 - Reads a floating number from the input.
- skip_to_end
 - Skip to the end of a record

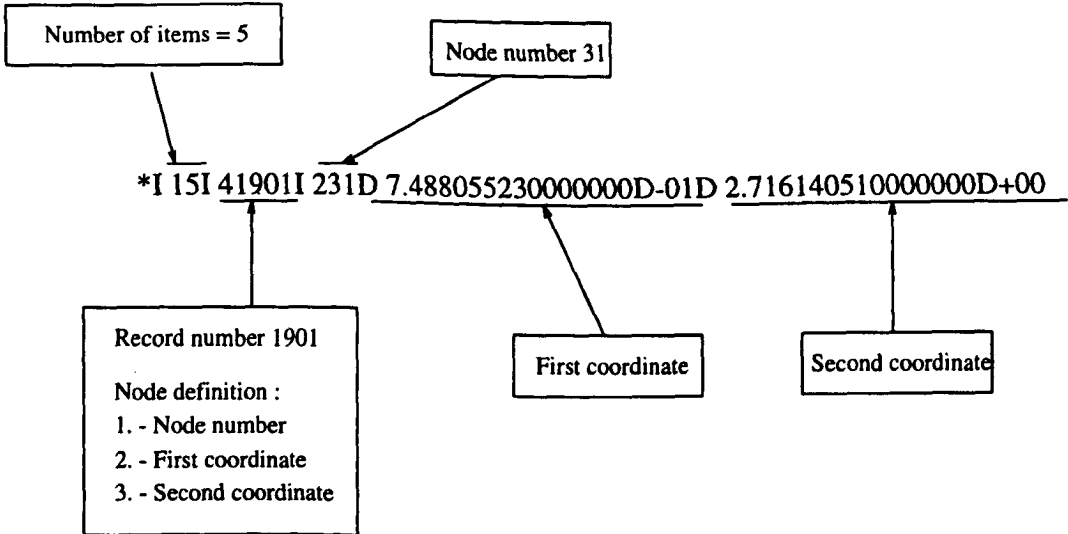


Figure 4.5: *Examples of a record in a FIL file.*

The variables obtained from the FEA analysis and read into Matlab are shown in Table 4.3, the directions 1,2 and 3 correspond to those defined on Figure 4.3 and refer to global axes in the model.

4.2.2 Program: Constraint

The constraint program is a series of sub-programs each of which is used to determine different parameters. Within this program there are various routines for filtering nodes in the ligament, matching with the coordinates and calculating the radius from the coordinates. The more important functions will be described in detail.

Variable	Description
stress11	First stress component
stress22	Second stress component
stress33	Third stress component
stress12	Shear stress
miss	von Mises stress
tres	Tresca stress
hydr	Hydrostatic pressure
princ1	First principal stress
princ2	Second principal stress
princ3	Third principal stress
inv3	Third invariant
strain11	First total strain component
strain22	Second total strain component
strain33	Third total strain component
strain12	Fourth total strain component
pstrain11	First plastic strain component
pstrain22	Second plastic strain component
pstrain33	Third plastic strain component
pstrain12	Fourth plastic strain component
pequist	Equivalent plastic strain
reac_set1	First component of reaction force
reac_set2	Second component of reaction force
Tese	Total elastic strain energy
Tew	Total external work
Tpd	Total plastic dissipation
J	The J integral
coord	Node coordinates in 1 and 2 direction

Table 4.3: Variables from ABAQUS into Matlab.

In fracture mechanics the stresses for different levels of deformation are often compared at a non dimensional distance $\frac{r\sigma_0}{J}$ from the crack tip, the most common distance at which the stress level are compared is $r = \frac{2J}{\sigma_0}$. $\frac{r\sigma_0}{J}$ is a dynamic distance moving away from the crack tip as the deformation level increases. It may be compared with the crack tip opening, as the crack tip opening can be approximated to $\frac{J}{\sigma_0}$ and $\frac{2J}{\sigma_0}$ is then 2 crack tip openings. The program for calculating the stresses at a constant distance is called "Snd_dis": (Stress non dimensionalised with the yield stress for a specific distance $\frac{r\sigma_0}{J}$) and uses a linear interpolation method for calculating the stress at the required distance, which is often $\frac{r\sigma_0}{J}=2$.

The stress intensity factor K_I can be calculated from the applied load through:

$$K_I = \sigma_{app} \sqrt{a\pi} f\left(\frac{a}{W}\right) \quad (4.9)$$

The form functions $f(\frac{a}{w})$ depend on the mode of loading as well as the crack length; the form functions are given in Tada *et al.* (1973). For single edge bending $f(\frac{a}{w})$ was calculated from:

$$f_1(\frac{a}{W}) = 1.122 - 1.40(\frac{a}{W}) + 7.33(\frac{a}{W})^2 - 13.08(\frac{a}{W})^3 + 14.0(\frac{a}{W})^4 \quad (4.10)$$

For the single edge tension bars the form function is expressed by:

$$f(a/W) = 1.12 - 0.23(\frac{a}{W}) + 10.55(\frac{a}{W})^2 - 21.72(\frac{a}{W})^3 + 30.39(\frac{a}{W})^4 \quad (4.11)$$

The form function for centre crack panels as a function of a/W is given in Table 4.4.

a/W	$f(\frac{a}{W})$
0.0	1.0000
0.1	1.0060
0.2	1.0246
0.3	1.0577
0.4	1.1094
0.5	1.1867
0.6	1.3033
0.7	1.4882
0.8	1.8160
0.9	2.5776

Table 4.4: Numerical values of $f(\frac{a}{W})$ for centre crack panels.

The K calibration for the double edge crack was calculated from

$$f(a/W) = 1.122 - 0.561(\frac{a}{W}) - 0.205(\frac{a}{W})^2 + 0.407(\frac{a}{W})^3 - 0.190(\frac{a}{W})^4 \quad (4.12)$$

Equation (4.10), (4.11) and (4.12) and the numerical values given for CCP are shown graphically in Figure 4.6

The total value of the J integral was obtained directly from ABAQUS, J is then divided into two terms - a elastic part calculated from the stress intensity factor K_I and a plastic part calculated as the difference between the J_{Total} and J_E . The program used to calculate J_P , J_E and K_I was called "JK_calc". The elastic part of the J integral J_E is calculated from the stress intensity factor:

$$J_E = \frac{K_I^2}{E}(1 - \nu^2) \quad (4.13)$$

The T stress is calculated in a program called "T_stress". T is calculated from the applied load, the stress intensity factor form function (K -calibration) and the biaxiality parameter.

T is defined through a bi-axiality parameter β :

$$T = \frac{\beta K_I}{\sqrt{a\pi}} \quad (4.14)$$

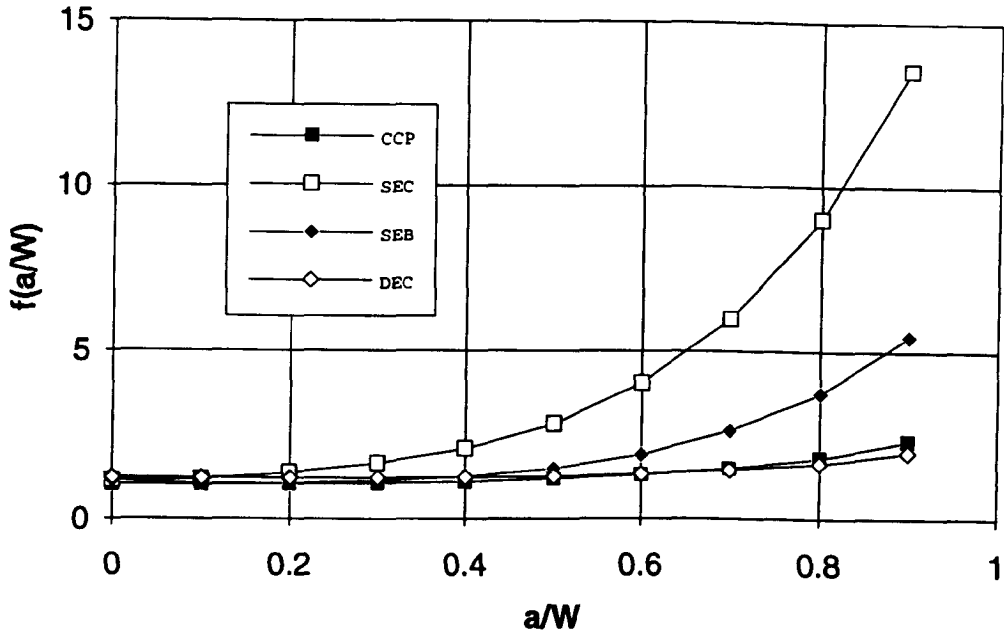


Figure 4.6: Form functions for single edge bend, single edge tension, centre crack panels and double edge cracked bars.

The bi-axiality parameters as given by Sham (1991) are given in Table 3.1 for single edge tension, and in Table 3.2 for single edge bending, the centre crack panels and double edge cracked bars are given in Table 3.3. The bi-axiality parameters for SECB, SECT, CCP and DEC are shown graphically in Figure 4.7.

By combining (4.9) with (4.14) the T stress was calculated more directly from the relation:

$$T = \sigma_{app} f\left(\frac{a}{W}\right) \beta \quad (4.15)$$

Q and σ_{MBLF} were calculated from a program called "Q_stress". Q was calculated as the difference between the stresses at a distance $\frac{r_{\sigma_0}}{2}$ from the crack tip and the small scale yielding field at the same distance. σ_{MBLF} was determined from T and the boundary layer formulation. Another fracture parameter calculated in this function is the hoop stress at a constant distance $\frac{r_{\sigma_0}}{2}$ non dimensionalised by the stress in the modified boundary layer formulation for the same distance from the crack tip.

Results are often presented in terms of the applied load non dimensionalised by the limit load. Limit loads have been determined numerically from non hardening plane strain solutions for the single edge geometries and for the double edge cracked bars. For the centre cracked panels the limit loads were obtained analytically from expressions given by Miller (1987). The limit load for each geometry whether they are calculated analytically or obtained from numerical solutions are determined in a program named "limit_load". The numerical results compare well with the

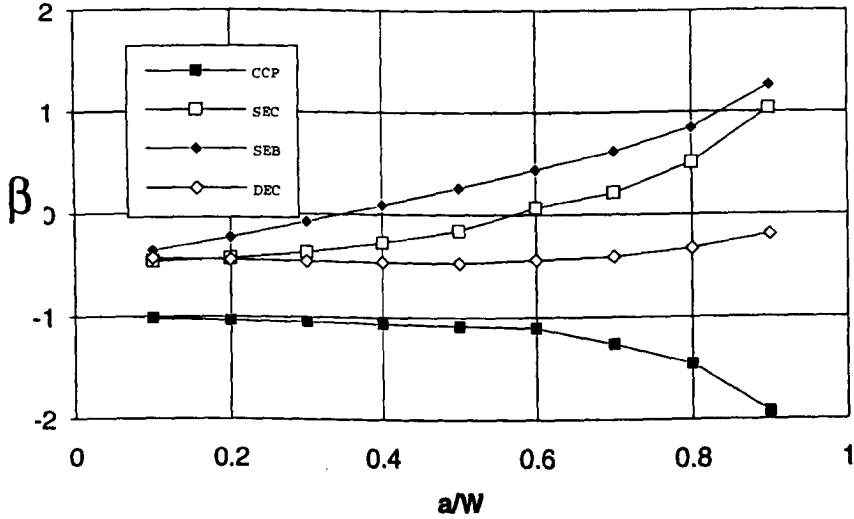


Figure 4.7: Bi-axiality ratio for single edge bend, single edge tension, centre cracked tension and double edge cracked bars geometries.

expressions given by Miller (1987) for edge cracked bars in bending with $a/W \leq 0.295$:

$$M_{Limit} = \frac{1.15W^2\sigma_0}{4} \left(1.261 - 2.72(0.31\frac{a}{W})^2 \right) \left(1 - \frac{a}{W} \right)^2 \quad (4.16)$$

For $a/W > 0.295$

$$M_{Limit} = \frac{1.15W^2\sigma_0}{4} \left(1.261(1 - \frac{a}{W})^2 \right) \quad (4.17)$$

Figure 4.8 compares the results from the non hardening numerical solution with Miller (1987).

For edge cracked bars in force loaded tension the limit load was curve fitted from the non-hardening solution to:

$$P_{Limit} = \left(3.6566(\frac{a}{W})^3 - 6.1261(\frac{a}{W})^2 + 1.4353(\frac{a}{W}) + 1.0922 \right) c\sigma_0 \quad (4.18)$$

Figure 4.9 shows a comparison of the numerical results with those expression given by the curve fit in Equation (4.18).

The limit load for the centre cracked panels were calculated from:

$$P_{Limit} = 2.3094\sigma_0 \frac{(W - a)}{2} \quad (4.19)$$

The limit load for the double edge cracked bars was obtained from the non-hardening solution.

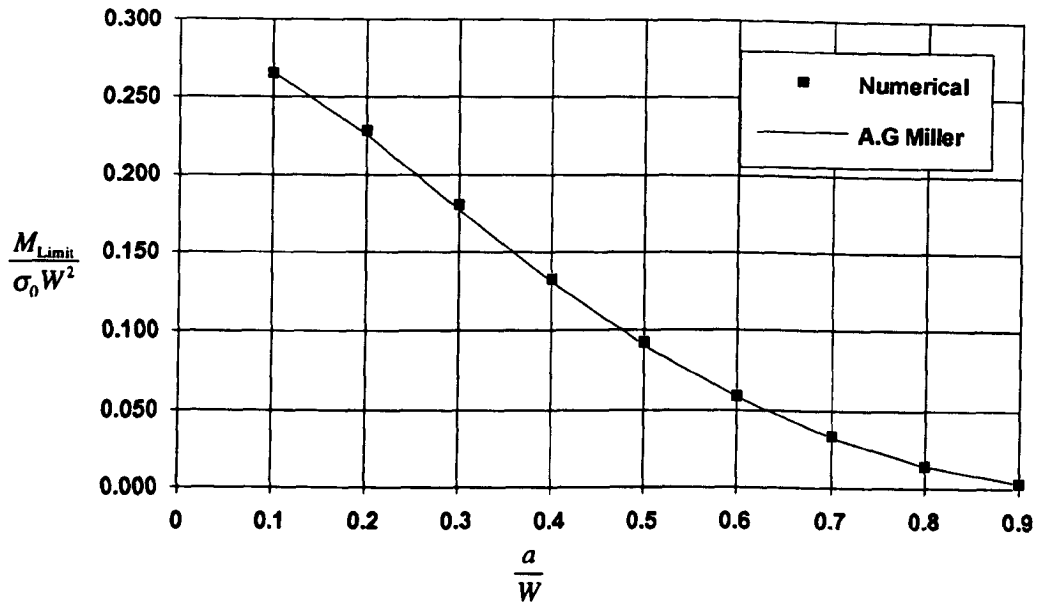


Figure 4.8: Numerical results for the non-dimensionalised limit load of SECB bars compared with Miller's (1987) formula.

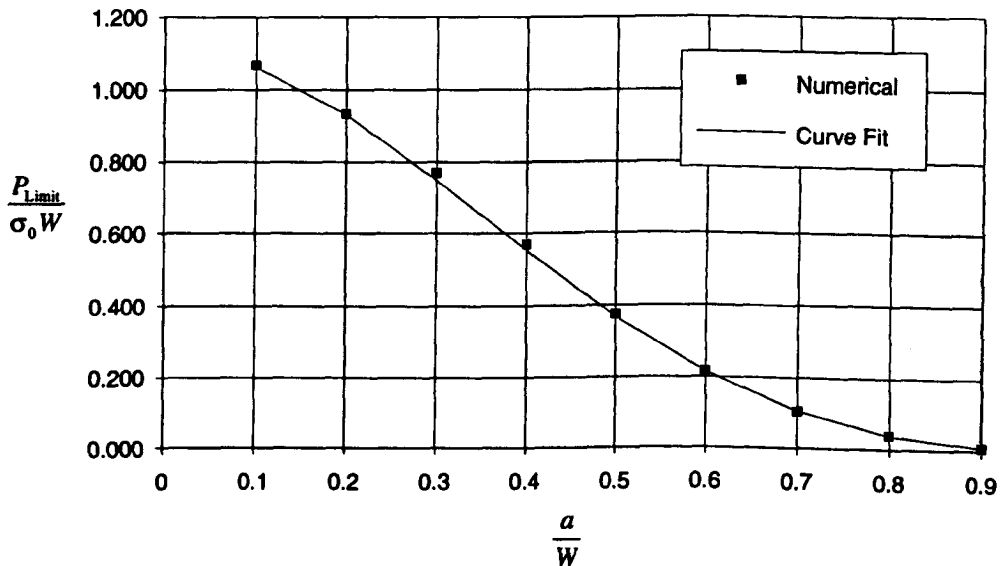


Figure 4.9: Numerical results for the non-dimensionalised limit load of SECT bars compared with a curve fit formula.

Blank Page

Limits to the Characterisation of Crack Tip Fields by One and Two Parameters

In Chapter 3 discussion centred on the characterisation of J dominated crack tip fields. However, McClintock (1971) has argued that single parameter fracture mechanics breaks down for weakly hardening materials in full plasticity due to the lack of uniqueness of the fully plastic flow field. Fracture toughness and the crack tip conditions depend on the size, geometry and loading mode. In this chapter original work is presented using modified boundary formulations to investigate the loss of crack tip constraint. Small scale yielding solutions ($T=0$) are compared with full field solutions and used to define the limits of single parameter fracture mechanics. The limits of two parameter characterisation are defined by comparing full field solutions with modified boundary layer solution. The geometries which have been analysed are single edge crack bars in tension and bending, and centre cracked panels.

5.1 Modified Boundary Layer Formulation Results

Modified boundary layer formulations are now used as a tool to investigate the limits of J dominance and the limits of applicability of J - T characterisation. The model used for the analysis is shown in Figure 4.1, and the applied boundary displacements are given in Equation (4.1). The value of $\frac{T}{\sigma_0}$ applied on the model ranged from -0.9 to 0.9 . Numerical calculations were performed with strain hardening exponents 3, 6, 13 and non-hardening material response in the Ramberg-Osgood stress-strain relation given in Equation (4.3).

Figure 5.1 shows the tangential stress $\sigma_{\theta\theta}$ directly ahead of the crack ($\theta = 0$), for a hardening exponent $n=6$ and $\frac{T}{\sigma_0} = -0.7$. The stresses are normalised by the yield stress σ_0 , while the radial distance r is non-dimensionalised by $\frac{J}{\sigma_0}$. The stress profiles are shown for a range of different deformation levels as an example of self similarity. The data are self similar in the sense that the data obtained for a given value of J falls on the same curve as that for a different value of J . However the stresses fall below the HRR field determined from the tabulated constants of Shih (1983).

Negative values of the T stress reduced the stress level ahead of the crack by an amount independent of the distance $\frac{r\sigma_0}{J}$, but dependent on T , following the observations of Betegón and Hancock (1991). For each hardening rate this gives rise to a family of curves parameterised by T , as shown for the four hardening rates in

Figures 5.2-5.5. Figure 5.2 shows the profile of the tangential stress directly ahead of the crack tip ($\theta=0$) for a range of $\frac{T}{\sigma_0}$ values for a hardening rate $n=3$. The solid line is the HRR field. Similar results are shown for hardening rates $n=6, 13$ and non hardening in Figures 5.3, 5.4 and 5.5.

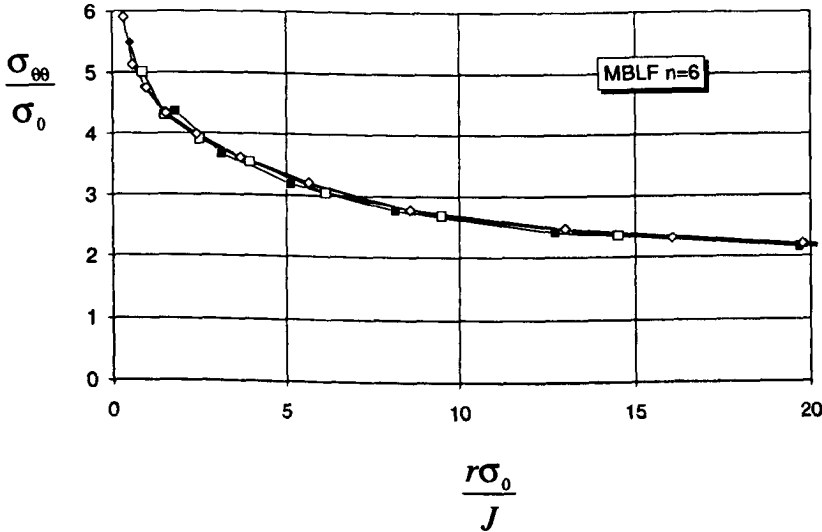


Figure 5.1: *The tangential stress directly ahead of the crack in a boundary layer formulation, $\frac{T}{\sigma_0} = -0.7$, ($n=6$).*

For positive values of T , the stress profile approaches the HRR field and can be characterised by J alone. In contrast negative values of T cause the stresses to fall below the HRR field, requiring a two parameter characterisation. This effect is most significant for materials with a low hardening rate, and weak for strongly hardening materials ($n=3$).

In Figures 5.6 - 5.9 the tangential stress directly ahead of the crack tip has been plotted as a function of T non-dimensionalised by the yield stress for distances $1 \leq \frac{r\sigma_0}{J} \leq 6$ ahead of the crack tip. The stress profiles for the various distances are broadly parallel, which indicates that crack tip constraint (described by T) is independent of distance.

The results in this analysis are compared with results of similar analyses by Wang and Parks (1993) denoted (YW&DP), and by Betegón and Hancock (1991) denoted (CB&JWH). In Figure 5.10 data are given at a distance $\frac{r\sigma_0}{J} = 2$; the non-dimensionalised stress ($\frac{\sigma_{\theta\theta}}{\sigma_0}$) for $\theta = 0$ is plotted against the T -stress normalised by the yield stress. The results from the present analysis are denoted (ADK) and compare favourably with analyses from other sources.

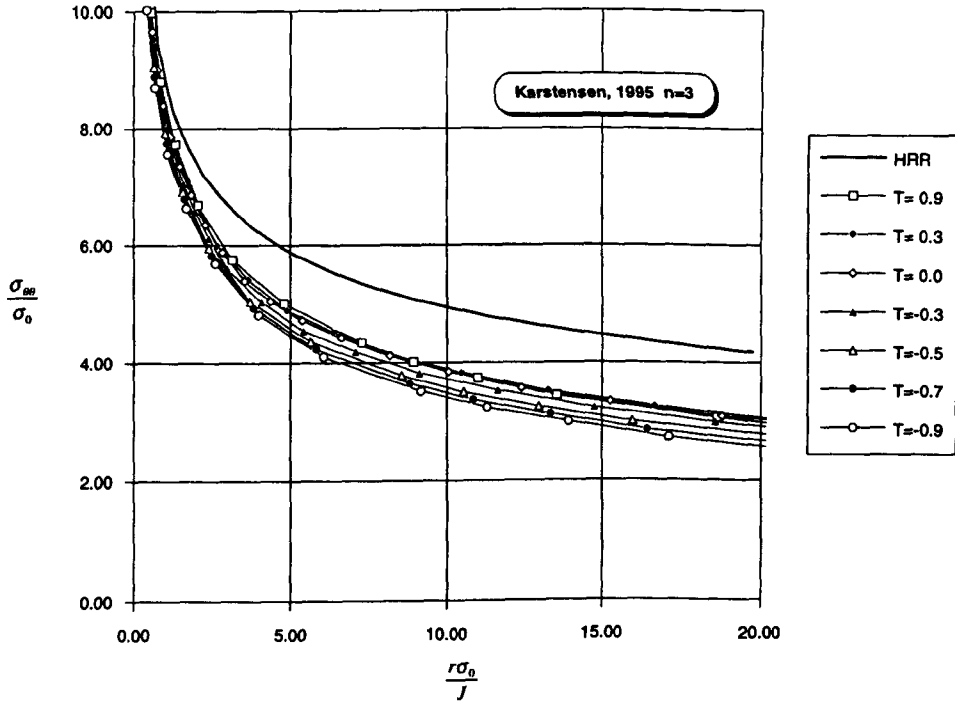


Figure 5.2: *The tangential stress normalised by the yield stress directly ahead of the crack in a modified boundary layer formulation for different values of $\frac{T}{\sigma_0}$, $n=3$.*

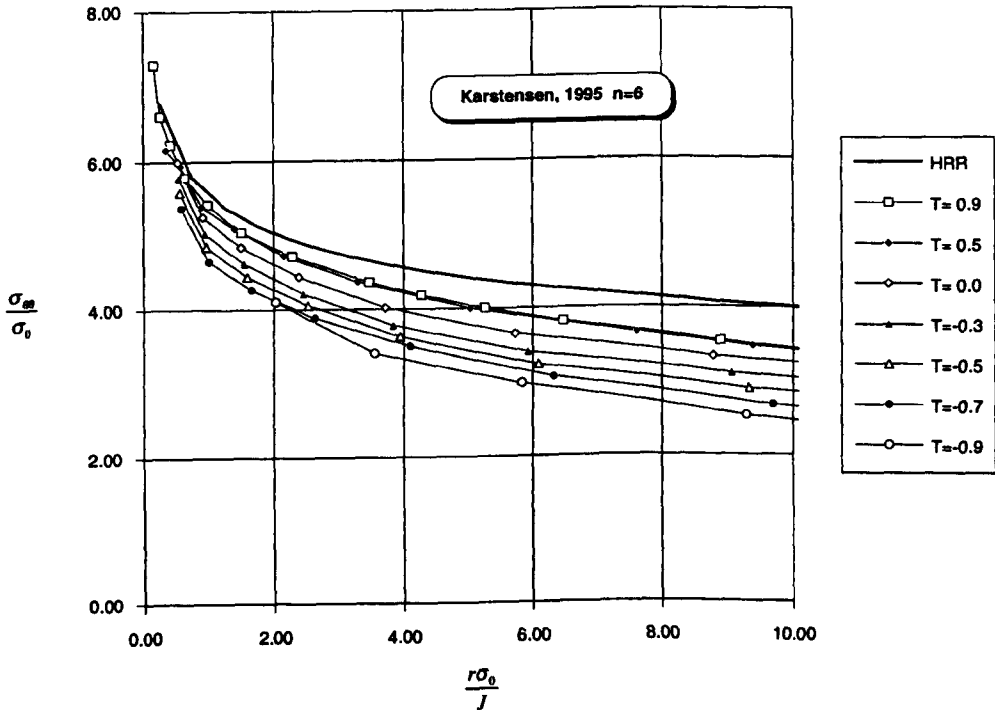


Figure 5.3: *The tangential stress normalised by the yield stress directly ahead of the crack in a modified boundary layer formulation for different values of $\frac{T}{\sigma_0}$, $n=6$.*

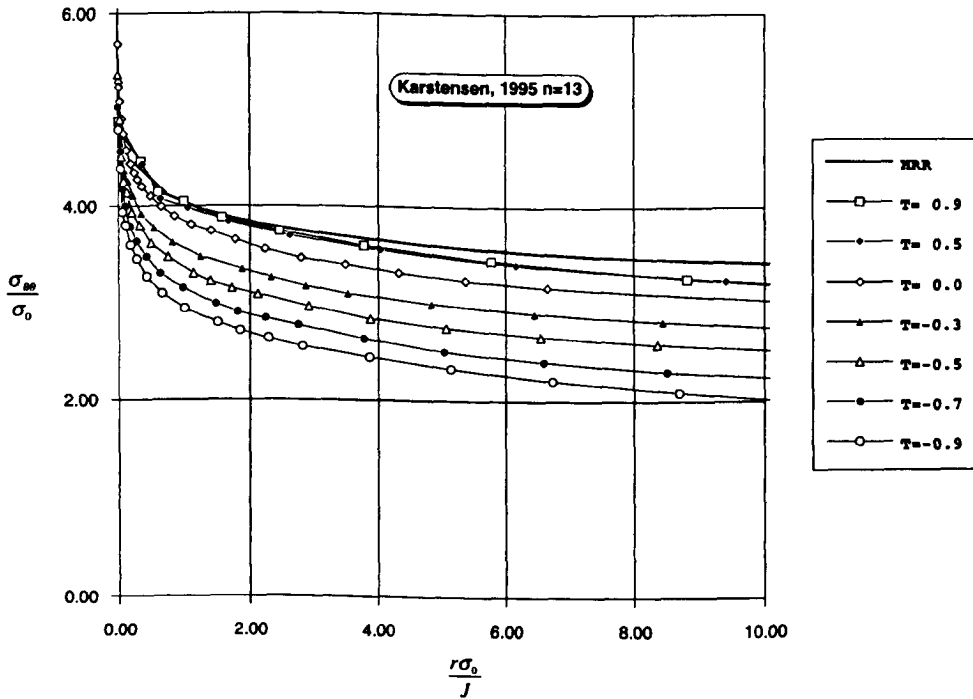


Figure 5.4: The tangential stress normalised by the yield stress directly ahead of the crack in a modified boundary layer formulation for different values of $\frac{T}{\sigma_0}$, $n=13$.

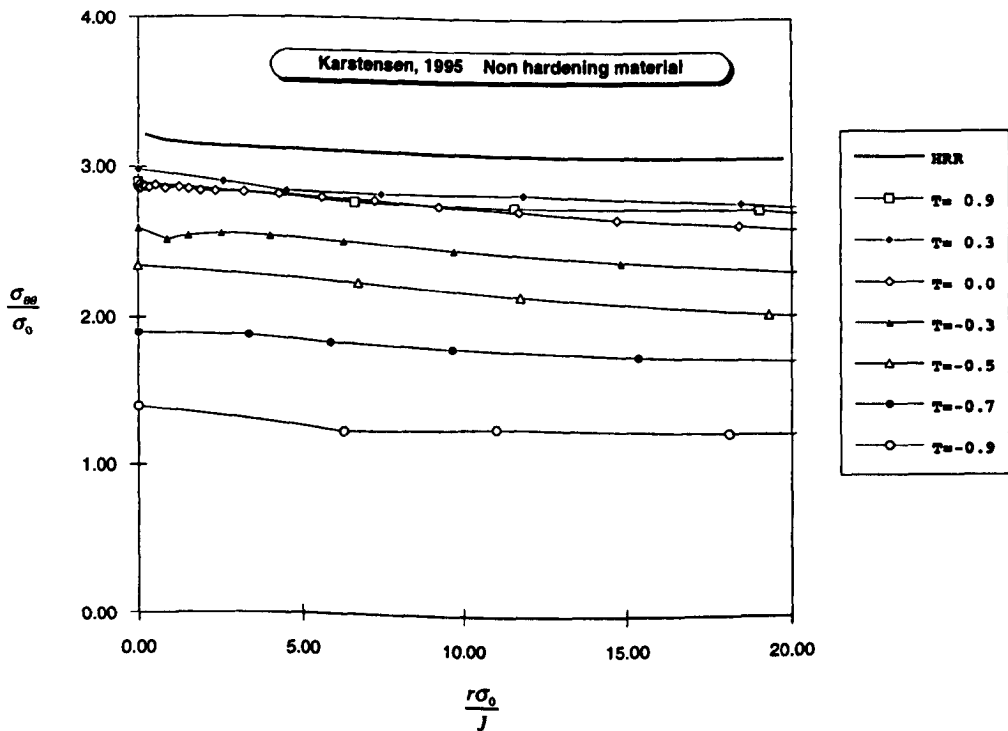


Figure 5.5: The tangential stress normalised by the yield stress directly ahead of the crack in a modified boundary layer formulation for different values of $\frac{T}{\sigma_0}$, non-hardening.

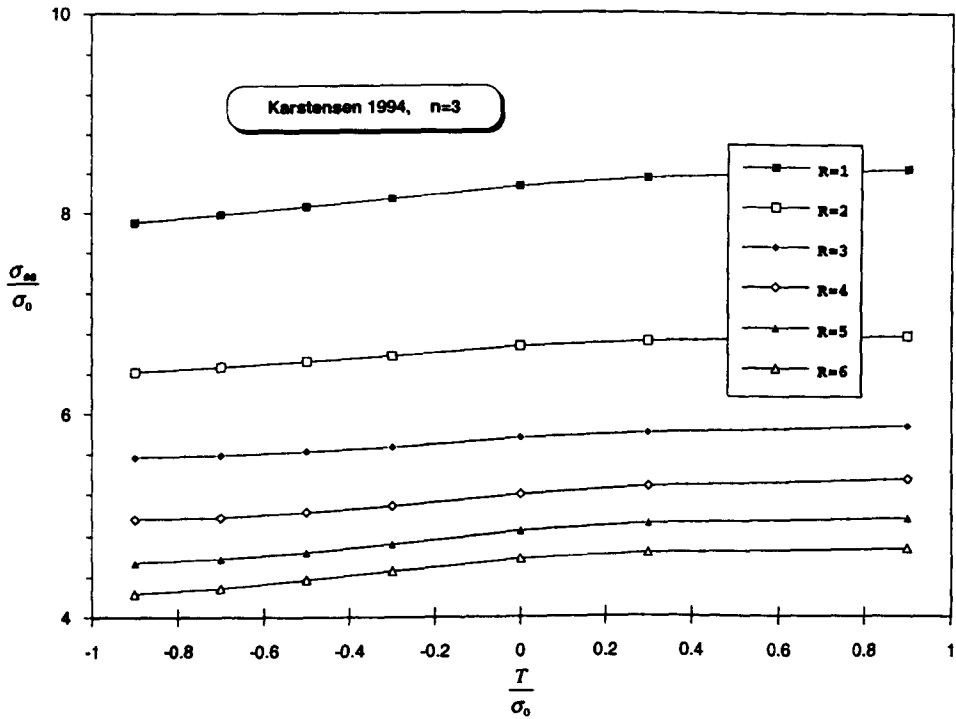


Figure 5.6: The tangential stress normalised by the yield stress at different distances ahead of the crack tip ($R = \frac{r\sigma_0}{T}$) in a modified boundary layer formulation with different values of $\frac{T}{\sigma_0}$, $n=3$.

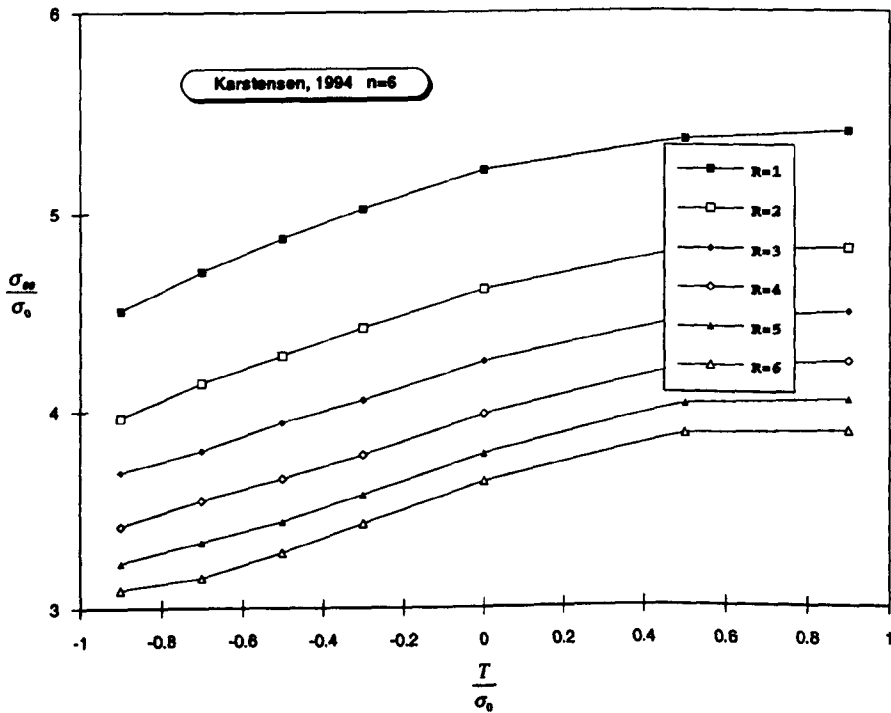


Figure 5.7: The tangential stress normalised by the yield stress at different distances ahead of the crack tip ($R = \frac{r\sigma_0}{T}$) in a modified boundary layer formulation with different values of $\frac{T}{\sigma_0}$, $n=6$.

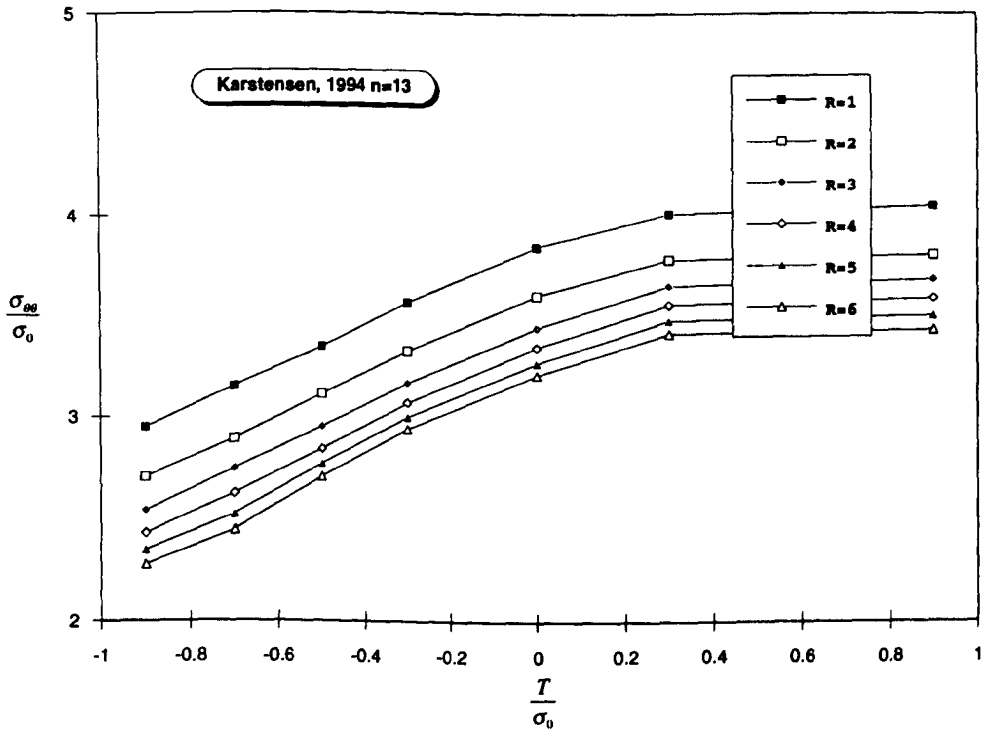


Figure 5.8: The tangential stress normalised by the yield stress at different distances ahead of the crack tip ($R = \frac{r\sigma_0}{T}$) in a modified boundary layer formulation with different values of $\frac{T}{\sigma_0}$, $n=13$.

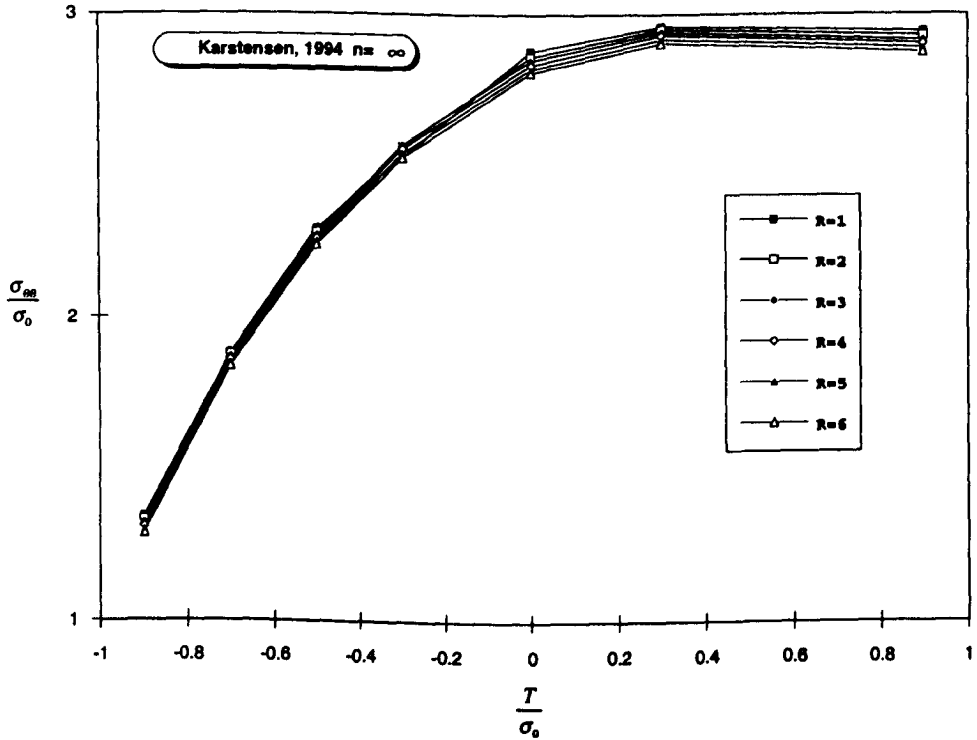


Figure 5.9: The tangential stress normalised by the yield stress at different distances ahead of the crack tip ($R = \frac{r\sigma_0}{T}$) in a modified boundary layer formulation with different values of $\frac{T}{\sigma_0}$, non-hardening.

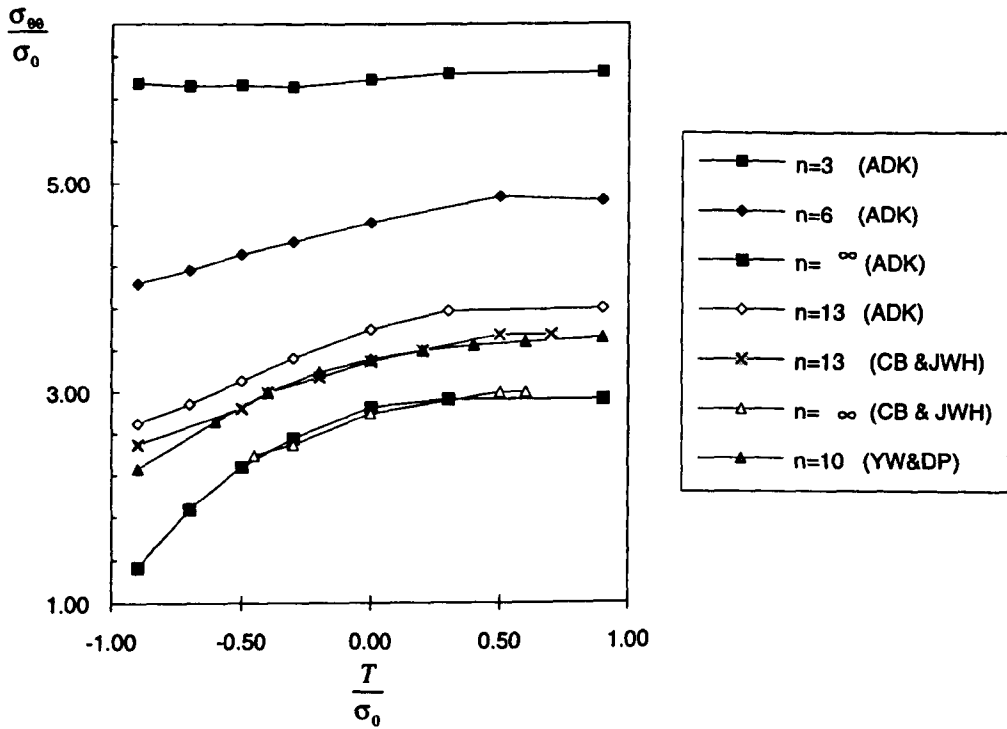


Figure 5.10: The modified boundary layer formulation compared for different strain hardening rates, as the tangential stress normalised by the yield stress directly ahead of the crack tip at a distance $r = \frac{2J}{\sigma_0}$ as a function of $\frac{T}{\sigma_0}$.

In general the stress field in a MBLF can be expressed in the form:

$$\frac{\sigma_{\theta\theta}^{MBLF}(r, J, \frac{T}{\sigma_0})}{\sigma_0} = \frac{\sigma_{\theta\theta}^{SSY}(\frac{r\sigma_0}{J})}{\sigma_0} + \sum_{i=1}^m A_i \left(\frac{T}{\sigma_0}\right)^i \quad (5.1)$$

where A_i are constants which depend on the strain hardening exponent n . A three-term polynomial fit was suggested by Wang (1993) as a modification of the two-term polynomial initially used by Betegón and Hancock (1991). Wang's three-term polynomial fit covered both positive and negative values of T , whereas Betegón and Hancock's two-term polynomial fit was only valid for negative values of T . However a good approximation can be obtained by using a two-term polynomial fit over the whole range of T , positive and negative.

For analysing the limits of J dominance the small scale yielding field (σ_{SSY}) has been chosen as a reference field rather than the HRR field. This field is obtained by applying a pure K field as the boundary conditions ($T=0$). The stress profile has been curve fitted using a least-squares fit as implemented in Matlab V.4. (1991) to an equation of the form:

$$\frac{\sigma_{SSY}}{\sigma_0} = A \left(\frac{J}{\sigma_0 r}\right)^t \quad (5.2)$$

Agreement between the small scale yielding field and the HRR field corresponds to t equal to $\frac{1}{n+1}$. For the four different values of n (3,6,13, ∞) the results for A and t are given in Table 5.1.

n	A	t
3	8.06	0.32
6	5.28	0.21
13	3.83	0.10
∞	2.86	0.02

Table 5.1: *Curve fitting constants for the small scale yielding field.*

The MBLF fields were expressed by two-term polynomials of the form:

$$\frac{\sigma_{MBLF}}{\sigma_0} = \frac{\sigma_{SSY}}{\sigma_0} + a_1 \left(\frac{T}{\sigma_0}\right) + a_2 \left(\frac{T}{\sigma_0}\right)^2 \quad (5.3)$$

Values for a_1 and a_2 in (5.3) for distances $1 < \frac{r\sigma_0}{J} < 5$ are given in Table 5.2, for $\frac{T}{\sigma_0}$ in the range from -1 to 1.

The modified boundary layer formulation for the 4 different hardening rates can be expressed by the equations:

$n=3$:

$$\frac{\sigma_{MBLF}}{\sigma_0}(r, T) = 8.06 \left(\frac{J}{r\sigma_0}\right)^{0.32} + 0.21 \left(\frac{T}{\sigma_0}\right) - 0.08 \left(\frac{T}{\sigma_0}\right)^2 \quad (5.4)$$

$n=6$:

$$\frac{\sigma_{MBLF}}{\sigma_0}(r, T) = 5.28 \left(\frac{J}{r\sigma_0}\right)^{0.21} + 0.48 \left(\frac{T}{\sigma_0}\right) - 0.25 \left(\frac{T}{\sigma_0}\right)^2 \quad (5.5)$$

n	a_1	a_2
3	0.21	-0.08
6	0.48	-0.25
13	0.64	-0.4
∞	0.83	-0.88

Table 5.2: Curve fitting constants for the modified boundary layer formulation.

$n=13$:

$$\frac{\sigma_{MBLF}}{\sigma_0}(r, T) = 3.83 \left(\frac{J}{r\sigma_0} \right)^{0.10} + 0.64 \left(\frac{T}{\sigma_0} \right) - 0.40 \left(\frac{T}{\sigma_0} \right)^2 \quad (5.6)$$

Non-hardening material :

$$\frac{\sigma_{MBLF}}{\sigma_0}(r, T) = 2.86 \left(\frac{J}{r\sigma_0} \right)^{0.02} + 0.83 \left(\frac{T}{\sigma_0} \right) - 0.88 \left(\frac{T}{\sigma_0} \right)^2 \quad (5.7)$$

Equations (5.4)-(5.7) are valid for the range $-1 \leq \frac{T}{\sigma_0} \leq 0$. For positive values of T the small scale yielding field is applied. The results indicate that the second term in the elastic-plastic expansion is a function of T , which is also the second term in the elastic expansion. In both the elastic and elastic-plastic problems the strength of the second term is much weaker than the first term, and is independent of the distance $\frac{r\sigma_0}{J}$.

5.2 T-stress in Full Field Solutions

A series of full field solutions has been analysed. The T stress for single edge bars in tension and bending and centre cracked panels have been calculated and the stress fields have been compared with the modified boundary layer formulations at the same value of $\frac{T}{\sigma_0}$. The methods of the numerical analysis were described in Chapter 4.

The crack tip opening stresses directly ahead of the crack at a distance $\frac{r\sigma_0}{J} = 2$ were determined at each load increment and are shown as a function of $\frac{T}{\sigma_0}$ in Figures 5.11-5.22. T is defined through a biaxiality parameter β and from the stress intensity factor, K :

$$T = \frac{\beta K}{\sqrt{a\pi}} \quad (5.8)$$

Some results of β for the important crack geometries have been given by Sham (1991), Leever and Radon (1983), Kfoury (1986) and Nekkal (1991). Figures 5.11-5.14 show data for the single edge bend bars for hardening rates $n=3,6,13$ and non-hardening. Figures 5.15-5.18 show, results for single edge tension bars, while Figures 5.19-5.22 show the data for centre crack panels. The solid lines indicates the modified boundary layer formulation with $\pm 10\%$ lines. T is proportional to the remote load level, and the curves start at $\frac{T}{\sigma_0} = 0$ corresponding to small scale

yielding. However at very low levels of deformation the distance $\frac{r\sigma_0}{J} = 2$ is very close to the crack tip and the stress gradient is too high to show sensible results. The stress values in Figures 5.11-5.22 are shown for deformation levels from contained yielding to large scale plasticity. At low loads the full field solutions follow the modified boundary layer formulation. As the load increases the full field solutions gradually deviate from the MBL solutions. This is particularly significant for the centre crack panels where even at low level of deformations the stress fields deviate from MBLF solutions as the T-stress for moderate load levels exhibit negative values well beyond $\frac{T}{\sigma_0} = -1$ where the boundary layer formulation is valid. The results shown in Figures 5.11- 5.22 establish a basis for the analysis of limits for J dominance and the limits for J - T characterisation which will now be examined.

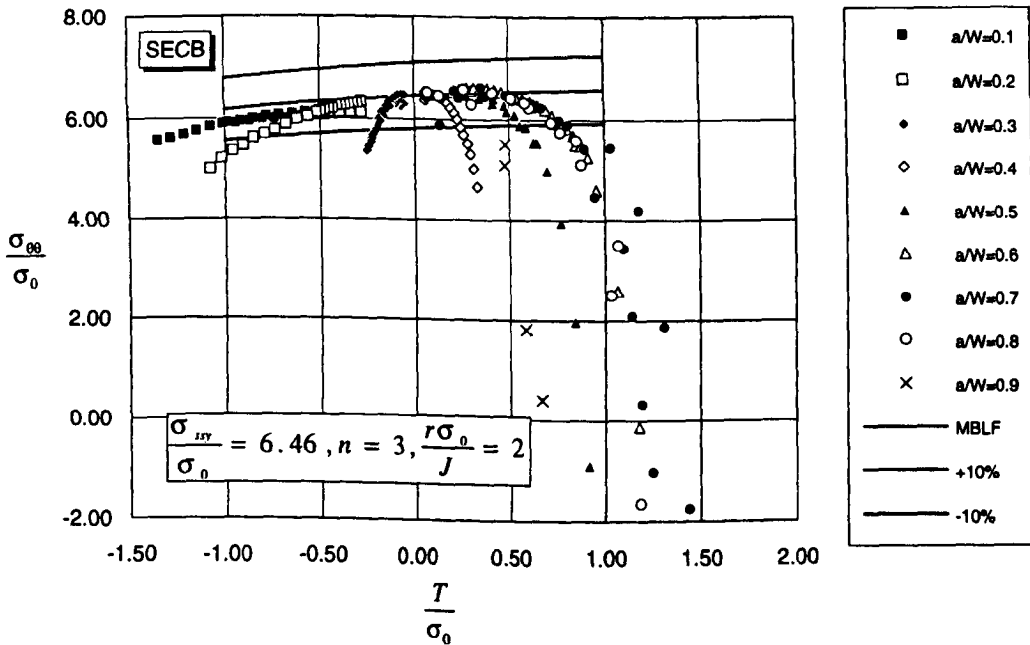


Figure 5.11: *The tangential stress normalised by the yield stress as a function of $\frac{T}{\sigma_0}$ directly ahead of the crack tip at a distance $\frac{r\sigma_0}{J} = 2$. Single edge cracked bend bars, $n=3$.*

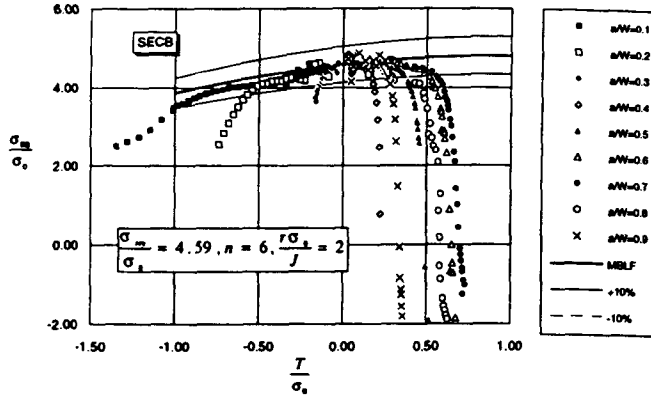


Figure 5.12: The tangential stress normalised by the yield stress as a function of $\frac{T}{\sigma_0}$ directly ahead of the crack tip at a distance $\frac{r\sigma_0}{J} = 2$. Single edge cracked bend bars, $n=6$.

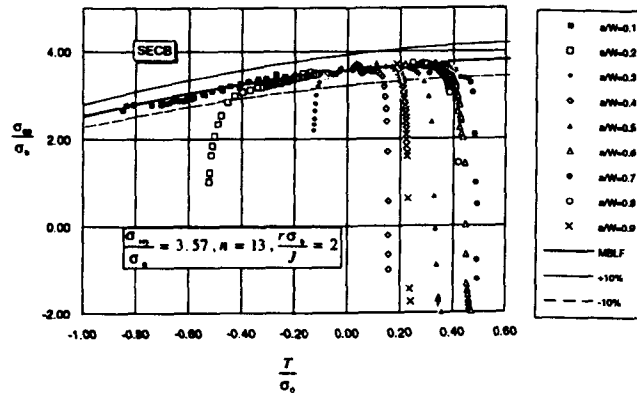


Figure 5.13: The tangential stress normalised by the yield stress as a function of $\frac{T}{\sigma_0}$ directly ahead of the crack tip at a distance $\frac{r\sigma_0}{J} = 2$. Single edge cracked bend bars, $n=13$.

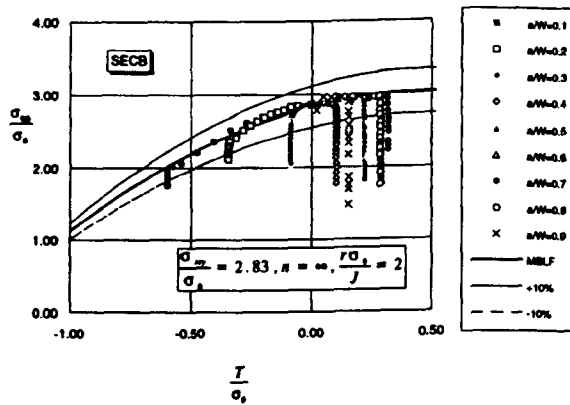


Figure 5.14: The tangential stress normalised by the yield stress as a function of $\frac{T}{\sigma_0}$ directly ahead of the crack tip at a distance $\frac{r\sigma_0}{J} = 2$. Single edge cracked bend bars, non-hardening.

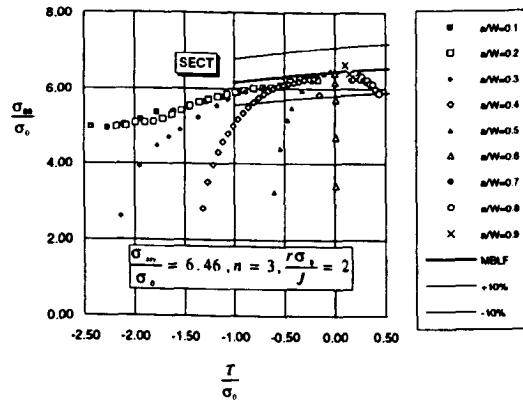


Figure 5.15: The tangential stress normalised by the yield stress as a function of $\frac{T}{\sigma_0}$ directly ahead of the crack tip at a distance $\frac{r\sigma_0}{J} = 2$. Single edge cracked bars in tension, $n=3$.

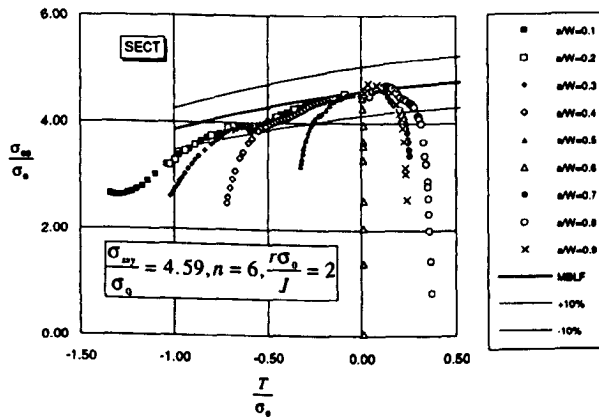


Figure 5.16: The tangential stress normalised by the yield stress as a function of $\frac{T}{\sigma_0}$ directly ahead of the crack tip at a distance $\frac{r\sigma_0}{J} = 2$. Single edge cracked bars in tension, $n=6$.

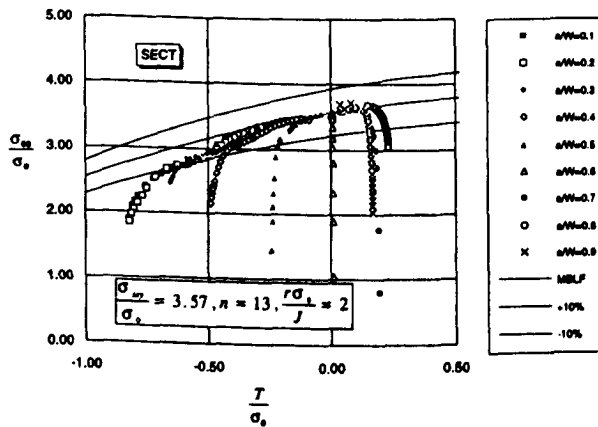


Figure 5.17: The tangential stress normalised by the yield stress as a function of $\frac{T}{\sigma_0}$ directly ahead of the crack tip at a distance $\frac{r\sigma_0}{J} = 2$. Single edge cracked bars in tension, $n=13$.

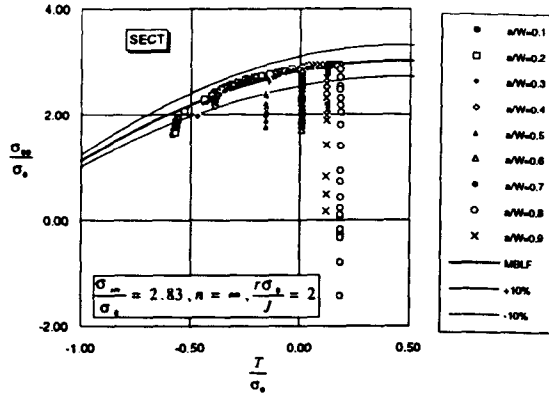


Figure 5.18: The tangential stress normalised by the yield stress as a function of $\frac{T}{\sigma_0}$ directly ahead of the crack tip at a distance $\frac{r\sigma_0}{J} = 2$. Single edge cracked bars in tension, non-hardening.

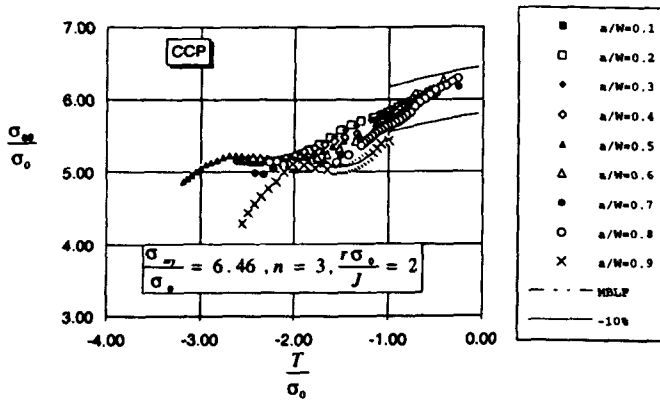


Figure 5.19: The tangential stress normalised by the yield stress as a function of $\frac{T}{\sigma_0}$ directly ahead of the crack tip at a distance $\frac{r\sigma_0}{J} = 2$. Centre cracked panels, $n=3$.

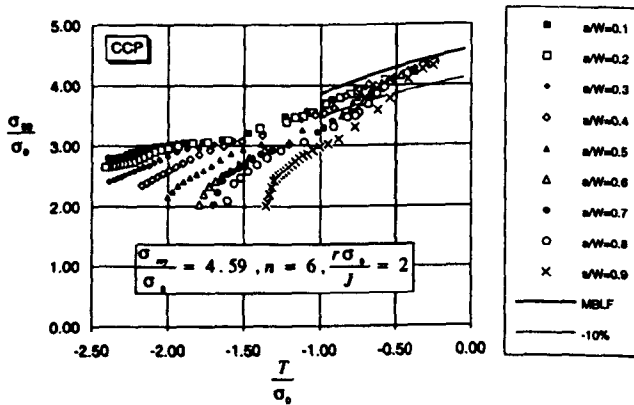


Figure 5.20: The tangential stress normalised by the yield stress as a function of $\frac{T}{\sigma_0}$ directly ahead of the crack tip at a distance $\frac{r\sigma_0}{J} = 2$. Centre cracked panels, $n=6$.

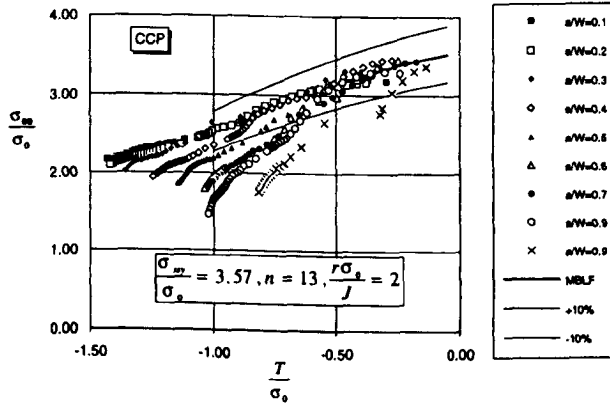


Figure 5.21: The tangential stress normalised by the yield stress as a function of $\frac{T}{\sigma_0}$ directly ahead of the crack tip at a distance $\frac{r\sigma_0}{J} = 2$. Centre cracked panels, $n=13$.

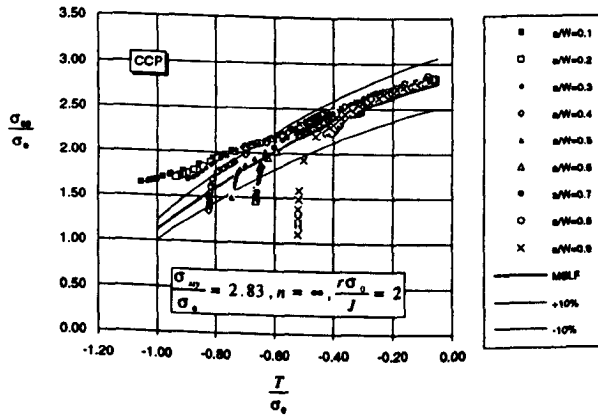


Figure 5.22: The tangential stress normalised by the yield stress as a function of $\frac{T}{\sigma_0}$ directly ahead of the crack tip at a distance $\frac{r\sigma_0}{J} = 2$. Centre cracked panels, non-hardening.

5.3 Limits for One Parameter Characterisation

Shih and German (1981) suggested a J -dominance criterion which requires that the stress field is within 10 % of the HRR field at a distance $r_y^{\sigma_0} = 2$ ahead of the crack tip. In the current work the small scale yielding field has been used as a reference field, rather than the HRR field. However the Shih and German 10% principle for the limits of J -dominance has been maintained. Figure 5.23 shows the stresses for single edge bend bars at a distance $r_y^{\sigma_0} = 2$ ahead of the crack; in Figure 5.24 the results for single edge tension bars are shown, while Figure 5.25 shows results for centre cracked panels. Results for each geometry are shown at 4 different hardening rates.

The stresses non-dimensionalised by the small scale yielding field are plotted as a function of the deformation level given in terms of $\frac{\sigma}{\sigma_0}$, where c is the width of the ligament ($W-a$). The graphs also show the small scale yielding field $\pm 10\%$. The breakdown of single parameter characterisation, is defined as the level of deformation, although the stress field is no longer described as the small scale yielding field $\pm 10\%$. The values of $\frac{\sigma}{\sigma_0}$ under which single parameter characterisation breaks down are given in Table 5.3 for the SECB, in Table 5.4 for the SECT and for the CCP in Table 5.5. Those data are shown graphically in Figure 5.26, where $\frac{\sigma}{\sigma_0}$ are plotted as a function of the a/W ratio for hardening rates $n=3, 6, 13$ and non-hardening.

Deeply cracked edge geometries, $a/W \geq 0.3$ for bending and $a/W \geq 0.5$ for tension, exhibit deformation fields in which the plasticity is confined to the uncracked ligament where the deformation field consists of a plastic hinge which is independent of the a/W ratio. As the deformation for deeply cracked bars is independent of a/W the stress fields all break down at the same level of deformation independent of the a/W ratio as shown in Figures 5.23 and 5.24. For the shallow cracked bars, plasticity extends to the cracked face and the stress field breaks down at a deformation level which is dependent on the a/W ratio.

Linear elastic fracture mechanics (LEFM) can be applied when crack tip plasticity is a minor perturbation of the elastic ($T=0$) field. Under these conditions the material can largely be regarded as linear elastic given that the well contained plastic zone is dominated by a surrounding linear elastic field. Valid LEFM is ensured if the specimen dimensions are large compared to the size of the plastic zone r_y . The plastic zone maybe compared with either the crack length a , the ligament ($W - a$) or the thickness B . The requirements given by ASTM (1983) are:

$$a, (W - a), B \geq 2.5 \left(\frac{K_{Ic}}{\sigma_0} \right)^2 \quad (5.9)$$

K_{Ic} is the critical plane strain value of the stress intensity factor. For plane strain LEFM the relation between J and K is

$$J = \frac{K^2}{E} (1 - \nu^2) \quad (5.10)$$

Inserting the J - K relationship into the ASTM size requirement

$$a, c \geq \frac{2.5JE}{(1 - \nu^2)\sigma_0^2} \quad (5.11)$$

for $\frac{\sigma_0}{E} = 1 - 2 \cdot 10^{-3}$ the ASTM requirement for small scale yielding conditions at fracture, and valid LEFM is then given as ($\nu = 0.3$)

$$\frac{a\sigma_0}{J}, \frac{c\sigma_0}{J} \geq 1000 - 2000 \quad (5.12)$$

Under small scale yielding conditions, a single parameter (e.g. K , J or CTOD) characterises the crack tip conditions and can be used as a geometry-independent fracture criterion. To identify the limits for one parameter characterisation of the crack tip stress field, the hoop stress at a distance $\frac{2J}{\sigma_0}$ ahead of the crack has been compared with the small scale yielding fields.

A valid K_{Ic} result is a material property that does not depend on the size or geometry of the cracked body. However geometries such as centre cracked panels and shallow edge cracked bars are incapable of maintaining significant triaxiality even within contained yielding in material with very weak strain hardening. Shallow cracked edge bars which exhibit a compressive T stress lose J dominance at low levels of deformation. For the shallow single edge cracked bars in bending and tension, single parameter characterisation seems to be lost for very low level of deformation characterised by $\frac{a\sigma_0}{J}$. This indicates that the crack length is the controlling dimension rather than the ligament. For a single edge crack bar in tension and bending $a/W = 0.1$, non-hardening and $n=13$ the breakdown of a K -characterisation occurs at $\frac{a\sigma_0}{J} = 3200$, the limit calculated in terms of the crack length extend the single parameter characterisation to $\frac{a\sigma_0}{J} = 360$. For a SECB $a/W = 0.2$, $n=13$ the breakdown occurs at $\frac{a\sigma_0}{J} = 500$. The deeply edge crack bars do not break the $\pm 10\%$ line until a typical value of $\frac{a\sigma_0}{J} = 25$, independent of a/W ratio and hardening rate.

The J -integral extends single parameter characterisation beyond the limits of LEFM, however single parameter characterisation by J eventually breaks down too. In non-hardening for an $a/W = 0.2$ bend bar single parameter characterisation breaks down at $\frac{a\sigma_0}{J} = 1200$. However strain hardening extends single parameter characterisation, for example for $n=6$ the SECB $a/W = 0.2$ breakdown is at $\frac{a\sigma_0}{J} = 100$. Specimens with positive T stress maintain J dominance until the crack tip opening becomes a significant fraction of the ligament and J dominance is lost at $25J/\sigma_0$, due to the compressive part of the bending field approaching the crack tip field.

a/W	n=3	n=6	n=13	n=∞
	$\frac{c\sigma_0}{J} \geq$	$\frac{c\sigma_0}{J} \geq$	$\frac{c\sigma_0}{J} \geq$	$\frac{c\sigma_0}{J} \geq$
0.1	160	1600	≈ 3200	≈ 5000
0.2	60	100	500	1200
0.3	40	40	40	50
0.4	20	20	20	30
0.5	20	20	20	30
0.6	20	20	20	30
0.7	20	20	20	30
0.8	20	20	20	30
0.9	20	20	20	30

Table 5.3: *Limits for one parameter characterisation of single edge cracked bend bars.*

a/W	n=3	n=6	n=13	n=∞
	$\frac{c\sigma_0}{J} \geq$	$\frac{c\sigma_0}{J} \geq$	$\frac{c\sigma_0}{J} \geq$	$\frac{c\sigma_0}{J} \geq$
0.1	280	≈ 3000	≈ 5000	≈ 5000
0.2	60	1000	2000	3500
0.3	40	500	1000	1000
0.4	25	120	300	450
0.5	20	45	60	100
0.6	20	20	20	25
0.7	20	20	20	25
0.8	20	20	20	25
0.9	20	20	20	25

Table 5.4: *Limits for one parameter characterisation for single edge cracked tension bars.*

a/W	n=3	n=6	n=13	n=∞
	$\frac{c\sigma_0}{J} \geq$	$\frac{c\sigma_0}{J} \geq$	$\frac{c\sigma_0}{J} \geq$	$\frac{c\sigma_0}{J} \geq$
0.1	3000	≈ 5000	≈ 5000	≈ 5000
0.2	1200	4800	≈ 5000	≈ 5000
0.3	800	3200	4600	≈ 5000
0.4	550	2000	2800	≈ 5000
0.5	400	1300	1800	≈ 5000
0.6	350	950	1600	4000
0.7	280	800	1200	2800
0.8	250	750	1100	2000
0.9	250	600	900	1800

Table 5.5: *Limits for one parameter characterisation for centre cracked panels.*

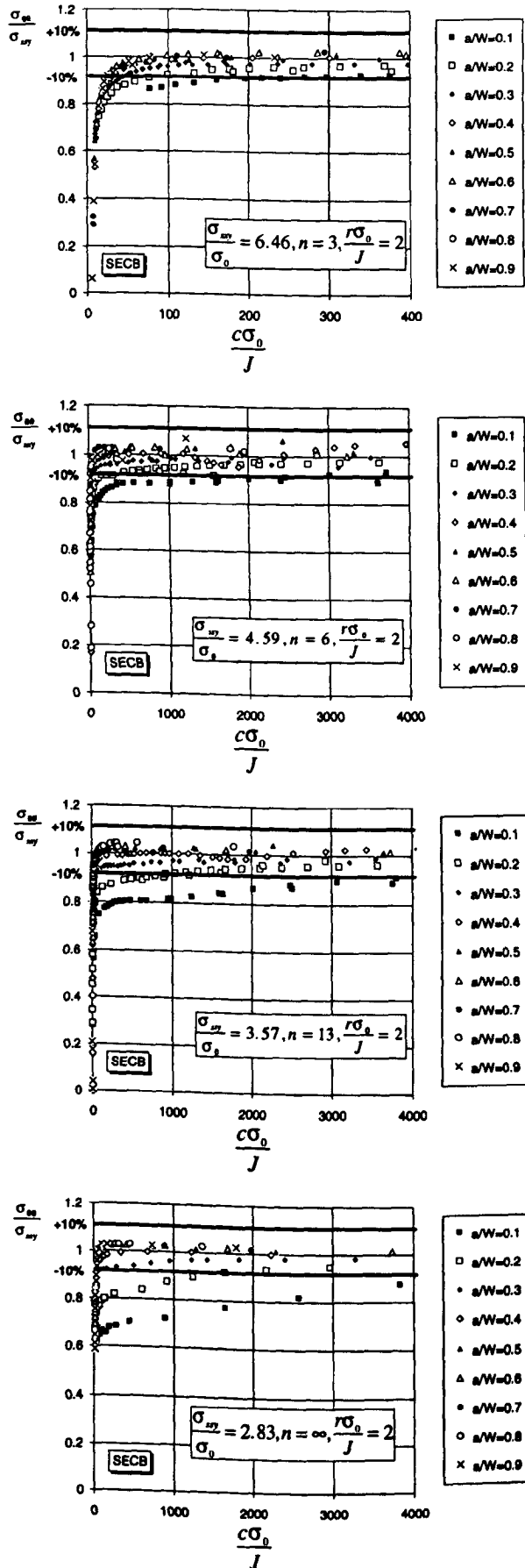


Figure 5.23: The stresses directly ahead of a crack in edge cracked bend bars normalised by the small scale yielding field at a distance $\frac{r\sigma_0}{J} = 2$ as a function of $\frac{c\sigma_0}{J}$.

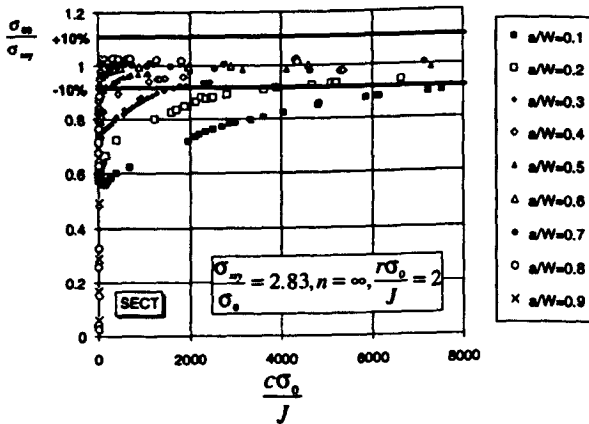
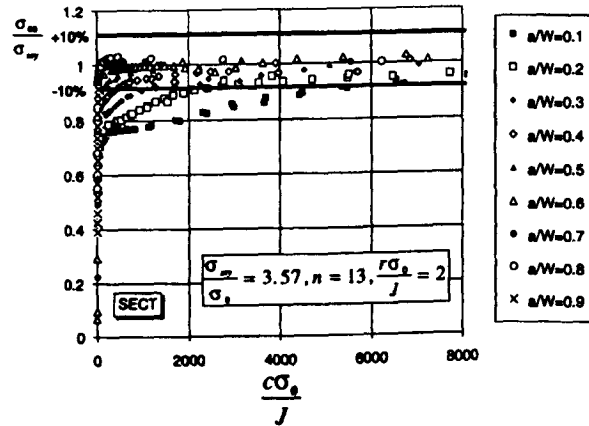
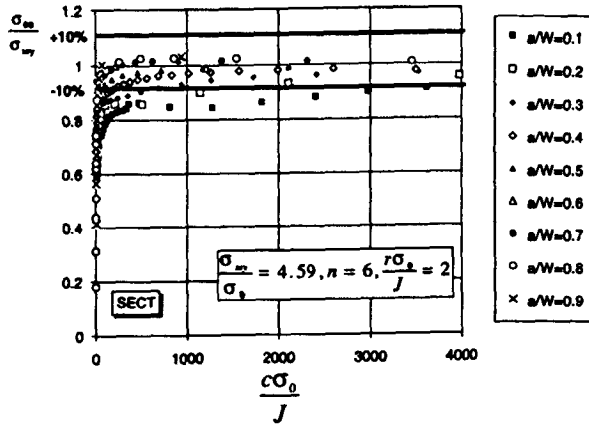
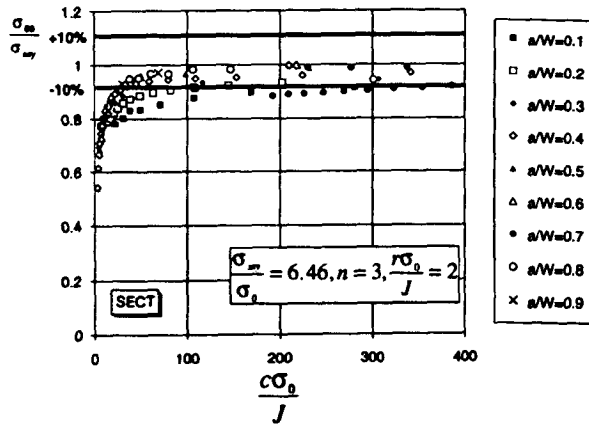


Figure 5.24: The stresses directly ahead of a crack in edge cracked bars in tension normalised by the small scale yielding field at a distance $\frac{r\sigma_0}{J} = 2$ as a function of $\frac{c\sigma_0}{J}$.

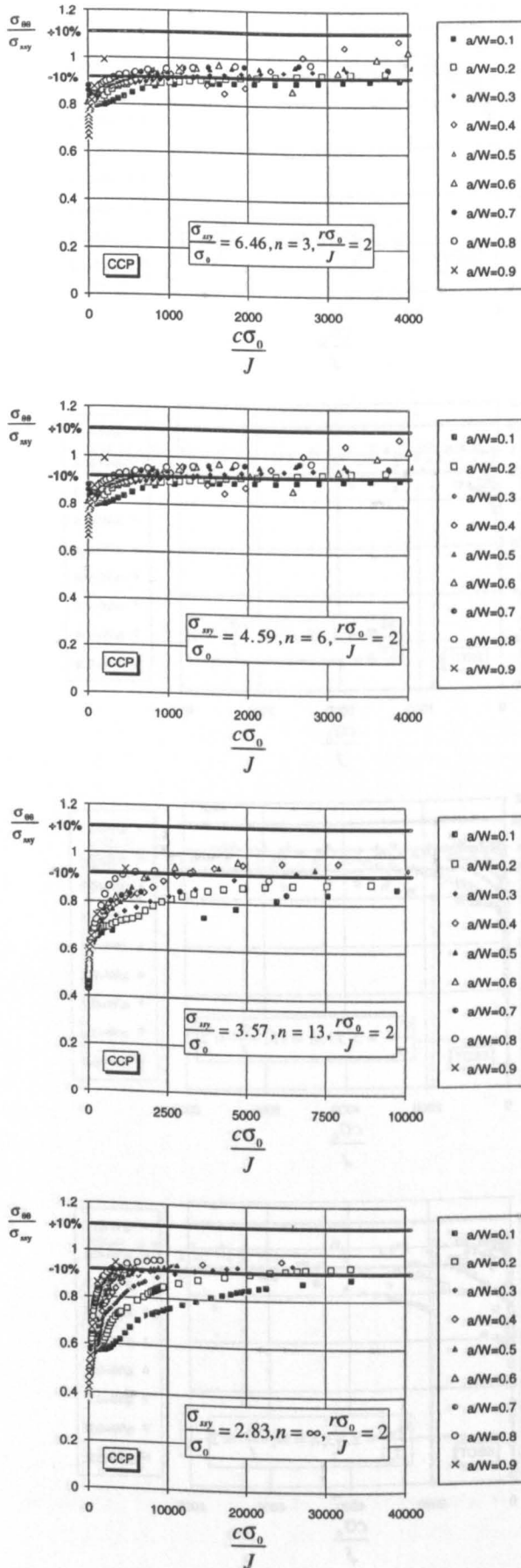


Figure 5.25: The stresses directly ahead of a crack in centre cracked panels normalised by the small scale yielding field at a distance $\frac{r\sigma_0}{J} = 2$ as a function of $\frac{c\sigma_0}{J}$.

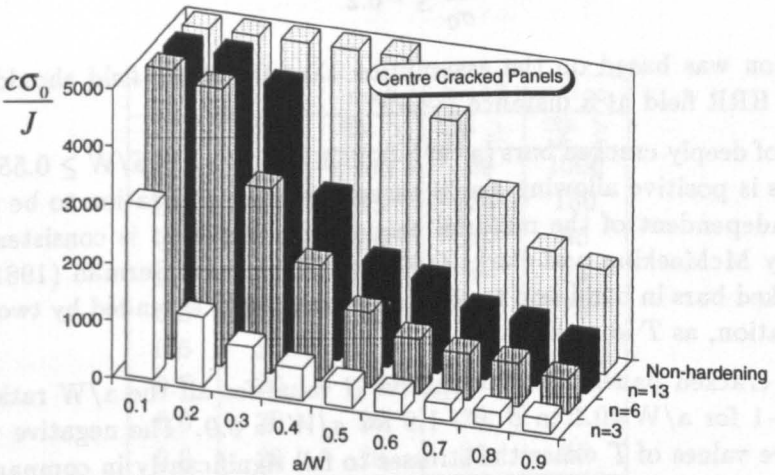
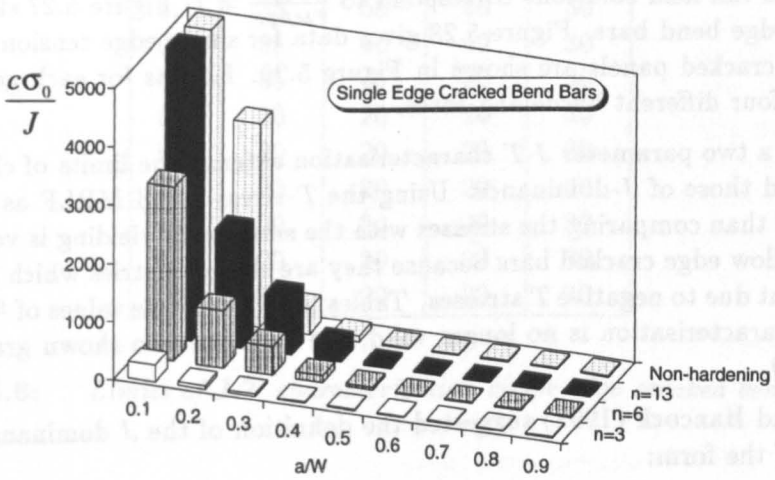
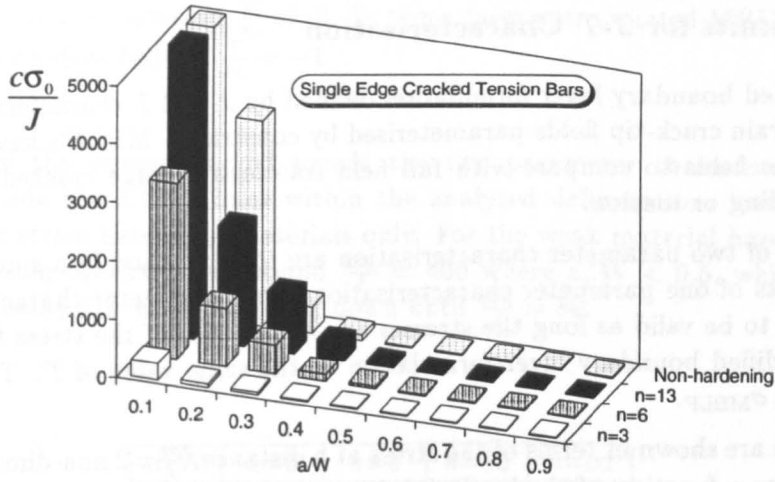


Figure 5.26: $\frac{c\sigma_0}{J}$ at the break down of single parameter characterisation for SECB, SECT and CCP, for hardening rates $n=3, 6, 13$ and non-hardening.

5.4 Limits for Two Parameter Characterisation

5.4.1 Limits for J - T Characterisation

The modified boundary layer formulation defined by J and T characterises a family of plane strain crack-tip fields parameterised by constraint. MBLF's have been used as reference fields to compare with full field solutions of edge cracked bars under either bending or tension.

The limits of two parameter characterisation are to be defined in a similar manner to the limits of one parameter characterisation. Two parameter characterisation is considered to be valid as long the stresses are within 10% of the stress field defined by the modified boundary layer formulation at the same value of T . This stress is denoted as σ_{MBLF} .

The results are shown in terms of the stress at a distance $r\sigma_0=2$ non-dimensionalised by σ_{MBLF} as a function of the level of deformation $\frac{\sigma_{\theta\theta}}{\sigma_0}$. Perfect agreement between MBLF's and full field solutions correspond to $\frac{\sigma_{\theta\theta}}{\sigma_{\text{MBLF}}} = 1$. Figure 5.27 shows results for single edge bend bars. Figure 5.28 gives data for single edge tension bars, while the centre cracked panels are shown in Figure 5.29. Results for each geometry are shown for four different hardening rates.

The use of a two parameter J - T characterisation extends the limits of characterisation beyond those of J -dominance. Using the T -stress based MBLF as a reference field rather than comparing the stresses with the small scale yielding is very effective for the shallow edge cracked bars because they are the geometries which display loss of constraint due to negative T stresses. Tables 5.6-5.8 give the values of $\frac{\sigma_{\theta\theta}}{\sigma_0}$ at which the J - T characterisation is no longer valid, the data are also shown graphically in Figure 5.30.

Betegón and Hancock (1991) suggested the definition of the J dominance criterion could be of the form:

$$\frac{T}{\sigma_0} \leq -0.2 \quad (5.13)$$

This criterion was based on the assumption that the stress field should be within 10% of the HRR field at a distance $r\sigma_0=2$.

In the case of deeply cracked bars ($a/W \geq 0.35$ in bending and $a/W \geq 0.55$ in tension) the T stress is positive allowing single parameter characterisation to be maintained until $\frac{20J}{\sigma_0}$ independent of the material hardening. This limit is consistent with $\frac{25J}{\sigma_0}$ proposed by McMeeking and Parks (1979) and Shih and German (1981). For the deeply cracked bars in bend and tension, this limit is not extended by two parameter characterisation, as T is positive.

The centre cracked panels have a negative β value for all the a/W ratios, ranging from $\beta = -1$ for $a/W=0.1$ to $\beta = -1.9$ for $a/W = 0.9$. The negative values of β and negative values of T cause the stresses to fall significantly in comparison to the small scale yielding field, and single parameter characterisation to break down even for very low levels of deformation.

Two parameter J - T characterisation extends the characterisation of the stress field for the centre cracked panels, but this depends on the way the modified

boundary layer formulation is extended beyond $\frac{T}{\sigma_0} = -1$ as some of the shallow cracked geometries result in values of $\frac{T}{\sigma_0}$ of -3. In these cases extrapolated MBLF solutions were used for values beyond $\frac{T}{\sigma_0} = -1$.

For some of the centre cracked panels the two parameter characterisation did not fall outside the $\pm 10\%$ lines within the analysed deformations level; this was observed for strain hardening materials only. For the weak material hardening J - T characterisation breaks down around $\frac{c\sigma_0}{J} = 400$ where $a/W < 0.5$, while for high hardening ($n=3$) J - T does not break down until $\frac{c\sigma_0}{J} = 80$.

a/W	$n=3$	$n=6$	$n=13$	$n=\infty$
	$\frac{c\sigma_0}{J} \geq$	$\frac{c\sigma_0}{J} \geq$	$\frac{c\sigma_0}{J} \geq$	$\frac{c\sigma_0}{J} \geq$
0.1	35	50	65	30
0.2	35	40	40	30
0.3	35	40	30	30
0.4	20	20	20	30
0.5	20	20	20	30
0.6	20	20	20	30
0.7	20	20	20	30
0.8	20	20	20	30
0.9	20	20	20	30

Table 5.6: *Limits of J-T characterisation single edge cracked bend bars.*

a/W	$n=3$	$n=6$	$n=13$	$n=\infty$
	$\frac{c\sigma_0}{J} \geq$	$\frac{c\sigma_0}{J} \geq$	$\frac{c\sigma_0}{J} \geq$	$\frac{c\sigma_0}{J} \geq$
0.1	30	100	180	1000
0.2	20	25	120	160
0.3	20	20	20	50
0.4	20	20	20	25
0.5	20	20	20	25
0.6	20	20	20	25
0.7	20	20	20	25
0.8	20	20	20	25
0.9	20	20	20	25

Table 5.7: *Limits of J-T characterisation for single edge cracked tension bars.*

a/W	n=3	n=6	n=13	n=∞
	$\frac{\sigma_0}{J} \geq$	$\frac{\sigma_0}{J} \geq$	$\frac{\sigma_0}{J} \geq$	$\frac{\sigma_0}{J} \geq$
0.1	-	75	200	≈ 5000
0.2	-	25	50	3200
0.3	-	-	-	2000
0.4	-	-	-	280
0.5	-	-	300	420
0.6	-	260	350	500
0.7	80	280	400	400
0.8	80	250	400	450
0.9	80	300	500	450

Table 5.8: Limits of J - T characterisation for centre cracked panels.

5.4.2 Limits for J - Q Characterisation

In loading modes which involve opening bending moments on the ligament J - Q characterisation also breaks down. Shih and O'Dowd (1992) have discussed criteria for the limits of J - Q characterisation. At low levels of deformation Q is independent of distance and is identical to the constraint characterisation based on T . However at high deformation levels Q varies with distance for the edge cracked bars and the criterion suggested by Shih and O'Dowd (1992) is a limit on the Q gradient term Q' :

$$Q' = \frac{dQ}{d\frac{\sigma_0}{J}} \quad (5.14)$$

In practise Shih and O'Dowd (1992) have used the mean gradient of Q over the interval $1 \leq \frac{r\sigma_0}{J} \leq 5$ from the crack tip.

$$Q' = \frac{Q(\frac{r\sigma_0}{J} = 5) - Q(\frac{r\sigma_0}{J} = 1)}{4} \quad (5.15)$$

Shih and O'Dowd (1992) have suggested $|Q'| \leq 0.03$ as the limit for J - Q characterisation. In the context of J - Q characterisation only the shallow cracked bars in bending and tension are considered, as the deeply cracked bars are within the limits of single parameter characterisation to high levels of deformation. These limits are not extended by J - Q characterisation. For example for all the deeply cracked tension and bending bars with moderate hardening the limit for single parameter characterisation is $\frac{\sigma_0}{J} \geq 20$.

Neither a J - T nor a J - Q characterisation extends the characterisation because the deeply cracked single edge geometries break down due to global bending which is not described through the J - T or a genuine J - Q characterisation. Figure 5.31 shows an example of Q' as a function of deformation level $\frac{\sigma_0}{J}$. The geometries are single edge bend bars $a/W=0.1, 0.2, 0.3$ and 0.7 at a strain hardening rate, $n=13$. Figure 5.32 shows Q' as a function of $\frac{\sigma_0}{J}$ for CCP ($a/W=0.1, 0.3, 0.5, 0.7$) and SECB ($a/W=0.2$) for strain hardening exponent $n=13$. It can be seen that $|Q'| \leq 0.03$ is only satisfied for deformation levels $\frac{\sigma_0}{J} \geq 100$.

An alternative requirement for the single edge bend geometries can be developed by adopting relations between Q' and the level of deformation expressed as $\frac{J}{c\sigma_0}$, anticipating a result which will be discussed in Chapter 6.

$$Q' = k_1(n)\left(\frac{J}{c\sigma_0}\right) \quad (5.16)$$

$k_1(n)$ is a calibrated function of strain hardening rate given in Chapter 6, $k_1(13) = -5.12$. With this relationship the ASTM requirement for J dominance of deeply cracked bars corresponds to $Q' \leq -0.20$. With this approach the criteria for deep and shallow cracked bars become identical at:

$$\frac{c\sigma_0}{J} \geq 25 \quad \text{and} \quad Q' \geq -0.2 \quad (5.17)$$

J - T characterisation is valid when the stress field differs from the reference field by less than 10%. J - Q characterisation is valid as long as the distance dependency of the stress field compared to the reference field is small. Table 5.9 gives the values of $\frac{c\sigma_0}{J}$ for single edge bend bars for hardening rates $n=3, 6, 13$ and non-hardening at which the J - Q characterisation breaks down under the criterion that $Q' \leq -0.2$. The distance dependency is measured by the constraint gradient Q' . Both J - Q and J - T characterisation break down simultaneously due to global bending on the ligament which causes the stress profile to become distance dependent.

n	$k_1(n)$	$\frac{c\sigma_0}{J}$
3	-13.4	67
6	-8.01	40
13	-5.12	26
∞	-6.12	31

Table 5.9: Limits for J - Q characterisation for single edge cracked bars in tension and bending

In Figure 5.32 Q' vs. $\frac{c\sigma_0}{J}$ is shown for a range of centre cracked panel geometries compared with a single edge cracked bend bar. It is significant to note that all the CCP fall on the same curve and initially have a small positive value of Q' , while the SECB have negative values. This indicates that the moment on the ligament for the CCP is a closing moment and for the SECB it is an opening moment. The values of Q' are much lower for CCP because the moment is small. Q' for CCPs never exceed 0.03 indicating that the J - Q characterisation is a better measure of constraint than the J - T characterisation.

5.5 Conclusion

The limits of one and two parameter characterisation for single edge bars in bending and tension and centre cracked panels have been analysed. Single parameter characterisation is dictated by the stress intensity factor K , and the two parameter approach is characterised either in terms of J - T or J - Q .

For single parameter characterisation the hoop stress ahead of the crack tip was compared with the small scale yielding field and the values of $\frac{\sigma_0}{\sigma_y}$ for which the two fields differ by more than $\pm 10\%$ have been given as the limitation for single parameter characterisation. The values of $\frac{\sigma_0}{\sigma_y}$ were then compared with ASTM size requirements for valid fracture toughness test (K_{IC} or J_{IC}).

For the edge cracked bars it was found that the limitation of single parameter characterisation for shallow cracks ($a/W=0.1$) was controlled by the crack length rather than the ligament in both tension and bending. Deeply cracked single edge specimens were well described with single parameter characterisation. Centre cracked panels are all known to develop unconstrained flow fields and negative values of T , and CCPs are therefore not well characterised by a single parameter description.

The J - T limits were found by comparing the tangential hoop stress with the corresponding stress obtained in the modified boundary layer formulation at the same value of T . Two parameter characterisation was found to extend the limits of characterisation beyond J -dominance for the shallow cracked single edge geometries. For single edge geometries the extend of J - T characterisation is comparable with the J - Q characterisation. The limits of J - Q characterisation were defined though the gradient $Q' = \frac{dQ}{dT}$ which defines the distance dependency of the constraint term.

The breakdown of the characterisation occurs when Q' exceed a critical value, corresponding to the ASTM requirement for J dominance ($Q' \leq -0.2$). There was no significant difference between the limits for J - T characterisation and J - Q characterisation. The limits of two parameter characterisation of centre cracked panels can be extended compared to single parameter characterisation. However in terms of a J - T characterisation the level of lost constraint exceeds the range of constraint which can be modelled by the modified boundary layer formulations. At all levels of deformation CCP fields are well described by J - Q .

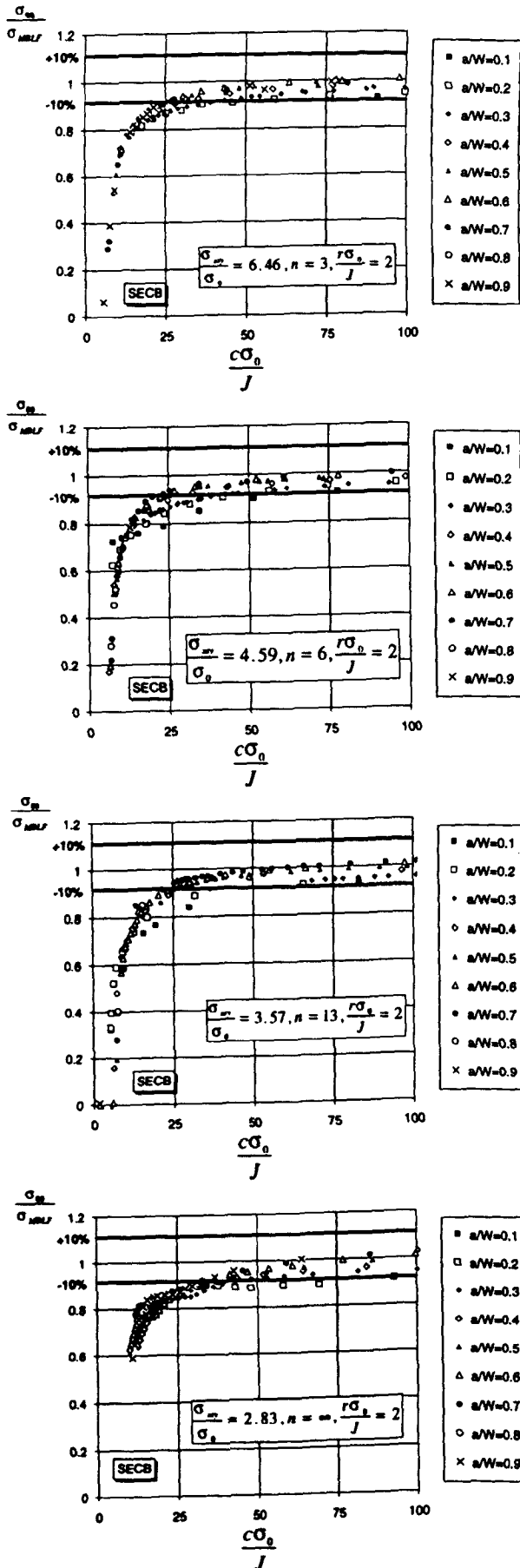


Figure 5.27: The stresses directly ahead of crack in an edge cracked bend bars normalised by the MBLF stress field at a distance $\frac{r\sigma_0}{J} = 2$ as a function of $\frac{c\sigma_0}{J}$.

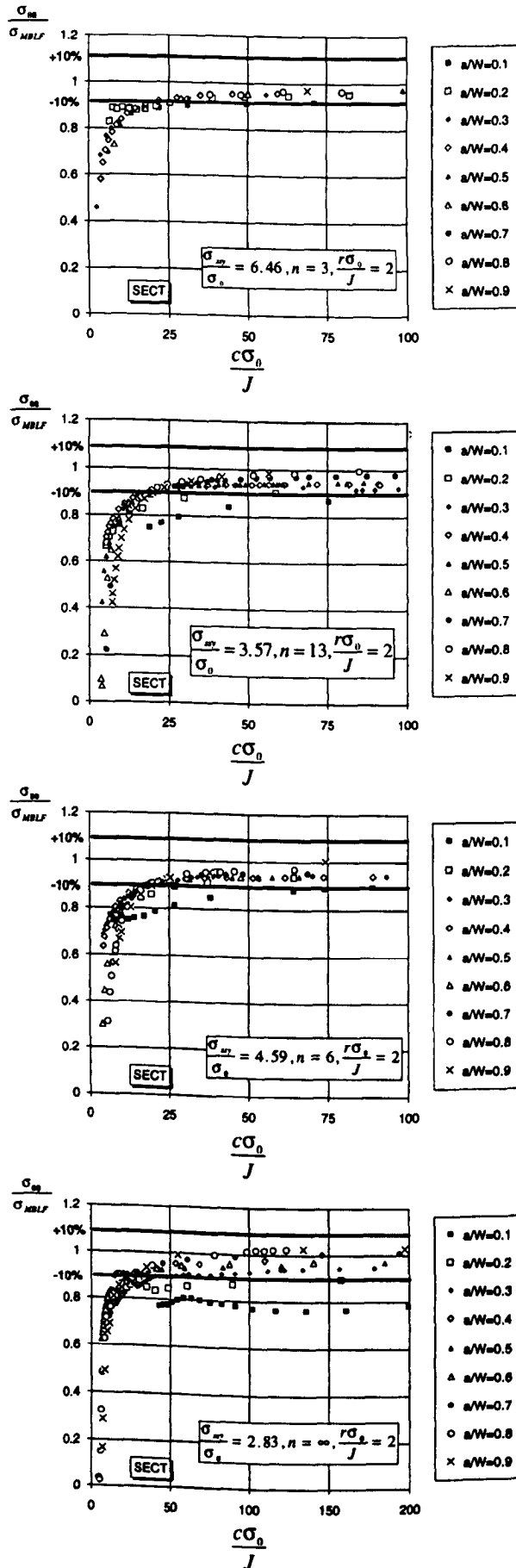


Figure 5.28: The stresses directly ahead of a crack in edge cracked bars in tension normalised by the MBLF stress field at a distance $\frac{r\sigma_0}{J} = 2$ as a function of $\frac{c\sigma_0}{J}$.

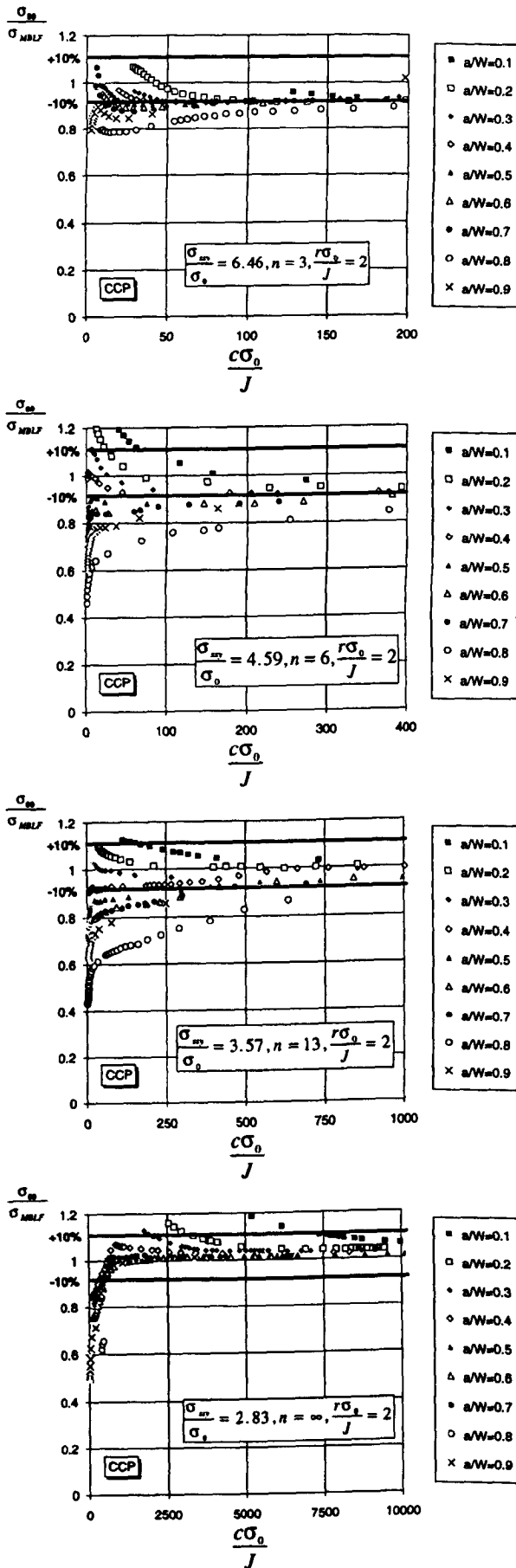


Figure 5.29: The stresses directly ahead of crack in a centre cracked panels normalised by the MBLF stress field at a distance $\frac{r\sigma_0}{J} = 2$ as a function of $\frac{c\sigma_0}{J}$.

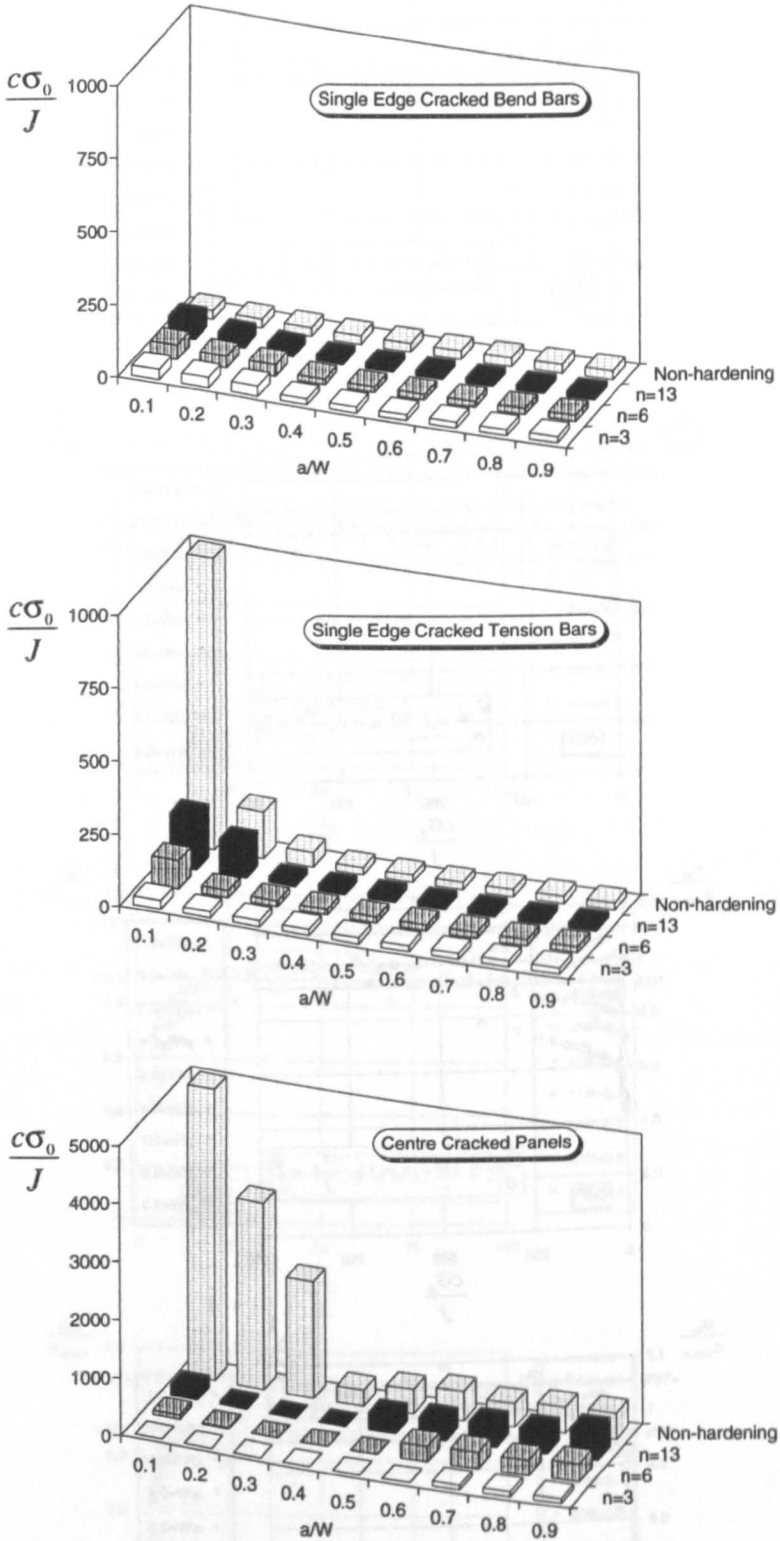


Figure 5.30: $\frac{c\sigma_0}{J}$ at the break down of J - T characterisation for SECB, SECT and CCP, for hardening rates $n=3, 6, 13$ and non-hardening.

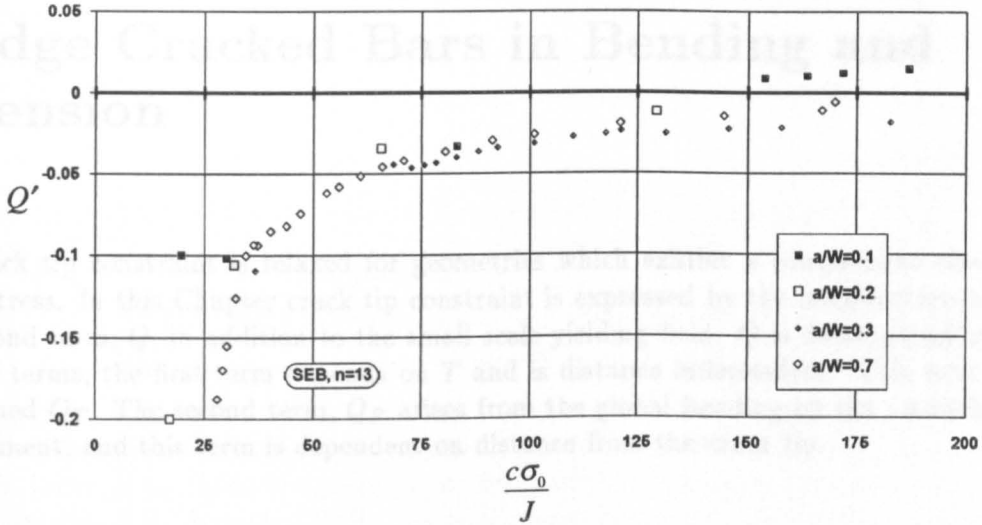


Figure 5.31: Q' as a function of $\frac{c\sigma_0}{J}$ for single edge bend bar, $n=13$

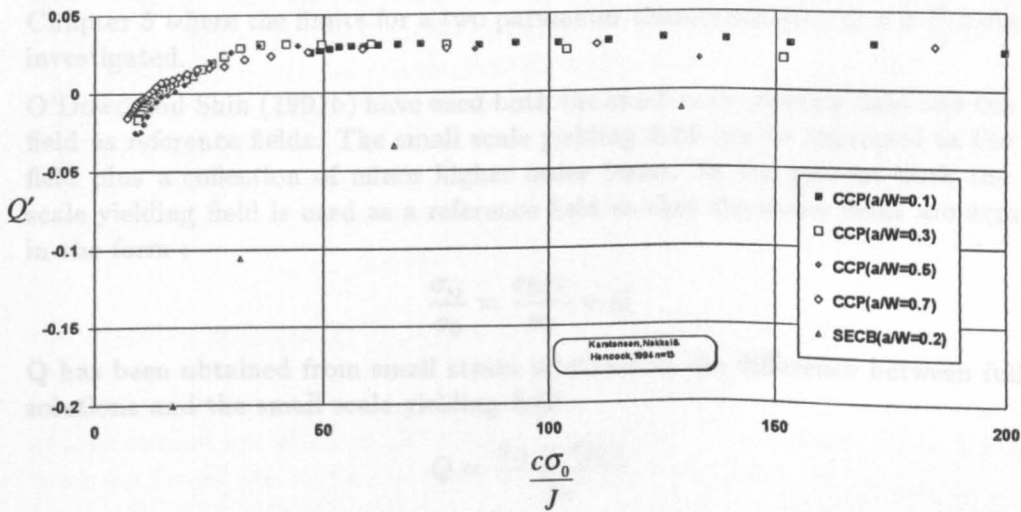


Figure 5.32: Q' as a function of $\frac{c\sigma_0}{J}$ for CCPs and SECB, $n=13$

Blank Page

Constraint Estimation Schemes for Edge Cracked Bars in Bending and Tension

Crack tip constraint is relaxed for geometries which exhibit a compressive elastic T -stress. In this Chapter crack tip constraint is expressed by the introduction of a second term, Q , in addition to the small scale yielding field. Q is decomposed into two terms, the first term depends on T and is distance independent. This term is named Q_T . The second term, Q_P arises from the global bending on the uncracked ligament, and this term is dependent on distance from the crack tip.

6.1 J - Q Crack Tip Fields

Betegón and Hancock (1991) argued that all geometries which develop constrained flow fields feature positive values of T stress, while geometries which exhibit unconstrained flow field feature negative values of T . In single edge cracked bend bars geometries with $a/W \geq 0.3$ exhibit positive values of T and fully constrained fields, as do single edge cracked bars in tension with $a/W \geq 0.5$.

To predict the level of crack tip constraint in fully plastic specimens Betegón and Hancock (1991) suggested that the full field solutions can be related to the modified boundary layer formulation at the same value of T . This technique was used in Chapter 5 where the limits for a two parameter characterisation in a J - T locus were investigated.

O'Dowd and Shih (1991b) have used both the small scale yielding field and the HRR field as reference fields. The small scale yielding field can be expressed as the HRR field plus a collection of minor higher order terms. In the present work the small scale yielding field is used as a reference field so that the stress fields are expressed in the form :

$$\frac{\sigma_{ij}}{\sigma_0} = \frac{\sigma_{SSY}}{\sigma_0} + Q \quad (6.1)$$

Q has been obtained from small strain solutions as the difference between full field solutions and the small scale yielding field:

$$Q = \frac{\sigma_{ij} - \sigma_{SSY}}{\sigma_0} \quad (6.2)$$

Full field solutions have been obtained for a range of geometries and material response as described in Chapter 5. In this chapter edge cracked bars are estimated in bending and tension.

Figure 6.1 shows numerical results for a shallow edge cracked bar ($a/W=0.2$, $n=13$). The hoop stress directly ahead of the crack is given as a function of $\frac{r\sigma_0}{J}$ for several levels of deformation. The stress profiles are compared with the small scale yielding field which applies at very small levels of deformation when plasticity is limited to a small contained area around the crack tip. The small scale yielding field ($T=0$) occurs at very low levels of deformation where the load is close to zero.

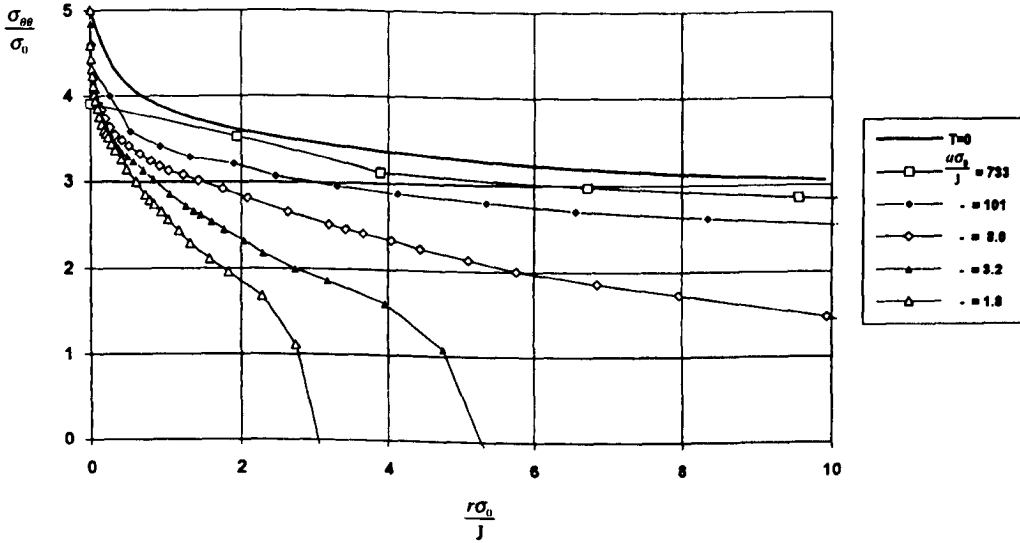


Figure 6.1: The hoop stress directly ahead of a crack SECB, $a/W=0.2$, $n=13$ at several levels of deformation.

At the lowest levels of deformation the crack tip field can be expressed as the small scale yielding field plus a distance independent term. This can be seen in Figure 6.1 where the lowest level of deformation $\frac{a\sigma_0}{J} = 733$. The difference between the small scale yielding field and the full field solution is independent of distance until $\frac{r\sigma_0}{J} = 10$. At greater distances this difference term becomes distant dependent as the global bending field is encountered. Since the bar is subjected to a bending moment the ligament remote from the tip is in compression. The global bending field thus causes the difference between the small scale yielding solution and the full field solution to become distance dependent. Therefore Q has been decomposed into two components Q_T and Q_P

$$Q = Q_T + Q_P \quad (6.3)$$

Q_T is obtained from the modified boundary layer formulation as a function of T . It is independent of the distance $\frac{r\sigma_0}{J}$ but dependent on the strain hardening rate.

Q_T is related to T and calculated from the elastic component of J as described in Chapter 5. The expression for Q_T is equal to the stress field denoted $\frac{\sigma_{MBLE}}{\sigma_0}$, which has the form :

$$Q_T = f\left(\frac{T}{\sigma_0}, n\right) = a_1\left(\frac{T}{\sigma_0}\right) + a_2\left(\frac{T}{\sigma_0}\right)^2 \quad (6.4)$$

Values of a_1 and a_2 are given in Table 5.2. The decomposition of Q can be understood as paralleling to the way in which the J -integral is decomposed into an elastic and a plastic part:

$$J = J_E + J_P \quad (6.5)$$

Here J_P is the plastic component of the J and J_E is the elastic part.

6.2 Constraint Estimation for Single Edge Crack Bars in Bending

In the full field solutions the stress at a distance $\frac{r_{\sigma_0}}{J} = 2$ were examined and compared with those in modified boundary layer formulations, using the scheme suggested by Betegón and Hancock (1991). In this case a notional value of T is calculated from K or the elastic component of J using the biaxiality data given by Sham (1991). The results, for four strain hardening rates, are shown in Figures 6.2-6.5. In these figures, the stresses in the full field solutions are normalised by those in the modified boundary layer formulation, σ_{MBLF} , at the same value of T . The level of deformation is assessed in terms of the applied load normalised by the limit load. The limit loads were determined numerically from the non-hardening analyses, but agree closely with the expression given by Miller (1987). For the non-hardening analyses the expression given by Miller (1987) is used as the limit load.

The distance dependency of Q_P is shown in the example in Figure 6.6, by plotting Q_P as a function of level of deformation given as $\frac{P}{P_{Limit}}$. The Figure shows results for single edge bend bars for all the geometries for a strain hardening exponent $n=13$, at distances $\frac{r_{\sigma_0}}{J}=1,2$ and 5 from the tip of the crack. It is significant to note that the results for all the a/W ratios fall on a common curve which depends on the distance from the crack tip. The shape of the curve is simply a function of n . The relationship between Q_P and $\frac{P}{P_{Limit}}$ can be fitted to the general form

$$Q_P = f\left(\frac{r_{\sigma_0}}{J}, n\right)\left(\frac{P}{P_{Limit}}\right)^{1+n} \quad (6.6)$$

Curve fitting functions $f\left(\frac{r_{\sigma_0}}{J}, n\right)$ for Q_P distances $\frac{r_{\sigma_0}}{J}=1,2$ and 5 are shown for the hardening rates 3, 6 and 13 in Tables 6.1-6.3. The curve fitting constants cannot be obtained for non-hardening materials, as $n=\infty$, however results for $n=100$ as an approximation are given in Table 6.4. Q_P vs. $\frac{P}{P_{Limit}}$ at a distance $\frac{r_{\sigma_0}}{J} = 2$ from the crack tip for all the hardening rates is shown in Figures 6.7 - 6.10.

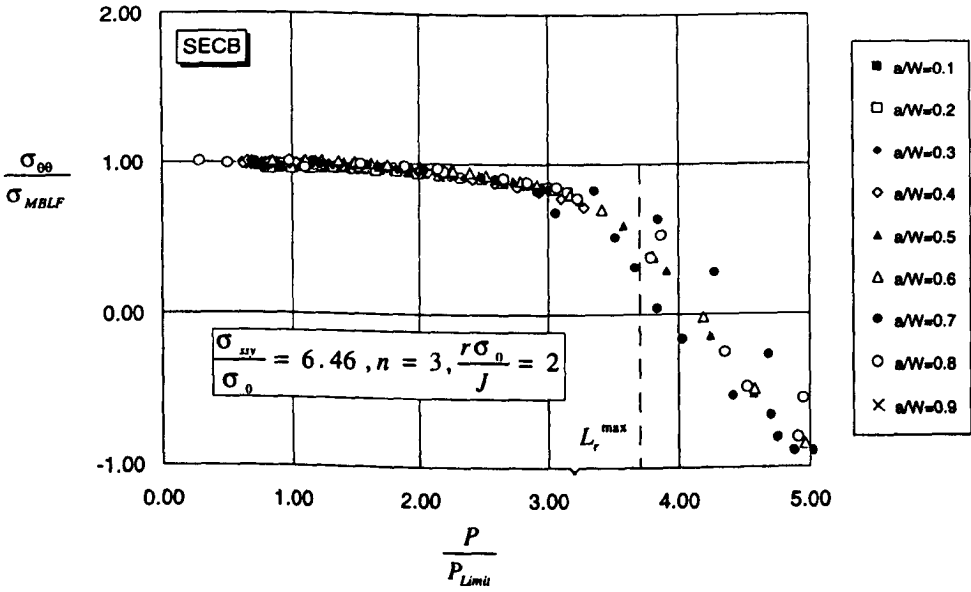


Figure 6.2: The hoop stress in SECB, normalised by the stress from a modified boundary layer formulation at the same value of T , as a function of load normalised by the limit load, $n=3$.

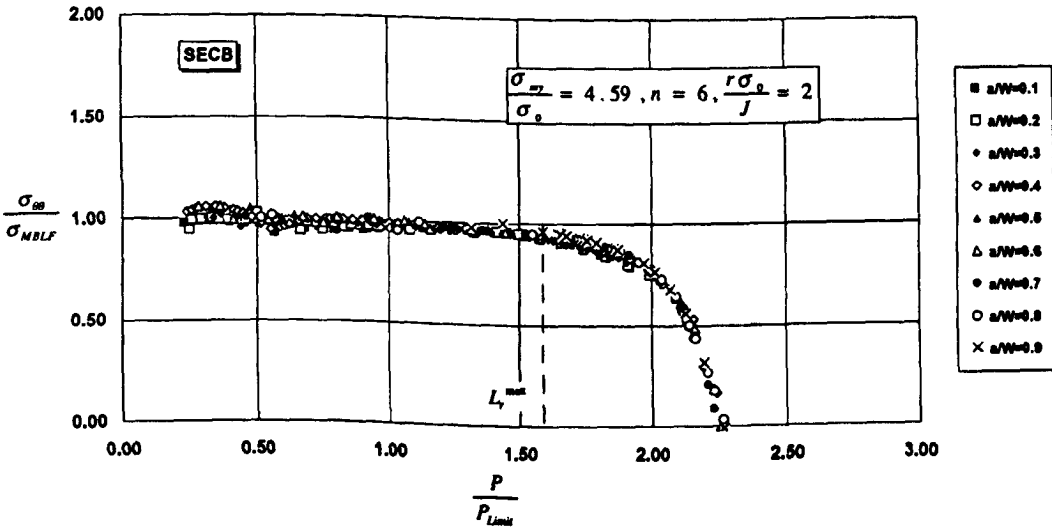


Figure 6.3: The hoop stress in SECB, normalised by the stress from a modified boundary layer formulation at the same value of T , as a function of load normalised by the limit load, $n=6$.

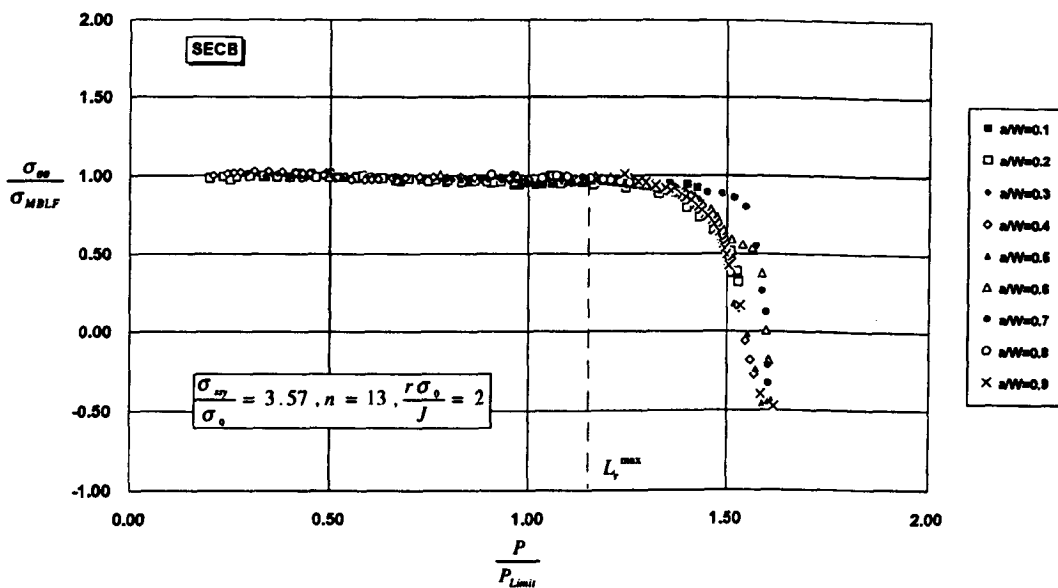


Figure 6.4: The hoop stress in SECB, normalised by the stress from a modified boundary layer formulation at the same value of T , as a function of load normalised by the limit load, $n=13$.

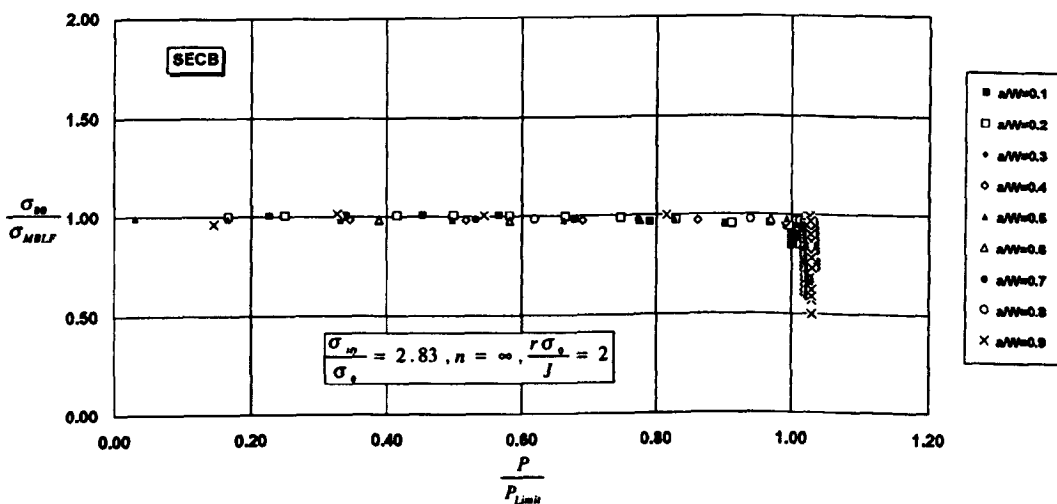


Figure 6.5: The hoop stress in SECB, normalised by the stress from a modified boundary layer formulation at the same value of T , as a function of load normalised by the limit load, non hardening.

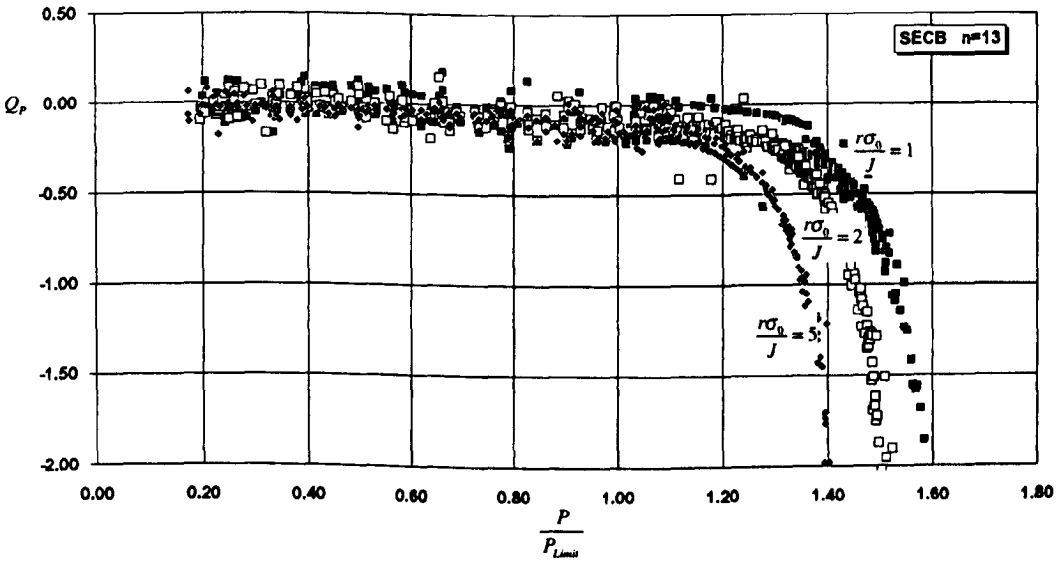


Figure 6.6: Q_P as a function of $\frac{P}{P_{Limit}}$ for Single edge bend bars at distances $\frac{r\sigma_0}{J} = 1, 2$ and 5 from the crack tip.

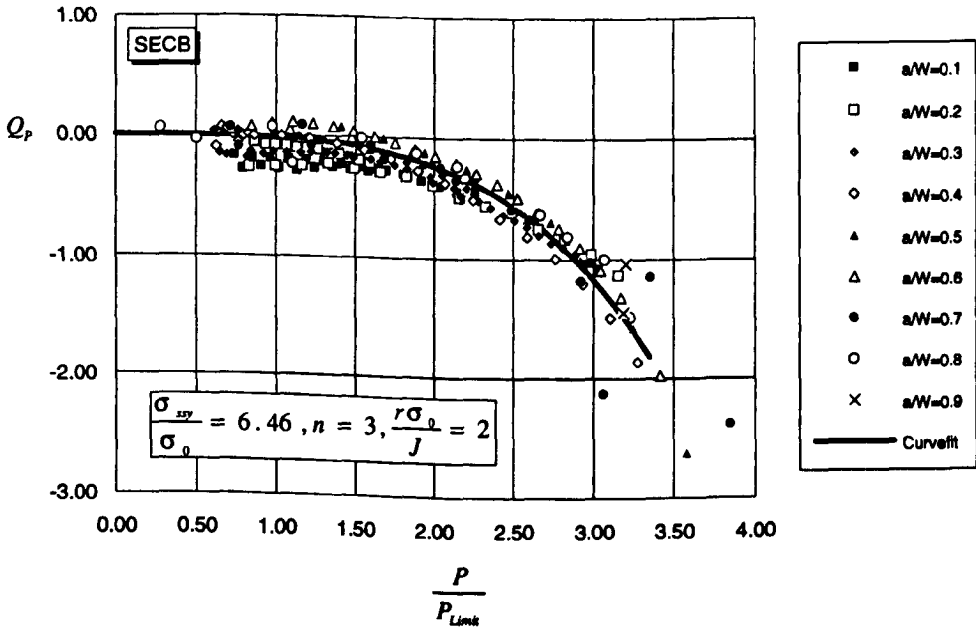


Figure 6.7: Q_P as a function of $\frac{P}{P_{Limit}}$ for single edge bend bars at a distance $\frac{r\sigma_0}{J} = 2$ from the crack tip, for all a/W ratios and $n=3$.

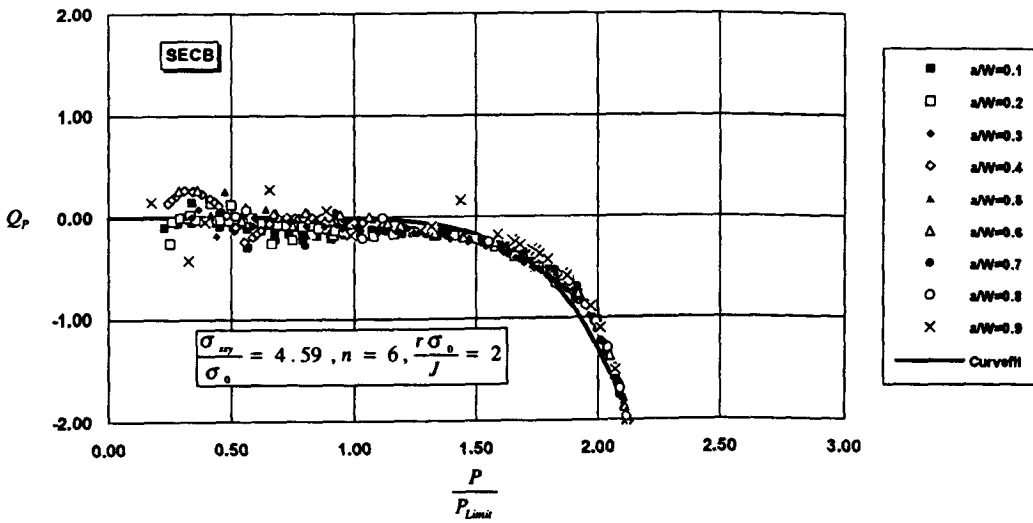


Figure 6.8: Q_P as a function of $\frac{P}{P_{Limit}}$ for single edge bend bars at a distance $\frac{r\sigma_0}{\sigma_y} = 2$ from the crack tip, for all a/W ratios and $n=6$.

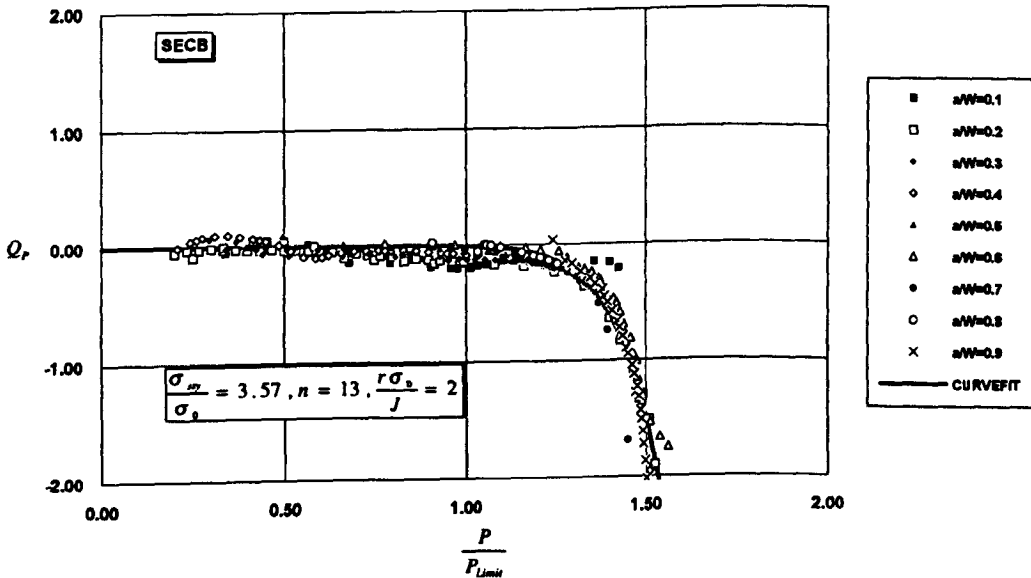


Figure 6.9: Q_P as a function of $\frac{P}{P_{Limit}}$ for single edge bend bars at a distance $\frac{r\sigma_0}{\sigma_y} = 2$ from the crack tip, for all a/W ratios and $n=13$.

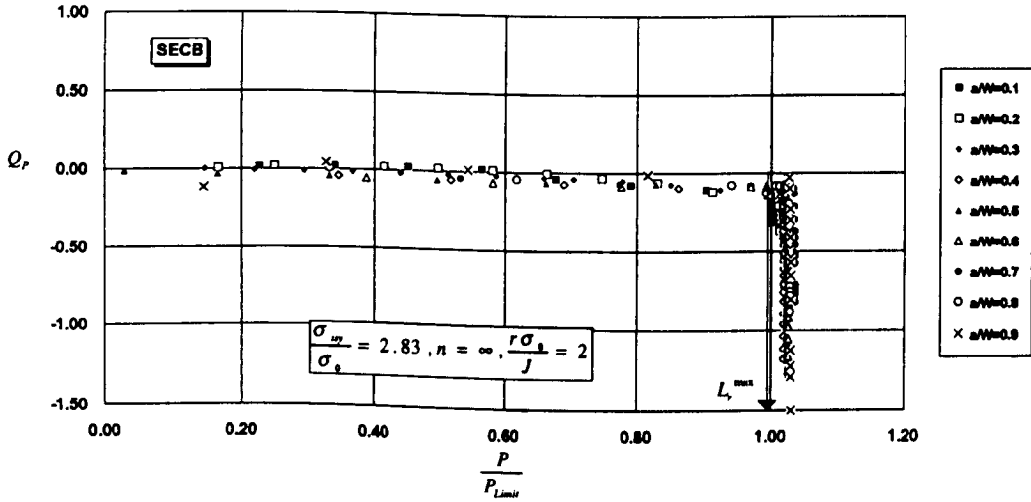


Figure 6.10: Q_P as a function of $\frac{P}{P_{Limit}}$ for single edge cracked bend bars at a distance $\frac{r\sigma_0}{J} = 2$ from the crack tip, for all a/W ratios, $n = \infty$.

a/W	$\frac{r\sigma_0}{J} = 1$	$\frac{r\sigma_0}{J} = 2$	$\frac{r\sigma_0}{J} = 5$
0.1			
0.2	-0.0123	-0.0133	-0.022
0.3	-0.0113	-0.0143	-0.0278
0.4	-0.008	-0.0133	-0.0379
0.5	-0.0121	-0.0105	-0.0364
0.6	-0.0055	-0.0118	-0.0356
0.7	-0.0064	-0.0143	-0.0286
0.8	-0.0063	-0.0177	-0.0417
0.9	-0.007	-0.0136	-0.0331

Table 6.1: Curve fittings results for the proportionality constant $k_2(n)$ which relates Q_P and $\frac{P}{P_{Limit}}$ for Single Edge Cracked Bend bars, $n=3$.

Figures 6.2-6.4 also show an important structural cut off used in the assessment of structural integrity by Failure Assessment Diagrams (Chell (1979)), and which is usually denoted L_r^{max}

$$L_r^{max} = \frac{\sigma_0 + \sigma_{UTS}}{2\sigma_0} \tag{6.7}$$

Numerical values of L_r^{max} for the constitutive relations used in this work are given in Table 6.5. Engineering structures are not operated at loads greater than L_r^{max}

a/W	$\frac{r\sigma_0}{J} = 1$	$\frac{r\sigma_0}{J} = 2$	$\frac{r\sigma_0}{J} = 5$
0.1	-0.0034	-0.004	-0.0074
0.2	-0.0044	-0.0064	-0.0189
0.3	-0.0039	-0.0070	-0.0192
0.4	-0.0033	-0.0065	-0.0196
0.5	-0.0031	-0.0065	-0.0190
0.6	-0.0034	-0.0066	-0.0188
0.7	-0.0031	-0.0064	-0.0206
0.8	-0.0033	-0.0065	-0.0191
0.9	-0.0035	-0.0064	-0.0175

Table 6.2: Curve fittings results for the proportionality constant $k_2(n)$ which relates Q_P and $\frac{P}{P_{Limit}}$ for Single Edge Cracked Bend bars, $n=6$.

a/W	$\frac{r\sigma_0}{J} = 1$	$\frac{r\sigma_0}{J} = 2$	$\frac{r\sigma_0}{J} = 5$
0.1	-0.0045	-0.0064	-0.0086
0.2	-0.0033	-0.0058	-0.0152
0.3	-0.0029	-0.0053	-0.0148
0.4	-0.0027	-0.0052	-0.0153
0.5	-0.0029	-0.0057	-0.0145
0.6	-0.0028	-0.0056	-0.0148
0.7	-0.0026	-0.0057	-0.0145
0.8	-0.0029	-0.0051	-0.0142
0.9	-0.0024	-0.0053	-0.0139

Table 6.3: Curve fittings results for the proportionality constant $k_2(n)$ which relates Q_P and $\frac{P}{P_{Limit}}$ for Single Edge Cracked Bend bars, $n=13$.

times the limit load. In this context the important result is that the J - T constraint estimation scheme provides acceptable predictions of constraint up to L_{max}^r for all but the highest hardening rate ($n=3$) when characterisation breaks down at approximately 2.5 times the limit load. It would be very unusual for a structure to operate at such load levels even under serious overload conditions, and even under these circumstances for all hardening rates, the J - T approach gives an overestimate of the stress and thus provides a conservative estimate of toughness and ensures structural integrity.

When Q_P is plotted as a function of $\frac{P}{P_{Limit}}$ it is noteworthy that the data for all the geometries falls on the same curve as shown in Figures 6.7-6.10. The shape of the curve only depends on the strain hardening rate n , and the distance $\frac{r\sigma_0}{J}$ at which Q is measured. Whereas the level of deformation expressed as $\frac{P}{P_{Limit}}$ where Q_P becomes significant depends on the distance $\frac{r\sigma_0}{J}$ in a linear manner as shown in Tables 6.1-6.4. The relation between Q_P and the applied load can be described by

a/W	$\frac{r\sigma_0}{J} = 1$	$\frac{r\sigma_0}{J} = 2$	$\frac{r\sigma_0}{J} = 5$
0.1	-0.206	-0.1741	-0.3975
0.2	-0.079	-0.0779	-0.1804
0.3	-0.0458	-0.0861	-0.3143
0.4	-0.0451	-0.0923	-0.2729
0.5	-0.0395	-0.0756	-0.237
0.6	-0.0329	-0.0544	-0.1704
0.7	-0.0099	-0.0162	-0.0567
0.8	-0.0239	-0.0418	-0.131
0.9	-0.0162	-0.0396	-0.1183

Table 6.4: Curve fittings results for the proportionality constant $k_2(n)$ which relates Q_P and $\frac{P}{P_{Limit}}$ for Single Edge Cracked Bend bars, non-hardening, $n=100$ is used for the fit.

n	L_r^{max}
3	3.8
6	1.6
13	1.2
∞	1.0

Table 6.5: L_r^{max} for different values of strain hardening exponent.

a relation of the form:

$$Q_P = k_2(n) \left(\frac{r\sigma_0}{J} \right) \left(\frac{P}{P_{Limit}} \right)^{n+1} \quad (6.8)$$

where $k_2(n)$ is a proportionality constant which depends on the strain hardening rate but is independent of the geometry (a/W ratio or the ligament size c). Values of $k_2(n)$ for hardening rates $n=3, 6$ and 13 are given in Table 6.10. The values are given as the averages for all a/W ratios.

Kumar *et al.* (1981) expressed the relation between the plastic component of the J integral J_P and the load as

$$J_P = \alpha \sigma_0 \epsilon_0 c h_1 \left(\frac{a}{W}, n \right) \left(\frac{P}{P_{Limit}} \right)^{n+1} \quad (6.9)$$

where h_1 is a function of the $\frac{a}{W}$ ratio and the strain hardening exponent, also tabulated by Kumar *et al.* (1981).

Equations (6.8) and (6.9) suggest that Q_P is linearly dependent on J_P . Figure 6.11 shows Q_P as a function of $\frac{J_P}{c\sigma_0}$ for $n=13$ and for different distances $\frac{r\sigma_0}{J}=1, 2$ and 5 from the tip of the complete range of edge cracked bars (a/W=0.1 to 0.9). It can be seen that Q_P is insensitive to the geometry (a/W), as all the curves fall on the same straight line. Similar data for the complete range of (a/W) and the other hardening rates $n=3, 6, 13$ and ∞ are given in figures 6.12 - 6.15 at a distance $\frac{r\sigma_0}{J}=2$ from the crack tip.

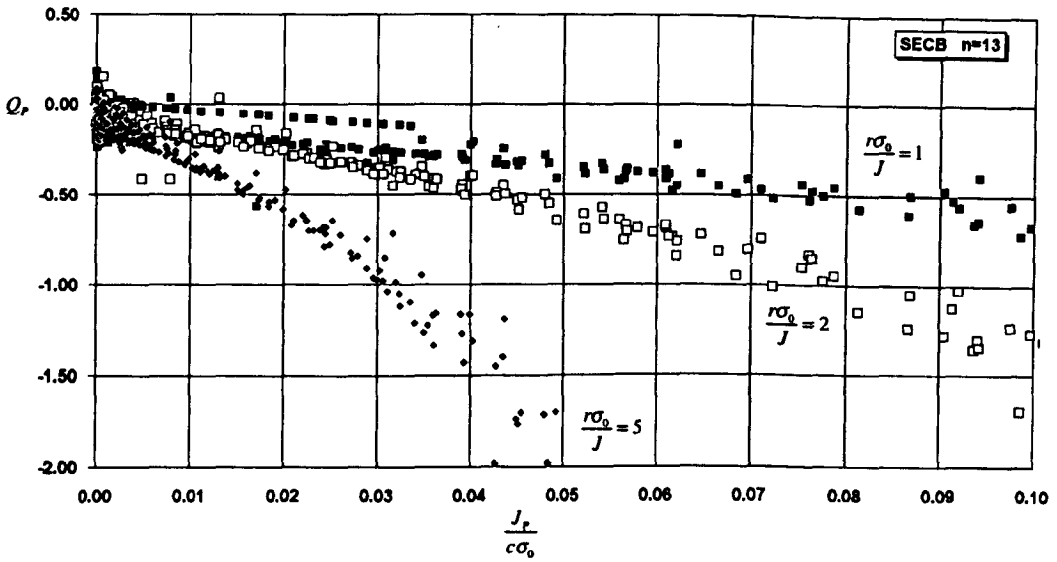


Figure 6.11: Q_P as a function of $\frac{J_P}{c\sigma_0}$ for single edge cracked bars in bending for all a/W at distances $\frac{r\sigma_0}{J} = 1, 2, 5$ from the crack tip.

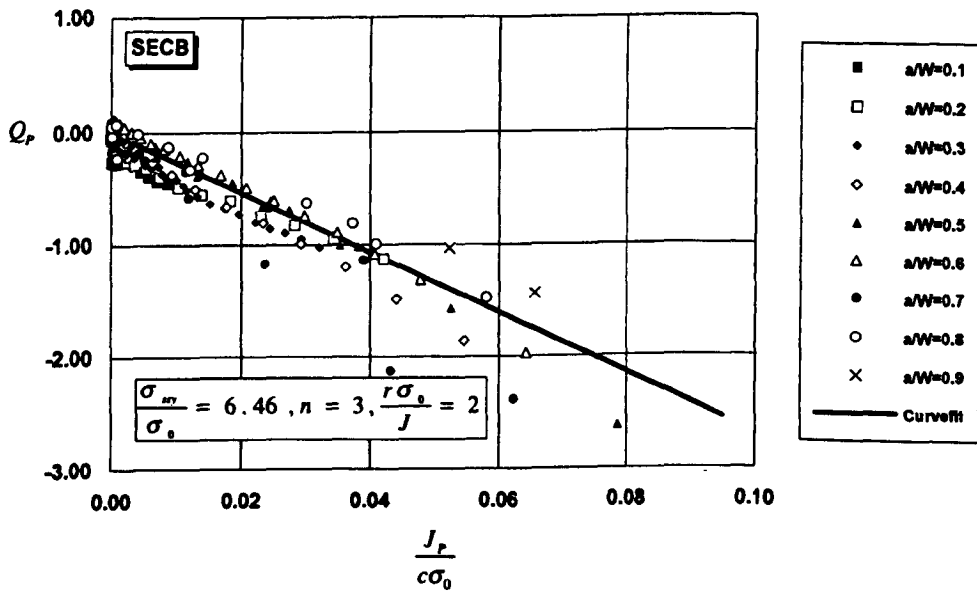


Figure 6.12: Q_P as a function of $\frac{J_P}{c\sigma_0}$ for single edge cracked bars in bending for all a/W at a distance $\frac{r\sigma_0}{J} = 2$ from the crack tip, $n=3$.

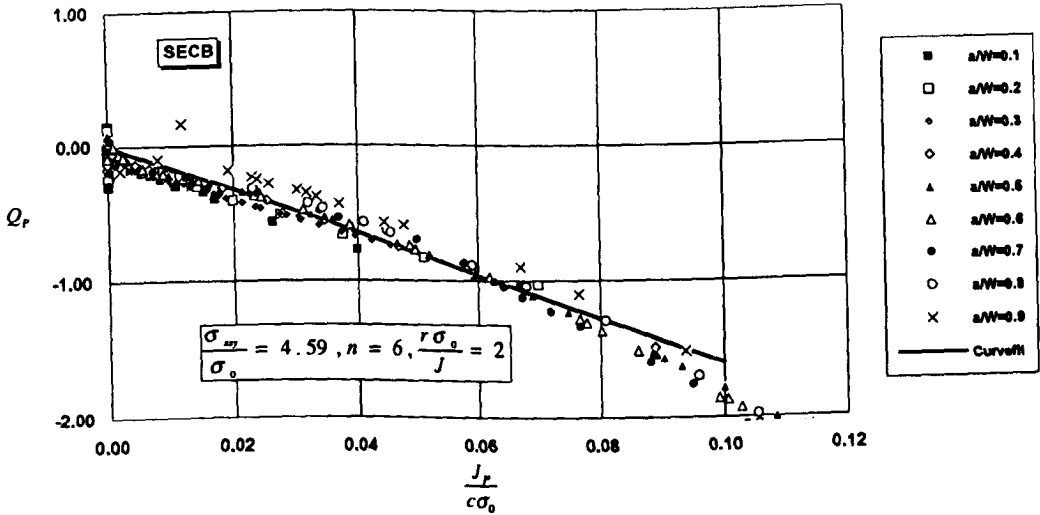


Figure 6.13: Q_P as a function of $\frac{J_P}{c\sigma_0}$ for single edge cracked bars in bending for all a/W at a distance $\frac{r\sigma_a}{J} = 2$ from the crack tip, $n=6$.

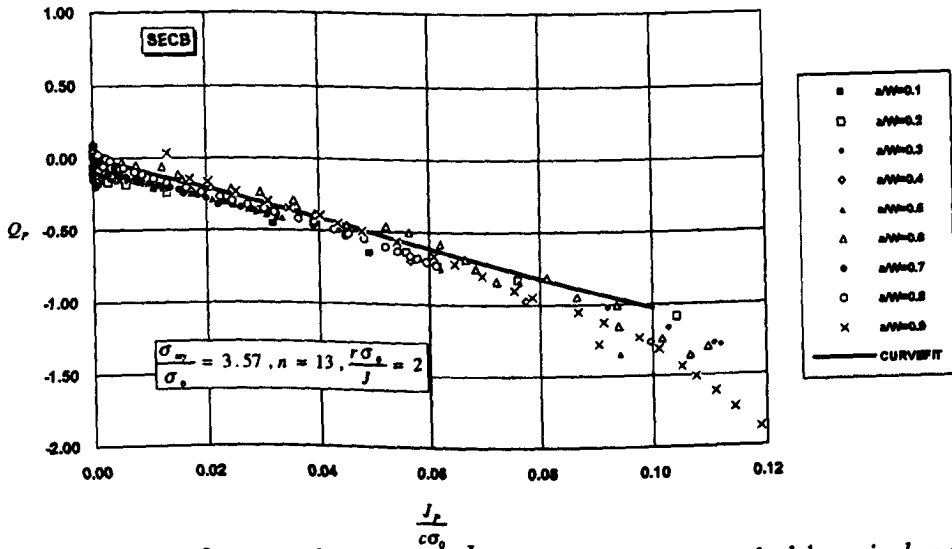


Figure 6.14: Q_P as a function of $\frac{J_P}{c\sigma_0}$ for single edge cracked bars in bending for all a/W at a distance $\frac{r\sigma_a}{J} = 2$ from the crack tip, $n=13$.

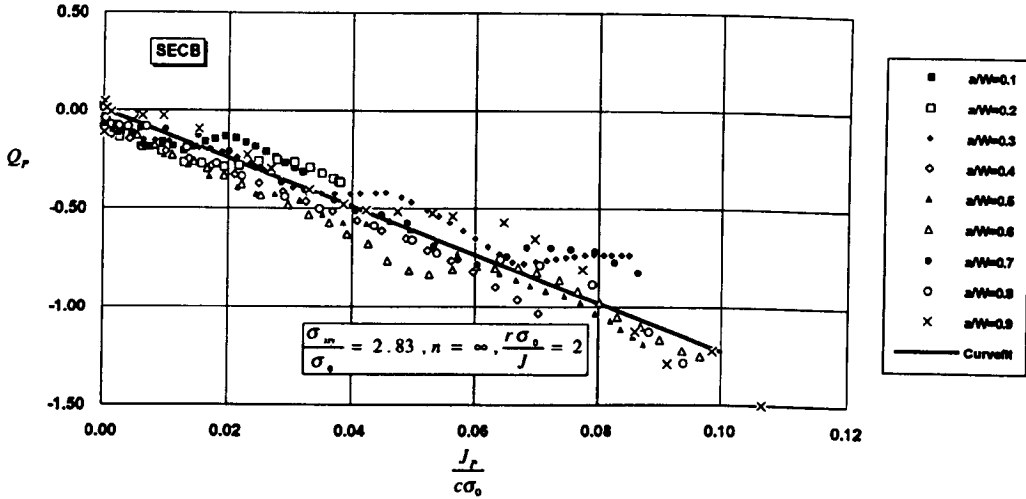


Figure 6.15: Q_P as a function of $\frac{J_P}{c\sigma_0}$ for single edge cracked bars in bending for all a/W at a distance $\frac{r\sigma_0}{J} = 2$ from the crack tip, non-hardening material.

Curve fitting Q_P as a function of J_P demonstrates that Q_P increases with the distance $\frac{r\sigma_0}{J}$ from the crack tip in a systematic manner. For low and moderate hardening rates the distance dependence of Q_P can be approximated by the relation

$$Q_{P(\frac{r\sigma_0}{J})} = k_1(n) \left(\frac{r\sigma_0}{J} \right) \left(\frac{J_P}{c\sigma_0} \right) = k_1(n) \left(\frac{r}{c} \right) \left(\frac{J_P}{J} \right) \tag{6.10}$$

Values of the constant k_1 are given in Tables 6.6-6.9 for the range of strain hardening exponents.

a/W	$\frac{r\sigma_0}{J} = 1$	$\frac{r\sigma_0}{J} = 2$	$\frac{r\sigma_0}{J} = 5$
0.1			
0.2	-25.0	-27.4	-48.3
0.3	-24.0	-31.3	-60.2
0.4	-16.9	-27.4	-77.8
0.5	-14.8	-35.5	-81.9
0.6	-10.8	-24.8	-77.8
0.7	-11.5	-29.8	-83.4
0.8	-7.9	-20.6	-64.7
0.9	-10.33	-17.7	60.9

Table 6.6: Curve fittings results for the proportionality constant $k_1(n)$ which relates Q_P and $\frac{J_P}{c\sigma_0}$ for Single Edge Bend bars, $n=3$.

Complete expressions for the stress field may now be assembled.

Firstly the results are assembled in a form which enables the stress field to be determined from the applied load.

$$\frac{\sigma_{\theta\theta}}{\sigma_0} = \frac{\sigma_{SSY}}{\sigma_0} + f\left(\frac{T}{\sigma_0}, n\right) + k_2(n) \left(\frac{r\sigma_0}{J} \right) \left(\frac{P}{P_{Limit}} \right)^{n+1} \tag{6.11}$$

a/W	$\frac{r\sigma_0}{J} = 1$	$\frac{r\sigma_0}{J} = 2$	$\frac{r\sigma_0}{J} = 5$
0.1	-32.5	-26.6	-26.2
0.2	-15.0	-11.6	-12.5
0.3	-5.81	-6.32	-15.2
0.4	-5.29	-7.01	-18.1
0.5	-7.34	-8.86	-26.99
0.6	-8.13	-12.6	-27.27
0.7	-10.04	-12.94	-36.41
0.8	-8.47	-13.68	-29.59
0.9	-7.35	-16.88	-38.24

Table 6.7: Curve fittings results for the proportionality constant $k_1(n)$ which relates Q_P and $\frac{J_P}{c\sigma_0}$ for Single Edge Bend bars, $n=6$.

a/W	$\frac{r\sigma_0}{J} = 1$	$\frac{r\sigma_0}{J} = 2$	$\frac{r\sigma_0}{J} = 5$
0.1	-11.29	-14.87	-19.87
0.2	-6.08	-10.34	-23.33
0.3	-6.62	-11.54	-30.55
0.4	-6.94	-12.61	-30.46
0.5	-7.34	-13.52	-31.68
0.6	-7.01	-13.73	-33.72
0.7	-6.82	-11.71	-32.45
0.8	-6.87	-11.70	-31.11
0.9	-5.69	-12.15	-28.86

Table 6.8: Curve fittings results for the proportionality constant $k_1(n)$ which relates Q_P and $\frac{J_P}{c\sigma_0}$ for Single Edge Bend bars, $n=13$.

$$Q_{\left(\frac{r\sigma_0}{J}\right)} = a_1\left(\frac{T}{\sigma_0}\right) + a_2\left(\frac{T}{\sigma_0}\right)^2 + k_2\left(\frac{r\sigma_0}{J}\right)\left(\frac{P}{P_{Limit}}\right)^{n+1} \quad (6.12)$$

Secondly the results are expressed in a form which enables the stress field to be determined from the elastic and plastic components of J .

$$\frac{\sigma_{\theta\theta}}{\sigma_0} = \frac{\sigma_{SSY}}{\sigma_0} + f\left(\frac{\beta}{\sigma_0}\sqrt{\frac{J_E}{E'\pi a}}, n\right) + k_1(n)\left(\frac{r\sigma_0}{J}\right)\left(\frac{J_P}{c\sigma_0}\right) \quad (6.13)$$

$$Q_{\left(\frac{r\sigma_0}{J}\right)} = f\left(\frac{\beta}{\sigma_0}\sqrt{\frac{J_E}{E'\pi a}}, n\right) + k_1(n)\left(\frac{r\sigma_0}{J}\right)\left(\frac{J_P}{c\sigma_0}\right) \quad (6.14)$$

In Table 6.10 data for k_1 and k_2 are given, as both k_1 and k_2 are insensitive to the a/W ratio for the SECB. The data has been averaged over the range of a/W for the distances $\frac{r\sigma_0}{J}=1,2$ and 5 .

a/W	$\frac{r\sigma_0}{Y} = 1$	$\frac{r\sigma_0}{Y} = 2$	$\frac{r\sigma_0}{Y} = 5$
0.1	-8.89	-9.40	-23.31
0.2	-8.96	-9.78	-24.02
0.3	-5.06	-10.08	-37.86
0.4	-5.90	-13.43	-40.98
0.5	-6.06	-12.59	-39.68
0.6	-7.36	-12.57	-40.33
0.7	-6.44	-11.18	-40.07
0.8	-6.70	-12.69	-40.67
0.9	-5.36	-12.69	-39.72

Table 6.9: Curve fittings results for the proportionality constant $k_1(n)$ which relates Q_P and $\frac{J_P}{\sigma_0}$ for Single Edge Bend bars, non-hardening.

n	k_1	k_2
3	-13.4	-0.0072
6	-8.01	-0.0051
13	-5.12	-0.0038
∞	-6.12	-

Table 6.10: k_1 and k_2 constants for Single Edge Cracked Bend Bars.

6.3 Constraint Estimation for Single Edge Cracked Bars in Tension

A similar approach to that adopted for edge cracked bend bars (SECB) has been used for the edge cracked tension bars (SECT). In figures 6.16 - 6.19 a comparison of the full field solution at a distance $\frac{r\sigma_0}{J} = 2$ is normalised by that in a modified boundary layer formulation at the same value of T and plotted as a function of $\frac{P}{P_{Limit}}$.

$Q_P(\frac{r\sigma_0}{J})$ at a distance $\frac{r\sigma_0}{J}=2$ from the crack tip as a function of $\frac{P}{P_{Limit}}$ is shown in Figures 6.20-6.23.

The data has a load dependency of the form $(\frac{P}{P_{Limit}})^{n+1}$ and the proportionality constant k_2 which is similar to that for bending, a function of the strain hardening exponent, n , and independent of the a/W ratio, are given in Table 6.11 for $n=6$ and in Table 6.12 for $n=13$. As in the case of the SECB data Q_P is linearly dependent on $\frac{J_P}{c\sigma_0}$ as shown in Figures 6.24-6.27. However the proportionality constant k_1 depends on the a/W ratio as well as the strain hardening exponent, as shown in Table 6.13 for $n=6$ and Table 6.14 for $n=13$.

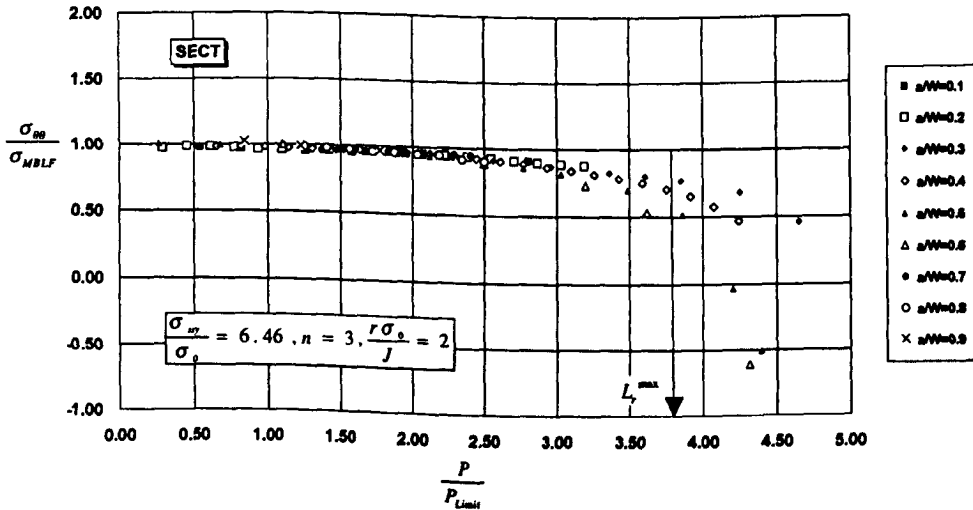


Figure 6.16: The hoop stress normalised by the stress from a modified boundary layer formulation for a distance $\frac{r\sigma_0}{J}=2$ at the same value of T , as a function of load normalised by the limit load, $n=3$.

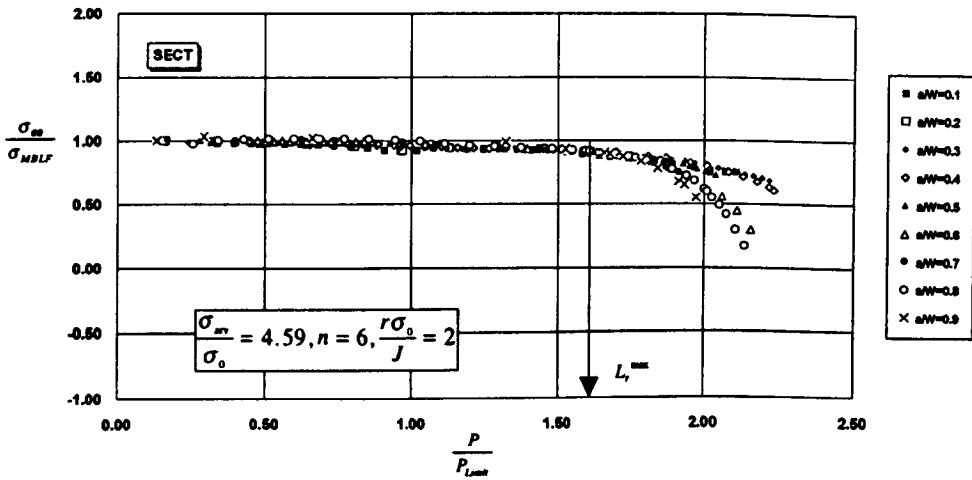


Figure 6.17: The hoop stress normalised by the stress from a modified boundary layer formulation for a distance $\frac{r\sigma_0}{J}=2$ at the same value of T , as a function of load normalised by the limit load, $n=6$.

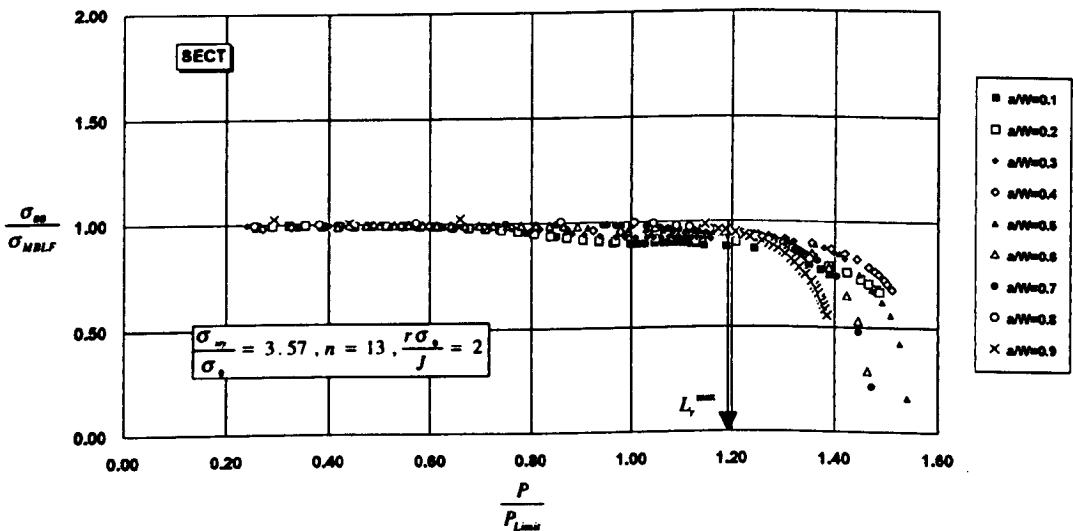


Figure 6.18: The hoop stress normalised by the stress from a modified boundary layer formulation for a distance $\frac{r\sigma_0}{J}=2$ at the same value of T , as a function of load normalised by the limit load, $n=13$.

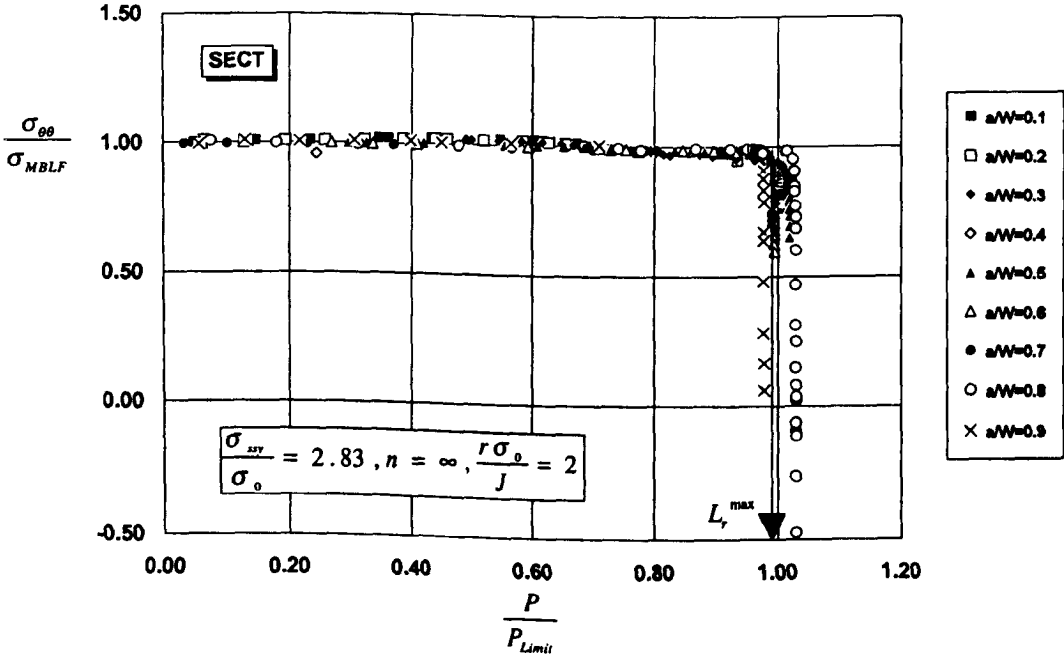


Figure 6.19: The hoop stress normalised by the stress from a modified boundary layer formulation for a distance $\frac{r\sigma_o}{J} = 2$ at the same value of T , as a function of load normalised by the limit load, non-hardening.

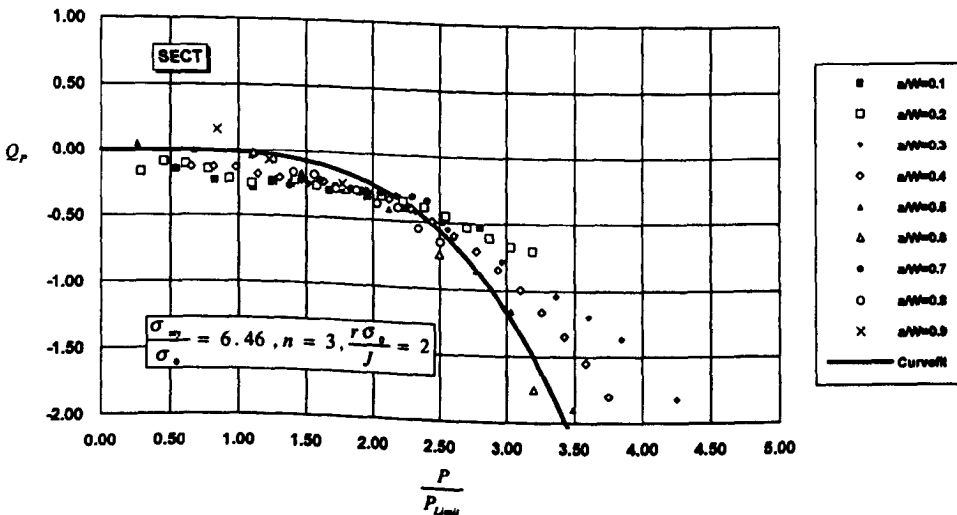


Figure 6.20: Q_P as a function of $\frac{P}{P_{Limit}}$ for single edge cracked bars in tension for all a/W at a distance $\frac{r\sigma_o}{J} = 2$ from the crack tip, $n=3$. Curve fitting value for $k_2(n)=-0.0087$

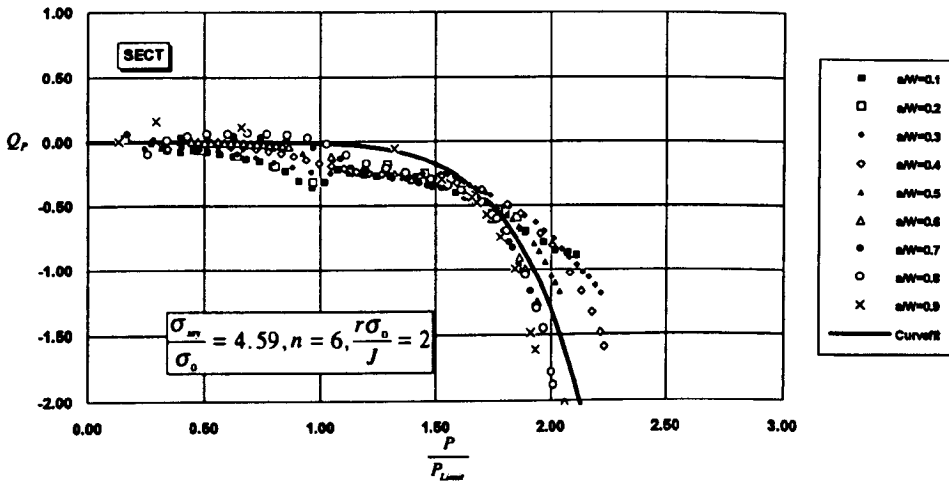


Figure 6.21: Q_P as a function of $\frac{P}{P_{Limit}}$ for single edge cracked bars in tension for all a/W at a distance $\frac{r\sigma_0}{J} = 2$ from the crack tip, $n=6$. Curve fitting value for $k_2(n) = -0.0072$

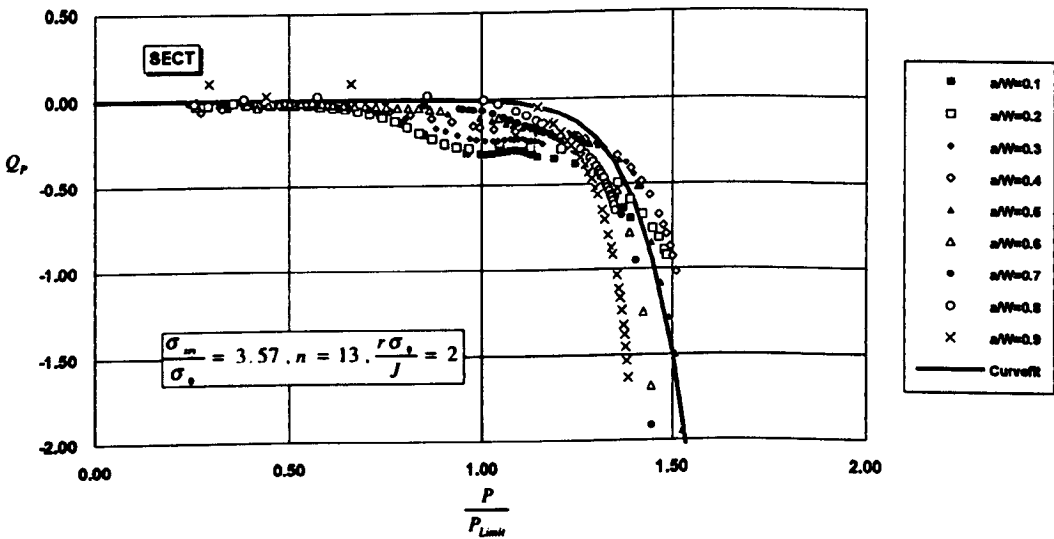


Figure 6.22: Q_P as a function of $\frac{P}{P_{Limit}}$ for single edge cracked bars in tension for all a/W at a distance $\frac{r\sigma_0}{J} = 2$ from the crack tip, $n=13$. Curve fitting value for $k_2(n) = -0.0041$

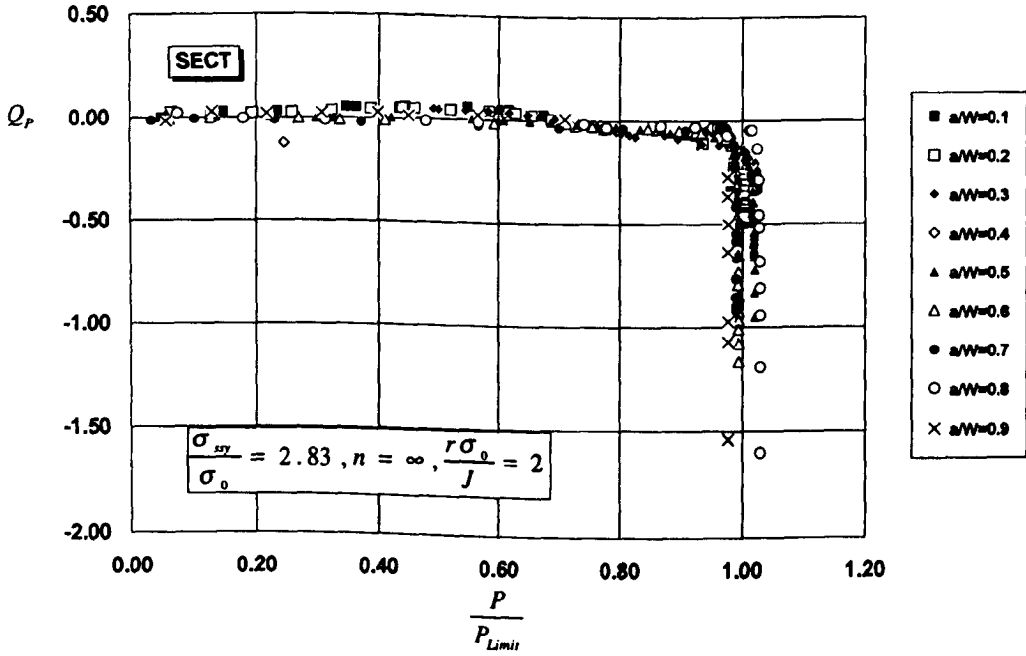


Figure 6.23: Q_P as a function of $\frac{P}{P_{Limit}}$ for single edge cracked bars in tension for all a/W at a distance $\frac{r\sigma_0}{J} = 2$ from the crack tip, non-hardening.

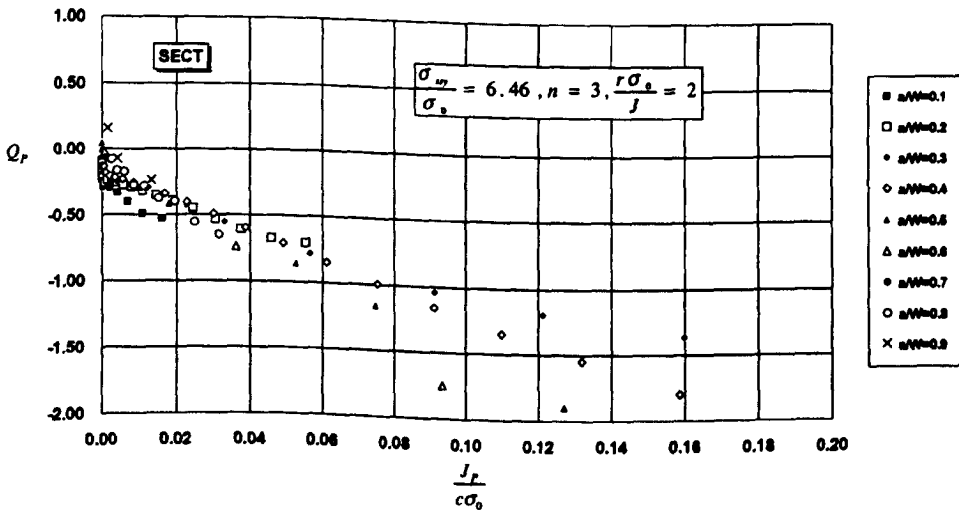


Figure 6.24: Q_P as a function of $\frac{J_P}{c\sigma_0}$ for single edge cracked bars for all a/W at a distance $\frac{r\sigma_0}{J} = 2$ from the crack tip, $n=3$.

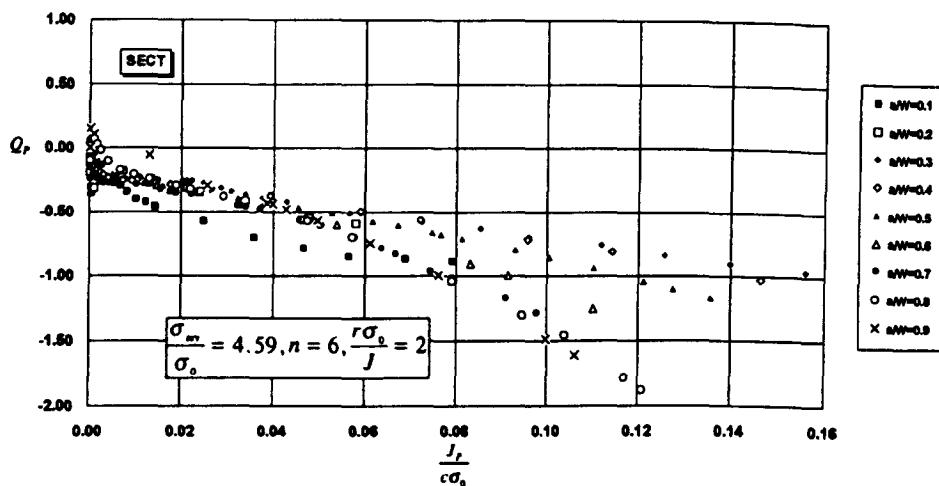


Figure 6.25: Q_P as a function of $\frac{J_P}{c\sigma_0}$ for single edge cracked bars for all a/W at a distance $\frac{r\sigma_0}{J} = 2$ from the crack tip, $n=6$.

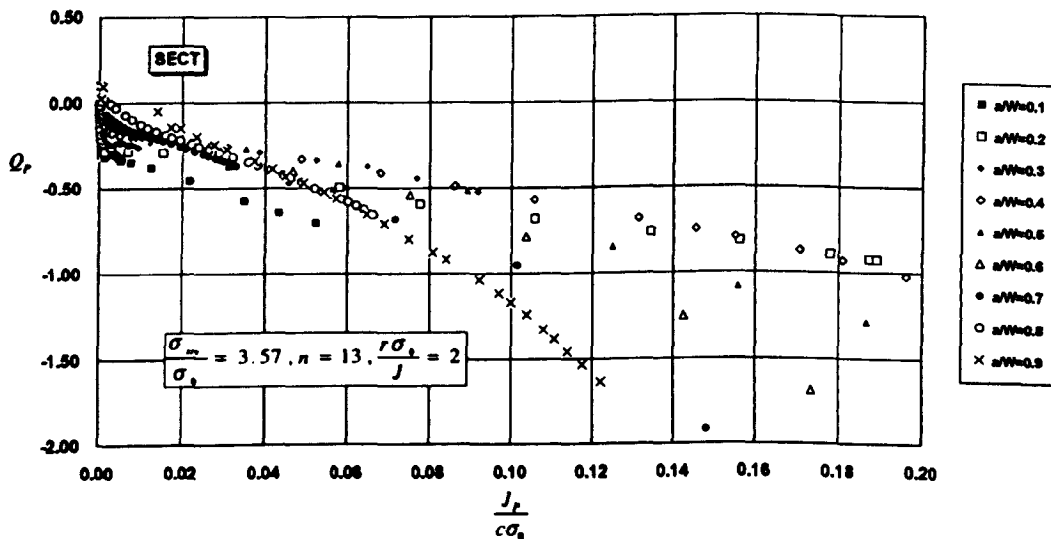


Figure 6.26: Q_P as a function of $\frac{J_P}{c\sigma_0}$ for single edge cracked bars for all a/W at a distance $\frac{r\sigma_0}{J} = 2$ from the crack tip, $n=13$.

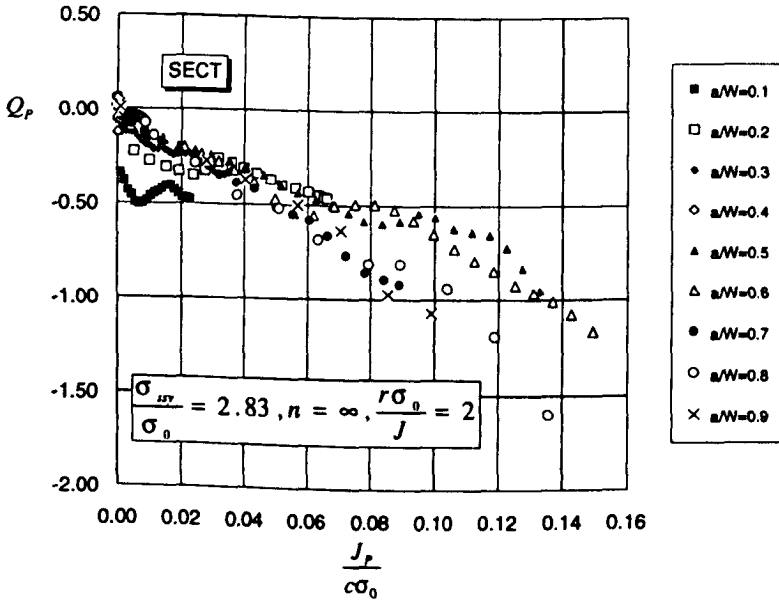


Figure 6.27: Q_P as a function of $\frac{J_P}{c\sigma_0}$ for single edge cracked bars for all a/W at a distance $\frac{r\sigma_0}{J} = 2$ from the crack tip, non-hardening.

a/W	$\frac{r\sigma_0}{J} = 1$	$\frac{r\sigma_0}{J} = 2$	$\frac{r\sigma_0}{J} = 5$
0.1	-0.0137	-0.0113	-0.0111
0.2	-0.0118	-0.0092	-0.0010
0.3	-0.0057	-0.0063	-0.0152
0.4	-0.0056	-0.0074	-0.0192
0.5	-0.0079	-0.0096	-0.0295
0.6	-0.0082	-0.0129	-0.0284
0.7	-0.0090	-0.0117	-0.0332
0.8	-0.0095	-0.0174	-0.0374
0.9	-0.0073	-0.0126	-0.0292

Table 6.11: Curve fittings results for proportionality constants $k_2(n)$ which relates Q_P and $\frac{P}{P_{Limit}}$ for Single Edge Cracked Tension bars, $n=6$.

a/W	$\frac{r\sigma_0}{J} = 1$	$\frac{r\sigma_0}{J} = 2$	$\frac{r\sigma_0}{J} = 5$
0.1	-0.0082	-0.0095	-0.0117
0.2	-0.0032	-0.0040	-0.0064
0.3	-0.0046	-0.0059	-0.0098
0.4	-0.0033	-0.0050	-0.0122
0.5	-0.0032	-0.0065	-0.0166
0.6	-0.0038	-0.0084	
0.7	-0.0041	-0.0089	-0.0246
0.8	-0.0093	-0.0161	-0.0560
0.9	-0.0061	-0.0136	-0.0376

Table 6.12: Curve fittings results for proportionality constant $k_2(n)$ which relates Q_P and $\frac{P}{P_{Limit}}$ for Single Edge Tension bars, $n=13$.

a/W	$\frac{r\sigma_0}{J} = 1$	$\frac{r\sigma_0}{J} = 2$	$\frac{r\sigma_0}{J} = 5$
0.1	-30.51	-23.57	-28.15
0.2	-13.99	-10.51	-14.52
0.3	-6.01	-7.33	-15.52
0.4	-5.29	-6.51	-20.08
0.5	-8.34	-8.86	-30.00
0.6	-7.93	-12.63	-29.26
0.7	-12.14	-15.94	-38.41
0.8	-7.99	-13.68	-30.79
0.9	-7.98	-13.59	-28.92

Table 6.13: Curve fittings results for proportionality constant $k_1(n)$ which relates Q_P and $\frac{J_P}{c\sigma_0}$ for Single Edge Cracked Tension bars, $n=6$.

a/W	$\frac{r\sigma_0}{J} = 1$	$\frac{r\sigma_0}{J} = 2$	$\frac{r\sigma_0}{J} = 5$
0.1	-14.98	-17.15	-20.85
0.2	-4.21	-5.25	-8.33
0.3	-4.63	-5.92	-9.77
0.4	-3.50	-5.28	-12.44
0.5	-3.38	-7.14	-16.23
0.6	-4.06	-8.88	
0.7	-5.50	-11.45	-24.32
0.8	-6.22	-10.64	-36.83
0.9	-5.96	-14.28	-39.56

Table 6.14: Curve fittings results for proportionately constant $k_1(n)$ which relates Q_P and $\frac{J_P}{c\sigma_0}$ for Single Edge Cracked Tension bars, $n=13$.

6.4 Discussion

The stresses in a series of full field solutions of edge cracked bars in bending and tension have been compared with the stresses predicted from a modified boundary layer formulation at the same value of T . The results are shown in Figures 6.2-6.5 for SECT and Figures 6.16-6.19 for SECT. It is firstly significant to note that the stress normalised by that obtained from the modified boundary layer formulation has the same dependence on the load normalised by the limit load for all the deep and shallow cracked bend bars. The cause of the loss of constraint in deeply cracked bars has been clearly identified with the global bending field impinging on the local crack tip field (McMeeking and Parks (1979), Shih and German (1981)).

Using the criterion that the stresses should be within 10% of the HRR field leads to the well known criterion for J dominance or single parameter characterisation, that the ligament should exceed $\frac{25J}{\sigma_0}$ ASTM (E 339-83 1983). The observation that the stress field deviates from that of the modified boundary layer formulation for deeply cracked and shallow cracked bars in exactly the same manner is strong evidence that the deviation from J - T characterisation is entirely due to the global bending field.

In Chapter 5 it has been shown that the deviation from J - T characterisation for both deep and shallow cracked bend bars breaks down at the same criterion for ligaments less than $\frac{25J}{\sigma_0}$. There can be little doubt therefore that both J - T and J - Q characterisation of the crack tip fields of edge cracked bend bars breaks down at the same deformation level due to the global bending field. Defect assessment schemes based on failure assessment diagrams, require that structures operate at loads less than L_r^{max} . Except for the highest strain hardening rate ($n=3$) the stress levels can be predicted to within 10% by estimates based on T without the need for full field numerical solutions with crack tip resolution.

The difference between the prediction based on T and the crack tip field in full field solutions has been denoted Q_P through Equation (6.3). The existence of a valid Q field beyond the predictions based on T requires the existence of a distance independent term. Figures 6.6 and 6.11 all clearly show that at levels of deformation at which significant deviations occur from the modified boundary layer formulation, Q_P increases with distance from the tip. The necessary conclusion is that in the case of edge cracked bars, the distance independent Q term is entirely accounted for by T , and that the deviation from J - T characterisation arises from the global bending field. This difference cannot be described by a valid distance independent term, and it is therefore necessary to conclude that Q does not extend the two parameter characterisation of force loaded edge cracked bars in tension and bending beyond the limits of J - T characterisation.

Having established the physical reasons for the simultaneous breakdown of J - T and J - Q characterisation in tension and bending, it is appropriate to turn to attempts to describe Q_P quantitatively. Firstly we note the almost linear dependence of Q_P on the plastic component of J shown by Figures 6.12- 6.15 and 6.24-6.27. This implies that Q_P is dependent on $\left(\frac{P}{P_{Limit}}\right)$ as supported by the data shown in Figures 6.7- 6.10 and 6.20-6.23. The Q_P - J_P relation has been fitted by a linear relation, and the proportionality constant, k_1 , is given in Table 6.10 as a function of the strain hardening exponent n . In bending the relationship is almost completely insensitive to the a/W ratio.

Similarly the Q_P - P relation has been independently fitted by a relation of the form $(\frac{P}{P_{Limit}})^{n+1}$. The proportionality constant k_2 is given in Table 6.10, as a function of n , but it is again noteworthy that the relation is closely similar for all a/W ratios. Given that the J_P - P relation is of the form proposed by Kumar Shih and German (1981) in Equation (6.9), there is a relation between the proportionality constants k_1 and k_2 such that

$$k_2 = k_1 \alpha \epsilon_0 h_1 \quad (6.15)$$

In bending both k_1 and k_2 are relatively insensitive to the a/W ratio. This in part arises from the strength of the $(\frac{P}{P_{Limit}})^{n+1}$ term, such that curve fitting with terms of this order is necessarily insensitive to the value of the proportionality constant k_2 . The Q_P - J_P and Q_P - P relations have been fitted independently. Consistency checks through Equation 6.15 have not been pursued, in view of controversy of independent consistency checks on h_1 itself. However it is worth noting that in bending the h_1 term is not strongly sensitive to the a/W ratio, whereas in tension it changes by almost a factor of ten. This leads to the result that in bending k_1 and k_2 are insensitive to a/W . In tension only k_2 is insensitive to a/W as both k_1 and h_1 depend strongly on a/W . In Table 6.15 $k_1(n)$ and $k_2(n)$ are given for bending, and $k_2(n)$ are given for tension.

	Bending		Tension
n	k_1	k_2	k_2
3	-13.4	-0.0072	-0.0087
6	-8.01	-0.0051	-0.0072
13	-5.12	-0.0038	-0.0041
∞	-6.12	-	-

Table 6.15: k_1 and k_2 constants for Single Edge Cracked Bars.

Equation (6.11) provides a convenient way of determining Q from the applied load in a form which parallels the J estimation schemes advanced by Kumar *et al.* (1981). Like the J -estimation scheme itself, it suffers from being very sensitive to the exact form of the stress-strain relation and is very sensitive to the exact value of the applied load. An alternative route which is necessarily less sensitive to the exact form of the stress-strain relation is given by Equation (6.13) and requires the ability to determine J .

It is convenient to focus initially on the deeply cracked bend geometries ($a/W > 0.3$) in which T is positive. For these geometries the fully plastic field initially develops high constraint, and is well described by J through the HRR field, within the limitations of J dominance. Further deformation leads to a loss of crack tip constraint and a loss of J -dominance which has been clearly identified to arise from the global bending field.

Deviations from the fully constrained field thus arise only from the distance dependent term Q_P . A knowledge of J and k_2 thus characterises the crack tip field. This provides a two parameter characterisation of deeply cracked geometries in which loss of constraint arises from the global bending field, and extends crack

tip characterisation beyond the limits of J -dominance. At small load levels, deeply cracked bars develop a highly constrained small scale yielding field which is maintained into full plasticity. This degenerates as the global bending field impinges on the local crack tip field producing an additional term which increases with distance from the crack tip in an initially linear manner,

$$Q_P = k_1(n) \left(\frac{r}{c}\right) \left(\frac{J_P}{J}\right) \quad (6.16)$$

At large levels of plasticity in which J_P is very much greater than J_E , and J_P is approximately equal to J , this produces a limiting form of crack tip field.

$$Q_P = k_1(n) \left(\frac{r}{c}\right) \quad \left(r \leq \frac{c}{4}\right) \quad (6.17)$$

$$\frac{\sigma_{\theta\theta}}{\sigma_0} = \frac{\sigma_{SSY}}{\sigma_0} k_1(n) \left(\frac{r}{c}\right) \quad (Q_T = 0, T \geq 0, r \leq \frac{c}{4}) \quad (6.18)$$

The field which is approached at high levels of plastic deformation thus comprises the small scale yielding field plus a term which increases linearly with distance across the ligament accounting for the influence of the global bending. There are of course limits on the distance over which such a description is adequate. Very close to the crack tip the stress directly ahead of the crack is close to the small scale yielding field, but at finite distances from the tip the stress decays through the global bending field. However, the stress level eventually drops to such a level that plasticity does not occur. That is to say directly ahead of the crack there is an elastic enclave bounded by the formation of plastic hinges which develop through the ligament. At greater distances from the tip the stress field becomes sufficiently compressive to induce plastic flow in compression. The effect of the central elastic enclave can be seen in Figure 6.1 at the largest levels of plastic deformation when the stress drops abruptly at distances from the crack tip of the order of $\frac{r}{c} \approx \frac{1}{4}$

It is finally worth recalling that the object of characterising crack tip fields is to be able to describe the crack tip stress distribution, as this leads naturally to associated fracture criteria. In order to test the way in which the proposed schemes describe crack tip deformation, four representative geometries have been chosen. These are a shallow cracked bend bar, $a/W = 0.2$ for which T is negative and a deeply cracked bend bar for which T is positive, $a/W = 0.7$. Similar shallow and deeply cracked bars have been considered in tension, $a/W = 0.2$ and $a/W = 0.7$. In both cases results are given for a hardening exponent, $n = 13$.

In Figures 6.28 and 6.29 the stress field ahead of the shallow and deeply cracked bend bars is predicted from Equations (6.11) and (6.13) using load and J as the inputs and compared with the full field solution at four different levels of deformation. A similar comparison is given in Figures 6.30 and 6.31 for edge cracked tension bars. There is demonstrably good agreement between the predictions and the field through conditions in which constraint loss occurs both by the formation of genuine Q/T fields and through conditions in which constraint loss occurs by global bending.

6.5 Conclusions

The development of crack tip constraint has been systematically examined for edge cracked bars subject to tension and bending. The initial loss of crack tip constraint is controlled by the sign of the non-singular T stress which is associated with fields which can be described by the small scale yielding field plus a distance independent term (Q).

Within contained yielding crack tip characterisation can rigorously be achieved by T or equivalently Q . J - T characterisation does however extend in practice well beyond the formal limits of contained yielding if a notional value of T is calculated from the elastic component of J . At high levels of deformation this characterisation breaks down due to the global bending field impinging on the crack tip. This results in a distance dependent Q term. In this context Q has been decomposed into a distance independent term Q_T which is formally related to T and a distance dependent term which is related to the global bending field has been expressed in terms of far field parameters such as the applied load and J . This constitutes a two parameter characterisation, and associated fracture criterion for deeply cracked bend bars, beyond the limits of J -dominance.

Shallow cracked bars show a very limited region of single parameter characterisation, as constraint loss originates from the compressive T stress associated with the elastic field. Characterisation can be extended by the use of a two parameter approach using J and T (or equivalently J - Q). These fields eventually break down simultaneously due to the global bending field. At these deformation levels characterisation has been achieved by the use of three parameters, J , Q_T and Q_P , this provides a complete crack tip constraint estimation scheme for edge cracked bars in tension and bending.

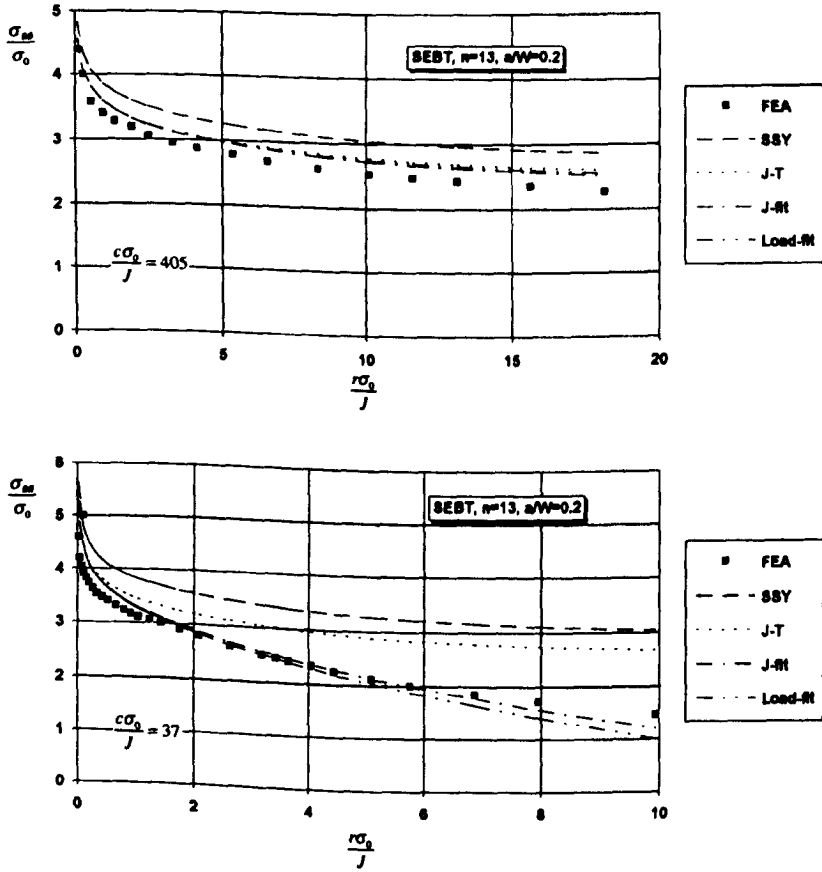


Figure 6.28: The hoop stress at a distance $\frac{r\sigma_0}{J} = 2$ directly ahead of a SECB, $a/W=0.2$, $n=13$ at several levels of deformation.

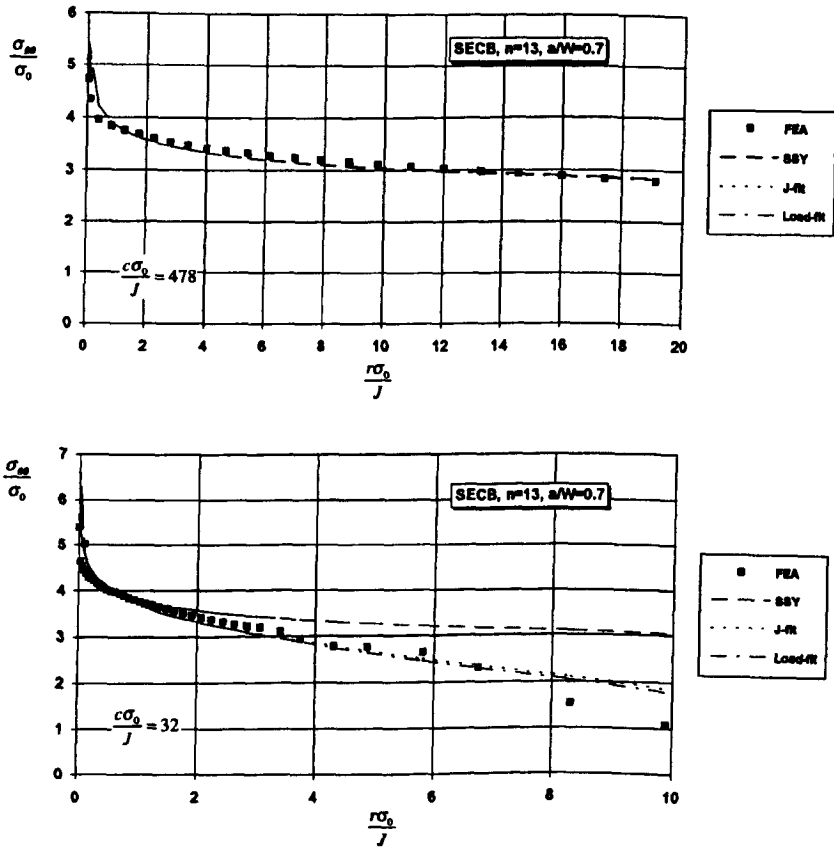


Figure 6.29: The hoop stress at a distance $\frac{r\sigma_0}{J} = 2$ directly ahead of a SECB, $a/W=0.7$, $n=13$ at several levels of deformation.

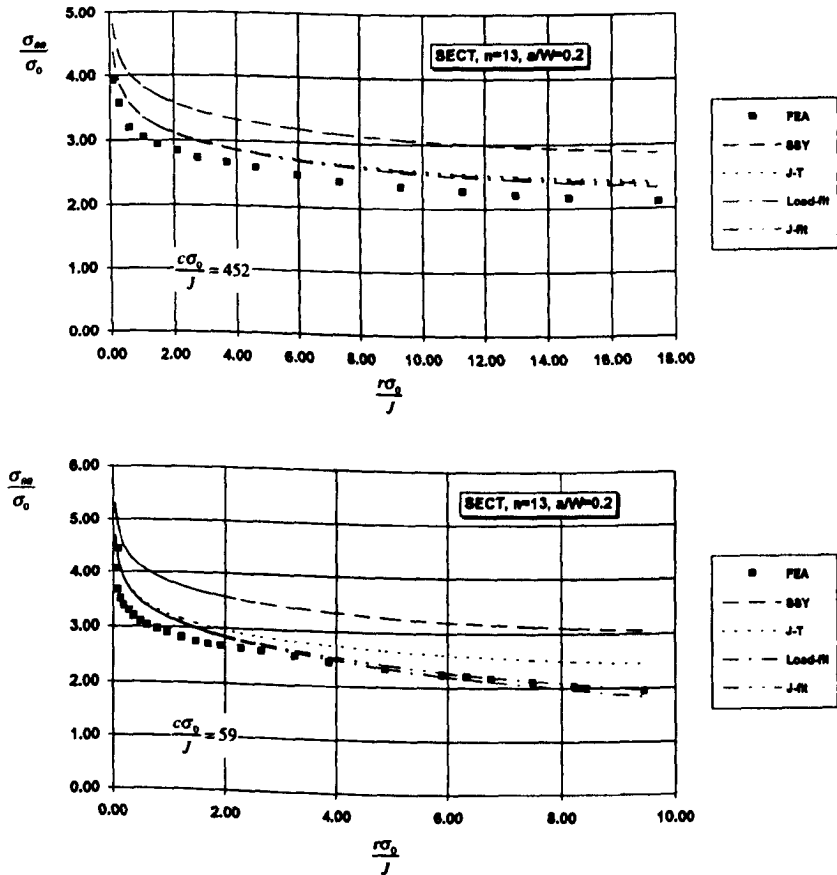


Figure 6.30: The hoop stress at a distance $\frac{r\sigma_0}{J} = 2$ directly ahead of a SECT, $a/W=0.2$, $n=13$ at several levels of deformation.

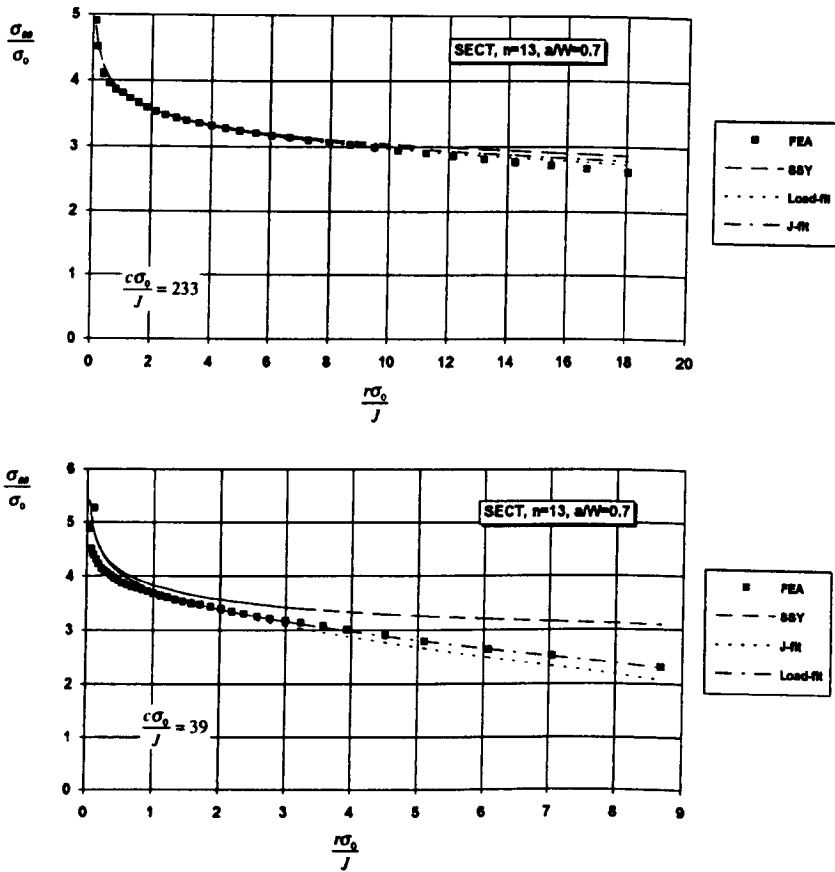


Figure 6.31: The hoop stress at a distance $\frac{r\sigma_0}{J}=2$ directly ahead of a SECT, $a/W=0.7$, $n=13$ at several levels of deformation.

Blank Page

Constraint Estimation Schemes for Centre Cracked Panels and Double Edge Cracked Bars

The development of crack tip constraint for centre crack panels and double edge cracked bars has been systematically examined for a range of geometries which have important displacement controlled symmetry boundary conditions. Crack tip constraint is expressed by the introduction of a second term, Q , in addition to the small scale yielding field.

7.1 Numerical Analysis

The numerical models of the centre crack panels and double edge cracked bars are described in Chapter 4. The geometries range from $a/W=0.1$ to $a/W=0.9$ with an interval of 0.1. The mesh comprises 8 biquadratic nodes isoparametric plane strain elements, with reduced integration and linear pressure interpolation, (ABAQUS element type CPE8RH). The boundary conditions on the centre crack panels and double edge cracked bars were displacement loading on the top boundary. Due to symmetry only a quarter of the structure was analysed, and analyses were performed at four different strain hardening rates ($n=3, 6, 13$ and non-hardening).

7.2 Stress Fields of Centre Cracked Panels

Single parameter characterisation of fully plastic crack tip fields occurs under restricted circumstances, as the flow fields of weakly strain hardening materials depend on geometry and loading (McClintock (1971)). Centre cracked panels develop unconstrained crack tip fields in full plasticity and a form of flow field which is radically different to the constrained fields developed by deeply cracked bend bars. In full plasticity, centre crack panels develop shear bands inclined at $\pm 45^\circ$ to the crack plane as shown schematically in Figure 7.1.

The loss of crack tip constraint associated with the field is illustrated by the numerical results in Figure 7.2. This Figure shows profiles of the hoop stress directly ahead of the crack as a function of r/ρ for a CCP ($n=13$ $a/W=0.3$), at different levels of deformation. The stress profiles are compared with the small scale yielding field which occurs when $T=0$. Even at very low levels of deformation within contained yielding the loss of constraint is significant. However even for the highest level of deformation $\frac{\sigma}{\sigma_0} \approx 10$ the stress profiles remain broadly parallel to the small scale

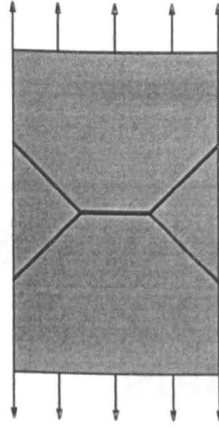


Figure 7.1: Development of plastic flow fields in centre cracked panels.

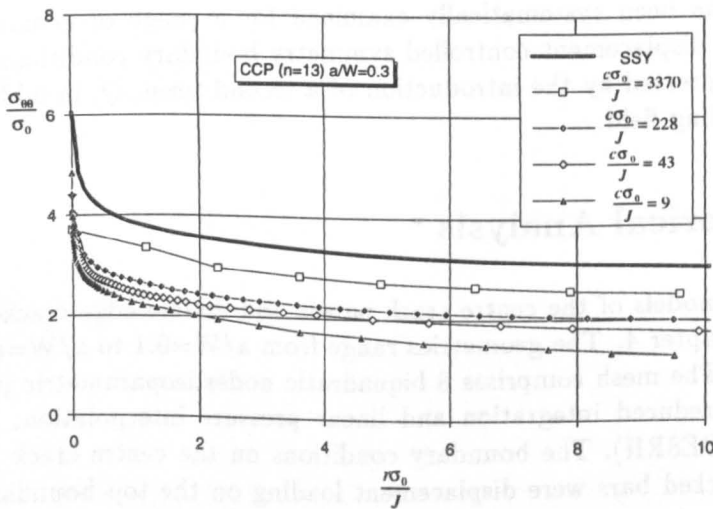


Figure 7.2: The hoop stress directly ahead of a crack in a centre crack panel, $a/W=0.3$, $n=13$ at several levels of deformations.

yielding field. The stress field can be simply expressed by a reference field being the small scale yielding field plus a difference term Q at all levels of deformation.

$$\frac{\sigma_{\theta\theta}}{\sigma_0} = \frac{\sigma_{SSY}}{\sigma_0} + Q \quad (7.1)$$

7.3 Numerical Results for Centre Cracked Panels

7.3.1 Numerical Results for Centre Cracked Panels

The stresses have been compared with modified boundary layer formulations at the same value of T and plotted as a function of applied load normalised by the limit load at a distance $r^*\sigma_0/J=2$ from the crack tip. T was calculated from the applied load or equivalently the stress intensity factor K . The bi-axiality values used were as given by Nekkal (1991) and displayed in Table 3.3 Chapter 3.

The results for four strain hardening rates are shown in Figures 7.3-7.6. The modified boundary layer formulation is only valid for $\frac{T}{\sigma_0} \leq -1$, and since some of the higher hardening rates give values for $\frac{T}{\sigma_0}$ as low as -3 it has been necessary to extrapolate the modified boundary layer formulation, and the values of σ_{MBLF} are necessarily sensitive to the way the extrapolation is done. Agreement between the MBLF and full field solutions corresponds to $\frac{\sigma_{\theta\theta}}{\sigma_{MBLF}} = 1$. To assess the extent of these correlations $\pm 10\%$ lines are also given in these figures.

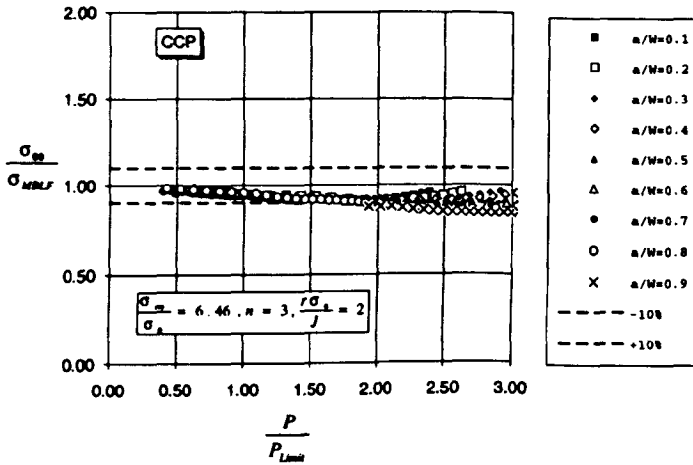


Figure 7.3: The stress directly ahead of a crack in a CCP, normalised by the MBLF stress field at a distance $\frac{r\sigma_0}{J} = 2$, as function of the load normalised by the limit load, $n=3$.

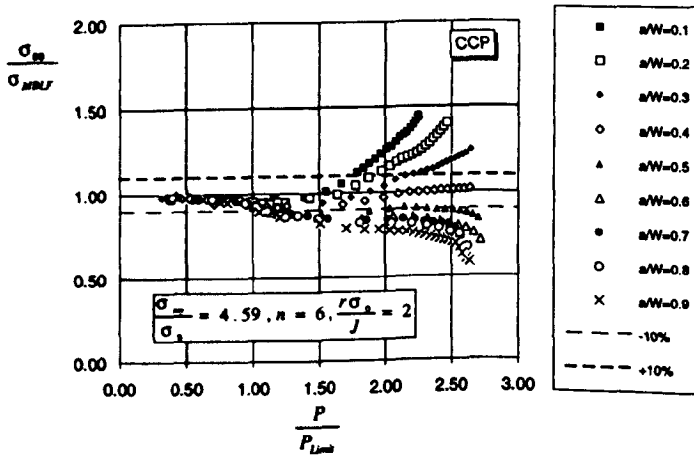


Figure 7.4: The stress directly ahead of a crack in a CCP, normalised by the MBLF stress field at a distance $\frac{r\sigma_0}{J} = 2$, as function of the load normalised by the limit load, $n=6$.

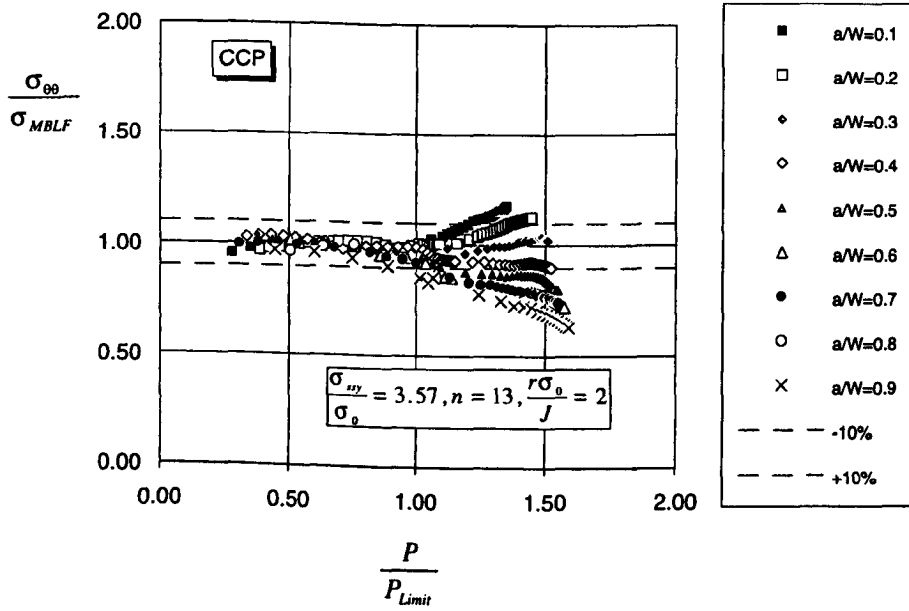


Figure 7.5: The stress directly ahead of a crack in a CCP, normalised by the MBLF stress field at a distance $\frac{r\sigma_0}{J} = 2$, as function of the load normalised by the limit load, $n=13$.

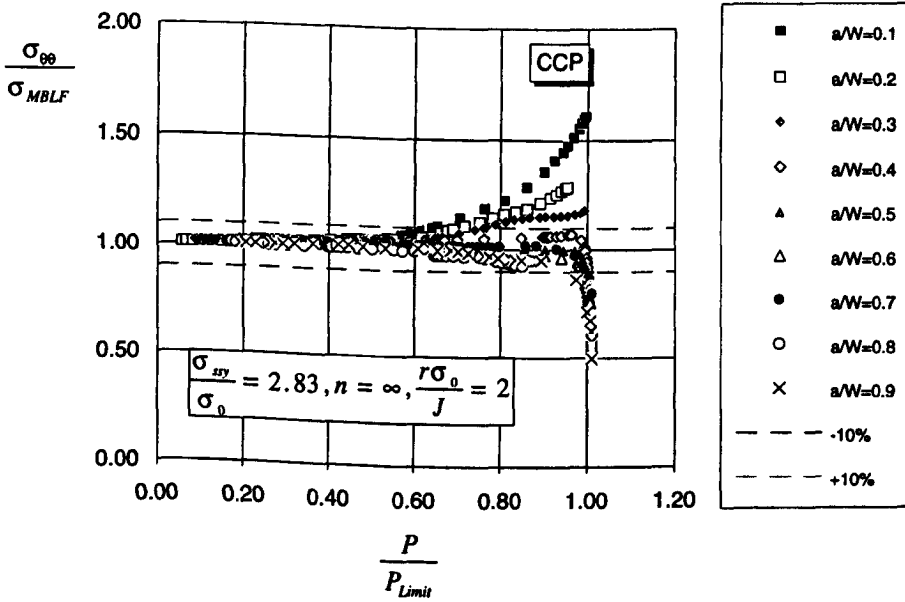


Figure 7.6: The stress directly ahead of a crack in a CCP, normalised by the MBLF stress field at a distance $\frac{r\sigma_0}{J} = 2$, as function of the load normalised by the limit load, non-hardening.

Figure 7.7 shows the difference term, Q , as defined in Equation (7.1) for all the geometries (full range of a/W ratios) at a strain hardening rate $n=13$. Q is plotted as a function of load normalised by the limit load at distances $r\sigma_0 = 1, 2$ and 5 from the crack tip.

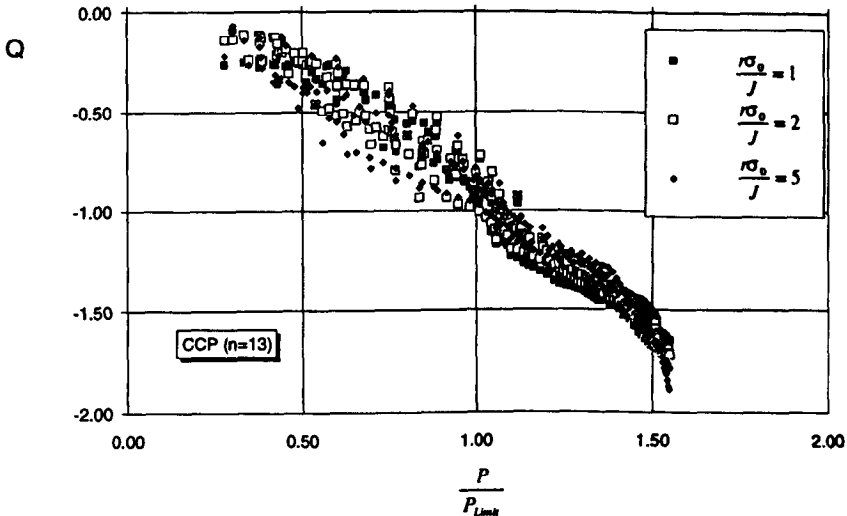


Figure 7.7: Q as a function of $\frac{P}{P_{Limit}}$ for CCP for distances $r\sigma_0 = 1, 2$ and 5, $n=13$.

The results shown in Figure 7.7 demonstrate that Q is independent of distance since the data for the three distances fall on approximately the same curve.

Q as a function of $\frac{P}{P_{Limit}}$ is shown for four different hardening rates ($n=3, 6, 13$ and non-hardening) at a distance $r\sigma_0 = 2$ from the crack tip, in Figures 7.8 - 7.11.

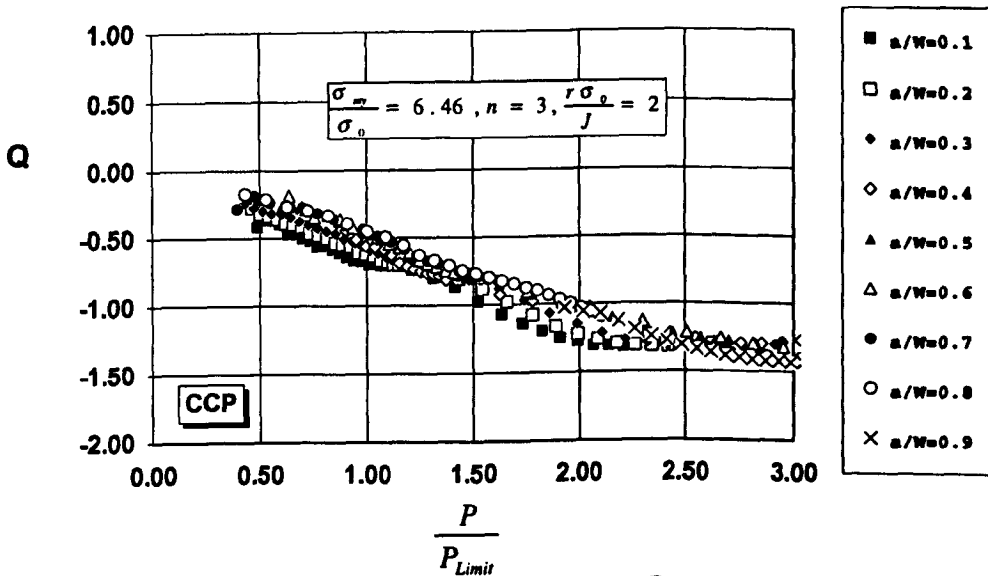


Figure 7.8: Q as a function of $\frac{P}{P_{Limit}}$ for CCP, $n=3$.

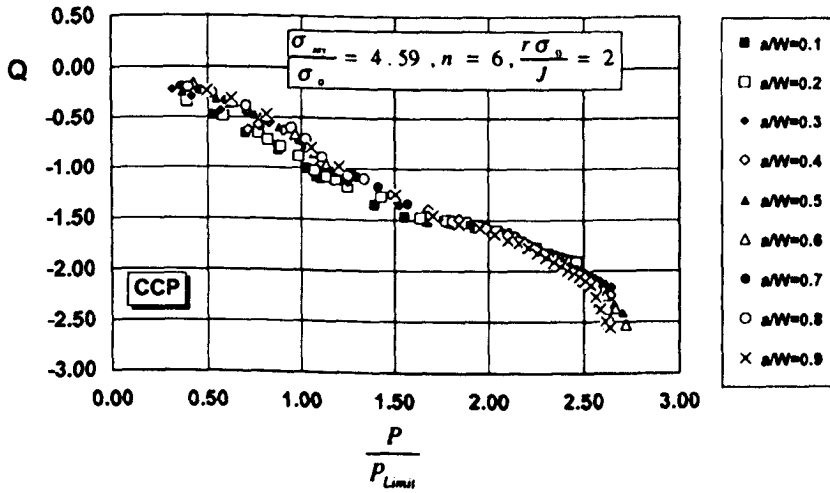


Figure 7.9: Q as a function of $\frac{P}{P_{Limit}}$ for CCP, $n=6$.

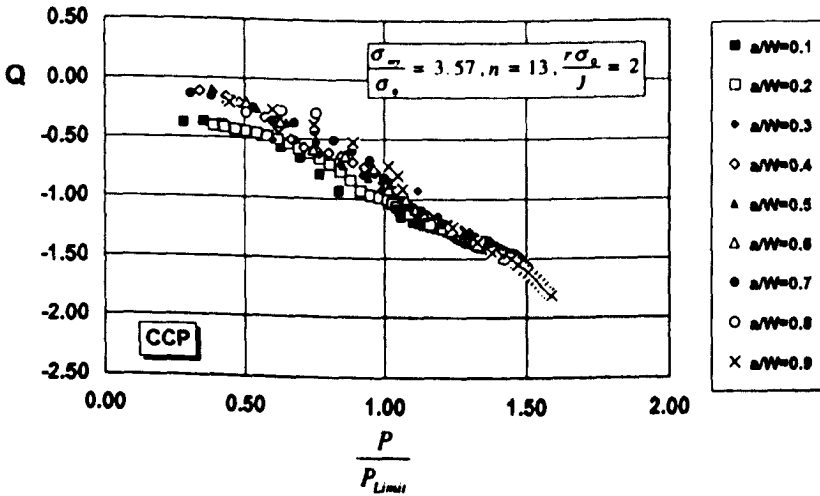


Figure 7.10: Q as a function of $\frac{P}{P_{Limit}}$ for CCP, $n=13$.

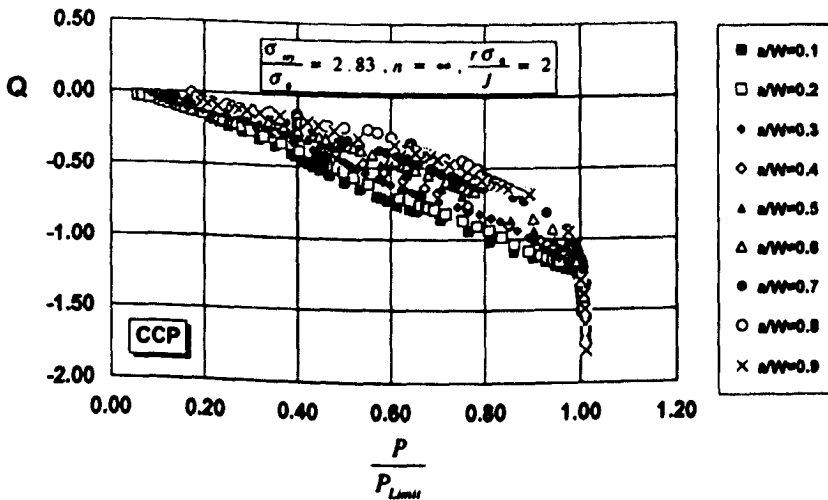


Figure 7.11: Q as a function of $\frac{P}{P_{Limit}}$ for CCP, non hardening material.

7.3.2 Force to Moment Ratios on the Ligaments of Centre Cracked Panels

Centre cracked panels are loaded with displacement boundary conditions and with displacement controlled symmetry conditions as shown schematically in Figure 7.12. A crack closing moment develops on the ligament as a reaction of the boundary condition along the symmetry line normal to the crack. The ligament is thus loaded with a combination of a crack opening force and a crack closing moment, as shown schematically in Figure 7.12.

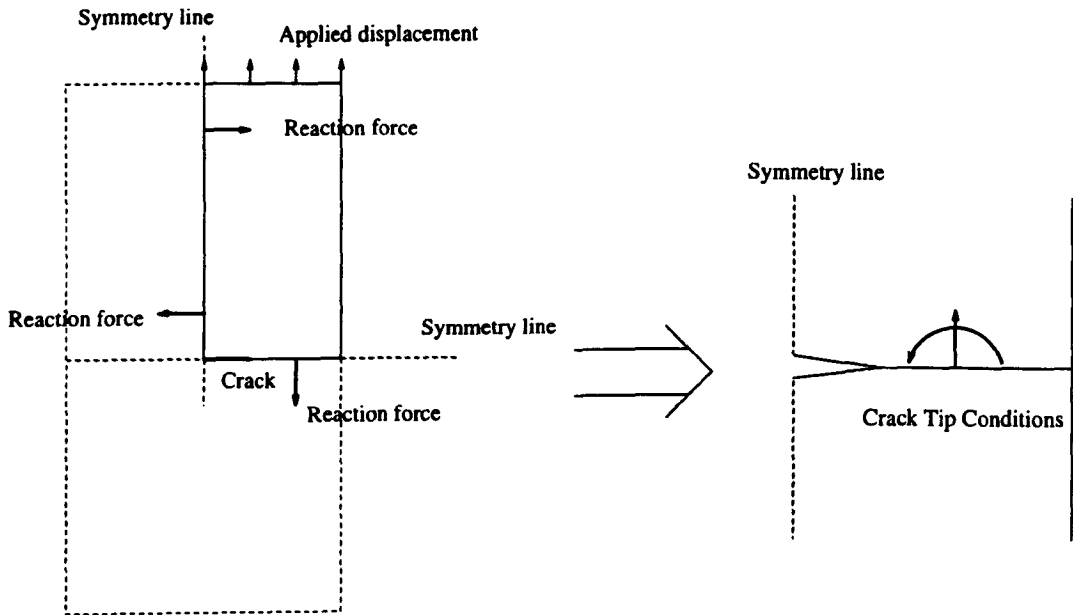


Figure 7.12: Boundary condition and reaction force and moment on the ligament for centre crack panels.

As the extent of plasticity increases, the ratio between force and moment changes, leading to a change in the crack tip conditions. The moment to force ratio $\frac{M}{P}$ can be regarded as a physical distance from the line where the moment is calculated to the line of action of the net force P . The line of action is shown schematically in Figure 7.13. e is the distance from the crack tip to the line of action, and e' is the distance from the centre line of the panel to the line of action.

If the force was applied in the line of action it would equilibrate the moment. The distance e from the crack tip to the line of action has been calculated numerically, and non-dimensionalised by the ligament c . The eccentricity ($\frac{e}{c}$) is shown as a function of $\frac{P}{P_{Limit}}$ in Figures 7.14 and 7.15 for all the geometries, for the hardening rate $n=13$ and for non hardening material. The moment about the centre line of the panel is calculated from the reaction forces on the ligament. This ensures that

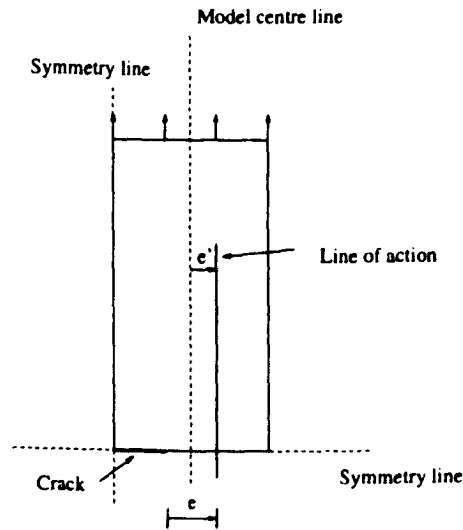


Figure 7.13: Force eccentricity.

there is no contribution to the moment from the applied load on the top boundary where the force is almost uniformly distributed.

The distance from the crack tip to the line of action as a fraction of the ligament was calculated as:

$$\left(\frac{e}{c}\right) = \left(\frac{1}{c}\right) \frac{\sum_{i=1}^n P_i (x_i - W/2)}{\sum_{i=1}^n P_i} - (a - W/2) \quad (7.2)$$

where n is the number of nodes on the ligament, P_i is the reaction force for the i 'th node and x_i is the x co-ordinate for the node with origin at the left hand side of the model.

In full plasticity the force to moment ratio approaches a steady state, and the eccentricity $(\frac{e}{c})$ falls on the same curve for all a/W ratios for $\frac{P}{P_{Limit}} \geq 1.2$ for $n=13$. For the non-hardening case the steady state is reached as the applied load reaches the limit load. At this level of deformation the crack tip condition approaches the same level of constraint for all the geometries. The fact that the crack tip condition approaches a steady state can also be seen in Figures 7.8-7.11, where the levels of constraint were described by Q as a function of $\frac{P}{P_{Limit}}$. As $(\frac{e}{c})$ approaches the same curve for all the geometries the crack tip conditions are the same and Q can be described uniquely for all geometries.

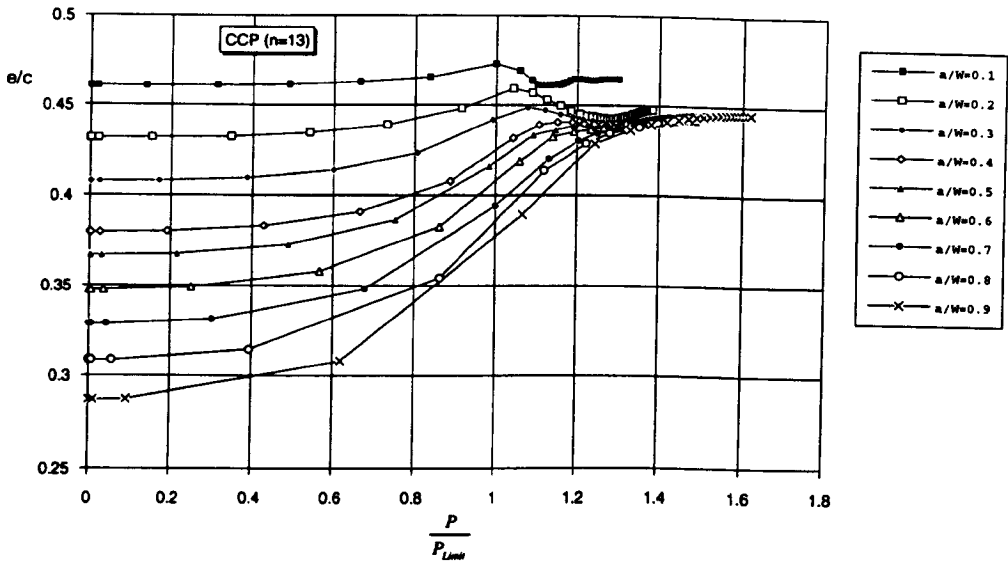


Figure 7.14: Line of action of the reaction force non dimensionalised by the size of the ligament showed as a function of $\frac{P}{P_{Limit}}$, $n=13$.

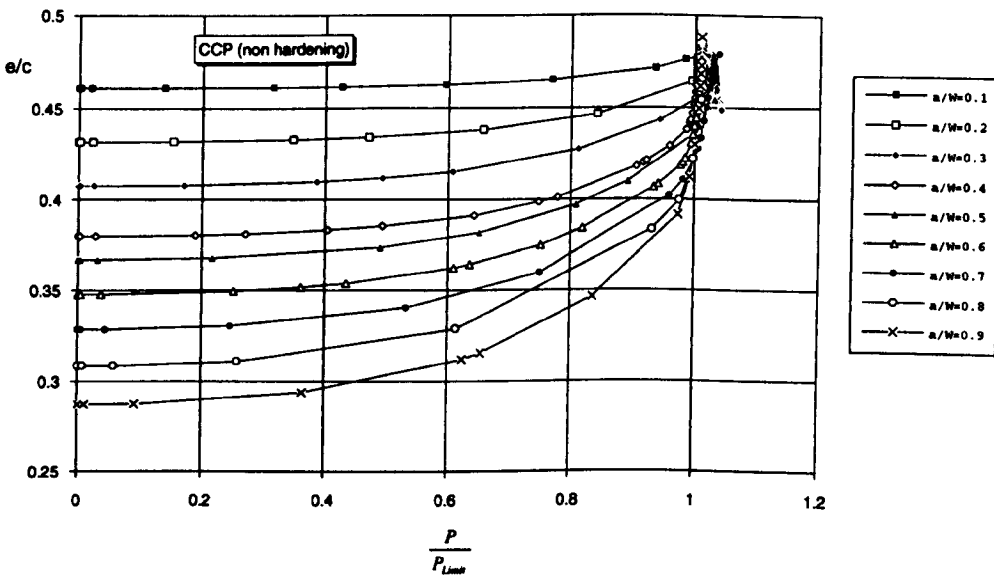


Figure 7.15: Line of action of the reaction force non dimensionalised by the size of the ligament showed as a function of $\frac{P}{P_{Limit}}$, no strain hardening.

7.4 Constraint Estimation for Centre Cracked Panels

7.4.1 Crack Tip Constraint Estimated by T

The hoop stress at a distance $\frac{r}{\rho} = 2$ from the crack tip normalised by the stresses in a modified boundary layer formulation at an equivalent value of T , are shown in Figures 7.3 - 7.6. Under largely elastic conditions the stress fields for centre cracked panels are described by the contained yielding field, characterised by K , plus the T field. Under those conditions the force to moment ratio acting on the ligament of each geometry can be obtained. At low levels of deformation the stress field for centre cracked panels is well defined by the modified boundary layer formulation. As the deformation level exceeds linear elastic characterisation, the force to moment ratios on the ligament changes and the associated bi-axiality obtained from for a linear elastic characterisation is no longer valid.

In full plasticity, centre crack tension panels in strain hardening materials can exhibit values of T beyond those that can be achieved in modified boundary layer formulations. It is therefore necessary to find a different way to characterise the constraint when T becomes very negative. Wang and Parks (1994) argued that the modified boundary layer formulation does not extend the characterisation compared with the one-parameter approach for CCP geometries. This contrasts with the data shown in Chapter 5 where single parameter characterisation is shown to breakdown long before $\frac{\sigma}{\sigma_0} = 200$.

By comparing the T stress obtained from the crack flanks with the T -stress calculated by the applied load they showed that the effective bi-axiality β changed as the load level increased. They suggested a weight function method to correct β . and defined a plastically-corrected T -stress. Wang and Parks (1994) analysed the $a/W=0.1$ geometry; while the results of analysis for $a/W=0.9$ are given in this thesis. These results are shown in Figure 7.16 where the tangential stress non-dimensionalised by the stresses in the modified boundary layer formulation at the same value of T is shown as a function of $\frac{b}{\rho}$. The dimension b is defined to be the smaller of either the crack length a or the ligament c . The results for the $a/W=0.9$ are obtained by applying force loading on the boundaries corresponding to a given level of elastic-plastic deformation. The load case is then analysed as a linear elastic case, and the T stress is calculated from K rather than from the applied load as is the case in the elastic-plastic analyses. Three different load cases have been analysed, as shown in Figure 7.16.

Further, centre cracked panels with a high strain hardening material, the levels of T stress get beyond the validity of the modified boundary layer formulation. The validity domain for the modified boundary layer formulation is $0 \geq \frac{T}{\sigma_0} \geq -1$, for the case when $\frac{T}{\sigma_0} < -1$ the modified boundary layer formulation stress needs to be extrapolated. For positive values of T the small scale yielding value is applied.

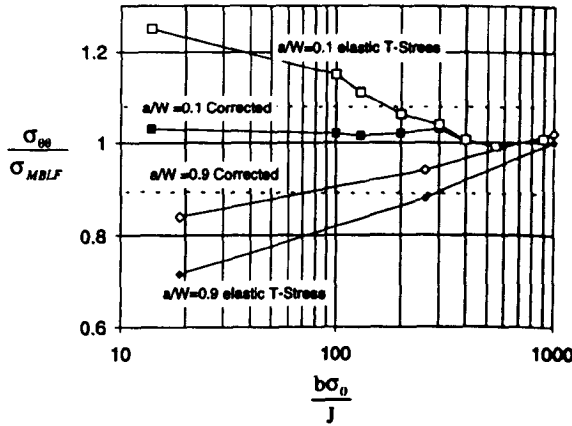


Figure 7.16: Comparison of hoop stress and MBLF solutions at $\frac{r_0}{J} = 2$. MBLF solutions were obtained using the elastic T-stress and the plastic corrected T-stress. Data for $a/W=0.1$ after Wang and Park (1994).

7.4.2 Crack Tip Constraint Estimated by Q

In Figures 7.8-7.11 the level of constraint given by Q was shown for hardening rates $n=3, 6, 13$ and non hardening. At low levels of deformation the scatter over the range of a/W is more significant than at higher levels of deformation. Q depends on the force to moment ratio, and as the force to moment ratio approaches a steady state the crack tip condition reaches a steady state for all the geometries and Q can be described by a single function of $\frac{P}{P_{Limit}}$.

The simplest way to estimate Q as a function of $\frac{P}{P_{Limit}}$ over the full deformation range is by a bi-linear approximation assuming that Q is proportional to applied load. The slope of the lines depends on the hardening rate

$$\begin{aligned}
 Q &= \alpha_1(n) \left(\frac{P}{P_{Limit}} \right) & \frac{P}{P_{Limit}} &\leq L_r^{max} \\
 Q &= Q(L_r^{max}) & \frac{P}{P_{Limit}} &= L_r^{max} \\
 Q &= \alpha_2 \left(\frac{P}{P_{Limit}} - L_r^{max} \right) + Q(L_r^{max}) & \frac{P}{P_{Limit}} &> L_r^{max}
 \end{aligned}
 \tag{7.3}$$

Values for $\alpha_1(n)$, $\alpha_2(n)$ and $Q(L_r^{max})$ are given in Table 7.1 for hardening rates $n=3, 6, 13$ and non-hardening. Values of L_r^{max} are given in Table 6.5, however for $n=3$ the line break is better described as being at $\frac{P}{P_{Limit}}=2$ rather than at L_r^{max} which is 3.8.

An example of the estimation schemes is shown in Figure 7.17 where Q is given as a function of $\frac{P}{P_{Limit}}$ using the bi-linear expression, for a hardening rate of $n=6$.

n	α_1	α_2	$Q_{L_r^{max}}$
3	-0.6	-0.2	-1.2
6	-0.9	-0.8	-1.4
13	-0.9	-1.7	-1
∞	-0.9	-	-

Table 7.1: Values of the Q estimation schemes for centre cracked panels for hardening rates $n=3, 6, 13$ and non-hardening.

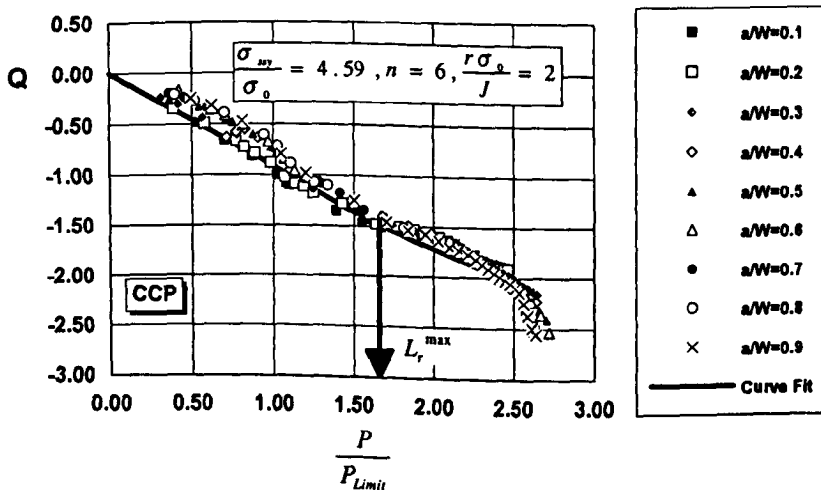


Figure 7.17: Q as a function of $\frac{P}{P_{Limit}}$ for centre cracked panel, $n=6$.

7.4.3 Discussion of Constraint Estimation for Centre Cracked Panels

A series of full field solutions of centre cracked panels have been analysed. The stresses at a distance $\frac{r\sigma_0}{J}=2$ from the crack tip non-dimensionalised by the stresses in modified boundary layer formulations are shown in Figures 7.3-7.6 as a function of $\frac{P}{P_{Limit}}$, for the hardening rates $n=3,6, 13$ and non-hardening materials. These results show that for the low levels of deformation the stress fields are well defined by the stresses obtained in a modified boundary layer formulation, but as $\frac{P}{P_{Limit}}$ increases the profiles start to diverge. The way the stresses differ from the small scale yielding field can be explained by the moment on the ligament changing due to the displacement boundary conditions. The conditions on the ligament due to the displacement boundary correspond to a crack closing moment. At low levels of deformation the force to moment ratio depends on the deformation level. At higher levels of deformation the force to moment ratio approaches a steady state and Q is well described by one relationship for all a/W ratios. This is because centre cracked panels all develop the same type of flow fields as shown in Figure 7.1.

Stress fields for crack geometries with low levels of constraint such as centre cracked

panels can be described by a reference field σ_{SSY} plus a second term characterising the level of constraint. It was demonstrated that for low levels of deformation the J - T characterisation works well for centre cracked panels, and the stress field under those conditions are characterised by the stresses obtained from a modified boundary layer formulation, as shown in Figures 7.3-7.6. However, as the load level increases the J - T characterisation breaks down and T is no longer a good description for the crack tip constraint, and therefore Q is proposed as the simplest way to complete the constraint estimation schemes for centre cracked panels.

n	(a/W)	Q (Equ. 7.6)	Q (Equ. 7.5)
∞	0.2	$-0.97 \frac{\sigma_{app}}{\sigma_0}$	$-0.83 \frac{\sigma_{app}}{\sigma_0}$
∞	0.5	$-1.57 \frac{\sigma_{app}}{\sigma_0}$	$-1.08 \frac{\sigma_{app}}{\sigma_0}$
6	0.3	$-1.11 \frac{\sigma_{app}}{\sigma_0}$	$-0.53 \frac{\sigma_{app}}{\sigma_0}$

Table 7.2: Values of Q calculated using two different approaches.

The level of constraint in the modified boundary layer formulation can be expressed as:

$$Q_T = a_1 \left(\frac{T}{\sigma_0} \right) - a_2 \left(\frac{T}{\sigma_0} \right)^2 \quad (7.4)$$

where constants a_1 and a_2 are given as a function of the hardening rate in Table 5.2. The T -stress is proportional to the load and for low levels of deformation, when $\frac{T}{\sigma_0} \ll 1$ the second term is very small and can be neglected. T can then be expressed in terms of the load as $T = \sigma_{app} \beta(a/W) f(a/W)$ and Q_T can now be written as

$$Q_T = a_1 \beta(a/W) f(a/W) \left(\frac{\sigma_{app}}{\sigma_0} \right) \quad (7.5)$$

σ_{app} is the applied stress, $f(a/W)$ is the K -calibration and $\beta(a/W)$ is the biaxiality parameter.

This term can be compared with the empirical expression for Q given by Equation (7.3), where $\frac{P}{P_{Limit}} \leq L_r^{max}$. The limit loads for centre cracked panels given by Miller (1987) are $P_{Limit} = \frac{2}{\sqrt{3}} \sigma_0 (W-a)$, and the load $P = \sigma_{app} W$, where both the load and the limit load are given per unit thickness.

$$Q = \frac{\sqrt{3}}{2} \left(\frac{\alpha_1(n)}{1 - (a/w)} \right) \left(\frac{\sigma_{app}}{\sigma_0} \right) \quad \frac{P}{P_{Limit}} \leq L_r^{max} \quad (7.6)$$

Equations (7.5) and (7.6) can be compared using a centre cracked panel $a/W=0.2$ in non-hardening material. The calculation shows that when Q is calculated from Equation (7.6) $Q = -0.97 \frac{\sigma_{app}}{\sigma_0}$, while Q calculated from Equation (7.5) gives $Q = -0.83 \frac{\sigma_{app}}{\sigma_0}$. Examples of other geometries and hardening rates are given in Table 7.2.

The data in Table 7.2 are only applied to low levels of deformation because that was the assumption which allowed Q_T to be reduced from a two term expression to a linear expression proportional to $\frac{T}{\sigma_0}$.

A comparison between the modified boundary layer formulation and the difference field Q is shown in Figure 7.18. Q is given as a function of $\frac{P}{P_{Limit}}$ for a hardening rate $n=13$, and Q_T as a function of $\frac{P}{P_{Limit}}$ is shown for the two extremes $a/W=0.1$ and $a/W=0.9$.

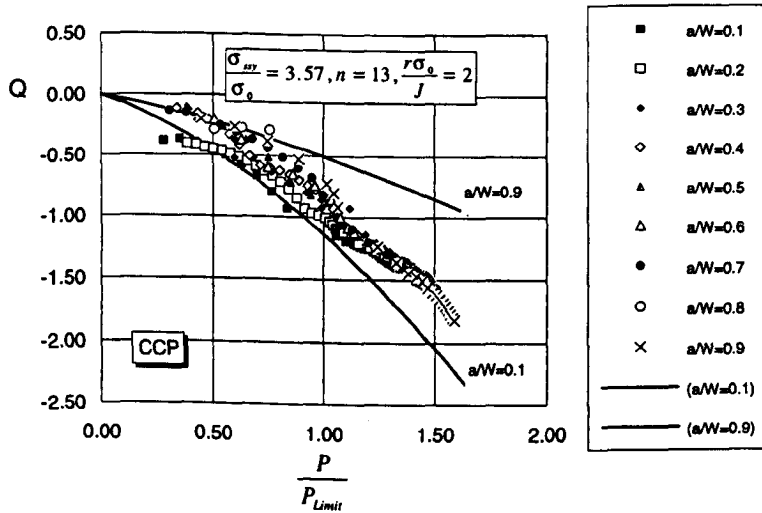


Figure 7.18: Q as a function of load normalised by limit load for $n=13$, with Q_T for $a/W=0.1$ and $a/W=0.9$.

7.5 Stress Field of Double Edge Cracked Bars

The slip line field for deeply and shallow double edge cracked bars in tension is shown in Figure 7.19. For deeply cracked double edge crack bars, plasticity is restricted to the ligament and leads to the Prandtl field. Plasticity in shallow cracked bars extends to the shoulder of the specimen as discussed by Ewing and Hill (1967). Shallow double edge cracked bars exhibit unconstrained flow fields and in this range of geometries T is negative. The bi-axiality parameter as a function of the a/W ratio is given in Table 3.3, after Leever and Radon (1983).

Figures 7.20 and 7.21 show the stress profiles for two different a/W ratios of double edge cracked bar at increasing levels of deformation. The stress profile shows the hoop stress directly ahead of the crack as a function of $\frac{r}{\rho}$. The geometry in Figure 7.20 is a shallow crack configuration ($a/W=0.3$) and in Figure 7.21 a deeply cracked configuration ($a/W=0.9$). At the lowest level of deformation ($\frac{\sigma_0}{\sigma_y} = 1013$) for $a/W=0.3$, the crack tip field can be expressed as the small scale yielding field, however as the load level increases an additional term is needed to describe the stress field. The fact that the stress field remains parallel indicates that the second parameter is distance independent. It also suggests that there is no significant opening moment on the ligament. For $a/W=0.9$ the stress field is slightly unconstrained at low levels of deformation. As plasticity develops, the fully constrained Prandtl field forms around the crack tip, as shown in Figure 7.19 and the stress fields approach the small scale yielding field.

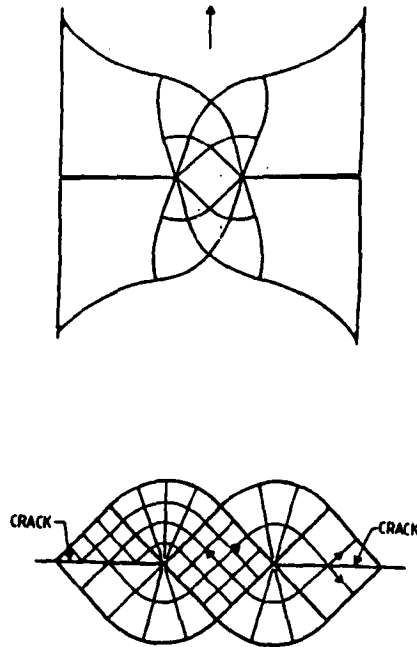


Figure 7.19: Slip line fields for double edge cracked bars.

7.6 Numerical Results for Double Edge Cracked Bars

The hoop stress directly ahead of the crack for the full field solutions of double edge cracked bar has been examined at a distance $\frac{r_{\sigma_0}}{c} = 2$ and compared with the modified boundary layer formulation at equivalent values of $\frac{T}{\sigma_0}$, as shown in Figure 7.22 for four different hardening rates. The stresses normalised by modified boundary layer formulation are plotted as a function of applied load normalised by the limit load. The limit loads for the double edge crack bars were calculated from numerical results as described in Chapter 4.

For the single edge crack bars in both tension and bending the level of constraint Q was expressed as a two term expression involving a distance dependent term and a distance independent term. Since the stress fields show no distance dependence the level of constraint will be expressed as a general Q term which is the difference between the stress field at a distance $\frac{r_{\sigma_0}}{c}$ from the crack tip and the small scale yielding field at the same distance. Values of Q at a distance $\frac{r_{\sigma_0}}{c} = 2$ from the crack tip as a function of $\frac{P}{P_{Limit}}$ are shown for the four different hardening rates in Figure 7.23.

The moment on the ligament was calculated for one quarter of the whole geometry and the eccentricity e/c calculated in the same manner as the centre cracked panels, given in Equation (7.2). The non-dimensionalised eccentricity e/c is shown in Figure 7.25 as a function of $\frac{P}{P_{Limit}}$ for all a/W ratios.

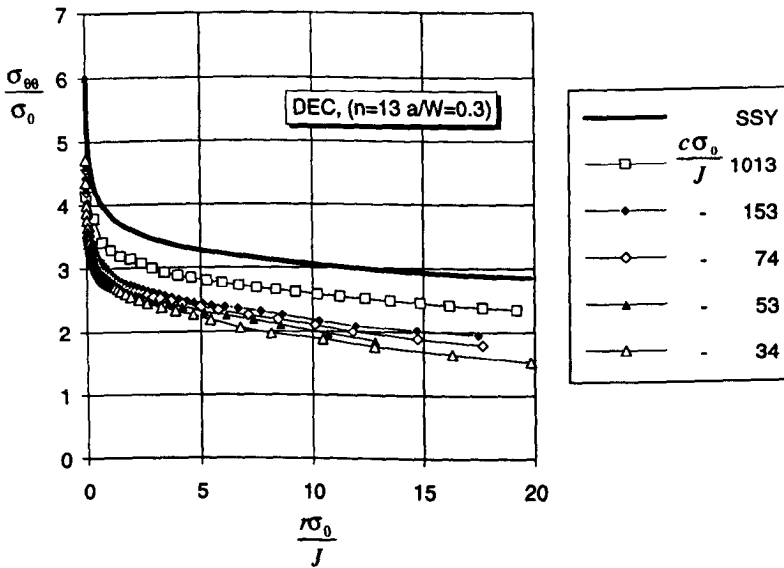


Figure 7.20: Hoop stress normalised by yield stress directly ahead of a crack in a double edge cracked bar at several levels of deformation, $a/W=0.3$ and $n=13$.

7.7 Constraint Estimation for Double Edge Cracked Bars

Constraint is expressed in terms of Q and given in Figure 7.23 as a function of $\frac{P}{P_{Limit}}$. The deeply cracked geometry $a/W=0.9$ behaves differently from the shallow cracked configurations. At very low levels of deformation there is a loss of constraint as T is slightly negative. As the load level increases the constraint rises again as the full Prandtl field appears around the crack tip. For $a/W=0.9$, $n=13$, Q reaches a positive value for $\frac{P}{P_{Limit}} = 1.2$; this occurs because for $a/W \geq 0.9$ the plastic flow field is restricted to the ligament, as shown in Figure 7.19.

Constraint has been estimated by Q as a function of $\frac{P}{P_{Limit}}$. For $n=3$ the simplest expression is a straight line, but for the lower hardening rates ($n=6, 13$ and non-hardening) Q as been estimated by a second order function:

$$\begin{aligned}
 Q &= -0.3 \frac{P}{P_{Limit}} & n &= 3 \\
 Q &= -28 \frac{P}{P_{Limit}}^2 - 0.21 \frac{P}{P_{Limit}} & n &= 6 \\
 Q &= -0.58 \frac{P}{P_{Limit}}^2 - 0.17 \frac{P}{P_{Limit}} & n &= 13 \\
 Q &= -2.13 \frac{P}{P_{Limit}}^2 + 0.93 \frac{P}{P_{Limit}} & & \text{non - hardening materials}
 \end{aligned}
 \tag{7.7}$$

An example of Q estimated as a function of $\frac{P}{P_{Limit}}$ using a second order curve fit is shown in Figure 7.24, for a hardening rate $n=6$.

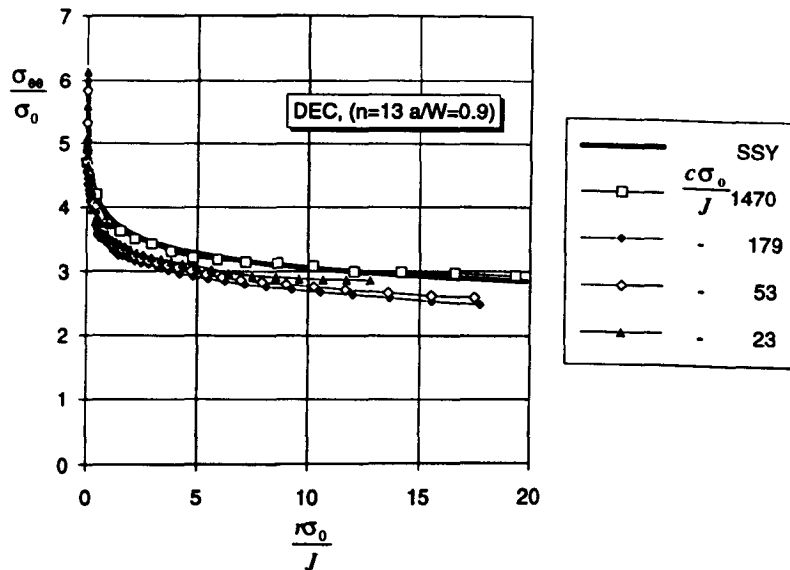


Figure 7.21: Hoop stress normalised by yield stress directly ahead of a crack in a double edge cracked bar at several levels of deformation, $a/W=0.9$ and $n=13$.

When the eccentricity normalised by the ligament was calculated from the force to moment ratio, it was also found that the deeply cracked geometry changes most. This can be seen in Figure 7.25 where the eccentricity normalised by the ligament is shown as a function of $\frac{P}{P_{Limit}}$ for $a/W=0.9$. (e/c) begins in the linear elastic case at 0.365 and at the highest level of deformation (e/c) becomes equal to 0.482. This may be compared with $a/W=0.4$ where for the lowest level of deformation (e/c)=0.39 and for the highest level of deformation (e/c) becomes 0.45. This explains why the constraint initially falls, but finally rises.

7.8 Conclusion

Crack tip constraint has been analysed for centre cracked panels and double edge cracked bars. Common to both geometries are important displacement boundary conditions and applied symmetry conditions. Because of the boundary conditions the ligament is loaded with a combination of a crack opening force and a crack closing moment. The evolution of the force/moment ratio as plasticity develops creates problems for constraint estimation schemes. For the centre cracked panels the crack tip conditions approach a steady state for all the a/W ratios, but for the double edge cracked bars this was not the case. The reason for this is the nature of the fully plastic flow fields. Centre cracked panels develop same type of the flow field for all a/W ratios. For deeply cracked double edge crack bars plasticity is restricted to the ligament and a full Prandtl field is developed around the crack tip, whereas for the shallow double edge cracked bars plasticity extends to the shoulder and results in a significant loss of constraint. Empirical constraint estimation formulas for centre cracked panels and double edge cracked bars have been given, and Q has been expressed as a function of the load non-dimensionalised by the limit load.

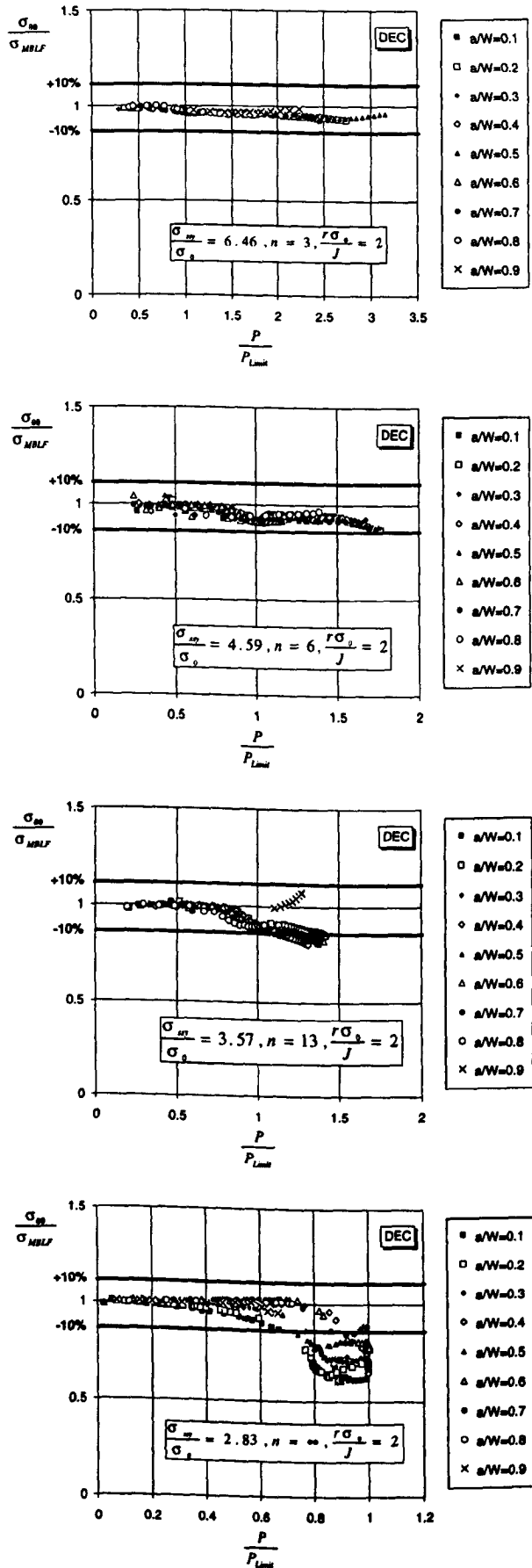


Figure 7.22: The hoop stress directly ahead of the crack at a distance $\frac{r\sigma_0}{J} = 2$ normalised by the modified boundary layer formulation as a function of the load normalised by limit load, strain hardening rates $n=3,6,13$ and non-hardening.

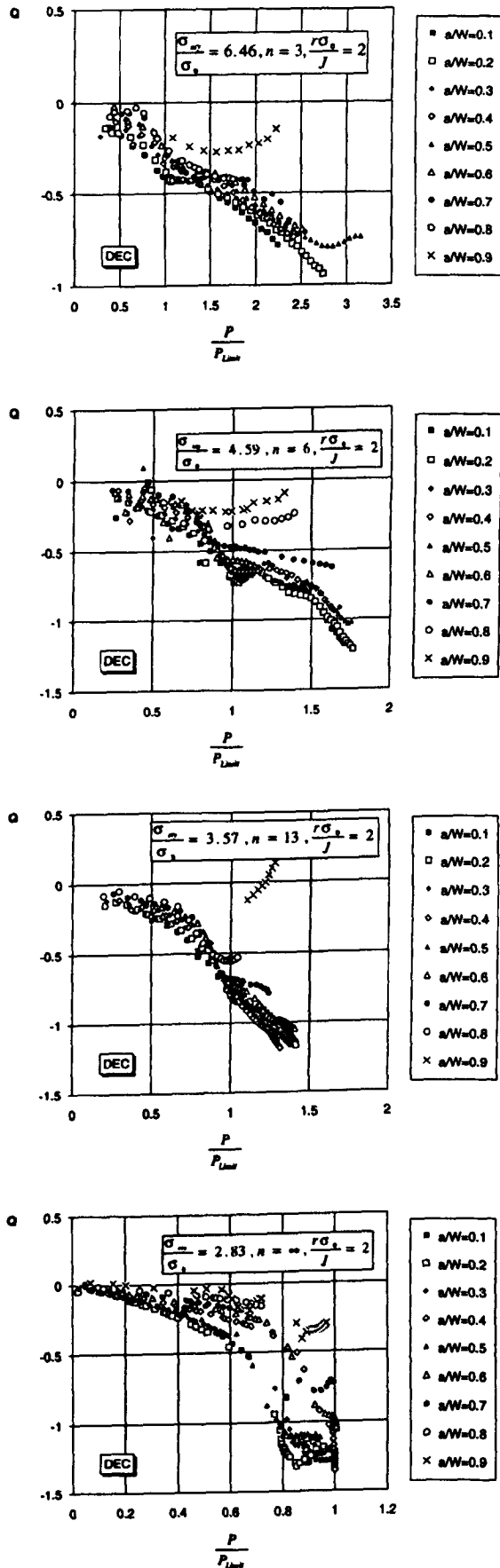


Figure 7.23: Q at a distance $\frac{r\sigma_0}{J} = 2$ as a function of the load normalised by limit load, strain hardening rates $n=3,6,13$ and non-hardening.

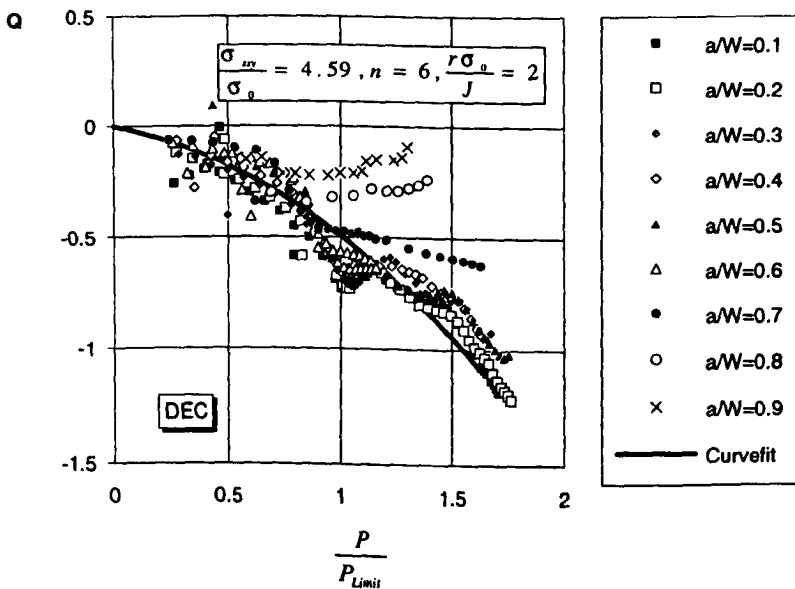


Figure 7.24: Q as a function of $\frac{P}{P_{Limit}}$ for double edge cracked bar with a second order curve fit, $n=6$.

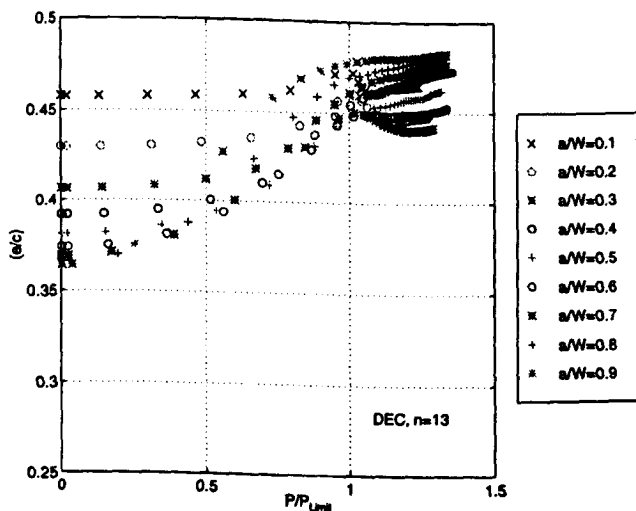


Figure 7.25: Line of action for reaction force non dimensionalised by the size of the ligament as a function of $\frac{P}{P_{Limit}}$, $n=13$.

Constraint Effects Modelled by Local Failure Criteria

8.1 Approach to a Local Failure Criteria in Cleavage

Temperature transitions in fracture toughness are important to the integrity of engineering structures. Three principal forms of fracture can be identified in plain carbon steels, of which the most dangerous is cleavage. Cleavage fracture is a low energy mode of fracture which occurs at low temperatures, by the direct separation of low index crystallographic planes.

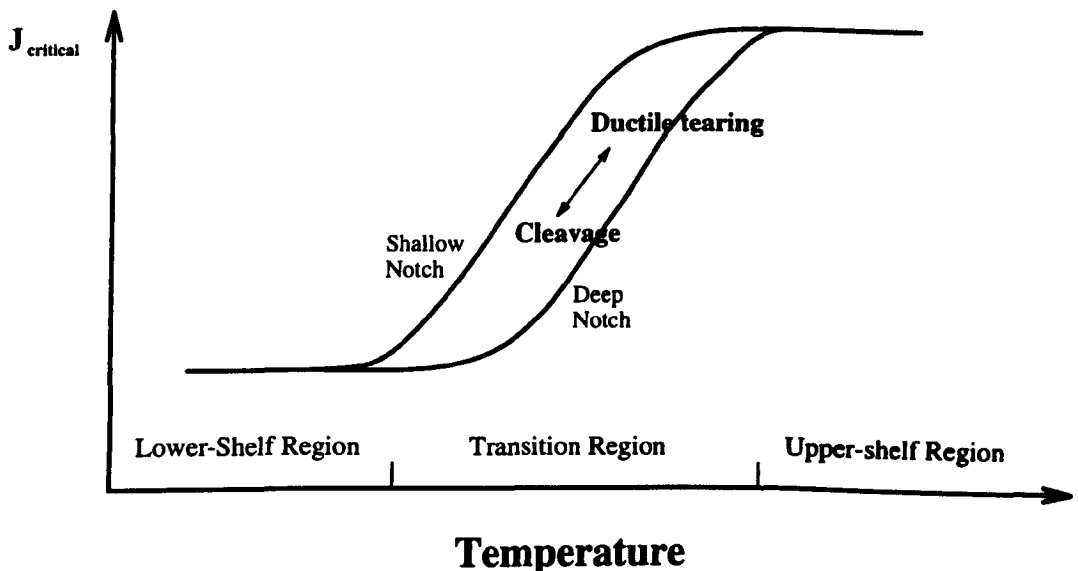


Figure 8.1: Schematic J -temperature curve for ductile-brittle transition.

As the temperature rises, the failure mode may pass through a transition region in which a ductile crack extension by void growth and coalescence from second phase particles followed by cleavage failure. At higher temperatures the toughness reaches the upper shelf, where the fracture process is completely ductile. The fracture process in the transition zone can be regarded as a competition between cleavage failure and ductile tearing. This competition has particular significance for structures operating near the transition temperature.

At the lowest temperatures the toughness and the associated plastic zone may be small enough to be described by linear elastic fracture mechanics LFM. However as the temperature increases the amount of plasticity invalidates LFM and requires the use of elastic plastic fracture mechanics EPFM, which introduces constraint effects.

8.1.1 The Scaling Approach

Anderson and Dodds (1991), Dodds *et al.* (1991) quantified the size requirement for single parameter characterisation of cleavage initiation under plastic deformation exceeding the K_{Ic} limits given in ASTM E339-83. The relation between different specimen geometries and fracture toughness is shown schematically in Figure 8.2.

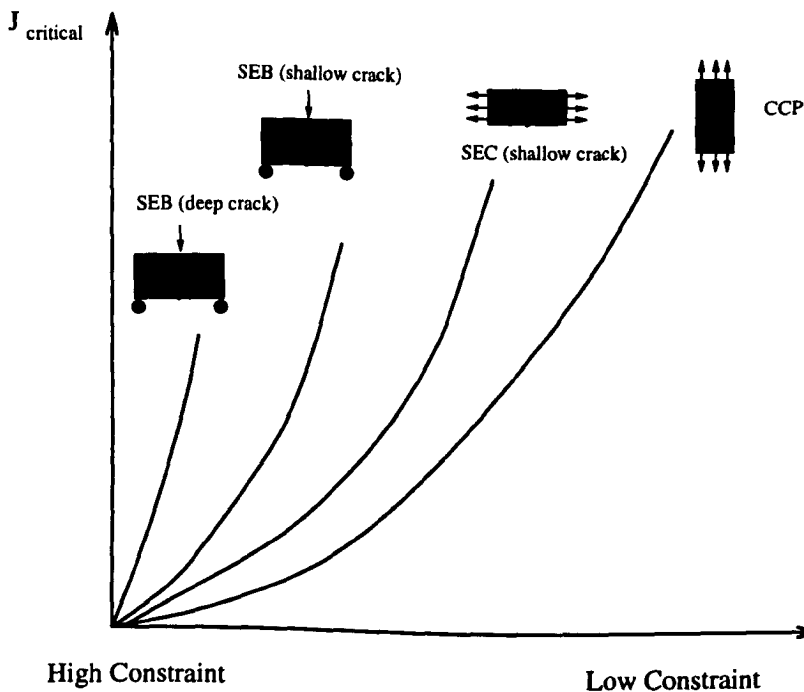


Figure 8.2: Fracture toughness for specimens with various levels of crack tip constraint.

Shallow cracked geometries where $T \leq 0$ exhibit increased toughness compared to deeply cracked bars when tested in the transition region. The increased toughness is caused by loss of constraint due to the decrease in crack-tip triaxiality. It was argued that the geometry dependence of toughness could be correlated with constraint. Consequently, cleavage fracture toughness in the transition region exhibits a strong geometry dependence.

The effect of constraint on toughness can be determined by testing different geometries. Deeply edge cracked bend bars are the most constrained, while centre cracked panels exhibit the lowest levels of constraint. This result indicates a strong geometry dependence of fracture toughness for cleavage in the transition zone, in which shallow cracked bend bars were much tougher than the deeply cracked at identical temperatures.

By comparing critical J -values for single edge cracked bend (SEB) bars with the value obtained in small scale yielding model, Dodds *et al.* (1991) proposed the use of a scaling factor, to correlate the fracture toughness between SEB and SSY. The scaling factor defined as J_{seb}/J_{ssy} relates the stress fields in bend bars in full plasticity and in small scale yielding at a fixed distance 4 crack tip opening displacements (δ) ahead of the crack. Dodds *et al.* (1991) suggest that the constraint scaling factor is applicable over a length-scale of $4-5\delta$. Figure 8.3 shows the effects of a/W on J_{seb}/J_{ssy} for a material with strain hardening $n=10$. For a given specimen size and material hardening the equivalent toughness (J_{ssy}) can be estimated from Figure 8.3.

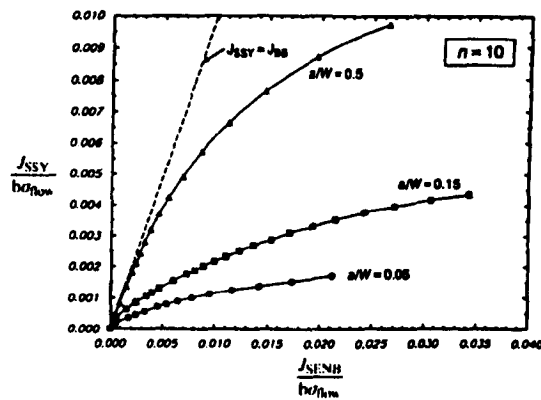


Figure 8.3: Relationship between the normalised J -integral values in SEB specimens with those of SSY conditions which generate equivalent opening mode stresses at $r=4\delta$ (COD) ahead of the crack tip for hardening exponent $n=10$. Dodds, Anderson and Kirk (1991).

8.1.2 The Local Approach

The *local approach* attempts to apply mechanistic failure criteria to crack tip stress and strain fields to determine fracture toughness. The fracture criterion is thus based on the local stress and strain fields acting over a critical micro structural distance which allows the operation of the failure mechanism.

Rice and Johnson (1970) argued that to propagate the crack, a critical fracture stress has to be exceeded over a micro structurally determined characteristic distance. This failure criteria was adopted by Ritchie, Knott and Rice (1973) to determine the fracture toughness for cleavage initiation in mild steel on the lower shelf. Cleavage fracture in mild steel initiates as microcracks are formed at the grain boundary carbides, and the microcracks propagate when the stress normal to the micro crack is sufficiently high.

Ritchie, Knott and Rice (1973) argued that unstable cleavage fracture can occur only if the tensile stress is high enough to initiate a crack at the first grain boundary directly ahead of the crack and maintain the stress level over the next grain.

They concluded therefore that the crack opening stress must exceed the fracture stress at a characteristic fixed distance of approximately two grain diameters from the crack tip, as shown in Figure 8.4.

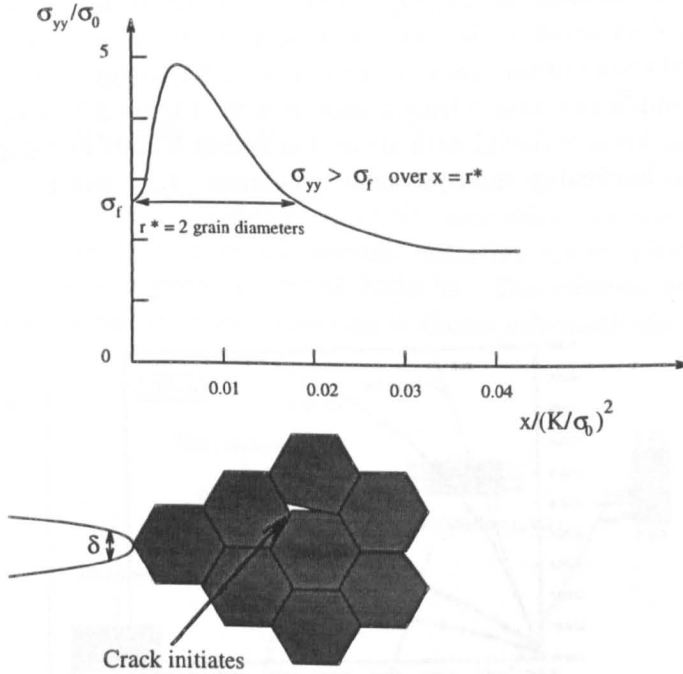


Figure 8.4: Schematic illustration of the Ritchie, Knott and Rice model for stress-controlled cleavage fracture directly ahead of a sharp crack.

Recall the nature of the HRR field and assume that fracture initiates when the maximum principal stress reaches a critical value σ_f at a distance ahead of the crack tip $r = r_c$, for $\theta = 0$. The HRR field can then be written as:

$$\frac{\sigma_f}{\sigma_0} = \left[\frac{J_c}{\alpha r_c \sigma_0 I_n \varepsilon_0} \right]^{\frac{1}{1+n}} \tilde{\sigma}_{\theta\theta}(0, n) \quad (8.1)$$

The fracture toughness can be determined by re-arranging (8.1) to expose J_c :

$$J_c = \left[\frac{\sigma_f}{\sigma_0 \tilde{\sigma}_{\theta\theta}(0, n)} \right]^{n+1} \alpha r_c \sigma_0 I_n \varepsilon_0 \quad (8.2)$$

This approach was developed by Ritchie, Knott and Rice (1973), to predict the temperature dependence for cleavage on the assumption that the local fracture stress σ_f is independent of the temperature as proposed by Orowan (1948), Knott (1966) and Oates (1969). At very low temperatures, the fracture stress was reached in the stress field just behind the plastic-elastic interface and the crack propagates even at low load levels because of the high yield stress.

However at increased temperatures, when the size of the plastic zone increases, the fracture stress is only reached within the plastic zone, close to the crack tip. Because of the nature of the singular stress field at the crack tip the fracture stress is exceeded even at low loads without developing fracture. In order to apply this technique it is necessary to determine the local fracture stress σ_f . This is usually achieved using notched bend or tension bars.

RKR (after Ritchie, Knott and Rice (1973)) determined the fracture stress using plane strain slip line field solutions for notched bars. The failure stress was determined using

$$\sigma_f = 2k\left(1 + \frac{1}{2}\pi - \frac{1}{2}\theta\right) \quad (8.3)$$

where k is the yield stress in shear, given as $1/\sqrt{3}\sigma_0$ for a Mises material, while θ is the notch angle.

Figure 8.5 shows Ritchie, Knott and Rice (1973)'s experimental results with notched bars loaded in pure bending (4 point-bending), which support the conclusion that the characteristic distance is two grain diameters.

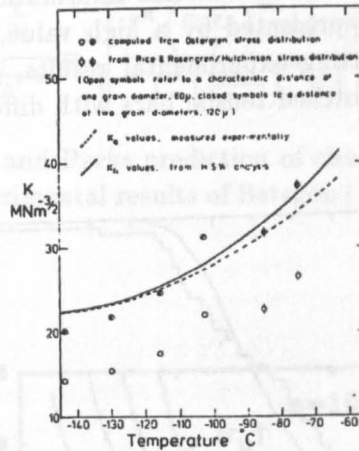


Figure 8.5: Comparison of the variation of fracture toughness with temperature between experimental values (K_Q and K_{Ic}) for characteristic distance of one and two grain diameters. H.S.W analysis: Heald, Spink and Worthington (1972)., diagram from Ritchie, Knott and Rice (1973).

8.1.3 Statistical Approach to Local Cleavage Failure

Following RKR local criteria for brittle cleavage, fracture based on Weibull statistics have been developed, Curry and Knott (1979), Beremin (1983), Lin *et al.* (1986) and Wang and Park (1992).

Cleavage fracture is essentially a weakest link process which involves several independent variables. The distribution of particle sizes gives a distribution of critical fracture strength σ_f , where the largest carbides have the lowest strength. The crystallographic orientation of the particles also influences the fracture process. The probability of failure below a stress σ_w can be given as a Weibull distribution of the form:

$$P_R = 1 - \exp\left(-\left(\frac{\sigma_w}{\sigma_u}\right)^m\right) \quad (8.4)$$

where σ_u is a temperature independent material constant (Beremin (1983)), and σ_w is the Weibull stress, defined as:

$$\sigma_w = \sqrt[m]{\sum_j (\sigma_1^j)^m \frac{V_j}{V_0}} \quad (8.5)$$

The stressed volume is divided into sub-volumes V_0 . The sub-volumes have to be of a size such that there is a finite probability of containing an existing microcrack with a reasonable length. It is assumed that the volumes are statistically independent of their neighbours.

In the Beremin analysis (1983), V_0 was chosen as a cube of $50 \times 50 \times 50 \mu m$ containing about 8 grains. V_j is the volume and σ_1^j is the maximum principal stress in the j 'th volume. The material constant m contains information about the material's reliability. High reliability is represented by a high value of m . Beremin (1983) found m to be 22 by curve fitting experimental results, on conventional tensile specimen and axis-symmetric notched tensile bars with different radii (20,10,4 and 2 mm), as shown in Figure 8.6.

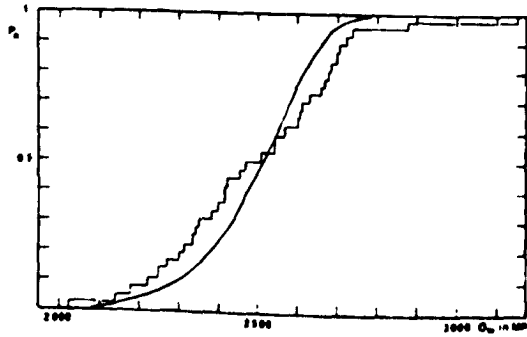


Figure 8.6: Plot of the experimental results as a function of the Weibull stress σ_w . Each vertical segment corresponds to one experiment. Comparison is made with the theoretical prediction of the cumulative probability of failure. Ferritic grain, test temperature 77K, after Beremin (1983).

Wang and Parks (1992) also used a statistical approach to estimate the effect of constraint on cleavage failure, by incorporating the T stress into the weakest link model to examine the effect of the T stress on the cleavage toughness.

If the particle strength is S , $g(S)$ defines the particle strength distribution, described by a Weibull three-parameter distribution. The particle strength distribution $g(S)$ gives the number of particles per unit volume having the strength S as:

$$\int_{\sigma_u}^{\sigma} g(S) dS = \left(\frac{\sigma - \sigma_u}{S_0} \right)^m f N \quad (8.6)$$

N is the number of particles per unit volume, σ is the crack opening stress ahead of the crack, and S_0 is a scaling parameter with the dimension of stress. The fraction of the particles N which can cleave is denoted f . The total failure probability Φ is

then given in the form of a weakest link statistic as:

$$\ln(1 - \Phi) = -fNb \left(\frac{\sigma_0}{S_0}\right)^m \int^A \left(\frac{\sigma - \sigma_u}{\sigma_0}\right)^m dA \tag{8.7}$$

Where A is the area ahead of the crack in which $\sigma \geq \sigma_u$ and $\sigma \geq \sigma_0$. f,N,b, σ_0 , S_0 ,m and σ_u are material constants.

The stress fields for different T values were calculated from a modified boundary layer formulation. For each level of T, there is a different value of the probability for failure calculated by Equation (8.7). Based on a dimensional analysis of (8.7), Wang and Parks (1992) expressed the ratio of the cleavage fracture toughness for any $\frac{T}{\sigma_0}$ to the cleavage toughness for $\frac{T}{\sigma_0} = 0$ in the form:

$$\frac{J_c^{\frac{T}{\sigma_0}}}{J_c^{\frac{T}{\sigma_0}=0}} = \sqrt{\frac{\int^A \left(\frac{\sigma - \sigma_u}{\sigma_0}\right)^m dA | \frac{T}{\sigma_0} = 0}{\int^A \left(\frac{\sigma - \sigma_u}{\sigma_0}\right)^m dA | \frac{T}{\sigma_0}}} \tag{8.8}$$

Figure 8.7 shows Wang and Parks prediction of cleavage fracture toughness, which was compared with experimental results of Betegón (1990), shown in the lower graph in Figure 8.7.

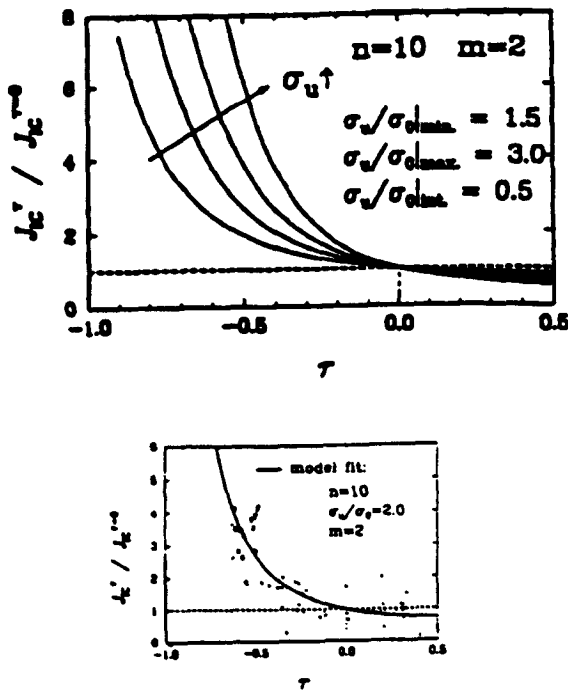


Figure 8.7: Variation of cleavage fracture toughness vs. τ at various values of σ_u . σ_u is the fracture stress and $\tau = \frac{T}{\sigma_0}$. The lower graph shows the analysis compared with the experimental data of Betegón (1990), after Wang and Parks (1992).

Shih and O'Dowd (1992) applied the RKR fracture criteria to $J - Q$ fields. The criterion is expressed as a critical stress σ_f , at a micro structurally significant distance r_c , and Equation (8.1) can be expressed in the form:

$$\frac{\sigma_f}{\sigma_0} = \left[\frac{J_c}{\alpha r_c \sigma_0 I_n \epsilon_0} \right]^{\frac{1}{1+n}} \bar{\sigma}_{\theta\theta}(0, n) + Q \quad (8.9)$$

The fracture toughness can be expressed as a function of Q . The toughness value at $Q=0$ is denoted J_{Ic} and the fracture toughness is now given as:

$$J_c = J_{Ic} \left(1 - \frac{Q \sigma_0}{\sigma_f} \right)^{n+1} \quad (8.10)$$

This approach may be compared with that of Dodds, Anderson and Kirk (1991). The Dodds-Anderson approach implies that unconstrained flow fields can be expressed as the HRR field multiplied by a scaling factor. As a result, the ratio $\left(\frac{J_c}{J_{Ic}}\right)$ is independent of σ_f .

In contrast $J-Q$ and $J-T$ description of crack tip fields create the field in the form of the HRR field plus a higher order term (Q) which is distance independent. This leads to relations as (8.10) in which the ratio $\left(\frac{J_c}{J_{Ic}}\right)$ is strongly dependent on σ_f . The probability of cleavage fracture is related to the contoured area in which the maximum principal stress is greater than a given value $\frac{\sigma_1}{\sigma_0}$. The area depends on the level of deformation in a low constraint geometry. The loss of constraint becomes more significant as the deformation level increases, as shown in Figure 8.8.

In the present study the contoured area ahead of a deeply cracked bend bar has been examined, as shown in Figure 8.8. The variation of stresses along rays of constant θ in a single edge bar in bending has been analysed, $a/W=0.5$ and $n=13$. Figure 8.8 compares non-dimensional contours of principal stresses for different levels of deformation. A single edge bend bar with $a/W=0.5$ has a positive bi-axiality value, and loss of constraint cannot be due to a negative T -stress, but must appear because of global bending. The contours maintain a self-similar shape but the size decrease for increasing load and extent of global bending. The actual size of the contour increases with J , but the contour in Figure 8.8 is normalised by J . The decrease in area indicates that a scaling factor must be applied to relate the SSY with the SECB.

8.1.4 Thickness effect

The constraint model used to predict fracture toughness in a local failure criteria only considers the stressed area in front of the crack tip; however Nevalainen and Dodds (1995), Koppenhoefer *et al.* (1995) and Wallin (1993) have argued that the volume of the material ahead of the crack tip controls the cleavage fracture. Wallin (1993) used a weakest link method to obtain the following statistical correction for fracture toughness data of specimens with two different thickness, B and B_0 . The method was used for experiments which failed in cleavage, and consequently he developed the following series-empirical expression:

$$K_{Ic2} = K_{min} + (K_{Ic1} - K_{min}) \left(\frac{B}{B_0} \right)^{1/4} \quad (8.11)$$

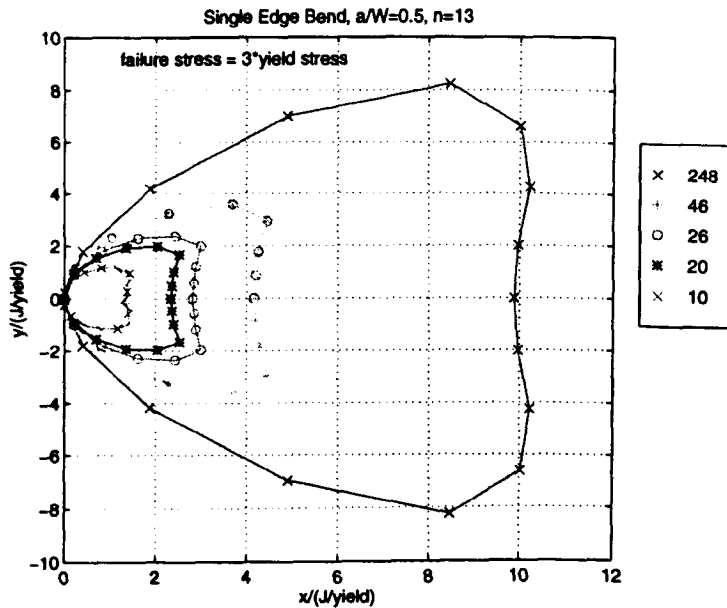


Figure 8.8: Comparison of shapes for contours of principal stresses, for increasing levels of applied loading for hardening exponent, $n=13$ and $a/W=0.5$. The levels of deformation is given in terms of $\frac{\sigma_0}{J}$.

where K_{min} denotes the threshold toughness of the material for an infinitely long crack front. This equation can also be expressed in terms of J :

$$J_{c2} = J_{c1} \sqrt{\frac{B_1}{B_2}} \quad (8.12)$$

The J equivalent of K_{min} has been neglected as a small term. The correction in Equation (8.12) relates different volumes of material to the fracture toughness. The cleavage failure is controlled by the weak metallurgical defects, and therefore the fracture toughness decreases with increasing probability of finding a defect. The increasing probability scales with increasing thickness.

The volume of material along the crack front over which the principal stress exceeds σ_c is given by :

$$V(\sigma_c) = \int_{-B/2}^{B/2} A(s, \sigma_c) ds \quad (8.13)$$

where $A(s, \sigma_c)$ is the area enclosed by the contour which lies on s . The maximum value of A , $A_{max} = A(s_{max}, \sigma_c)$. Nevalainen and Dodds (1995) suggest that the effective thickness as $B_{eff} = V/A_{max}$, and replaced the effective thickness with the actual specimen thickness in Equation (8.12). They also suggest to replacing J_{c1} with the critical value of J in a small scale yielding test $J_{c,ssy}$. A measured toughness value obtained from a specimen which has lost constraint, for example a shallow crack bend bar, can now be related to the value of the small scale yielding toughness using a modified form of Equation (8.12):

$$J_{c,ssy} = J_C \sqrt{B_{eff}/B_{ref}} \quad (8.14)$$

B_{ref} is the reference thickness related to the small scale yielding.

Figure 8.9 shows the B_{eff}/B as a function of increasing levels of deformation $J_{avg}/b\sigma_0$. The data is obtained from a 3-D finite element analysis of single edge bend bars by Navalainen and Dodds, the material strain hardening is $n=10$, and $E/\sigma_0=500$, $\nu=0.3$. They investigated the thickness effect for various W/B ratios and a range of principal stress ratios. The principal stress ratio shown in Figure 8.9 is $\sigma_1/\sigma_0=3$.

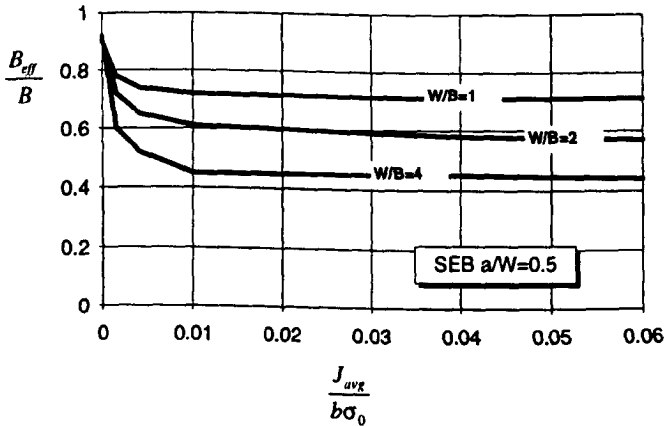


Figure 8.9: Effective thicknesses for a single edge bend bar $a/W=0.5$, $\frac{\sigma_1}{\sigma_0}=3$. Data after Navalainen and Dodds (1995), $n=10$ and $E/\sigma_0=500$.

8.2 Local Fracture Criteria for Cleavage

Crack tip constraint for single edge bend bars were discussed in Chapter 6. The level of constraint is defined by Q as defined in Equation (6.2). Q is decomposed into a two term expression in Equation (6.3). The first term is related to T and is a distance independent term in Equation (6.4). The second term is distance dependent and is related to the global bending field on the ligament. The distance dependent term is denoted Q_P and can be determined either from the load as given in Equation (6.8) or from the plastic component of J expressed in Equation (6.10).

In the present work the Ritchie, Knott and Rice fracture criteria is applied to the stress fields expressed by Equation (6.13). Cleavage fracture is assured when the stress directly ahead of the crack $\sigma_{\theta\theta}$ reaches a critical local fracture stress σ_f at a significant micro structural distance $r = r^*$. The fracture criterion is now given by:

$$\frac{\sigma_f}{\sigma_0} = \frac{\sigma_{SSY}}{\sigma_0} + Q_T + k_1(n) \left(\frac{r^*}{c} \right) \left(\frac{J_P}{J} \right)_c \quad (8.15)$$

A reference value for the fracture toughness J_c can be found from the small scale yielding field, in which $Q_T = 0$, and $\frac{r^*}{c} = 0$. This value is denoted $J_{c,ssy}$ and depends on the strain hardening exponent and the critical local fracture stress. $J_{c,ssy}$ is then given by

$$J_{c,ssy} = r^* \sigma_0 \left(\frac{\sigma_f}{A\sigma_0} \right)^{\frac{1}{n}} \quad (8.16)$$

At low levels of deformation there is no effect from the global bending field, as the plastic zone is very small and unaffected by the global bending field. The fracture criterion in Equation (8.15) is then reduced to a two term expression of the form as originally developed by O'Dowd and Shih (1991a,b):

$$\frac{\sigma_f}{\sigma_0} = A \left(\frac{J_c}{r^* \sigma_0} \right)^t + Q \quad (8.17)$$

Q represents the level of constraint, and in Figure 8.10, $\frac{J_c}{J_{c,cr}}$ are shown for different values of Q_T . This corresponds to a graphical presentation of Equation (8.17) for two different strain hardening exponents, $n=6$ and $n=13$. The critical local fracture stress is taken to be $3\sigma_0$.

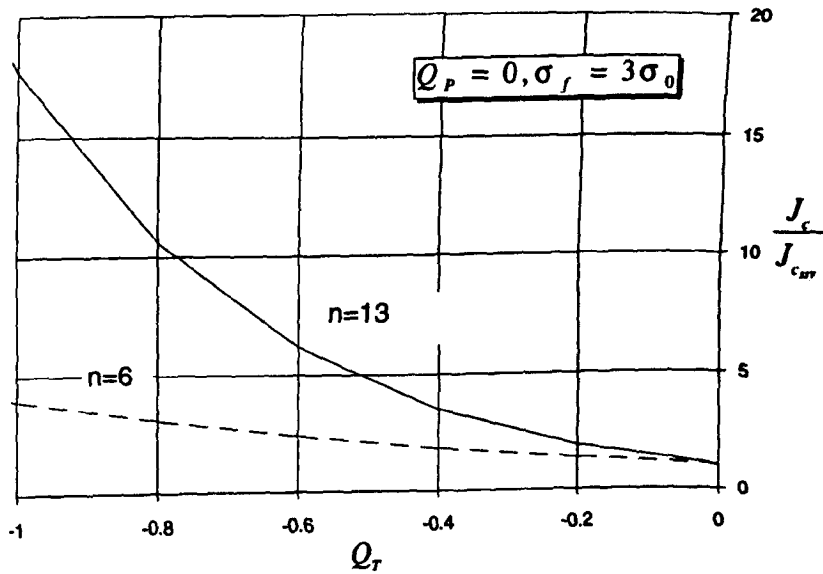


Figure 8.10: *The local failure criteria applied on a stress field described by a two parameter characterisation.*

For deeply cracked bend bars $a/W \geq 0.35$, $Q_T \geq 0$ and the loss of constraint arises only from the global bending field as quantified by Q_P . The fracture criterion can then be written in the form:

$$\frac{\sigma_f}{\sigma_0} = A \left(\frac{J_c}{r^* \sigma_0} \right)^t + k_1(n) \left(\frac{r^*}{c} \right) \quad (8.18)$$

Figure 8.11 shows $\frac{J_c}{J_{c,cr}}$ as a function of $\frac{r^*}{c}$ following Equation (8.18) at a strain hardening $n=13$ and local fracture stresses $\sigma_f = 3\sigma_0$ and $\sigma_f = 2.5\sigma_0$. Since r^* is a fixed micro structural distance the ratio $\frac{r^*}{c}$ indicates different sizes of test specimen.

For shallow cracked bend bars, $a/W \leq 0.35$, the loss of constraint can arise from a combination of a negative T stress and the global bending field. In this case the failure criterion is given by:

$$\frac{\sigma_f}{\sigma_0} = A \left(\frac{J_c}{r^* \sigma_0} \right)^t + Q_T + k_1(n) \left(\frac{r^*}{c} \right) \quad (8.19)$$

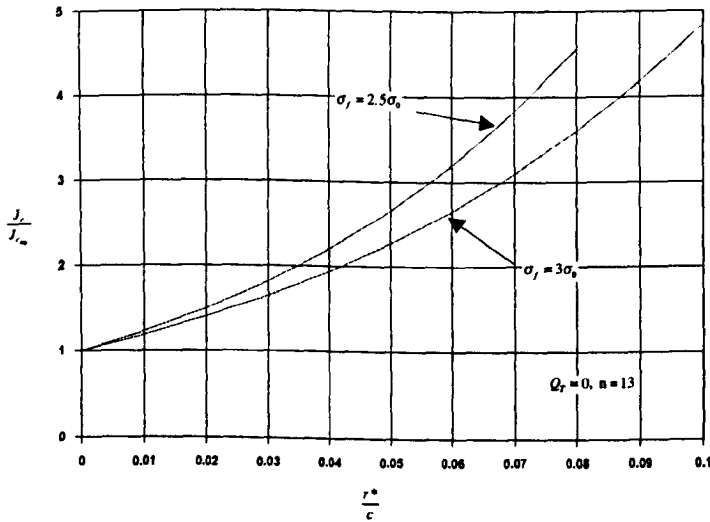


Figure 8.11: Local cleavage criteria for deeply crack bend bars; $Q_T = 0$, $n=13$.

This is shown graphically in Figures 8.12 and 8.13. Figure 8.12 shows $\frac{J_c}{J_{c,ssy}}$ as a function of Q_T for different values of $\frac{r^*}{c}$. The hardening exponent is $n=13$ and the fracture stress is $\sigma_f = 3\sigma_0$ for both Figures.

Finally it is appropriate to relax the requirement that $J_P \gg J_E$ and show results for the case in which J_E is a significant proportion of J . For Q_T and $n=13$:

$$\frac{\sigma_f}{\sigma_0} = \frac{\sigma_{SSY}}{\sigma_0} + k_1(n) \left(\frac{r^*}{c} \right) \left(\frac{J_P}{J} \right)_c \quad (8.20)$$

In Figure 8.14 results are given for a local fracture stress $\sigma_f = 3\sigma_0$ and $n=13$ as a function of $\frac{r^*}{c}$ where the values of $\frac{J_P}{J}$ vary from $\frac{J_P}{J}=0$ to $\frac{J_P}{J}=1$ of increments 0.1. At very high deformations levels $\frac{J_P}{J} = 1$ and for small scale yielding $\frac{J_P}{J}=0$.

8.3 Discussion

The increase in toughness of single edge cracked bars due to loss of constraint has been demonstrated for unstable cleavage fracture. There are two different reasons both for the loss of constraint and for the corresponding increase in fracture toughness. For shallow cracked specimens loaded to moderate levels of deformation the increase in fracture toughness is due to loss of constraint caused by a compressive T stress. As the level of deformation increases the bending field in the uncracked ligament increases and causes the crack tip stress field to lose constraint due to global bending.

Betegón and Hancock (1991) argued that J dominance is maintained for T stresses greater than $-0.2\sigma_0$ for $n=13$ when they compared the stress field in shallow cracked bend bars with the HRR field at a distance $\frac{r^*}{J} = 2$. The corresponding value of Q_T can be calculated from the modified boundary layer formulation as given by Betegón and Hancock (1991):

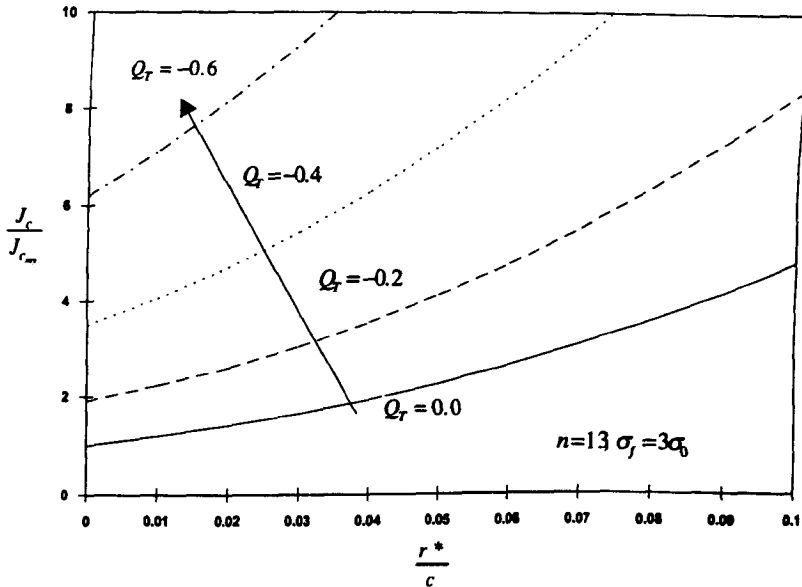


Figure 8.12: $\frac{J_c}{J_{c,ssy}}$ as a function of $\frac{r^*}{c}$ with increments of 0.01 for different values of Q_T . $n=13$ and $\sigma_f = 3\sigma_0$.

$$Q_T = 0.64 \left(\frac{T}{\sigma_0} \right) - 0.4 \left(\frac{T}{\sigma_0} \right)^2, \quad n = 13, \quad T < 0 \quad (8.21)$$

Using Betegón and Hancock's argument that $T \geq -0.2$, the value of Q_T may be calculated to be $Q_T = -0.14$. Assuming the fracture stress is $\sigma_f = 3\sigma_0$, the requirement in terms of a $J_{Ic}/J_{c,ssy}$ is that J-dominance is maintained for values of $J_{Ic}/J_{c,ssy} \leq 1.6$. For other values of the fracture stress the results are given in Table 8.1.

n	$\frac{\sigma_f}{\sigma_0}$	$\frac{T}{\sigma_0}$	Q_T	$\frac{J_c}{J_{c,ssy}}$
13	3.0	-0.2	-0.14	1.6
13	2.5	-0.2	-0.14	1.7

Table 8.1: Data of the fracture toughness for maintaining J-dominance for $T \geq -0.2\sigma_0$ $n=13$, $Q_P=0$.

When J_P is a significant fraction of J the increase of toughness is only due to global bending. Assuming the same level of constraint, $Q=-0.14$ but for deeply edge cracked bars $T \geq 0$ and therefore $Q_T=0$. With $Q_P=-0.14$ the requirement can be expressed in terms of a size requirement for $\frac{r^*}{c}$. For $n=13$ this result gives $\frac{r^*}{c} \geq 0.03$, and consequently the size requirement for applying a local failure criterion to a single parameter characterisation of the stress and strain fields is now $c \geq 33r^*$.

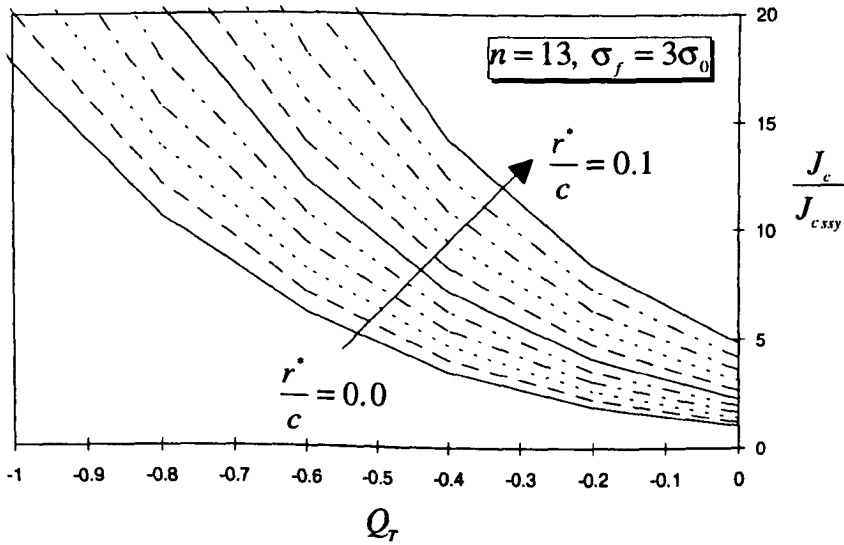


Figure 8.13: $\frac{J_c}{J_{c,asy}}$ as a function of Q_T for different values of $\frac{r^*}{c}$. $n=13$ and $\sigma_f = 3\sigma_0$.

8.4 Conclusion

An important feature in this scheme of estimation of constraint effect on fracture toughness is that it is now possible to obtain the value of a valid J_{Ic} , from a test which does not satisfy the J -dominance conditions. For example, if the fracture toughness is obtained from shallow crack bend bars which show enhanced toughness due to negative T , it is now possible to determine the corresponding valid $J_{Ic} = J_{c,asy}$, which is the fracture toughness independent of the geometry.

Further, is it also possible to test a sample which does not satisfy the size requirements and then transfer the fracture toughness to a valid J_{Ic} . $J_{c,asy}$ can be determined from an invalid test for example by reading of Figure 8.12. r^* is a material parameter which can be obtained from metallographic observations.

To obtain the fracture toughness for other shallow cracked geometries with negative values of Q_T it is necessary to make use of an iterative process to estimate under which load the critical value of J will occur.

Prediction of fracture toughness by constraint estimation in local failure in cleavage may also be used to transfer fracture toughness data from a test specimen to a real structure. When the geometry and the load conditions are known on the structure, a standard test fracture toughness can be used to estimate the toughness of the structure containing the crack. From a standard bend test with $a/W = 0.5$ geometry $T=0$, it is now possible to estimate the fracture toughness even if the structure exceeds the limits for single parameter characterisation.

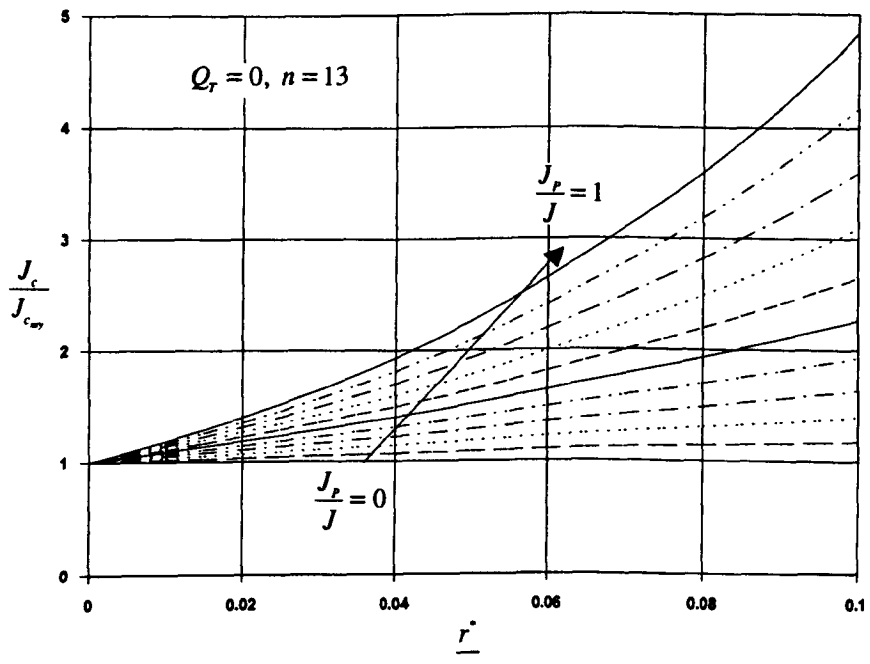


Figure 8.14: $\frac{J_c}{J_{casy}}$ as a function of $\frac{r_c^*}{c}$, $Q_T = 0$ and $n=13$.

Blank Page

Mixed Mode and Mode I Crack Tip Fields Unified by Constraint

Plane strain boundary layer formulations have been widely used to study the nature of Mode I and Mode II crack tip fields in contained yielding. In Mode I, constraint loss has been correlated with T which is the second term in the Williams expansion. This leads to a family of fields which are deviatorically similar but differ mainly hydrostatic. In the present work mixed mode fields are shown to belong to the same family. At the angle of maximum hoop stress, the constraint of mixed mode fields can be related to Mode I J - Q / T fields. Mode I constraint based failure loci have then been used to infer mixed mode failure.

9.1 Non-hardening Mode I Fields

Non-hardening plasticity has been widely used to describe the structure of plane strain crack tip plasticity. Such studies notably include the work of McClintock (1971) in the use of slip line fields to study crack tip plasticity under both fully plastic conditions and contained yielding. In contained yielding, crack tip plasticity is encompassed by an elastic field. If, in plane strain Mode I deformation, it is assumed that plasticity surrounds the crack tip, then the slip lines must leave the traction free surfaces of the crack flanks at $\frac{\pi}{4}$ and approach the plane of symmetry ahead of the crack at $\frac{\pi}{4}$ having rotated through an angle of $\frac{\pi}{2}$. This leads to a field, which consists of constant stress sectors in which the slip lines are straight, and a centred fan with an angular span of $\frac{\pi}{2}$, as illustrated in Figure 9.1. This field, which was originally discussed by Prandtl (1920), is also recognised as a limiting case of the HRR field, after Hutchinson 1968b, Rice and Rosengren (1968), for non-hardening plasticity. The HRR field can be regarded as the first term of an asymptotic series describing the non linear crack tip field as discussed by Sharma and Aravas (1991) and Xia *et al.* (1993).

Single parameter fracture mechanics is based on the premise that crack tip fields can be accurately described by a parameter, such as J , which describes the amplitude of the dominant singularity to the neglect of higher order terms. There is now considerable evidence that higher order terms are significant in many geometries and loading modes (Betegón and Hancock (1991), O'Dowd and Shih (1991a,b)).

In the case of contained yielding the structure of the crack tip fields can be elucidated by boundary layer formulations (Rice and Tracey 1974) in which the displacements corresponding to the first two terms of the Williams expansion are applied as boundary conditions to an arbitrary region surrounding the crack tip. With the

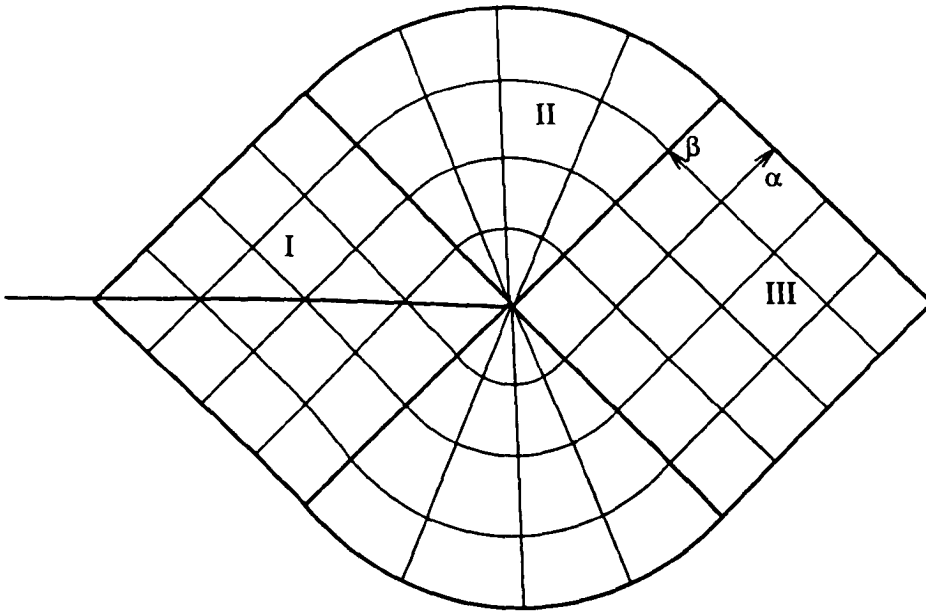


Figure 9.1: Prandtl slip stress field in a region around a crack tip.

limitation that plasticity is restricted to a small fraction of the radius of the outer boundary, the structure of the fields within the plastic zone can be investigated. This technique has been used by Bilby et al (1986), Betegón and Hancock (1991) and Du and Hancock (1991) to examine the effect of higher order terms such as T on the crack tip field. Du and Hancock (1991) examined the structure of non-hardening Mode I crack tip fields and constructed plane strain slip line fields for different levels of T . The Prandtl field is a limiting example of this family of fields which is recovered only for positive values of T .

As T is proportional to the applied load, the $T=0$ field is significant in the sense that it is the field which applies in all geometries at very small load levels, and is thus identified as the small scale yielding field. In this case, ($T=0$), plasticity was not observed to completely surround the crack tip, and elastic wedges were left on the crack flanks, as shown in Figure 9.2. This accounts for the small but consistent difference found in numerical solutions between the HRR (Prandtl) field and the small scale yielding ($T=0$) field.

For increasingly negative values of T the angular span of the centred fan decreased, paralleling the forward rotation of the lobes of the plastic zone. In non-hardening plasticity, changes of the stress state in the leading sector ahead of the crack can only arise from changes in the mean stress. Following O'Dowd and Shih (1991a,b) this can be described by the introduction of a second parameter, Q :

$$\sigma_{\theta\theta} = \sigma_{SSY} + Q\sigma_0 \quad (9.1)$$

In the case of contained yielding there is a unique relation between Q and T , which in general depends on the strain hardening rate. For non-hardening plasticity, Karstensen, Nekkal and Hancock (1995) give:

$$Q_T = 0.83\left(\frac{T}{\sigma_0}\right) - 0.88\left(\frac{T}{\sigma_0}\right)^2 \quad (9.2)$$

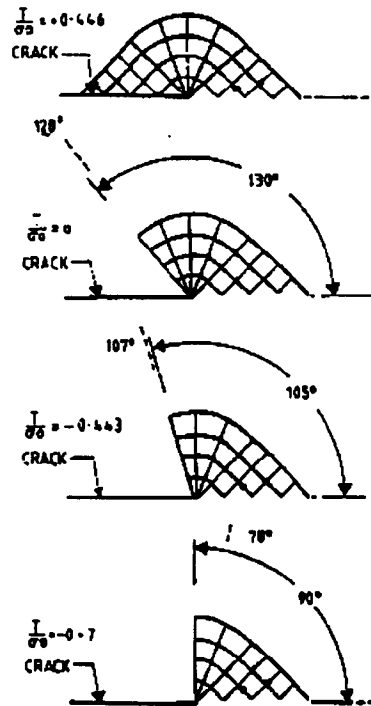


Figure 9.2: *The Effect of the T stress on the plastic zone shape in small scale yielding, after Du and Hancock (1991).*

The stress state ahead of the crack can be deduced from the Hencky Equations (Hill 1950), which express the equilibrium requirements in terms of the rotation of the slip lines. In the Prandtl field the rotation of the slip lines can be followed from the flank into the constant stress diamond ahead of the crack. However, for the fields in which plasticity does not surround the tip, this is not possible. In this case, the fields can instead be expressed in terms of the maximum hydrostatic stress directly ahead of the crack, σ_m . The hydrostatic stress ahead of the fully constrained Prandtl field can thus be written in terms of the yield stress in shear as:

$$\sigma_m = k(1 + \pi) \quad (9.3)$$

The corresponding hydrostatic stress in the unconstrained fields is thus

$$\sigma_m = k(1 + \pi) + \sqrt{3}kQ \quad (9.4)$$

Here it is convenient to define Q using the Prandtl field as the reference state. Using cylindrical co-ordinates (r, θ) centred at the crack tip, the stress field in the diamond

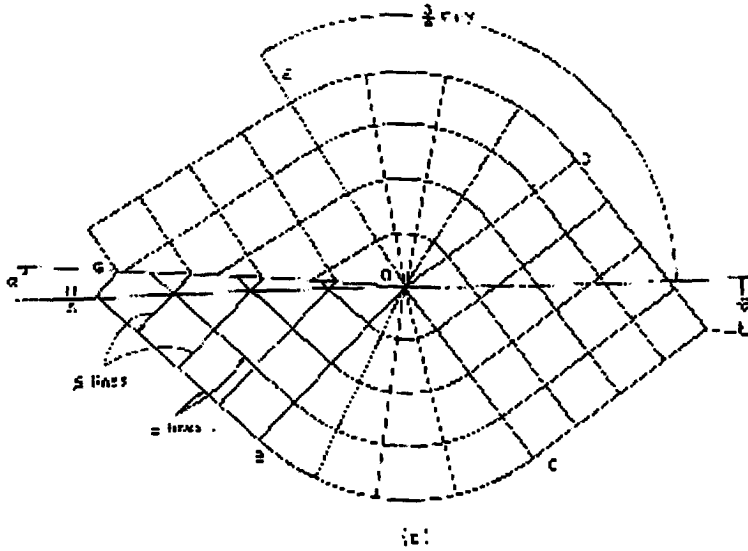


Figure 9.3: A mixed mode field with a stress discontinuity (Shih 1974).

ahead of the crack, can be written:

$$\begin{aligned}
 \sigma_{\theta\theta} &= \sigma_m + \sqrt{3}kQ + k \cos 2\theta \\
 \sigma_{rr} &= \sigma_m + \sqrt{3}kQ - k \cos 2\theta \\
 \sigma_{zz} &= \sigma_m + \sqrt{3}kQ = \sqrt{3}kQ + k(1 + \pi) \\
 \tau_{r\theta} &= k \sin 2\theta
 \end{aligned}
 \tag{9.5}$$

In the centred fans the field becomes:

$$\begin{aligned}
 \sigma_{\theta\theta} &= \sigma_{rr} = \sigma_{zz} = \sigma_m + \sqrt{3}kQ + k\left(\frac{\pi}{2} - 2\theta\right) \\
 \tau_{r\theta} &= k
 \end{aligned}
 \tag{9.6}$$

A constant stress sector only exists on the crack flanks for the Prandtl field ($Q=0$, $T>0$), where the stress is:

$$\begin{aligned}
 \sigma_{\theta\theta} &= k(1 - \cos 2\theta) \\
 \sigma_{rr} &= k(1 + \cos 2\theta) \\
 \tau_{r\theta} &= k \sin 2\theta \\
 \sigma_m &= k
 \end{aligned}
 \tag{9.7}$$

9.2 Non-hardening Mixed Mode Fields

In the case of non-hardening plasticity it is of course only possible for crack tip fields to differ by a hydrostatic term. However O'Dowd and Shih (1991a,b) have argued that even in the presence of hardening, Q is largely hydrostatic in nature. The family of Mode I fields are thus claimed to be deviatorically similar, but hydrostatically different. The nature of the dominant singularity in mixed mode fields were identified by Shih (1974) as belonging to the HRR family. Under contained yielding the nature of loading can be loading defined by an elastic mixity M^e

$$M^e = \frac{2}{\pi} \tan^{-1} \left(\frac{K_I}{K_{II}} \right)
 \tag{9.8}$$

Starting from the Prandtl field, in Mode I ($M^e = 1$), Shih sought mixed mode fields in which the number of constant stress and centred fan sectors was constant but each was distorted. Although this procedure led to inadmissible stress fields, the problem was resolved by postulating a stress discontinuity along a radial line emanating from the crack tip. Equilibrium demands that the hoop and shear stresses (σ and τ_{xy}) are continuous across the discontinuity, but the equilibrium equations allow a jump in the radial stress, σ_{rr} . Fields of this type are illustrated in Figure 9.3. In both the limiting case of pure Mode I and Mode II deformation, it was not necessary to postulate a stress discontinuity. For pure Mode I the Prandtl field illustrated in Figure 9.1 arises and in pure Mode II the field shown in Figure 9.4 was identified.

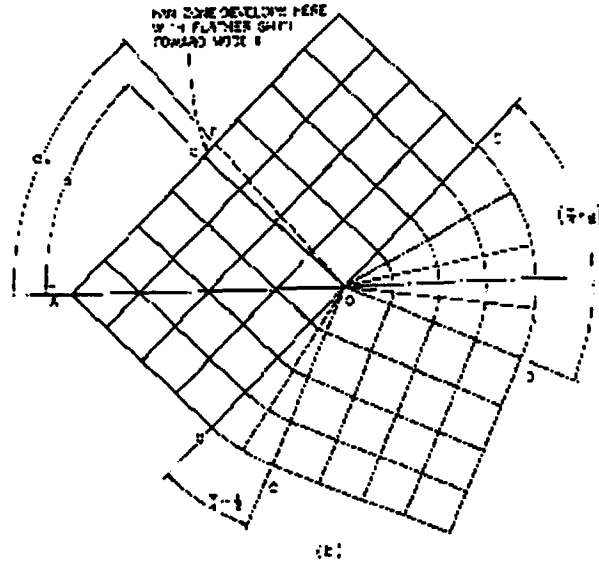


Figure 9.4: The Mode II field after Shih (1974).

In the present work the structure of the slip line fields for mixed mode problems under small scale yielding conditions have been re-examined using a boundary layer formulation approach. This is used as a precursor to examining the effect of hardening. The present work has attempted to demonstrate that mixed mode fields can be related to Mode I two parameter field described by J and a second constraint parameter (Q/T), and that Mixed Mode loading can be simply regarded as a mechanism leading to the loss of in-plane constraint.

9.3 Numerical Model

Crack tip fields have been examined by the finite element method using the mesh shown in Figure 9.5. The mesh comprised 360 first order quadrilateral elements implemented in ABAQUS (1992). The crack tip was represented by twelve collapsed quadrilaterals such that the crack tip comprised 25 coincident but independent nodes. The mesh was highly focused such that the size of the crack tip elements were approximately one millionth of the radius of the outer boundary.

Remote from the tip displacement boundary conditions associated with the displace-

ments (u,v) were calculated from the Westergaard Equations 2.10, for a plane strain mixed mode problem characterised by the Mode I stress intensity factor K_I and the Mode II stress intensity factor K_{II} . Mixed Mode problems with the mixities given in Table 9.1, have been examined numerically.

$$\begin{aligned}
 u &= \sqrt{\frac{r}{2\pi}} \frac{1}{2G} \left[K_I \cos\left(\frac{\theta}{2}\right) (\kappa - 1 + 2 \sin^2\left(\frac{\theta}{2}\right)) + K_{II} \sin\left(\frac{\theta}{2}\right) (\kappa + 1 + 2 \cos^2\left(\frac{\theta}{2}\right)) \right] \\
 v &= \sqrt{\frac{r}{2\pi}} \frac{1}{2G} \left[K_I \cos\left(\frac{\theta}{2}\right) (\kappa + 1 - 2 \cos^2\left(\frac{\theta}{2}\right)) - K_{II} \cos\left(\frac{\theta}{2}\right) (\kappa + 1 + 2 \cos^2\left(\frac{\theta}{2}\right)) \right]
 \end{aligned}
 \tag{9.9}$$

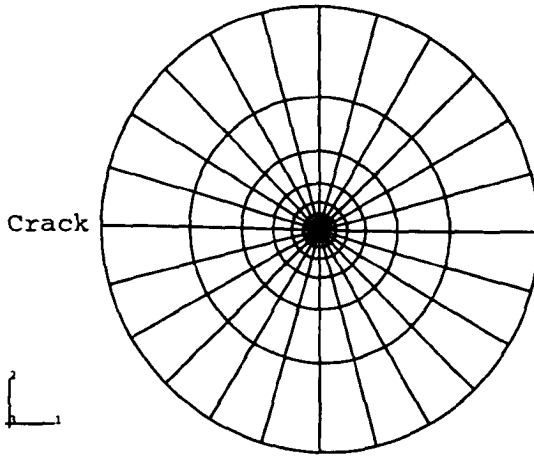


Figure 9.5: The mesh for the mixed mode problems.

	M^e
K_I	1.00
$K_I = 4K_{II}$	0.84
$K_I = 2K_{II}$	0.71
$K_I = K_{II}$	0.50
$K_I = 0.5K_{II}$	0.30
K_{II}	0.00

Table 9.1: Elastic mixity for range of plane strain mixed mode fields.

Calculations were performed under the restriction that the plastic zone was a very small fraction of the radius of the outer boundary. In uniaxial tension the material response was described by an isotropic elasticity with a value of Poisson's ratio as 0.3. Yield was governed by the von Mises yield criterion and subsequent plastic flow occurred under incremental plasticity using the Prandtl-Reuss flow rules. Data were written to a file which was subsequently interrogated with the post-processing

programme described in Chapter 4. The stress field at the crack tip was determined by extrapolating the stress to the tip ($r=0$) along radial lines such that the tip was approached asymptotically from different angles.

9.4 Results

9.4.1 Slip line Fields

During plastic deformation, the plastic strains at the crack tip were assumed to dominate the elastic components, such that deformation was almost incompressible. Under these circumstances the stress field is determined by the hydrostatic or mean stress σ_m ($\sigma_m = \sigma_{kk}/3$) and the yield criterion. The hydrostatic stress at the tip ($r=0$) is illustrated as a function of angle θ in Figure 9.6 for five levels of mixity, while the angular span of the Mises stress is shown in Figure 9.7.

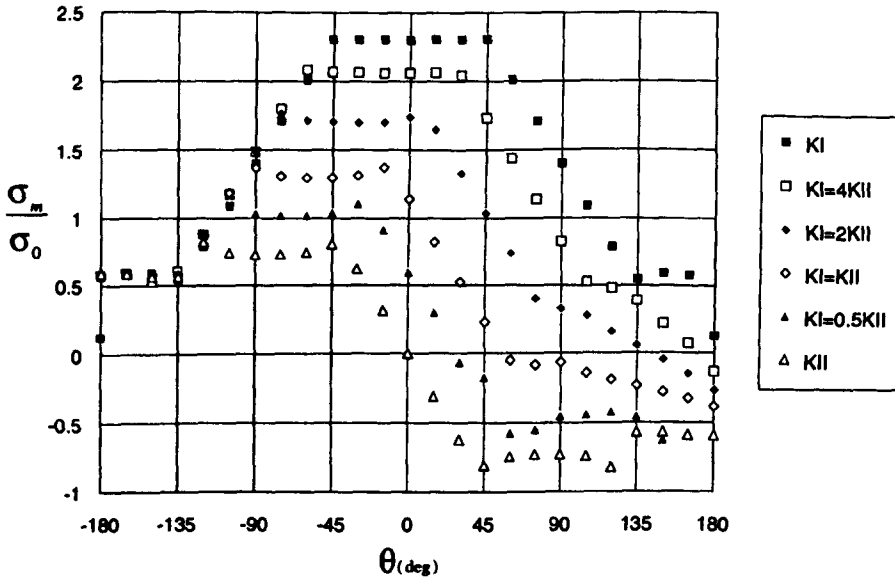


Figure 9.6: Mean stress non-dimensionalised by yield stress as a function of angle for a range of mixities, non-hardening material.

The structure of the plastic sectors of the field can be identified from the hydrostatic component. Rice (1968a) has shown that for incompressible plane strain deformation, combination of the yield criterion, the plane strain condition and the necessity for the crack tip stresses to be bounded allows the equilibrium equations to be written in the form:

$$\frac{\partial \sigma_{rr} + \sigma_{\theta\theta}}{\partial \theta} \times \frac{\tau_{r\theta}}{\partial \theta} = 0 \tag{9.10}$$

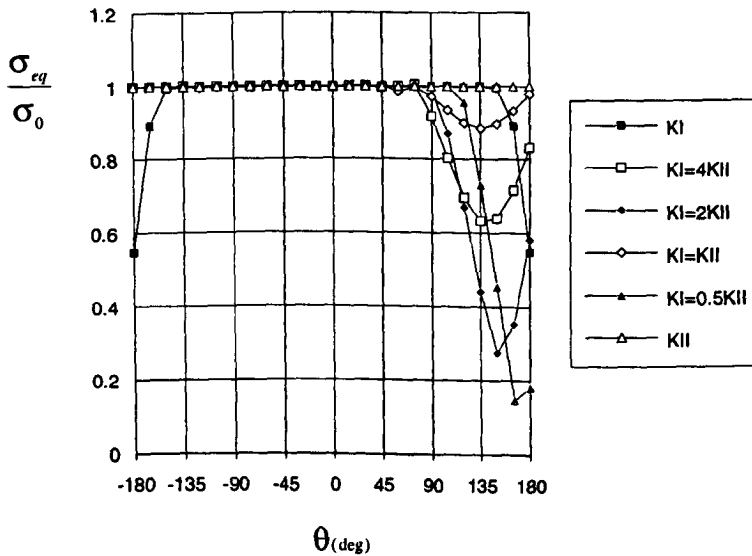


Figure 9.7: Equivalent stress non-dimensionalised by the yield stress as a function of angle for range of mixities, non-hardening material.

This leads to two possible forms for the plastic sectors, either

$$\frac{\partial \sigma_{rr} + \sigma_{\theta\theta}}{\partial \theta} = \frac{\partial \sigma_m}{\partial \theta} = 0 \quad (9.11)$$

or

$$\frac{\tau_{r\theta}}{\partial \theta} = 0 \quad (9.12)$$

The first condition corresponds to regions in which the mean stress does not change with angle around the tip, and thus comprises constant stress sectors in which the slip lines are straight. The second condition corresponds to the situation in which the shear stress in cylindrical co-ordinates does not change with angle. As the slip lines are trajectories of constant shear stress, this corresponds to centred fans, in which the hydrostatic stress varies linearly with angle.

In association with the yield criterion these observations enable the angular span of the elastic and plastic sectors to be identified and allows the field to be assembled. In all the numerical examples shown in Figure 9.6 the region of constant stress has an angular span of $\pi/2$, however the orientation of the constant stress diamond rotates with mixity. The angular span of the centred fans are determined from the span over the region in which the mean stress varies linearly with angle. Finally the fields are completed by noting the span over which the yield criterion is not satisfied, corresponding to elastic wedges. The complete family of fields is assembled in Figure 9.8, where the angles given to the left of the slip line fields in Figure 9.8 are the elastic displacement vectors on the crack flanks and the angle to the right are the orientation of the maximum hoop stress.

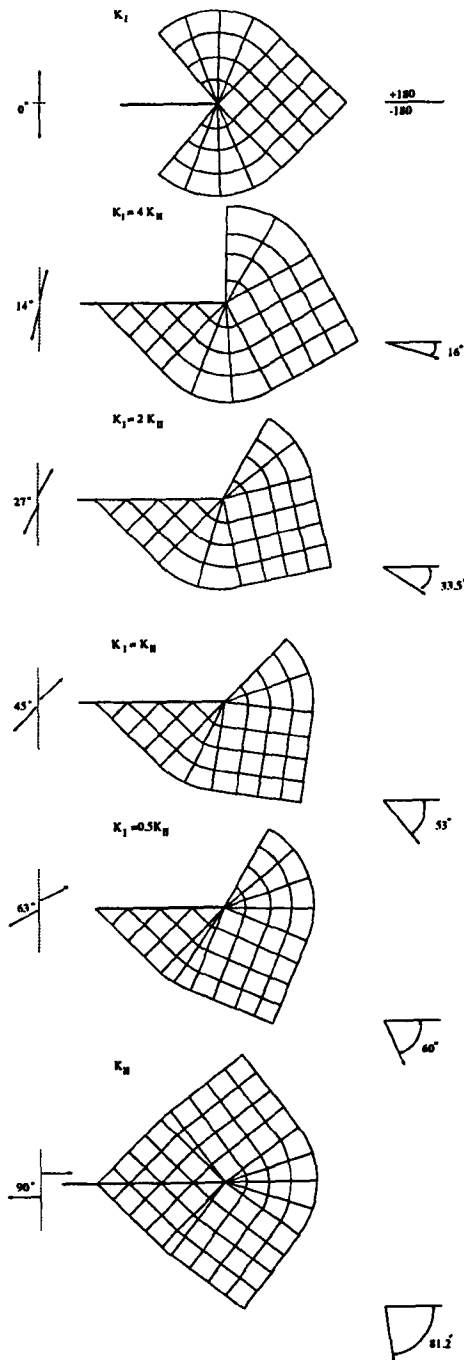


Figure 9.8: Slip Line field for the family of mixed mode problems.

The Mode I field is that discussed by Du and Hancock (1991). The main point of difference between the Mode I field and the Prandtl field is the presence of elastic sectors on the crack flanks. This corresponds to the small but consistent difference which has been found between the small scale yielding field and the HRR field in both non-hardening and hardening calculations.

The mixed mode fields are simple distortions of the Mode I field corresponding to a rotation of the main constant stress diamond. This allows the field to extend to the crack flanks with a uniform stress triangle on the tensile side, while the elastic wedge on the compressive flank increases its angular span. Figure 9.9 shows the distortion of a mixed mode field ($K_I = K_{II}$) in an exaggerated form.

This process continues with increase mixity until the pure Mode II field is recovered. This field is identical to that discovered by Shih (1974) as plasticity now fully surrounds the crack tip.

The Mode I and mixed mode fields differ from those discussed by Shih (1974) in that the necessity for a stress discontinuity is resolved by the formation of an elastic wedge on the crack flanks. The angle of maximum hoop stress given in Figure 9.8 is however very close to that given by Shih. The angle of maximum principal stress and also the maximum hydrostatic stress is the direction from the tip radial out through the constant stress diamond. This angle is of particular interest in terms of stress controlled brittle fracture. It is frequently argued that such failure occurs at the orientation at which the propagating crack extends in Mode I (Erdogan and Sih (1963), Williams and Ewing (1972), Budden (1987)).

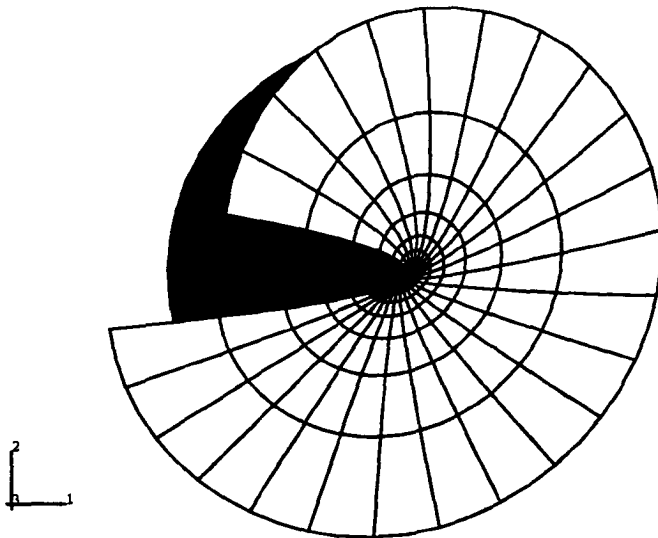


Figure 9.9: *The displaced model of a mixed mode problem for $K_I = K_{II}$.*

In the case of non-hardening plasticity the crack tip stress at this angle may be compared with the stress in an unconstrained Mode I field. In non-hardening plasticity it is convenient to focus attention at the tip, where mixed mode fields can be correlated with Mode I fields which have the same level of constraint. Recall, of course, that in the pure Mode I field the direction of interest is directly ahead of the crack, whereas in the mixed mode problem it is inclined at angle which is a

function of mixity. On this basis the constraint of Mode I fields parameterised by Q or T can be identified with the constraint of mixed mode fields parameterised by elastic mixity, as shown in Figures 9.13 and 9.14.

9.4.2 Strain Hardening

It is now appropriate to turn attention to the effect of strain hardening. The material response is described in Chapter 4. In uniaxial tension the material has an isotropic elastic response for stresses less than the uniaxial yield stress σ_0 . Yield is determined by the von Mises yield criterion and the associated flow rule. At stresses greater than the yield stress the material follows a law which approximates to a Ramberg-Osgood stress-strain relation.

Numerical calculations were performed for the elastic mixities given in Table 9.1 with strain hardening exponents, $n=13$ and 6. Attention has been focused on the plane on which the maximum principal stress and minimum shear stress occur. In Mode I this is directly ahead of the crack but in the mixed mode loading the angle is weakly dependent on the hardening rate over the range of interest (Shih 1974) and the numerical data have been taken from the radial node set closest to this angle. The stresses are non-dimensionalised with respect to the uniaxial yield stress, σ_0 , while the radial distance from the crack tip is non-dimensionalised by J/σ_0 .

Figures 9.10 and 9.11 show numerical results for a range of mixities ranging between 0 and 1 for strain hardening rates $n=13$ and $n=6$. The important point is that the stress profiles for all the mixities are parallel. At this orientation, they can therefore be regarded as a family of fields which differ by a second order term which is independent of distance.

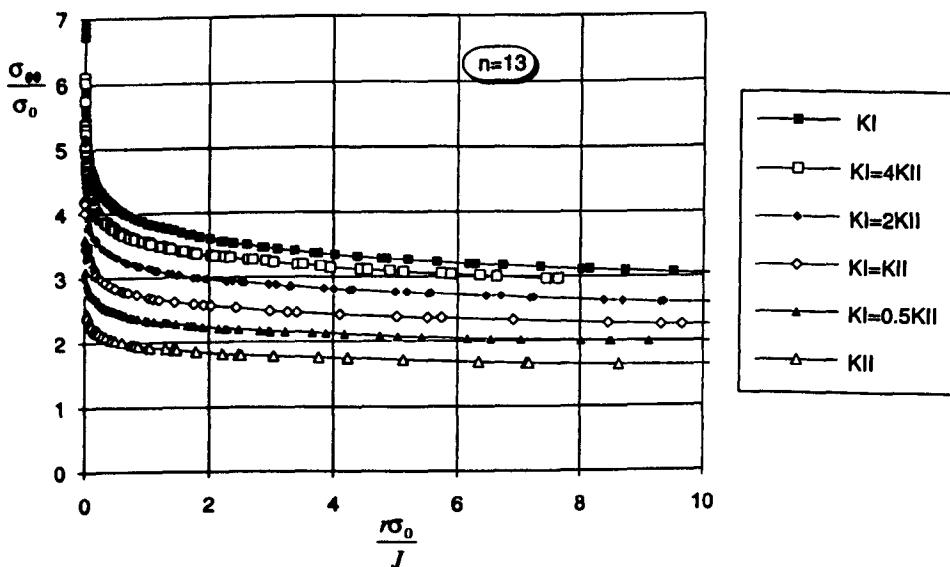


Figure 9.10: The maximum hoop stress as a function of the non-dimensionalised distance from the crack tip, $n=13$.

Figure 9.12 shows numerical results for Mode I modified boundary layer formulations, in which constraint loss is associated with T . Again the central observation is

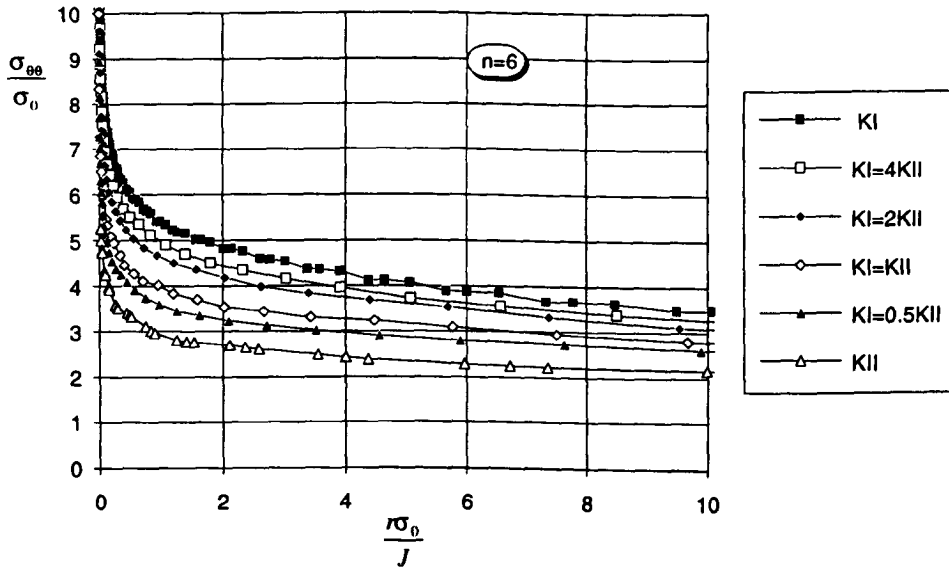


Figure 9.11: *The maximum hoop stress as a function of the non-dimensionalised distance from the crack tip, $n=6$.*

that for a given hardening rate all these stress profiles are parallel. That is to say, the stress level associated with a mixed mode problem can be identified with the loss of constraint in a Mode I loading. This relationship between mixity and Q and T is shown in Figures 9.13 and 9.14. O'Dowd and Shih (1991a,b) have argued that Mode I fields are deviatorically similar but differ hydrostatically through a parameter Q . In this context the maximum stress deviator, $s_{\theta\theta}$, directly ahead of the Mode I fields is given in Figure 9.15 for a hardening exponents $n=13$ and $n=6$.

Although the fields are not deviatorically identical, they are deviatorically very similar and differ mainly by a hydrostatic term, as discussed by O'Dowd and Shih (1991a,b). In the same spirit the maximum stress deviator, $s_{\theta\theta}$, has been determined for the mixed mode fields at the angle of maximum hoop stress, as shown in Figure 9.16. Comparison of Figures 9.15 and 9.16 indicates that the mixed mode fields are deviatorically similar to equivalent accuracy as the Mode I J - Q/T fields.

9.5 Fracture Criteria

The constraint dependent fracture toughness which is observed in Mode I can be expressed as a fracture locus in which the toughness is given as a function of a constraint parameter Q/T . The first example of this was given by Betegón and Hancock (1990) whose data on a series of shallow edge cracked bend bars, which failed by cleavage, is shown in Figure 3.7 as a function of T . Extensive data have been presented by Sumpter (1993b), Sumpter and Hancock (1994), Sumpter and Forbes (1992) and by Kirk et al (1993).

In Mode I, cleavage is often interpreted on the basis of local criteria which involve the attainment of a critical stress over a micro structurally significant distance directly ahead of the crack as proposed by Ritchie, Knott and Rice (1973). In mixed mode

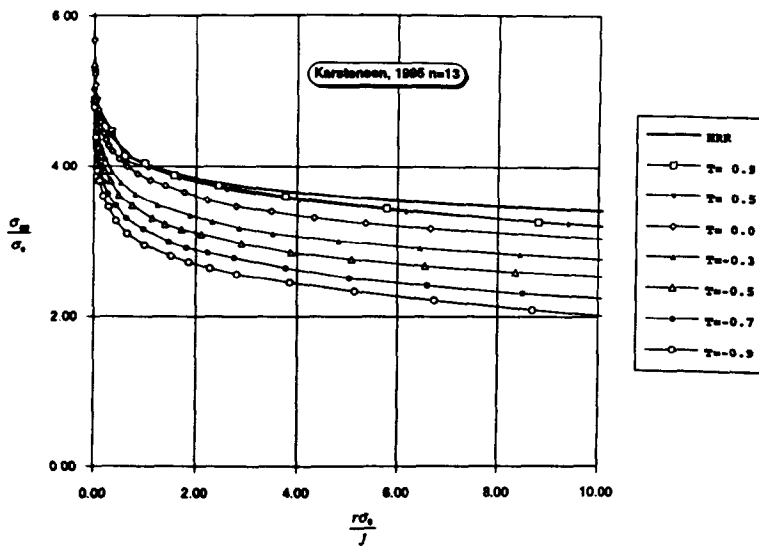


Figure 9.12: The hoop stress directly ahead of a crack in Mode I as a function of the non-dimensionalised distance from the crack tip for a range of $\frac{T}{\sigma_0}$ values, $n=13$.

loading, the direction of crack propagation has also been identified with the plane of maximum hoop stress (Erdogan and Sih (1963), Williams and Ewing (1972) and Budden (1987)) which occurs at an inclined angle, such that the propagating crack grows locally in Mode I.

The constraint of Mode I and mixed mode fields have been correlated in Figures 9.12, 9.13 and 9.14 for perfect plasticity and hardening exponents $n=13$ and $n=6$. It is thus now possible to map the constraint based Mode I failure loci into mixed mode data. As an illustration the experimental data of Betegón (1990) is considered. Betegón (1990) performed a range of experiments on deep and shallow edge cracked bend bars, in an experimental plain carbon steel with a strain hardening exponent $n=14$. Failure occurred in full plasticity by cleavage. The Mode I data are shown in Figure 9.17 as a J - Q locus. Using the relationship between mixity and Q given in Figure 9.14 for $n=13$, this data may be mapped into a J -mixity locus, which is shown in Figure 9.18.

9.6 Conclusions

In Mode I, constraint loss may give rise to a family of elastic-plastic crack tip fields which can be described by J and a second parameter which determines the level of crack tip constraint (Q). This family of fields differs in a largely hydrostatic manner. Mixed mode field can be interpreted as belonging to the same family such that constraint loss by mixed mode loading results in a family of fields which differ largely hydrostatically on the plane of maximum hoop stress. For stress controlled brittle fracture this allows the constraint enhanced toughness observed in unconstrained Mode I fields to be correlated with the constraint enhanced toughness in mixed mode loading.

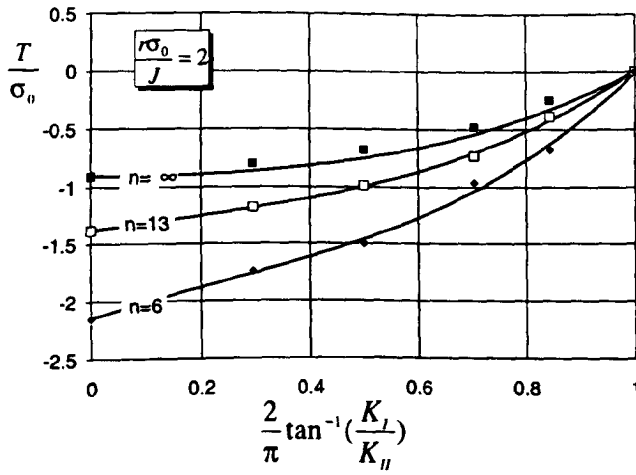


Figure 9.13: $\frac{T}{\sigma_0}$ as a function of mixity for a range of hardening rates.

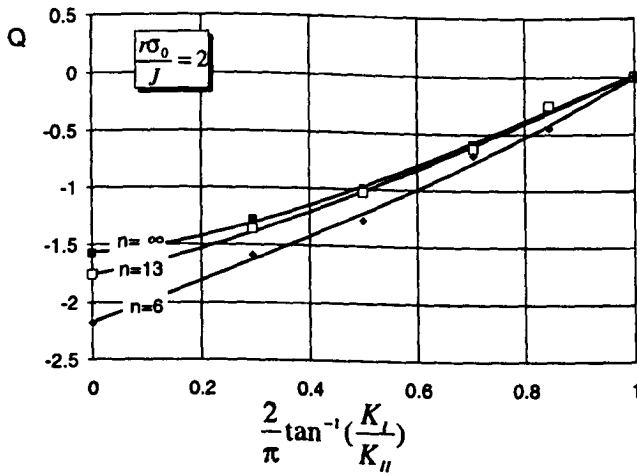


Figure 9.14: Q as a function of mixity for a range of hardening rates.

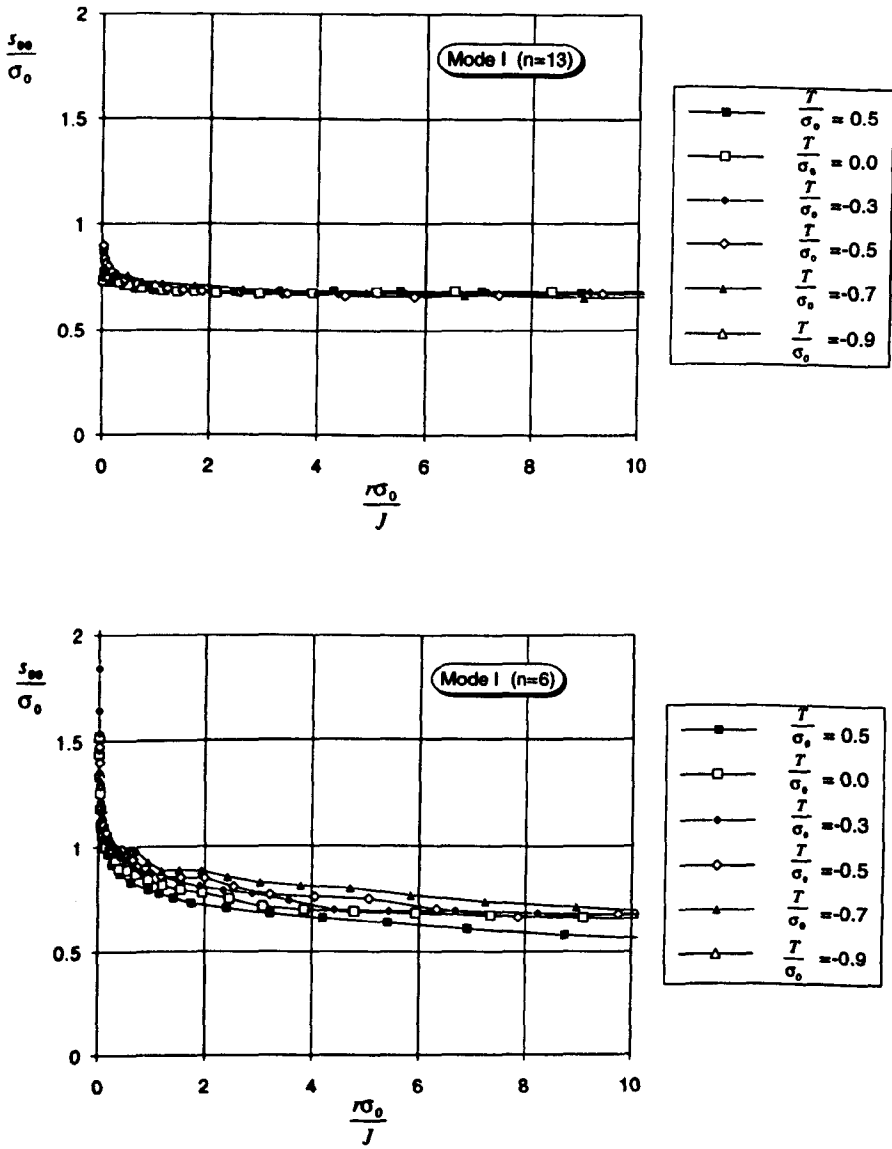


Figure 9.15: The stress deviation non-dimensionalised by the yield stress directly ahead of Mode I crack for a range of $\frac{T}{\sigma_0}$ values, $n=13$ and $n=6$.

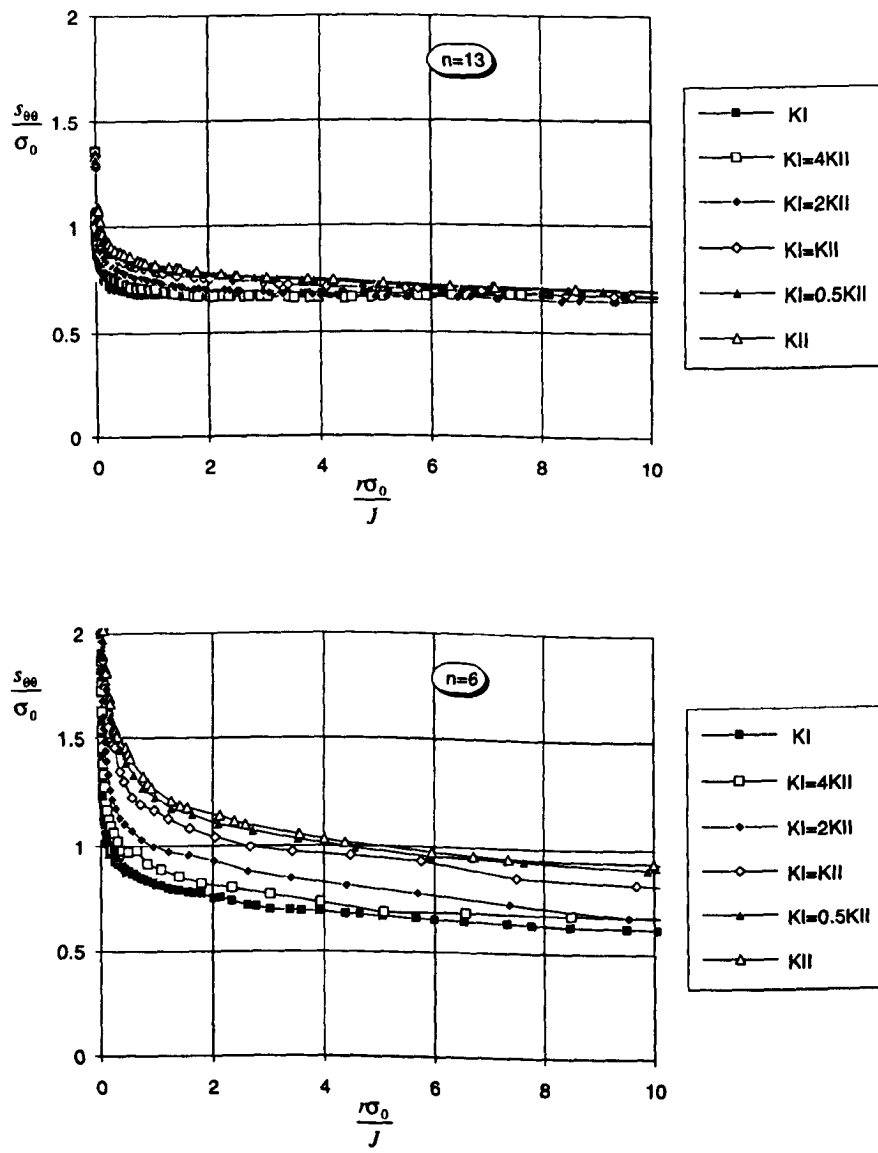


Figure 9.16: The stress deviation non-dimensionalised by the yield stress at the maximum stress angle for a range of mixities, $n=13$ and $n=6$.

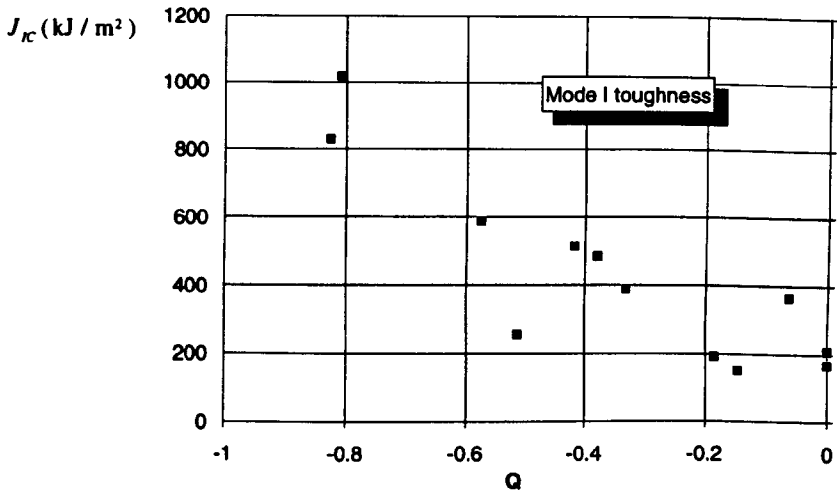


Figure 9.17: Experimental data in a J-Q locus for 3PB test from Betegón (1991), n=14.

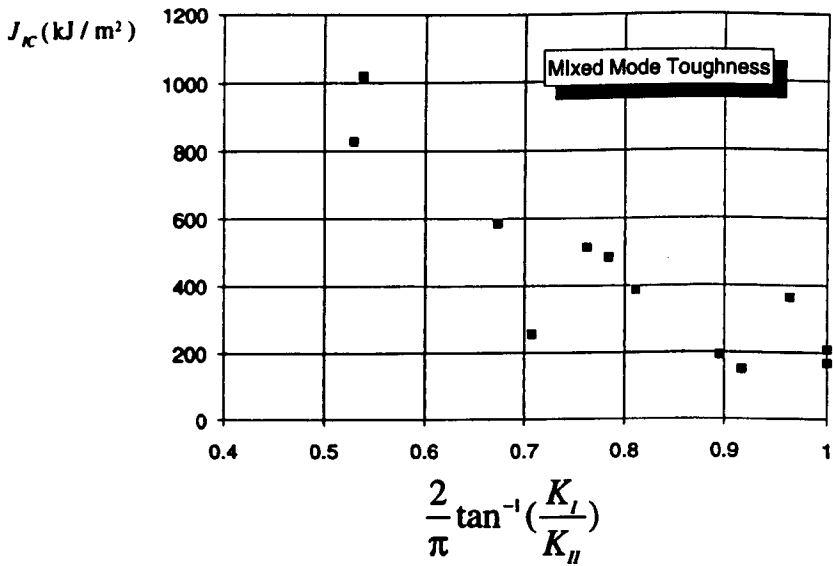


Figure 9.18: Experimental data obtained in 3PB tests and mapped into mixed mode data for n=13 in a J-M^e locus, 3PB tests after Betegón (1991).

Blank Page

Conclusion

Two parameter fracture mechanics has been shown to extend the range of applicability of defect assessment schemes. In particular it provides a framework for utilising the enhanced toughness associated with cracks which develop unconstrained flow fields.

The limits of one and two parameter characterisation have been defined, and two parameter characterisation has been shown to extend the range of characterisation of elastic-plastic crack tip fields, most notably for short cracks in edge cracked bars in tension and bending.

The development of crack tip constraint has been examined systematically; firstly for edge cracked bars in tension and bending and secondly for centre cracked panels and double edge cracked bars.

For single edge cracked bars it was shown that initial loss of constraint was controlled by the non-singular T stress. At high levels of deformation the J-T characterisation breaks down due to global bending on the ligament. This resulted in a distance dependent term Q_P to estimate the constraint expressed either in terms of load normalised by limit load or in terms of J. Q_T , estimated through T together with Q_P provides a complete crack tip constraint estimation scheme for edge cracked bars in tension and bending.

The constraint estimation of the centre cracked panels proved to be more difficult, due to the effect of displacement boundary conditions which alternate the force to moment ratio on the ligament as the applied load increases. The behaviour of the stress field has been explained and the simplest estimation of Q as a function of $\frac{P}{P_{Limit}}$ was suggested in term of a bi-linear expression.

Prediction of fracture toughness using constraint estimation scheme in a local failure criteria in cleavage has been applied. A method has been suggested to allow the transfer of fracture toughness data from a test specimen to a real structure or between test specimens of different sizes.

The family of J-Q fields in a mode I problem differ mainly in a hydrostatic manner. Mixed mode field can be described in an equivalent way, and the loss of constraint in elastic-plastic crack tip fields in a Mode I problem has been matched with the loss of constraint in mixed mode problems. This also allows the constraint enhanced toughness for unconstrained fields in Mode I to be correlated with the constraint enhanced toughness in mixed mode loading.

Blank Page

References

- ABAQUS V.5.3 (1992). ABAQUS Manual. *Hibbitt, Karlsson and Sorenson Inc.* Providence, Rhode Island.
- Ainsworth, R. and O'Dowd, N. (1995). 'Constraint in the failure assessment diagram approach for fracture assessment'. *Transaction of the ASME, Journal of Pressure Vessel Technology* **117**, 260-267.
- Al-Ani, A. (1988). J dominance of short cracks in bending and tension. Master's thesis. Department of Mechanical Engineering. University of Glasgow.
- Al-Ani, A. M. and Hancock, J. (1991). 'J-dominance of short cracks in tension and bending'. *Journal of Mechanics and Physics of Solids* **39**, No.1, 23-43.
- Andersen, T. (1995). *Fracture Mechanics; Fundamentals and Applications*. CRC Press, Inc.. Boca Raton, Florida. Second Edition.
- Anderson, T. and Dodds, R. (1991). 'Specimen size requirements for fracture toughness testing in the ductile-brittle transition region'. *Journal of Testing and Evaluation* **19**, 123-134.
- ASTM (E 339-83 1983). *Standard Method for Plane Strain Fracture Toughness Testing of Metallic Materials*. Vol. 03 01. American Society for Testing and Materials. Philadelphia. pp. 487-511. Metals Test Methods and Analytical Procedures.
- ASTM (E813-81 1981). *Standard Method for J_{IC} Fracture Toughness*. American Society for Testing and Materials. Metals Test Methods and Analytical Procedures.
- Beremin, F. M. (1983). 'A local criterion for cleavage fracture of a nuclear pressure vessel steel'. *Metallurgical Transactions A* **14**, 2277-2287.
- Betegón, C. (1990). Two parameter elastic-plastic fracture mechanics (in Spanish) "Caracterización biparamétrica de los campos tensionales en la mecánica de la fractura elastoplástica". PhD thesis. Universidad de Oviedo, Spain.
- Betegón, C. and Hancock, J. W. (1990). Two parameter characterisation of elastic-plastic crack tip fields and an associated failure criterion. In 'Fracture Behavior and the Design of Materials and Structures, ECF 8'. Vol. 2. EMAS, UK. pp. 999-1002.
- Betegón, C. and Hancock, J. W. (1991). 'Two-parameter characterization of elastic-plastic crack-tip fields'. *Journal of Applied Mechanics* **58**, 104-110.
- Bilby, B. A., Cardew, B. A., Goldthorpe, M. R. and Howard, I. C. (1986). A finite element investigation of the effect of specimen geometry on the field of stress and strain at the tip of stationary cracks. In 'Size Effect in Fracture'. Inst. Mech. Eng.. London, UK. pp. 37-46.
- Bilby, B. A., Cottrell, A. H. and Swindon, K. H. (1963). The spread of plastic yield from a notch. In 'Proceedings, Royal Society of London'. Vol. A-272. pp. 304-314.

- British Standard (BS-7448 1991b). *Method for determination of K_{IC} , critical CTOD and critical J values of metallic materials*. London.
- British Standard (PD6493 1991a). *Guidance on Methods for Assessing the Susceptibility levels of flaws in Fusion Welded Structures*. London. Welding Standards Policy Committee, Technical Committee WEE/37.
- Broek, D. (1991). *Elementary Engineering Fracture Mechanics*. 4 edn. Kluwer Academic Publisher. Dordrecht.
- Budden, P. J. (1987). 'The stress field near a blunting crack tip under mixed modes I and II'. *Journal of Mechanics and Physics of Solids* **35**(4), 457-478.
- Bueckner, H. F. (1973). Methods of analysis and solution of crack problems. In Sih, G. C. (Ed.). 'Mechanics of Fracture I'. Noordhoff, Leyden. pp. 239-314.
- Chao, Y. J. and Ji, W. (1994). Cleavage fracture quantified by J and A_2 . In 'Constraint Effects in Fracture: Theory and Applications, ASTM STP 1244'. American Society for Testing Materials. Philadelphia.
- Charpy, M. (1912). In 'Assoc. Intern. Essai Materiaux, 6th Congr.'. Vol. 4. New York. p. 5.
- Chell, G. G. (1979). A procedure for incorporating thermal and residual stresses into the concept of a failure assessment diagram. In J.D.Landes, Begley, J. and Clarke, G. (Eds.). 'Elastic Plastic Fracture, ASTM STP 700'. American Society for Testing and Materials. Philadelphia, PA. pp. 581-605.
- Cherepanov, G. P. (1967). 'Crack propagation in continuous media'. *International Journal of Solid Structures* **4**, 811-831.
- Curry, D. A. and Knott, J. F. (1979). 'Effect of microstructure on cleavage fracture toughness of quenched and tempered steels'. *Metal Science* pp. 341-345.
- Dean, R. H. and Hutchinson, J. W. (1980). Quasi-static steady crack growth in small-scale yielding. In 'Fracture Mechanics, ASTM STP 700'. American Society for Testing and Materials. Philadelphia, PA. pp. 383-405. Twelfth Conference.
- Dodds, R., Anderson, T. L. and Kirk, M. T. (1991). 'A framework to correlate a/W ratio effects on elastic-plastic fracture toughness (J_c)'. *International Journal of Fracture* **48**, 1-22.
- Dodds, R., Shih, C. F. and Anderson, T. L. (1993). 'Continuum and micromechanics treatment of constraint in fracture'. *International Journal of Fracture* **64**, 101-133.
- Dowling, A. R. and Townley, C. H. A. (1975). 'The effect of defects on structural failure: a two criteria approach'. *International Journal of Pressure Vessels and Piping* **3**, 77-137.
- Drugan, W. R., Rice, J. R. and Sham, T. L. (1982). 'Asymptotic analysis of growing plane strain cracks in elastic ideally plastic solids'. *Journal of Mechanics and Physics of Solids* **30**, 447-473.
- Du, Z. Z. and Hancock, J. W. (1991). 'The effect of non-singular stresses on crack tip constraint'. *Journal of Mechanics and Physics of Solids* **39**, 555-567.
- Dugdale, D. S. (1960). 'Yielding of steel sheets containing slits'. *Journal of Mechanics and Physics of Solids* **8**, 100-104.
- Erdogan, F. and Sih, G. C. (1963). *Journal of Basic Engineering* **85**, 519.
- Eshelby, J. D. (1968). 'Stress analysis of cracks'. *Journal of the Iron and Steel Institution* **121**, 13-48.

- Ewing, J. W. (1968). 'The plastic yielding of V notched tension bars with circular roots'. *Journal of Mechanics and Physics of Solids* **16**, 305.
- Ewing, J. W. and Hill, R. (1967). 'The plastic constraint of v-notched tension bars'. *Journal of Mechanics and Physics of Solids* **15**, 115.
- Gao, Y.-C. (1980). Elastic-plastic fields at crack tips in perfectly - plastic medium. In 'Acta Mech. Sin.'. ICTAM. Toronto.
- Green, A. P. (1953). 'The plastic yielding of notched bars due to bending'. *Quart. Journal of Mech. and Applied Mathematic* **6**, 223-239.
- Green, A. P. and Hundy, B. B. (1958). 'Initial plastic yielding in notch bend tests'. *Journal of Mechanics and Physics of Solids* **4**, 128-144.
- Griffith, A. A. (1921). 'The phenomena of rupture and flow in solids'. *Phil. Trans. R. Soc. A* **221**, 163-198.
- Hancock, J. W., Reuter, W. G. and Parks, D. M. (1993). Constraint and toughness parameterized by T. In Hackett, E. M., Schwalbe, K. H. and Dodds, R. H. (Eds.). 'Constraint Effect in Fracture, ASTM STP 1171'. American Society for Testing and Materials. Philadelphia, PA. pp. 21-40.
- Heald, P. T., Spink, G. M. and Worthington, P. J. (1972). *Material Science in Engineering* **10**, 129.
- Hellan, K. (1985). *Introduction to Fracture Mechanics*. McGraw-Hill. Singapore.
- Hill, R. (1950). *The Mathematical Theory of Plasticity*. Clarendon Press. Oxford.
- Hooke, R. (1678). 'Ut tensio sic vis "ceiinossstuv"'. *De Potentiâ Restitutiva*.
- Hutchinson, J. W. (1968a). 'Singular behavior at the end of a tensile crack in a hardening material'. *Journal of Mechanics and Physics of Solids* **16**, 13-31.
- Hutchinson, J. W. (1968b). 'Plastic stress and strain fields at a crack tip'. *Journal of Mechanics and Physics of Solids* **16**, 337-347.
- Ilyushin, A. A. (1946). *Prikadnia Matematika i Mekhanika, P.M.M.* **10**, 347.
- Inglis, C. E. (1913). 'Stresses in a plate due to the presence of cracks and sharp corners'. *Trans. Inst. Nav. Archit.* **55**, 219-241.
- Irwin, G. R. (1948). 'Fracture dynamics'. *Fracture of Metals* pp. 147-166. American Society for Metals, Cleveland.
- Irwin, G. R. (1957). 'Analysis of stresses and strains near the end of a crack traversing a plate'. *Journal of Applied Mechanics* **24**, 361-364. Trans. ASME.
- Irwin, G. R. (1960). Plastic zone near a crack tip and fracture toughness. In 'Proc. 7th Sagamore Ordnance Material Research Conference'. Vol. 5. pp. 63-78.
- Karstensen, A. D., Nekkal, A. and Hancock, J. W. (1995). 'Constraint estimation scheme for edge crack bars in tension and bending'. Submitted for publication in *Journal of Mechanics and Physics of Solids*.
- Kfouri, A. P. (1986). 'Some evaluations of the elastic T-term using Eshelby's methods'. *International Journal of Fracture* **30**, 301-315.
- Kirk, M. T. and Dodds, R. H. (1992). J and CTOD estimation equations for shallow cracks in single edge notch bend specimen. In Dawes, M. G. (Ed.). 'Shallow Crack Fracture Mechanics, Toughness Tests and Applications'. The Welding Institute. Publishing, Abington Cambridge, England. Paper 2.
- Kirk, M. T., Koppenhoefer, K. C. and Shih, C. F. (1993). Effect of constraint on specimen dimensions needed to obtain structurally relevant toughness measures. In Hackett, E. M., Schwalbe, K. H. and Dodds, R. H. (Eds.). 'Constraint Effect

- in Fracture, ASTM STP 1171'. American Society for Testing and Materials. Philadelphia, PA. pp. 79-103.
- Knott, J. (1966). 'Some effects of hydrostatic tension on fracture behavior of mild steel.'. *Journal of Iron Steel Institution* **204**, 104-111.
- Koppenhoefer, K. C., Dodds, R. H. and Kirk, M. T. (1995). Size and deformation limits to maintain constraint in K_{Ic} and J_c testing of bend specimens. In Kirk, M. and Bakker, A. (Eds.). 'Constraint Effects in Fracture Theory and Application: Second Volume, ASTM STP 1244'. American Society for Testing and Materials. Philadelphia, PA. pp. 445-460.
- Kumar, V., German, M. D. and Shih, C. F. (1981). 'An engineering approach for elastic-plastic fracture analysis'. Report to EPRI, (NP-1931), General Electric Company, Palo Alto, CA.
- Larsson, S. G. and Carlsson, A. J. (1973). 'Influence of non-singular stress terms and specimen geometry on small-scale yielding at crack tips in elastic plastic material'. *International Journal of Fracture* **19**, 263-278.
- Leevers, P. S. and Radon, J. C. (1983). 'Inherent stress biaxiality in various fracture specimen geometries'. *International Journal of Fracture* **19**, 942-955.
- Leggatt, R. H. and Gordon, J. R. (1992). 3-D elastic-plastic finite element analysis for CTOD and J in SENB, SENAB and SENT specimen geometries. In Dawes, M. G. (Ed.). 'Shallow Crack Fracture Mechanics, Toughness Tests and Applications'. The Welding Institute. Publishing, Abington Cambridge, England.
- Li, F. Z., Shih, C. F. and Needleman, A. (1985). 'A comparison of methods for calculating energy release rate'. *Engineering Fracture Mechanics* **21**, 405-421.
- Li, Y. and Wang, Z. (1986). 'High-order asymptotic field of tensile plane-strain nonlinear crack problem'. *Scientia Sinica (Series A)* **29**, 941-955.
- Lin, T., Evans, A. G. and Ritchie, R. O. (1986). 'A statistical model of brittle fracture by transgranular cleavage'. **34**(5), 477-497.
- MacLennan, I., Al-Ani, A. M. and Hancock, J. W. (1992). Determination of T-stress for semi-elliptical crack. In 'Proc. 7th ABAQUS Users' Groups Conference'. University of Cambridge, Cambridge.
- MacLennan, I. and Hancock, J. (1995). 'Constraint-based failure assessment diagrams'. *Proc. Royal Society of London* **45**, 1-21.
- MacLennan, I. and Hancock, J. W. (1992). The effect of constraint on the ductile-brittle transition. In Dawes, M. G. (Ed.). 'Shallow Crack Fracture Mechanics, Toughness Tests and Applications'. The Welding Institute. Publishing, Abington Cambridge, England.
- Matlab V.4. (1991). *Matlab Manual. The MathWorks Inc. Version 4.*
- McClintock, F. A. (1968). 'A criterion for ductile fracture by the growth of holes'. *Journal of Applied Mechanics* **35**, 363-371.
- McClintock, F. A. (1971). Plasticity aspects of fracture. In Liebowitz, H. (Ed.). 'Fracture'. Vol. 3. Academic Press. London. pp. 47-225.
- McClintock, F. A. and Argon, A. S. (1966). *Mechanical Behavior of Materials*. Addison-Wesley Publishing Company, Inc.. Reading, Massachusetts.
- McMeeking, R. A. and Parks, D. M. (1979). On criteria for J-dominance of crack tip fields in large scale yielding. In Landes, J. (Ed.). 'Elastic-Plastic Fracture,

- ASTM STP 668'. American Society for Testing and Materials. Philadelphia. pp. 175-194.
- McMeeking, R. M. (1977). 'Finite deformation analysis of crack-tip opening in elastic-plastic material and implications for fracture'. *Journal of Mechanics and Physics of Solids* **25**, 357-381.
- Miller, A. G. (1987). *Review of limit loads of structures containing defects*. Nuclear Electric Report. TPRD/B/0093/N82.
- Milne, I., Ainsworth, R., Dowling, A. and Stewart, A. (1986). Assessment of the integrity of structures containing defects (r6). Technical report. Central Electricity Generating Board, CA. Report, Revision 3.
- Mises, R. (1913). *Göttinger Nachrichten Math. Phys. Klasse* p. 582.
- Murakami, Y. (1987). *Stress Intensity Factor Handbook, Vol I*. Pergamon Press. New York.
- Nekkal, A. (1991). A two parameter approach to elastic-plastic fracture mechanics. Master's thesis. Department of Mechanical Engineering. University of Glasgow.
- Nevalainen, M. and Dodds, R. H. (1995). Numerical investigation of 3-D constraint effects on brittle fracture in SE(B) and C(T) specimens. Technical report. University of Illinois at Urbana-Champaign, Dept. of Civil Eng. Urbana, Illinois. Report no SRS 598.
- Oates, G. (1969). 'Effect of temperature and strain rate on cleavage fracture in a mild steel and a low-carbon manganese steel'. *Journal of the Iron and Steel Institution* **207**, 353-357.
- O'Dowd, N. P. and Shih, C. F. (1991a). 'Family of crack-tip fields characterized by a triaxiality parameter: Part I - structure of fields'. *Journal of Mechanics and Physics of Solids* **39**, 939-963.
- O'Dowd, N. P. and Shih, C. F. (1991b). 'Family of crack-tip fields characterized by a triaxiality parameter: Part II - fracture applications'. *Journal of Mechanics and Physics of Solids* **40**, 989-1015.
- Orowan, E. (1948). 'Fracture and strength of solids'. *Report Program Physics* **12**, 185-230.
- Orowan, E. (1955). 'Energy criteria of fracture'. *Welding Journal* **34**, 157-160.
- Parks, D., Lam, P. and McMeekings, R. (1981). Some effects of inelastic constitutive models on crack tip fields in steady quasistatic growth.. In Francois, D. (Ed.). 'Advances in Fracture Research, 5th Int. Conf. on Fracture'. Vol. 5. pp. 2607-2614.
- Parks, D. M. (1974). 'A toughness derivative finite element technique for determination of crack tip stress intensity factors'. *Internal Journal of Fracture* **10**, 487-502.
- Parks, D. M. (1977). 'The virtual crack extension method for non-linear material behavior'. *Computer Methods in Applied Mechanics and Engineering* **12.**, 353-364.
- Parks, D. M. (1991a). Engineering methodologies for assessing crack front constraint. In 'Proc. Spring Meeting of the Soc. Experimental Mechanics'. Milwaukee, USA.
- Parks, D. M. (1991b). Advances in characterization of elastic-plastic crack-tip fields. In Argon, A. (Ed.). 'Topics in Fracture and Fatigue'. Springer Verlag. pp. 59-98.
- PATRAN v.2.4.5 (1988). *Patran User's Manual*. PDA Engineering, California.

- Pineau, A. (1992). Global and local approaches of fracture - transferability of laboratory test results to components. In Argon, A. (Ed.). 'Topics in Fracture and Fatigue'. Springer Verlag. pp. 197-234.
- Prandtl, L. (1920). 'Über die härte plastischer körper'. *Nachr. Ges. Wiss.* pp. 74-85.
- Reid, C. R. and Drugan, W. J. (1992). 'Asymptotic finite deformation fields of analysis of growing cracks in elastic - perfectly plastic materials'. *Journal of Mechanics and Physics of Solids* **39**, 989-1015.
- Rice, J. (1968a). Mathematical analysis in the mechanics of fracture. In Liebowitz, H. (Ed.). 'Fracture: An Advanced Treatise'. Vol. II. Academic Press. London. pp. 191-311.
- Rice, J. R. (1968b). 'A path independent integral and the approximate analysis of strain concentration by notches and cracks'. *ASME Journal of Applied Mechanics* **35**, 379-386.
- Rice, J. R. (1972). *International Journal of Solids and Structures* **8**, 751-758.
- Rice, J. R. (1974a). 'Limitations to the small scale yielding approximation for crack tip plasticity'. *Journal of The Mechanics and Physics of Solids* **22**, 17-26.
- Rice, J. R. (1974b). Elastic-plastic models for stable crack growth. In M.J.May (Ed.). 'Conf. Proc. Mechanics and Mechanisms of Crack Growth'. British Steel Corp.. Physical Metallurgy Centre Publication. Cambridge, U.K.
- Rice, J. R. and Johnson, M. A. (1970). The role of large crack tip geometry changes in plane strain fracture. In Kanninen, M., Adler, W., Rosenfields, A. and Jaffee, R. (Eds.). 'Inelastic Behavior of solids'. McGraw-Hill Series in Material Science and Engineering, New York. pp. 641-672.
- Rice, J. R. and Levy, N. (1972). 'The part through surface crack in an elastic plate'. *ASME Journal of Applied Mechanics* **39**, 185-194.
- Rice, J. R. and Rosengren, G. F. (1968). 'Plane strain deformation near a crack tip in a power law hardening material'. *Journal of Mechanics and Physics of Solids* **16**, 1-12.
- Rice, J. R. and Sorensen, E. P. (1978). 'Continuing crack tip deformation and fracture for plane strain crack growth in elastic-plastic solids'. *Journal of Mechanics and Physics of Solids* **26**, 163-186.
- Rice, J. R. and Tracey, D. M. (1974). 'Computational fracture mechanics'. *Journal of Mechanics and Physics of Solids* **22**, 17-26.
- Rice, J. R., Paris, P. C. and Merkle, J. G. (1973). Some further results of J-integral analysis and estimates. In 'ASTM STP 536'. pp. 231-245.
- Ritchie, R. O., Knott, J. and Rice, J. R. (1973). 'On the relationship between critical tensile stress and fracture toughness in mild steel'. *Journal of Mechanics and Physics of Solids* **21**, 395-410.
- Rooke, D. P. and Cartwright, D. J. (1976). *Compendium of stress intensity factors*. Her Majesty's Stationary Office. London.
- Sham, T. L. (1991). 'The determination of the elastic T-term using higher order weight functions'. *International Journal of Fracture* **48**, 81-102.
- Sharma, S. M. and Aravas, N. J. (1991). 'Determination of higher order terms in asymptotic elastoplastic crack tip solutions'. *Journal of Mechanics and Physics of Solids* **39**, 1043-1072.

- Sharma, S. M., Aravas, N. J. and Zelman, M. G. (1994). Two-parameter characterization of crack tip fields in edge-cracked geometries: Plasticity and creep solutions. In Erdogan, F. and Hartranft, R. J. (Eds.). 'Fracture Mechanics, ASTM STP 1220'. American Society for Testing and Materials. Philadelphia.
- Shih, C. F. (1974). Small-scale yielding analysis of mixed mode plane-strain crack problems. In 'Fracture Analysis, ASTM STP 560'. American Society for Testing and Materials. Philadelphia, PA. pp. 187-210.
- Shih, C. F. (1981). 'Relationship between the J-integral and the crack opening displacement for stationary and extending cracks'. *Journal of Mechanics and Physics of Solids* **29**, 305-326.
- Shih, C. F. (1983). Tables of Hutchinson-Rice-Rosengren singular field quantities. Technical report. Materials Research Laboratory, Brown University. Providence, RI.
- Shih, C. F. (1985). 'J-dominance under plane strain fully plastic conditions: the edge bar subjected to combined tension and bending'. *International Journal of Fracture Mechanics* **29**, 73-83.
- Shih, C. F. and German, M. D. (1981). 'Combined loading of a fully plastic ligament ahead of an edge crack'. *Journal of Applied Mechanics* **53**, 27-43.
- Shih, C. F. and Hutchinson, J. W. (1986). *Journal of Applied Mechanics* **53**, 271-277.
- Shih, C. F. and O'Dowd, N. P. (1992). A fracture mechanics approach based on a toughness locus. In Dawes, M. G. (Ed.). 'Shallow Crack Fracture Mechanics, Toughness Tests and Applications'. The Welding Institute. Publishing, Abington Cambridge, England.
- Shih, C. F., O'Dowd, N. P. and Kirk (1993). A framework for quantifying crack tip constraint. In Hackett, E. M., Schwalbe, K. H. and Dodds, R. H. (Eds.). 'Constraint Effect in Fracture, ASTM STP 1171'. American Society for Testing and Materials. Philadelphia, PA. pp. 2-20.
- Slepyan, L. (1974). *Izv. Nauk. SSSR. Mekhanika Tverdogo Tela* **9**, 57. Translated from Russian.
- Sumpter, J. and Hancock, J. W. (1994). Status review of the J plus T stress fracture analysis method. In '10th Eur. Conf. on Fracture'. pp. 617-626.
- Sumpter, J. and Turner, J. W. (1976). Method for the laboratory determination of J_C . In 'Cracks and Fracture, ASTM STP 601'. American Society for Testing and Materials. Philadelphia, PA. pp. 3-18.
- Sumpter, J. D. G. (1993a). An experimental investigation of the T stress approach. In Hackett, E. M., Schwalbe, K. H. and Dodds, R. H. (Eds.). 'Constraint Effect in Fracture, ASTM STP 1171'. American Society for Testing and Materials. Philadelphia, PA. pp. 492-502.
- Sumpter, J. D. G. (1993b). 'Fracture avoidance in welded steel structures. Are recent test standards useful to industry?'. *Institution of Engineers and Shipbuilders in Scotland*.
- Sumpter, J. D. G. and Forbes, A. T. (1992). Constraint based analysis of shallow cracks in mild steel. In Dawes, M. G. (Ed.). 'Shallow Crack Fracture Mechanics, Toughness Tests and Applications'. The Welding Institute. Publishing, Abington Cambridge, England.
- Tada, H., Paris, P. C. and Irwin, G. R. (1973). The stress analysis of cracks handbook. Technical report. Det Research Corporation. Hellertown, Pennsylvania.

- Tresca, H. (1864). *Comptes Rendus Acad. Sci, Paris* **59**, 754.
- Turner, J. W. (1973). *Material Science in Engineering* **11**, 275-282.
- Tvergaard, V. and Hutchinson, J. (1994). 'Effects of T-stress on Mode I crack growth resistance in a ductile solid'. *International Journal of Fracture* **34**, 213-241.
- Varias, A. G. and Shih, C. F. (1993). 'Quasi-static crack advance under a range of constraints - steady- state fields based on a characteristic length'. *Journal of Mechanics and Physics of Solids* **41**(5), 835-861.
- Wallin, K. (1993). Statistical aspects of constraint with emphasis on testing and analysis of laboratory specimens in the transition region. In Hackett, E. M., Schwalbe, K. H. and Dodds, R. H. (Eds.). 'Constraint Effect in Fracture, ASTM STP 1171'. American Society for Testing and Materials. Philadelphia, PA. pp. 264-288.
- Wang, Y. Y. (1993). On the two-parameter characterization of elastic-plastic crack-front fields in surface cracked plates. In Hackett, E. M., Schwalbe, K. H. and Dodds, R. H. (Eds.). 'Constraint Effect in Fracture, ASTM STP 1171'. American Society for Testing and Materials. Philadelphia, PA. pp. 120-138.
- Wang, Y. Y. and Gordon, J. R. (1992). The limits of applicability of J and CTOD estimation procedures for shallow-cracked SENB specimens. In Dawes, M. G. (Ed.). 'Shallow Crack Fracture Mechanics, Toughness Tests and Applications'. The Welding Institute. Publishing, Abington Cambridge, England.
- Wang, Y. Y. and Park, D. M. (1992). 'Evaluation of the T-stress in surface-cracked plates using line-spring method'. *International Journal of Fracture* **59**, 25-44.
- Wang, Y. Y. and Parks, D. M. (1994). Limits of J-T characterization of elastic-plastic crack-tip fields. In Kirk and Bakker (Eds.). 'Constraint Effects in Fracture: Theory and Applications, ASTM STP 1244'. American Society for Testing and Materials. Philadelphia, PA.
- Wells, A. A. (1961). Unstable crack propagation in metals, cleavage and fast fracture. In 'Proceedings of the Crack propagation Symposium'. Vol. 1. Cranfield, UK. pp. 210-230. Paper 48.
- Westergaard, H. M. (1939). 'Bearing pressure and cracks'. *Journal of Applied Mechanics* **6**, 49-53.
- Williams, M. L. (1957). 'On the stress distribution at the base of a stationary crack'. *ASME Journal of Applied Mechanics* **24**, 111-114.
- Williams, M. L. and Ewing, P. D. (1972). *International Journal of Fracture* **8**, 441.
- Xia, L., Wang, T. C. and Shih, C. F. (1993). 'Higher-order analysis of crack-tip fields in elastic power-law hardening materials'. *Journal of Mechanics and Physics of Solids* **41**, 665-687.
- Yang, S., Chao, Y. J. and Sutton, M. A. (1993a). 'Higher order asymptotic crack tip fields in a power-law hardening material'. *Engineering Fracture Mechanics* **45**(1), 1-20.
- Yang, S., Chao, Y. J. and Sutton, M. A. (1993b). 'Complete theoretical analysis for higher order asymptotic terms and the HRR zone at a crack tip for mode I and mode II loading of a hardening material'. *Acta Mechanica* **98**, 79-98.

